Development of Polymeric Nanoparticles and Complementary Diagnostics to Control Aberrant Immune Function

by

Kevin R. Hughes

A dissertation submitted in partial fulfillment
of the requirements for the degree of
Doctor of Philosophy
(Biomedical Engineering)
in the University of Michigan
2020

Doctoral Committee:

Professor Lonnie D. Shea, Chair
Associate Professor Marilia Cascalho
Research Assistant Professor Jessica J. O'Konek
Associate Professor Ariella Shikanov

Kevin R. Hughes

krhughes@umich.edu

ORCID iD: 0000-0002-1706-2799

© Kevin R. Hughes 2020

Dedication

This dissertation is dedicated to my incredible and loving wife

Acknowledgements

I cannot overexpress my gratitude to my graduate advisor, Dr. Lonnie Shea. You have been an incredible example of an exceptional mentor, scientist, communicator, and family man. Thank you for guiding me throughout my PhD work and for your commitment to the development of your students.

I am incredibly thankful for the expert interpretations and suggestions from my thesis committee members Dr. Jessica O'Konek, Dr. Marilia Cascalho, and Dr. Ariella Shikanov. Your dedication to guiding my experimental design and identifying areas where my work and expertise can improve have significantly improved my contributions to the field. Thank you for your patience and for helping me to become a better scientist and person.

I had the luxury of receiving incredible amounts of scientific and technical assistance from many Shea lab members over the years and am thankful for everyone within our group. I would be remiss if I did not specifically highlight Dr. Ryan Pearson for making certain that I had the technical understanding to be an effective material scientist, Dr. Liam Casey for his mentorship on topics of life and lab, and Dr. Aaron Morris for working closely with me and providing significant intellectual input in much of my thesis work. I've had the opportunity to work with many brilliant scientists and will always cherish the weeks, months, and years I've worked alongside Jeffrey Landers and Drs. Matthew Hall, Robert "Smitty" Oakes, and Yining Zhang. None of this work would have been possible without contributions from many individuals from many laboratory groups—thank you all for your efforts and friendship.

I would never have made it to a point where I had the opportunity to contribute to the advancement of this field without the unwavering support and love that my parents have provided. Thank you for always believing in me and by encouraging me, through example, to strive to be a better person. You continually make sacrifices to help your children and we are incredibly grateful.

I'm not able to adequately relay the contributions that my wife has made to my life and work, so I won't try. Anna, you are the most incredible person I have ever known and you make life worth living.

I am grateful to the sources of funding that have enabled this work, including funding through NIH grants EB-013198, NS-026543, EB-009910, AI-148076, DK-121462, and AI-147677; the Juvenile Diabetes Research Foundation, including 2-SRA-2014-287-Q-R and 2-SRA-2016-313-S-B; the Soft and Hybrid Nanotechnology Experimental (SHyNE) Resource (NSF ECCD-1542205); the MRSEC program (NSF DMR-1121262) at the Materials Research Center; the Nanoscale Science and Engineering Center (EEC-0118025/003); the International Institute for Nanotechnology (IIN); University of Michigan's Biomedical Engineering department; and the UM Precision Health Scholars grant. Certain cellular assays were performed in the Flow Cytometry Core Facility of the Interdepartmental ImmunoBiology Center at Northwestern University; the Michigan Center for Materials Characterization; the U-M Cancer Center Immunology Core; and the U-M Biointerfaces Institute. I'd like to thank Dr. Mohammed Javeed I Ansari for providing ABM mice; Christopher Krebs, PhD and the University of Michigan DNA Sequencing Core for assistance in OpenArray processing and analysis and the University of Michigan Flow Cytometry Core and In Vivo Animal Core for flow cytometry and histology resources, respectively. I have been supported through funding provided through the

University of Michigan's Rackham Pre-Doctoral Fellowship, Rackham Merit Fellowship, and the U.S. Department of Education's Graduate Assistance in Areas of National Need Fellowship.

Table of Contents

Dedication ii
Acknowledgements iii
List of Tables xiv
List of Figures xv
Abstract xxxii
Chapter 1 Introduction: Nanotechnology and Biomaterials for Immune Modulation and Monitoring 1
Authors 1
Preface 1
Background 1
Autoimmunity 3
Allergy 6
Transplant Rejection 9
Clinical Trials of Tolerogenic Nanotherapies 13
Liposomal 14
Virus-like Particles 18
Metallic 19
Polymeric 20
Precision Diagnostics 22
Liquid Biopsy 23
Immunological Niches 23
Outlook 25
Biomaterial Interventions Discussed in This Thesis 27
Contents 29
Chapter 2 In Vivo Rreprogramming of Immune Cells: Technologies for Induction of Antigen-Specific Tolerance 34
Authors 34
Abstract 34

Introduction 34
Peripheral tolerance mechanisms 37
Apoptotic cells 39
Naturally occurring exosomes 40
Non-specific deletion 41
APC Reprogramming 41
Cell-based therapeutics 41
Particle-based therapeutics 42
Autoantigen delivery 46
Cell-based approaches 47
Particle-based approaches 50
Alloantigen Delivery 55
Cell-based approaches 56
Particle-based approaches 58
Allergen Delivery 60
Cell-based approaches 62
Particle-based approaches 63
Carrier-free therapeutics 65
Fusion proteins 65
Soluble Ag arrays 67
Lymphocyte Reprogramming 67
Regulatory T cell induction 68
CAR T cells 69
Peptide-MHC complexes on particles 72
Immune privileged sites 74
Conclusion and future directions 75
Acknowledgement 77
Chapter 3 Controlled Delivery of Single or Multiple Antigens in Tolerogenic Nanoparticles Using Peptide-Polymer Bioconjugates 78
Authors 78
Abstract 78
Introduction 79
Results 81

Synthesis of antigen-polymer conjugates and particle preparation 81
Regulatory T cell induction by acNP-Ags is size and antigen loading-dependent 84
Regulatory T cell induction by acNP-Ag nanoparticles is concentration-dependent 86
acNP-Ags suppress EAE induced by $PLP_{139-151}$ immunization 88
acNP-Ags suppress EAE induced with a cocktail of encephalitogenic peptides ($PLP_{139-151}$ and $PLP_{178-191}$) 89
Discussion 91
Materials and Methods 95
PLG-Ag conjugation 95
Mice 96
Nanoparticle preparation 96
Nanoparticle characterization 97
$OVA_{323-339}$-IgG1 binding *in vitro* 97
Cell culture 98
Antibodies and flow cytometry 98
Cell isolation and *in vitro* Treg induction assay 99
R-EAE disease induction and measurement 99
Acknowledgements: 100
Supplementary Tables and Figures 100
Chapter 4 Conjugation of Transforming Growth Factor Beta to Antigen-Loaded Poly(lactide-co-glycolide) Nanoparticles Enhances Efficiency of Antigen-Specific Tolerance 106
Authors 106
Abstract 106
Introduction 107
Results 109
Bioactivity of TGF-β-coupled PLG nanoparticles 109
Antigen and TGF-β bioactive co-delivery by nanoparticles 110
PLG nanoparticles downregulate dendritic cell costimulatory molecules and reduce inflammatory cytokine secretion 113
Ag-NPs affect changes in the T cell compartment 115
Surface conjugation of TGF-β improves the tolerogenic effect of Ag-NPs 116
Subcutaneous delivery of TGF-β conjugated Ag-NPs reduces relapse scores in EAE 118
Discussion 119

Materials and Methods 125
Ag-PLG conjugation 125
Mice 126
Nanoparticle preparation and TGF-β conjugation 126
Cell culture 127
Antibodies and flow cytometry 127
Cell isolation and *in vitro* Treg induction assay 128
Ex vivo T cell analysis 128
EAE disease induction and measurement 129
Acknowledgements 129
Supplementary Figures 130
Chapter 5 Nanoparticle Delivery of Antigen Attenuates Anaphylactic Response in a Murine Model of Peanut Allergy 131
Authors: 131
Abstract: 131
Introduction: 132
Materials and Methods: 135
Synthesis of PLG(Greer) nanoparticles: 135
Nanoparticle Characterization 136
Mice and immunizations 136
Measurement of serum antibodies 137
Analysis of cytokine expression recall assays 137
Assessment of hypersensitivity reactions. 137
Statistics 138
Results: 138
Definition of safety parameters 138
Synthesis and characterization of nanoparticles 139
PLG(PE) administration is well-tolerated in pre-sensitized mice 140
Prophylactic administration of PLG(PE) prevents sensitization 141
Therapeutic administration of PLG(PE) provides benefit to clinical symptoms 143
Discussion: 144
Conclusion: 147
Acknowledgements: 148

Funding: 148
Chapter 6 Optimizing PLG Nanoparticle-Peptide Delivery Platforms for Transplantation Tolerance Using an Allogeneic Skin Transplant Model 149
Authors 149
Abstract 149
Introduction 150
Materials and Methods 153
Mice 153
Skin transplantation 153
Donor antigen preparations 153
PLG particle synthesis 153
Antigenic peptide encapsulation in PLG nanoparticles 154
Antigenic peptide conjugation to PLG nanoparticles 154
Particle characterization 155
In vivo biodistribution study 156
Recipient treatment schemes 156
Generation of bone marrow derived macrophages (BMDMs) 157
ABM T cell proliferation *in vitro* 157
Analysis of skin graft infiltrating cells and draining lymph node (DLNs) cells 158
Luminex liquichip microplate cytokine assays 159
Antibodies and flow analysis 159
Statistics 160
Results 160
Characterization of NPs conjugated or encapsulated with bm12 peptides 160
Peptide length and skin allograft survival 162
Biodistribution of NP-ECDI-P1 164
Graft-infiltrating cells in NP-ECDI-P1 treated recipients 166
Bm12-specific T cell proliferation and cytokine production 168
Peptide conjugation method and skin allograft survival 171
Antigen incorporation method and skin allograft survival 172
Whole donor cell lysate containing antigenic epitopes for tolerance delivery 175
Discussion 176
Conclusions 182

Author contributions 183
Conflicts of interest 183
Data availability 183
Acknowledgments 183
Chapter 7 Localized Immune Tolerance from FasL-Functionalized PLG Scaffolds 184
Authors 184
Abstract 184
Introduction 185
Materials and methods 188
Materials 188
Biotinylation of PLG and characterization 188
Particle and scaffold fabrication 189
Particle characterization 189
Protein loading and quantification 190
Apoptosis assay 190
Mice and recombinant proteins 190
Islet isolation and engineering with SA-FasL protein 191
Islet transplantation 191
Intraperitoneal Glucose Tolerance Test 192
Mixed Lymphocyte Reaction 192
Statistical analysis 193
Results 193
Transplantation of SA-FasL-engineered islets on microporous scaffolds 193
Synthesis and characterization of biotin-PLG conjugates and particle formation 195
SA-FasL loading on biotin-PLG scaffolds 198
SA-FasL scaffolds support allogeneic graft function without chronic immunosuppression 200
Discussion 201
Data availability 205
Conflicts of interest 206
Acknowledgments 206
Chapter 8 Engineered Immunological Niches to Monitor Disease Activity and Treatment Efficacy in Relapsing Multiple Sclerosis 207

Authors: 207
Abstract 207
Introduction 207
Results 209
EAE alters gene expression at implantable immunological niche 209
Characterization of populations within immunological niches and blood 212
Immunological niches are dynamic with disease state and reflect effectiveness of therapy 214
Preemptive intervention enabled by early detection abrogates disease. 217
Discussion 217
Methods 219
Scaffold Fabrication and Subcutaneous implantation 219
Disease Induction 220
Tissue isolation 221
RNA isolation and cDNA synthesis 221
OpenArray High-Throughput RT-qPCR 222
Selection of Genes of Interest 222
Gene Signature Scores and analysis 223
Histology 224
Flow cytometry 224
Nanoparticle Fabrication and Administration 225
Statistics 226
Data Availability: 227
Supplemental Figures 227
Acknowledgements 242
Conflict of Interest Statement: 243
Chapter 9 Conclusion and Future Directions 244
Summary of Findings 244
Significance and Impact 248
Future Directions 249
Development of strategies to conjugate proteins, lysates, and extracts to polymer backbones of NP formulations 249
Improvement of NP safety and efficacy in murine models of food allergy. 251
Understanding the mechanism of action of NP therapies 252

Further investigation of implantable complementary diagnostics 254
Appendices 256
Development of immunological niche in murine model of primary progressive multiple sclerosis 256
Introduction 256
Methods 257
Scaffold Fabrication and Subcutaneous implantation 257
Disease Induction 257
Tissue isolation 258
RNA isolation and cDNA synthesis 258
OpenArray High-Throughput RT-qPCR 259
Selection of Genes of Interest 259
Gene Signature Scores and analysis 260
Nanoparticle Fabrication and Administration 261
Statistics 261
Characterization of PLG nanoparticle efficacy in murine model of primary progressive MS 261
Investigation of PLG NP efficacy in murine model of egg allergy 265
Materials and Methods: 265
Synthesis of PLG(Greer) nanoparticles: 265
Nanoparticle Characterization 266
Mice and immunizations 266
Assessment of hypersensitivity reactions. 266
Statistics 267
Timing of therapeutic application of PLG(OVA) impacts efficacy. 267
Bibliography 269

List of Tables

Table 1.1: Role of direct, indirect, and semi-direct recognition in allorejection 10

Table 1.2: Clinical trials harnessing nanotherapeutics to target immune dysfunction 17

Table 2.1: Nanoparticles investigated for antigen-specific immune regulation delivering protein or peptide antigens. 44

Table 3.1: Size and zeta potential of the nanoparticle formulations used in this study. Ag loading (μg Ag/mg PLG) was precisely controlled by combining PLG-Ag conjugates with unmodified PLG at predetermined mixing ratios. *ac-PLG-PLP139-151, 178-191 particles contained 8 μg/mg of both PLP139-151 and PLP178-191. 82

Table 3.2: Determination of acNP-Ag loading using ^{1}H-NMR. Lyophilized acNP-Ag particles were dissolved in DMSO-d6 and the protein content was determined by comparing the integration values of the overlapping methyl proton peaks of leucine and isoleucine to the methylene proton peak present in PLG..... 100

Table 3.3: Concentration (ng/mL) of antigen delivered per well as a function of acNP-$OVA_{323-339}$ concentration and loading. Orange colored cells represent the protein loadings evaluated in Figure 3.3..... 100

.

List of Figures

Figure 1.1 Overview of the intersection of tolerogenic therapies and precision diagnostics for monitoring patient health and response to therapies 3

Figure 2.1: Highlighted approaches of technologies implemented for antigen-specific tolerance induction. Most antigen-specific tolerance strategies result in reprogramming lymphocytes through antigen presenting cells (APCs), however, there are platforms that target T cells and specifically recognize their autoreactive T cell receptors. Inspired by the natural clearance of apoptotic cells which results in peripheral tolerance maintenance, antigen has been delivered by various platforms including antigen-coupled splenocytes (Ag-SP), erythrocyte-targeted peptides (Ag-RBC), and antigen-loaded synthetic particles. These carriers are internalized, processed by APCs, and induce tolerogenic costimulation and soluble signaling pathways that direct T cell phenotypes away from immunogenic effector T cell activation and toward regulatory T cells (Tregs), anergy, or deletion. Direct interaction of particle-bound peptide-major histocompatibility complexes (pMHC-NPs) with antigen-experienced T cells can induce a tolerogenic regulatory-like TR1 phenotype that can mitigate immune-mediated disease progression. 37

Figure 2.2: Mode of antigen-association with particles affects the risk of anaphylaxis following intravenous administration in individuals with prior antigen sensitization. Antigen is associated with particles by surface-coupling (NP-Ag) or by encapsulation (NP(Ag)) methods. In vivo, granulocyte activation occurs when NP-Ag or soluble antigen is recognized by circulating IgE antibodies or binds to pre-bound IgE on granulocytes. Cross-linking of IgE on granulocytes triggers degranulation and subsequent release of histamine and other inflammatory mediators that cause increased permeability, distension of blood capillaries, and anaphylaxis. (i) Binding of antigen-specific IgE to NP-Ag can trigger granulocyte activation. (ii) Binding of antigen-specific IgG to NP-Ag reduces potential granulocyte activation but can result in off-targeted biodistribution and reduce tolerance induction. (iii) Pre-mature antigen release from NP(Ag) can result in granulocyte activation but to a lesser extent than NP-Ag. (iv) NP(Ag) with negligible rate of antigen release reduces the risk of granulocyte activation and enables unaffected distribution to the liver and spleen to induce tolerogenic responses. 47

Figure 2.3: Erythrocyte-binding TER119 scFv antibodies fused with autoantigen (p31) specifically target red blood cells in situ after intravenous administration and induce antigen-specific tolerance in type 1 diabetes model. (A) TER119-p31 induces tolerance and results in normoglycemia. Normoglycemic NOD/ShiLtJ mice received adoptive transfer of diabetogenic BDC2.5 CD4+ T cells and 3 intravenous treatments of saline, p31, or TER119-p31 (n =8, n = 9, and n = 9, respectively) over the first week. ***P < 0.0001. (B) Immunohistochemistry of pancreatic islets excised 4 days

after treatment and stained for CD3ε T cells (green), insulin (red), and nuclei (blue). Saline-treated and untargeted autoantigen mimetope p31 resulted in T cell infiltration and islet destruction in contrast to mice treated with red blood cell-binding autoantigen (TER119-p31) which prevented T cell infiltration and preserved insulin production. (Scale bar = 100 μm). Reproduced from [146] with permission. 49

Figure 2.4: Antigen-polymer conjugate nanoparticles display favorable physicochemical and biological properties for tolerance induction. (A) Release profile of NP($OVA_{323-339}$), NP-$OVA_{323-339}$, and acNP-$OVA_{323-339}$. (B) Regulatory T cell induction is dependent on nanoparticle concentration. BMDCs were treated for 3 h with various concentrations of 400 nm of acNP-$OVA_{323-339}$ (2, 8, 25, 150 μg/mg loading) formulation. Excess acNP-$OVA_{323-339}$ particles were subsequently washed from the cell surface prior to addition of OT-II T cells and 2 ng/mL of TGF-β1. (C) Schematic representation of antigen-polymer conjugate nanoparticles delivering multiple Ags. (D) Clinical scores of SJL/J mice treated with 1.25 mg of acNP-$OVA_{323-339}$ (8 μg/mg $OVA_{323-339}$), acNP-$PLP_{139-151}$ (8 μg/mg $PLP_{139-151}$), acNP-$PLP_{178-191}$ (8 μg/mg $PLP_{178-191}$), or acNP-$PLP_{139-151,178-191}$ (8 μg/mg $PLP_{139-151}$ and 8 μg/mg $PLP_{178-191}$) and immunized with $PLP_{139-151}$ and $PLP_{178-191}$ in CFA to induce R-EAE 7 days later. (E) Corresponding cumulative clinical score for mice treated with particles (n = 5). Differences between disease courses of different treatment groups were analyzed for statistical significance using the Kruskal-Wallis test (one-way ANOVA non-parametric test) with Dunn's multiple comparisons test ($p < 0.05$). 52

Figure 2.5: A short course of low dose rapamycin synergizes with PLG-donorAg (dAg) to enhance tolerance efficacy. Recipient mice (C57BL/6) receiving donor (BALB/c) PLG-dAg injections at days 7 and +1 in combination with a 4-day course (days 1, 0. +1, and +2) of low dose (0.1 mg/kg) rapamycin demonstrated significantly greater islet allograft survival (n=11) compared with mice treated with rapamycin alone (n=9), BALB/c PLG-dAg alone (n=17), or PLG particles coupled with lysate proteins from a third party donor SJL/J (n=4). **$p < 0.01$. Reproduced from [72] with permission from Elsevier. 59

Figure 2.6: Prophylactic treatment with PLG(OVA) inhibits Th2-induced airway inflammation. Naive female BALB/c mice (n = 5) were treated i.v. with 2.5 mg PLG(OVA) or control PLG(LYS) on days −7 and +7 relative to i.p. immunization with 10 μg of OVA in 3 mg of alum or alum alone on days 0 and +14 before aerosol challenge with 10 mg/mL OVA for 20 min on days +28–30 and sample collection on day +31. LYS, lysozyme. (A) Concentration of serum OVA-IgE was determined by sandwich ELISA. (B) Lungs were flushed with BALF, total cell counts were determined, and samples were cytospun onto slides before DiffQuik staining for differential cell counts of bronchoalveolar lavage eosinophils. (C) Lungs were fixed in formalin and stained with H&E. (D) Cytokines from BALF supernatant were analyzed by Milliplex. Results are mean ± SEM and are representative of three separate experiments. *$P < 0.05$; **$P < 0.01$. Reproduced with permission from [169]. 64

Figure 2.7: pMHC-NPs suppress MOG-induced EAE in vivo. C57BL/6 mice were immunized with $pMOG_{35–55}$. (A) EAE scores of mice treated from day 14 (n=4 each). (B) EAE

scores of mice treated from day 21 (n=10, 7 and 3 from top). (C) Representative microglial IBA1 staining and relative rank scores in the cerebellum of mice from B (n=4–5). Reproduced with permission from [7]. ©2016 Macmillan Publishers Ltd... 74

Figure 3.1: Synthesis and characterization of PLG-antigen conjugates and nanoparticle formation. (A) ^{1}H-NMR spectrum of PLG, $OVA_{323-339}$, and PLG-$OVA_{323-339}$ measured in DMSO-d6 (calibrated at 2.5 ppm). (B) The coupling efficiency of $OVA_{323-339}$ to PLG was calculated by comparing the integration values of the overlapping methyl proton peaks of leucine and isoleucine present at 1.4 ppm in $OVA_{323-339}$ (d, d') to the methylene proton peak present at 5.3 ppm in PLG (b). (C) Schematic representation of nanoparticles used in this study. (D) PLG, NP($OVA_{323-339}$), NP-$OVA_{323-339}$, and acNP-$OVA_{323-339}$ were incubated with FITC-labeled anti-$OVA_{323-339}$ IgG to identify the presence of peptide on the surface of the particles. Results are geometric mean fluorescence intensity. (E) Release profile of NP($OVA_{323-339}$), NP-$OVA_{323-339}$, and acNP-$OVA_{323-339}$. Statistical differences between groups was determined by performing a one-way ANOVA and Tukey's Post-hoc test ($p<0.05$). Groups with similar letters indicates no statistical significance. 83

Figure 3.2 Figure 3.3: Regulatory T cell induction in vitro is dependent on nanoparticle size and Ag loading. BMDCs were treated for 3 h with 300 μg/mL of 400 nm (B and D) and 80 nm (C and E) acNP-$OVA_{323-339}$ or 100 ng/mL of soluble $OVA_{323-339}$. Excess acNP-$OVA_{323-339}$ was subsequently washed from the wells prior to addition of naïve $CD4^{+}$ OT-II T cells and 2 ng/mL of TGF-β1. Cells were co-cultured for 4 days prior to flow cytometric analysis. (A) Representative gating strategy for regulatory T cell induction. All cells, singlets, live, and CD4+ cells were examined for CD25 and Foxp3 expression. (B and c) The effect of antigen loading on CD25 and (D and E) Foxp3 expression of T cells was measured. Although both particles formulations increased CD25 expression similarly, only 400 nm acNP-$OVA_{323-339}$ particles could efficiently induce $CD4^{+}CD25^{+}Foxp3^{+}$ regulatory T cells. Statistical differences between groups was determined by performing a one-way ANOVA and Tukey's Post-hoc test ($p<0.05$). Groups with similar letters indicates no statistical significance. 85

Figure 3.4: Regulatory T cell induction is dependent on nanoparticle concentration. BMDCs were treated for 3 h with various concentrations of 400 nm of acNP-$OVA_{323-339}$ (2, 8, 25, 150 μg/mg loading) formulation. Excess acNP-$OVA_{323-339}$ particles were subsequently washed from the cell surface prior to addition of OT-II T cells and 2 ng/mL of TGF-β1. The cells were co-cultured for 4 days prior to using flow cytometry to measure CD25 (A) and Foxp3 expression (B) of T cells. OT-II splenocytes were treated with soluble $OVA_{323-339}$ (100 ng/mL) or acNP-$OVA_{323-339}$ (25 μg/mg loading; 75 μg/mL) in the presence or absence of 2 ng/mL of TGF-β1. (C) The cells were co-cultured for 4 days prior to using flow cytometry to measure CD25 and Foxp3 expression. Statistical differences between groups was determined by performing a one-way ANOVA and Tukey's Post-hoc test ($p<0.05$). Groups with similar letters indicates no statistical significance. 88

Figure 3.5: acNP-Ags prophylactically induce tolerance in R-EAE. Clinical scores for SJL/J mice treated with 2 doses of 2.5 mg of NP($OVA_{323-339}$), 2.5 mg of NP($PLP_{139-151}$) (2.6 μg/mg $PLP_{139-151}$), or 2.5 mg of acNP-$PLP_{139-151}$ (2.6 μg/mg $PLP_{139-151}$) and immunized with $PLP_{139-151}$/CFA to induce R-EAE. (A) Treatment of mice with nanoparticle formulations resulted in significantly abrogated clinical disease scores compared to the control. (B) Corresponding cumulative clinical score for mice treated with tolerogenic particles (n = 5). Differences between disease courses of different treatment groups were analyzed for statistical significance using the Kruskal-Wallis test (one-way ANOVA non-parametric test) ($p < 0.05$). 89

Figure 3.6: acNP-Ag particles induce protective tolerance against R-EAE induced with cocktail of autoantigens. Clinical scores of SJL/J mice treated with 1.25 mg of acNP-$OVA_{323-339}$ (8 μg/mg $OVA_{323-339}$), acNP-$PLP_{139-151}$ (8 μg/mg $PLP_{139-151}$), acNP-$PLP_{178-191}$ (8 μg/mg $PLP_{178-191}$), or acNP-$PLP_{139-151,178-191}$ (8 μg/mg $PLP_{139-151}$ and 8 μg/mg $PLP_{178-191}$) and immunized with $PLP_{139-151}$ and $PLP_{178-191}$ in CFA to induce R-EAE 7 days later. (A) Schematic representation of antigen-polymer conjugate nanoparticles delivering multiple Ags. (B) Treatment of mice with acNP-Ags formulated with both pathogenic epitopes resulted in significantly abrogated mean clinical disease scores compared to mice treated with only a single or irrelevant epitope. (C) Corresponding cumulative clinical score for mice treated with particles (n = 3-7). Differences between disease courses of different treatment groups were analyzed for statistical significance using the Kruskal-Wallis test (one-way ANOVA non-parametric test) ($p < 0.05$). 90

Figure 3.7: Synthesis and characterization of PLG-$PLP_{139-151}$ conjugates. ^{1}H-NMR spectrum of (i) PLG, (ii) $PLP_{139-151}$, and (iii) PLG-$PLP_{139-151}$ measured in DMSO-d6 (calibrated at 2.5 ppm). 102

Figure 3.8: Synthesis and characterization of PLG-$PLP_{178-191}$ conjugates. ^{1}H-NMR spectrum of (i) PLG, (ii) $PLP_{178-191}$, and (iii) PLG-$PLP_{178-191}$ measured in DMSO-d6 (calibrated at 2.5 ppm). 103

Figure 3.9: SEM images of various acNP particle formulations utilized in this study. (a) NP; (b) acNP-$OVA_{323-339}$ (8 μg/mg); (c) acNP-$OVA_{323-339}$ (25 μg/mg); (d) acNP-$OVA_{323-339}$ (50 μg/mg); (e) acNP-$OVA_{323-339}$ (150 μg/mg); (f) acNP-$PLP_{139-151,\ 178-191}$ (16 μg/mg). Scale bar: 2 μm. 104

Figure 3.10: Size-dependent cellular interactions and biodistribution of Cy5.5-labelled 80 nm or 400 nm PLG particles. (a) Bone marrow-derived dendritic cells were treated with particles at various concentrations for 3 hr. Maximum cellular associations were observed for both particles at 300 μg/mL and were not increased when the concentration was increased to 1 mg/mL (n=3). (b) Size-dependent biodistribution of 80 or 400 nm particles in the liver, spleen, and lungs. 1.25 mg of each particle type was intravenously administered to SJL/J mice and 24 h following particle administration, the mice were euthanized, and cellular fluorescence was analyzed. A significantly lower percentage of 80 nm particles accumulated in the organs evaluated. 400 nm particles accumulated significantly in the liver and to a much

lesser extent that was comparable to the 80 nm particle in the spleen and lungs (n=3). No Tx; no treatment. 104

Figure 4.1 Surface-coupled TGF-β is bioactively delivered by PLG nanoparticles. (A) A schematic depiction of the NP production and TGF-β conjugation procedure used to create the NPs in this study. TGF-β was conjugated to blank PLG, Ag-encapsulated, and Ag-polymer conjugate NPs. (B) Naïve $CD4^+CD25^-$ T cells were cultured in anti-CD3-coated plates for 4 days in the presence of 2 μg/mL anti-CD28, 10 ng/mL IL-2, and 2 ng/mL of soluble TGF-β, blank PLG NPs, or 300 μg/mL of PLG-TGF-β NPs (166 ng TGF-β/mg). T cells were characterized by flow cytometry for CD25 and intracellular Foxp3. 110

Figure 4.2: TGF-β and antigen are bioactively co-delivered by PLG particles to induce antigen-specific Tregs. (A) Characterization of Ag-NPs before and after TGF-β conjugation. Antigen-loaded NPs were prepared by encapsulating OVA peptide [PLG(OVA) NPs] or by incorporating PLG-Ag conjugates with unmodified PLG (acPLG NPs). (B-D) BMDCs were treated for 3 hours with 300 μg/mL of Ag-NPs. After 3 h, media was exchanged to remove excess particles. The BMDCs were then co-cultured for 4 days with naïve OT-II $CD4^+CD25^-$ T cells at a 1:1 ratio. Cells that were not treated with NPs received 100 ng/mL of OVA and 2 ng/mL of TGF-β. (B) Representative plots of flow cytometry data gated on live $CD4^+$ T cells. (C) Treg induction was compared between solubly derived TGF-β and NP-bound TGF-β co-delivered with PLG(OVA) NPs (3 μg OVA/mg) and acPLG-OVA NPs (2 μg OVA/mg). (D) Treg induction was evaluated with titrated amounts of TGF-β conjugated to acPLG-OVA NPs (OVA loading constant at 8 μg/mg). Statistical differences were determined using a two-tailed unpaired t-test. Error bars indicate SD. 112

Figure 4.3: NP treatment decreases BMDC costimulatory molecule expression and cytokine secretion. BMDCs were treated with soluble OVA or with NPs for 3 h. Excess NPs were washed away, and cells were incubated for 4 days. (A and C) BMDCs were unstimulated (immature) or (B and D) stimulated (mature) with 10 ng/mL of IFNγ and 10 ng/mL LPS after 3 h NP treatment. (A and B) BMDCs were evaluated by flow cytometry on day 4. Histograms show live cell surface molecule expression with red line histograms representing the indicated treatment and blue filled histograms representing untreated BMDCs. (C and D) The cytokines present in the BMDC media on day 4 were evaluated by ELISA. Statistical differences were determined by one-way ANOVA with Tukey's multiple comparisons test. Within data subsets, no significant difference was observed between conditions labeled with matching letters ($p>0.05$). Error bars indicate SD. 114

Figure 4.4: Ag-NPs cause Ag-specific changes in T cell populations in vivo. OT-II mice were untreated or injected with 1.25 mg of NPs (8 μg Ag/mg, 166 ng TGF-β/mg). (A-C) Mice treated i.v. received a single tail vein injection. (D-F) Mice treated s.c. received 4 injections distributed over the shoulders and hind limbs. After 7 days, the livers, spleens, and pooled brachial, axillary, and inguinal lymph nodes were excised and analyzed by flow cytometry for $CD4^+$ T cells and $CD25^+Foxp3^+$ Tregs. Statistical differences were determined by Fisher's Least Significant Difference (LSD) test.

Within data subsets, no significant difference was observed between conditions labeled with matching letters ($p>0.05$). Error bars indicate SEM. 116

Figure 4.5: TGF-β co-delivery improves the tolerogenic efficiency of Ag-loaded NPs in EAE model. (A,B) SJL mice were prophylactically injected i.v. with sub-therapeutic doses of Ag-NPs (A, 1.25 mg or B, 0.0625 mg at 8 μg Ag/mg and 166 TGF-β/mg). After 7 days, mice were immunized with PLP/CFA on day 0 to induce EAE (n=5). (C,D) SJL mice (n=7) were immunized (day 0) and injected with 1.25 mg of Ag-NPs (8 μg Ag/mg, 166 ng TGF-β/mg) on day 13 (the third day of disease presentation). 6 days after injection, 3 mice per cohort were euthanized and (D) the number of liver CD25+Foxp3+ Tregs was quantified using flow cytometry. Statistical differences between treatments for the indicated time periods were determined by (A and C) the Kruskal-Wallis test (one-way ANOVA non-parametric test) with Dunn's multiple comparisons test ($p < 0.05$) or (B) the Mann-Whitney (two-tailed non-parametric) test ($p<0.05$). Statistical differences between cell numbers (D) were determined using Fisher's Least Significant Difference (LSD) test. Within data subsets, no significant difference was observed between conditions labeled with matching letters ($p>0.05$). Error bars indicate SD. 118

Figure 4.6: Subcutaneous delivery of TGF-β-coupled Ag-NPs reduces the severity of relapse symptoms in EAE. SJL mice were injected s.c. with 1.25 mg of Ag-NPs (8 μg Ag/mg, 166 ng TGF-β/mg) 7 days before immunization with PLP/CFA to induce EAE (n=5). Statistical differences between treatments for the indicated time periods were determined by the Kruskal-Wallis test (one-way ANOVA non-parametric test) with Dunn's multiple comparisons test ($p < 0.05$). 119

Figure 4.7: In the EAE model, symptoms are suppressed with a dose of 2.5 mg Ag-relevant NPs. SJL mice were prophylactically injected i.v. with Ag-NPs (8 μg Ag/mg NP). After 7 days, mice were immunized with PLP/CFA on (day 0) to induce EAE (n=5). 130

Figure 5.1 Determination of safety parameters related to delivery of peanut extract via NP. Surface-conjugated NP (PLG-PE) were generated with relatively low, medium, or high loadings of peanut extract. Physicochemical properties are listed (A). Increased surface loading of peanut extract correlates with increased FITC anti-peanut antibody as measured by flow cytometric analysis (B). Relative amounts of surface or soluble peanut extract delivered intravenously and corresponding observation of anaphylactic response (C). C3H/HeJ mice were sensitized with i.p. injection of peanut and alum at Days -14 and -0 as described. Mice received injection of surface-conjugated PLG-PE or soluble peanut extract on Day +7 and were assessed for anaphylaxis as measured by core temperature (D and E). 139

Figure 5.2 Characterization of PLG NP used for in vivo studies. NP Size, Zeta, Polysdispersity (PDI), and antigen loading (μg antigen per mg NP) are characterized (A). Antigen release was measured over 2 hours (B). LAL Endotoxin testing indicates acceptable levels for all formulations utilized (C). 140

Figure 5.3 PLG(PE) is well-tolerized in pre-sensitized mice. C3H/HeJ mice were sensitized by i.p. injection of alum and Greer peanut extract on Day -7. Mice were treated on Day 0 with PLG(PE) or controls and assessed for anaphylactic response to therapy. Intravenous injection of PLG(PE), PBS, or PLG(PBS) were well tolerated, while injection of an equivalent total dose (25.75µg) of soluble Greer peanut extract resulted in anaphylactic temperature drop (A) and serum release of MCPT-1 (B) (n=5). Cyan 5.5-labeled, peanut extract-loaded NPs (PLG(PE, Cy5.5)) were injected intravenously. 24 hours post-injection, spleens, inguinal lymph nodes, mesenteric lymph nodes, lungs, and livers were collected and imaged by IVIS to determine relative organ distribution in naïve and pre-sensitized mice, presented as percent of total radiant efficiency (C). Statistical significance: * = P<0.05, ** = P <0.01..... 140

Figure 5.4 PLG(PE) provides prophylactic protection from peanut allergy. C3H/HeJ mice were sensitized by i.p. injection of alum and peanut extract on Day 0 and 14 and received treatment or controls on days 7 and 21. Data represent 7th and final oral challenge. Schematic of experimental timeline (A). Clinical anaphylaxis score was characterized (B) and serum MCPT-1 levels determined by ELISA (C). Serum peanut-specific IgE levels were characterized (D) and cytokine secretion in culture supernatants of recall assays were measured by Luminex multiplex (E). n=5 per group. Statistical significance: * = P<0.05, ** = P <0.01 **** = P <0.001 142

Figure 5.5. Attenuation of anaphylactic response with PLG(PE). Mice were sensitized with alum beginning on Day 0 and treated with PLG(PE) on Days 21, 28, and 35 (A) or 21 and 28 (B). Therapeutic efficacy in CTx-induced disease were tested by CTx sensitization on Day 0 and treatment on days 42, 49, and 65 (C and D). PLG(PE) provided protection from alum-induced serum MCPT-1 production (A). Serum cytokine recall assays of spleen and mesenteric lymph node cells by Luminex multiplex assay demonstrate significant reduction in allergic and inflammatory cytokines (B) in alum-induced disease. PLG(PE) provided protection from CTx-induced allergy as measured by post-challenge temperature drop (C) and serum MCPT-1 release (D). Statistical significance: * = P<0.05, ** = P <0.01 143

Figure 6.1 PLG NP characterization and quantification of antigen coupling. (A) Nanoparticles size (486.5 ± 26.4 nm) and (B) surface Zeta Potential distribution (-40.95 ± 2.66 mV) were obtained using dynamic light scattering ($n = 3$). (C) Representative scanning Electron Micrograph (SEM) image of PLG NPs used for antigen coupling. (D) Loading amount. After peptide coupling by different methods, the amount of peptide loaded on each platform was determined by CBQCA assay. Measurements were standardized to 1 mg of PLG NPs or 3.3×10^7 splenocytes ($n = 5$), as 3 mg of PLG NPs or 1×10^8 antigen-coupled splenocytes per dose were injected for subsequent in vivo experiments. (E) Loading efficiency. Calculated as the percentage of bound peptide following the conjugation/encapsulation reaction over the input peptide at the beginning of the conjugation/encapsulation reaction. For (A)–(C), data are representative of 3 independent experiments. For (D) and (E), data shown are average from 3 independent experiments. 158

Figure 6.2 The effect of peptide length on skin allograft survival. Indicated preparations of NPs (3mg/dose) or SPs (1×10^8/dose) were injected (i.v.) on day −7 and +1 to mice receiving tail to back bm12 to B6 skin transplantation on day 0. Skin grafts were monitored and rejection was determined when 80% of the graft area was necrotic. Statistical significance was determined by Log-rank (Mantel-Cox) tests. ***p < 0.001, ****p < 0.0001. 163

Figure 6.3 Biodistribution of NP-blank, NP-ECDI-P1, or bm12 ECDI-SP in the spleen 24 h post i.v. injection. (A) MHC I-A^b and Rhodamine/PKH67 double positive cells in the spleen of injected mice were gated out using the spleen from un-injected mice as a negative control (left dot plots). IA^{b+}Rhodamine/$PKH67^+$ cells were further analyzed for CD11c, CD8α, B220 and CD11b expressions (right dot plots). Plots shown are representative of 3 mice in each group. (B) Percentages of each splenic cell population uptaking NP-blank, NP-ECDI-P1 or bm12 ECDI-SP of total IA^{b+}Rhodamine/$PKH67^+$ cells. Statistical significance was determined by one-way ANOVA with Sidak's multiple comparisons test. *p < 0.05, **p < 0.01. Data shown were averaged from 3 mice in each group. 166

Figure 6.4 Graft-infiltrating $CD4^+CD44^+Foxp3^+$ and $CD8^+CD44^+IFN\text{-}\gamma^+$ cells in skin allografts from recipient mice treated with NP-blank, NP-ECDI-P1 or bm12 ECDI-SP. (A) Left bar graph: Percentage of graft-infiltrating $CD44^+Foxp3^+$ cells among graft-infiltrating $CD4^+$ cells; Right bar graph: Total number of $CD4^+CD44^+Foxp3^+$ cells in skin allografts. Representative contour plots show gating for $CD44^+Foxp3^+$ cells in skin allografts from recipients of each treatment group. (B) Left bar graph: Percentage of graft-infiltrating $CD44^+IFN\text{-}\gamma^+$ cells among graft-infiltrating $CD8^+$ cells; Right bar graph: Total number of $CD8^+$ $CD44^+IFN\text{-}\gamma^+$ cells in skin allografts. Representative contour plots show gating for $CD44^+IFN\text{-}\gamma^+$ cells in skin allografts from recipients of each treatment group. For (A) and (B), skin allografts were harvested and examined on day 8 post transplantation. Statistical significance was determined by one-way ANOVA with Sidak's multiple comparisons test. *p < 0.05, **p < 0.01. Data is representative or averaged from 3 mice per group. 168

Figure 6.5 In vitro bm12-specific CD4 T cell proliferation and cytokine production in response to stimulation by APCs pulsed with different bm12 antigen sources. (A) ABM $CD4^+$ T cell proliferation. ABM $CD4^+$ T cells were co-cultured with B6 BMDMs pulsed with various NP and SP formulations of P1 and P2 as the source of bm12 antigen. % proliferation of ABM $CD4^+$ T cells was determined by % of ABM $CD4^+$ T cells with VPD450 fluorescence lower than that of undivided ABM $CD4^+$ T cells. (B) Cytokine production from ABM $CD4^+$ T cells co-cultured with B6 BMDMs pulsed with NP-blank, NP-ECDI-P1 or bm12 ECDI-SP. IFN-γ, IL-12p70, IL-1β, and IL-5 levels were determined by Luminex liquichip microplate reader. For both (A) and (B), statistical significance was determined by one-way ANOVA with Sidak's multiple comparisons test or student's t-test. *p < 0.05, **p < 0.01, ***p < 0.001, ****p < 0.0001. Data is representative of n = 2 biological replicates per group. 170

Figure 6.6 The effect of peptide conjugation chemistry on skin allograft survival. (A) Indicated preparations of NPs (3mg/dose) were injected (i.v.) on day −7 and +1 to mice

receiving tail to back bm12 to B6 skin transplantation on day 0. Skin grafts were monitored and rejection was determined as in Fig. 2. Similarly, the bm12 ECDI-SP treated group served as a positive control whereas the NP-blank treated group served as a negative control. Statistical significance was determined by Log-rank (Mantel-Cox) tests. (B) ABM $CD4^+$ T cell proliferation. ABM $CD4^+$ T cells were co-cultured with B6 BMDMs pulsed with either NP-ECDI-P1 or NP-BMPH-P3 as the source of bm12 antigen. % proliferation of ABM $CD4^+$ T cells was similarly determined as in Fig. 5. Statistical significance was determined by one-way ANOVA with Sidak's multiple comparisons tests. Data is representative of n = 2 biological replicates per group. For both (A) and (B), *p < 0.05, ***p < 0.001, ****p < 0.0001, ns = no significance. 172

Figure 6.7 Surface conjugation or encapsulation of P1 peptide provides equivalent skin allograft survival. (A) Percent of peptide release over 196 h of NP-ECDI-P1 and NP-Encap-P1, as described in Materials and Methods. Note that the error bars are smaller than the size of symbols for the NP-Encap-P1 data points. (B) Confocal images of a single representative NP-ECDI-P1 particle and a single representative NP-Encap-P1 particle. Magnification: ×60. (C) Fluorescence intensity profiles calculated across the gray arrow in (B) of a single representative NP-ECDI-P1 particle and a single representative NP-Encap-P1 particle. (D) Indicated preparations of NPs (3mg/dose) were injected (i.v.) on day −7 and +1 to mice receiving tail to back bm12 to B6 skin transplantation on day 0. Skin graft monitoring, determination of rejection, positive and negative controls were similar to Fig. 2. Statistical significance was determined by Log-rank (Mantel-Cox) tests. (E) ABM $CD4^+$ T cell proliferation. ABM $CD4^+$ T cells were co-cultured with B6 BMDMs pulsed with either NP-ECDI-P1 or NP-Encap-P1 as the source of bm12 antigen. % proliferation of ABM $CD4^+$ T cells was similarly determined as in Fig. 5. Statistical significance was determined by one-way ANOVA with Sidak's multiple comparisons tests. Data is representative of n = 2 biological replicates per group. For both (D) and (E), ***p < 0.001, ****p < 0.0001, ns = no significance..... 174

Figure 6.8 The antigenic peptide P1 provides comparable skin allograft protection as donor cell lysate. (A) Indicated preparations of NPs (3mg/dose) or SPs (1×10^8/dose) were injected (i.v.) on day −7 and +1 to mice receiving tail to back bm12 to B6 skin transplantation on day 0. Skin grafts were monitored and rejection was determined as in Fig. 2. Statistical significance was determined by Log-rank (Mantel-Cox) tests. (B) ABM $CD4^+$ T cell proliferation. ABM $CD4^+$ T cells were co-cultured with B6 BMDMs pulsed with either NP-ECDI-lysate or SP-ECDI-lysate as the source of bm12 antigen. % proliferation of ABM $CD4^+$ T cells was similarly determined as in Fig. 5. Statistical significance was determined by one-way ANOVA with Sidak's multiple comparisons tests. Data is representative of n = 3 biological replicates per group. For (A) and (B), ns = no significance. 176

Figure 7.1 SA-FasL engineered islets establish allogeneic tolerance when transplanted on PLG scaffolds. (A) Schematic showing biotinylated islets functionalized with SA-FasL are loaded on microporous PLG scaffolds and implanted in the epididymal fat pad of mice. (B) Individual tracing of blood glucose levels for syngeneic islets modified

with SA-FasL and transplanted on scaffolds (SCF), with mice receiving a short course of rapamycin (n = 3, mean survival time > 100 days). (C) Kaplan Meier analysis of allogeneic BALB/c islets transplanted under the short cover of rapamycin on unmodified PLG scaffolds in C57BL/6 recipients. Conditions include SA-FasL-engineered islets on scaffolds with rapamycin (n = 5, mean survival time >200 days), naïve islets on scaffolds with rapamycin (n = 5, mean survival time = 23 ± 2.19 days). (D) Intraperitoneal glucose tolerance test of long-term islet grafts compared to naïve C57BL/6 mice after fasting for 6 h, followed by i. p. glucose injection. Blood glucose of mice was taken starting just before injection and at the indicated time points. (E) Area under curve for the intraperitoneal glucose tolerance test. The area for naïve mice compared to the transplanted mice is not significantly different (p = 0.16). (F–I) T cell proliferative response from recipients of long-term (>200 days) BALB/c SA-FasL-engineered islets mounted on unmodified PLG scaffolds plus rapamycin (n = 3) and naïve C57BL/6 as controls (n = 3). Responders were labeled with CFSE and used against BALB/c donor (F,H) and third party C3H (G,I) stimulators in a standard ex vivo mixed lymphocyte reaction. After 4 days of culture, cells were stained with antibodies against CD8 (F,G) and CD4 (H,I) molecules and incubated with 7AAD to gate out dead cells before flow cytometry analysis. (J) Representative dot plots of data presented in F, G, H and I. Bars represent mean and SEM. Asterisks represent level of significance (*p < 0.05, **p < 0.01) found by using a two-tailed Welch's t-test. 194

Figure 7.2 Characterization of biotin-PLG polymer. (A) Conjugation of NH_2-PEG_2-biotin to PLG via carbodiimide chemistry, resulting in biotin-PLG. (B) ^{1}H NMR in $(D_3C)_2SO$ of PLG (top), biotin linker (middle), and biotin-PLG (bottom)..... 196

Figure 7.3 Biotin-PLG particles can be efficiently conjugated with SA-FasL and induce apoptosis in mouse B lymphoma cell line. (A) Schematic of biotin-PLG particles being functionalized with SA-FasL. (B) The amount of fluorescently tagged SA bound to the particles was investigated by varying the protein concentration (0, 100, 200, 400, 800, and 40,000 ng SA/mL in 1 mL) incubated with 1 mg of biotin-PLG particles (“biotin particles”). As a control, 1 mg of unmodified PLG particles was incubated with the same SA concentrations (“blank particles”). After two spins and washes, particles were dissolved in DMSO and fluorescence was measured, n = 3. (C) The loading efficiency was calculated by dividing the bound SA by the incubated SA, n = 3. (D) Biotin-PLG particles functionalized with SA-FasL induce cell death in A20 cells. Particles were incubated with 400 ng/mL of SA-FasL in 1 mL with 1 mg of particles. After washing to remove unbound SA-FasL, particles were incubated with 1.5×10^5 A20 cells for 18 h and cell death was analyzed via propidium iodide stain and flow cytometry (n = 3). For comparison, soluble FasL was added to cells (0, 10 ng) and demonstrated the ability to induce cell death at low concentrations (n = 3). 197

Figure 7.4 Biotin-PLG scaffolds can be efficiently conjugated with SA-FasL and induce apoptosis in mouse B lymphoma cell line. (A) Schematic of biotin-PLG particles functionalization with SA-FasL. (B) The amount of fluorescently tagged SA bound to scaffolds was investigated by varying the protein concentration (0, 100, 200, 400,

and 800 ng SA/20 μL) incubated with 2.5 mg biotin-PLG scaffolds ("biotin"). As a control, unmodified PLG scaffolds were incubated with the same SA concentrations ("blank"). After two washes, scaffolds were dissolved in DMSO and fluorescence was measured, n = 3. (C) The loading efficiency was calculated by dividing the bound SA by the incubated SA, n = 3. (D) Scaffolds were incubated with SA-FasL (0, 40, 200, and 400 ng/20 μL). After washing to remove unbound SA-FasL, scaffolds were incubated with 1.5×10^5 A20 cells for 18 h. Apoptotic and dead cells were analyzed via propidium iodide and Annexin V staining and flow cytometry (n = 3). For comparison, 2.5 mg of soluble FasL was added to cells and induced apoptosis in the 98% of the cells (n = 3). (E) Scaffolds required a minimum loading of 200 ng FasL/mg scaffold to induce apoptosis in the majority of A20 cells..... 199

Figure 7.5 Islets on scaffolds conjugated with SA-FasL demonstrate robust long-term tolerance. (A) Survival of allogeneic BALB/c islets mounted on PLG scaffolds and transplanted in the epididymal fat pad of chemically diabetic C57BL/6 recipients. Groups included naïve islets mounted on SA-FasL-engineered PLG scaffolds plus rapamycin (n = 6, MST > 200 days, P = 0.0007 vs rapamycin alone), SA-FasL-engineered islets mounted on SA-FasL-engineered PLG scaffolds (n = 6, MST = 46 days, P = 0.0007 vs rapamycin alone), and naïve islets transplanted under a short cover of rapamycin (n = 5, MST = 23 ± 2.19 days). All mice received islets loaded on 2 PLG scaffolds. PLG scaffolds were engineered with 2.5 μg/scaffold, except 3 mice in the islet-FasL + PLG-SA-FasL that were transplanted with PLG scaffolds engineered with 0.5μg/scaffold and all 3 animals rejected their grafts. Rapamycin was given to the indicated groups through i. p. injection at 0.2 mg/kg daily for 15 days starting on the day of transplantation. Mice were monitored twice weekly for blood glucose levels. Those with >250 mg/dL for two consecutive readings 24 h apart were considered diabetic and rejecting the graft. Statistical analysis was performed using log-rank test, **P < 0.01, ***P < 0.001. (B) Blood glucose readings of two groups of mice from (A). (C) Intraperitoneal glucose tolerance test (IPGTT) of long-term islet grafts compared to naïve C57BL/6 mice after fasting for 6 h, followed by i. p. glucose injection. Blood glucose of mice was taken starting just before injection and at the indicated time points. (D) Area under the curve for (C). 201

Figure 8.1 IN gene expression changes enables scoring and segmenting of diseased and healthy during EAE onset. a) SJL mice were implanted with PCL scaffolds 14 days prior to adoptive transfer of T cells reactive to either $PLP_{139-151}$ (EAE) or $OVA_{323-339}$ (control). INs were subsequently removed at an asymptomatic (7 day - yellow) or symptomatic (9 day - green) time point for analysis via high-throughput qPCR (OpenArray). b) Clinical scores of the mice at each time point demonstrate that no mice displayed symptoms of EAE at day 7 post-implantation, but mice were symptomatic by day 9. c) Flow cytometry for immune cell surface markers demonstrates minor differences between OVA and PLP at day 9. Data are presented as mean + SEM. Statistical analysis performed by student's t-test, asterisk indicates change from control (*p=0.038). n=7 (PLP) or 8 (OVA) mice. d) Heatmap and hierarchical clustering of 21 identified genes of interest, expression levels standardized by gene (n=8 per condition, 4 at day 7, 4 at day 9). e) Radar plot demonstrates altered gene expression (as $\log_2$FC) for signature genes in pre-

symptomatic (yellow) and symptomatic (green) when compared to time-matched OVA controls (black), with a similar pattern at both time points. f) Plot of the bagged tree (BT) prediction score versus SVD indicates separation between groups. Black lines indicate 99.9% confidence intervals for pooled diseased or control mice. Filled ovals indicate mean (centroid) and standard error of the mean for each indicated group. Each point is from an individual mouse and increasing point size indicates sicker mice (as an average of the day of explant and day after). g) Heatmap and hierarchical clustering signature genes from blood (expression levels standardized by gene) indicate no clear clustering of controls from diseased samples, n=5 per condition. h) A radar plot of gene expression signature (as log_2FC) from blood during symptomatic onset clearly does not show the same patterns as that of the IN. Mouse cartoon from Servier image bank, https://servier.com/Powerpoint-image-bank. 210

Figure 8.2 Gene signature in IN effectively monitors disease dynamics and indicates relapse. For relapse studies, INs were implanted subcutaneously two weeks before disease induction by adoptive transfer. INs were isolated at day 21 (remission) and day 28 (relapse). Mice received a second adoptive transfer of T cells (either $PLP_{178-191}$ or SIINFEKL) on day 23 to induce relapse (indicated on graphs with black arrows). a-b) Radar plots demonstrate similar gene expression (as log_2FC) for signature genes in remission (purple) when compared to time-matched controls (black) (a), but altered expression in relapse (orange) (b). c) Plot of BT score versus SVD indicates no separation between healthy and remitting mice, but separation between relapse and healthy. Black lines indicate historic (from disease onset data) 99.9% confidence intervals for pooled diseased or control mice. Each point indicates a single mouse. d-f) SVD score ($F(3,19) = 5.391$, $p=0.0074$) (d), BT score ($F(3,19) = 9.421$, $p=0.0005$) (e), and a combined metric ($F(3,19) = 6.504$, $p=0.0033$) (f) plotted versus time (left y-axis, black lines) and corresponding clinical scores at each time point (right axis, red points) indicates only the remission t.p. (d21) is significantly different from peak disease (d9). Data are presented as mean ± SEM. A one-way ANOVA was used to compare scores over time for EAE mice. A Bonferroni-corrected post-hoc multiple comparisons test was used to compare each time point to symptomatic disease onset (d9). (n=9 OVA at d21, n=5 OVA at d28, n= 11 PLP at d21, n=4 PLP at d28)..... 215

Figure 8.3 Gene signatures indicate response to therapy and enable proactive treatment to prevent disease. To test the ability of the IN to indicate response to therapy, 2.5 mg PLG nanoparticles encapsulating either PLP or OVA peptides were administered I.V. two days after adoptive transfer and INs were isolated on day 9 (disease onset). a) Radar plot demonstrating similar gene expression (as log_2FC) for signature genes in EAE mice treated with PLP loaded particles (purple) when compared to time-matched controls treated with particles (grey), but altered expression in EAE mice treated with control (OVA) particles (orange). b) Plot of BT score versus SVD indicates no separation between healthy mice treated with control particles and EAE mice treated with PLP particles (responders to treatment), but a clear separation in EAE mice treated with OVA particles (nonresponders / control treatment). Black lines indicate historic (from disease onset data) 99.9% confidence intervals for pooled diseased or control mice. Each point indicates a single mouse. Another experiment was designed to test if early detection of disease by INs could enable

proactive treatment to prevent the development of EAE. Seven days post-transfer INs were explanted and mice proactively treated with either an I.V. injection of 2.5 mg PLG nanoparticles encapsulating $PLP_{139-151}$ or daily I.P. injections of 5 mg/kg dexamethasone. c) Mean clinical scores of the mice at each time point demonstrate that both pre-emptive treatments reduce disease severity when compared to an untreated control. A two-way ANOVA was used to compare scores ($F(2, 11) = 5.422$, $p=0.0230$). A Dunnett's multiple comparisons test was used to compare each treatment to the untreated control at each time point. (n=6 untreated and 4 treated, $^{**}p\leq0.0012$ and $^{***}p\leq0.0002$ on days 9-11). Pink arrows indicate dexamethasone administration and purple indicate particle administration. 216

Figure 8.4 Gene expression from entire OpenArray Panel. a) Heatmap and hierarchical clustering of gene expression from entire OpenArray panel (n=8 per condition, 4 at day 7, 4 at day 9). b) Volcano plot of OpenArray data. Black lines indicate a fold change of ±2 and red line indicates p = 0.05. In total, 130 genes are significantly differentially expressed at the INs between healthy and diseased mice. 227

Figure 8.5 Gene expression from OpenArray for 21 genes in gene signature. Log_2 FC is displayed in boxplots with $25\text{-}75^{th}$ percentiles and range of data for each group displayed (outliers indicated with red +). Black and white boxes demonstrate pooled OVA controls and diseased mice, while yellow and green boxes represent the log_2 (fold change) at days 7 and 9, respectively. Two-way ANOVA was used to compare pooled OVA controls vs diseased mice (# $p<0.05$). A Bonferroni-corrected post-hoc multiple comparisons test was used to compare diseased to time matched controls ($^{*}p<0.05$, $^{**}p<0.005$)..... 228

Figure 8.6 Development of SVD and BT model enable classification of mice as healthy or diseased. a) Gene expression data was used to train a bootstrap aggregated (bagged) decision tree ensemble to predict the probability that any given mouse was diseased ($F(1,12) = 26.84$, #p=0.0002) b) An unsupervised dimensionality reduction technique (singular value decomposition – SVD) was used to reduce the gene expression of the 21-gene signature to a score ($F(1,12) = 85.69$, # $p = 8.19e\text{-}07$). Two-way ANOVA was used to compare pooled OVA controls vs diseased mice. A Bonferroni-corrected post-hoc multiple comparisons test was used to compare diseased to time matched controls ($^{*}p<0.05$, $^{**}p<0.0005$). c) Three principle components of SVD plotted in a 3D scatter plot. The single SVD scores were computed by calculating the Euclidean distance from the OVA control centroid to any given point (each point represents an independent mouse)..... 229

Figure 8.7 INs isolated from healthy mice have similar scores to OVA controls. Plot of the bagged tree (BT) prediction score versus SVD in which pink points represent INs isolated from healthy mice (no adoptively transferred cells), black represent mice that received OVA adoptive transfers and yellow and green PLP adoptive transfers. Black lines indicate 99.9% confidence intervals for pooled diseased or control mice. Filled ovals indicate mean (centroid) and standard error of the mean for each indicated group. Clearly, the signature scores for healthy mice and OVA controls are similar..... 230

Figure 8.8 Gene expression analysis by qPCR confirms OpenArray findings. The same samples examined via OpenArray were analyzed in-house by qPCR in 384 well plates and signature scores plotted as bagged tree (BT) versus SVD. Black lines indicate 99.9% confidence intervals for pooled diseased or control mice. Filled ovals indicate mean (centroid) and standard error of the mean for each indicated group. Clearly, the results via qPCR indicate similar findings to OpenArray. 231

Figure 8.9 Evaluation of immune cells within INs. a) H&E stains indicate a normal FBR for a porous material in both OVA and PLP conditions demonstrating immune infiltrate, foreign body giant cell (FBGC) formation, and tissue ingrowth. b) Flow cytometry for immune cell surface markers demonstrates minor differences between OVA and PLP, but little change in the cell populations within the INs over time. Data are presented as mean + SEM. Statistical analysis performed by student's t-test at individual time points, asterisks indicate change from control (*$p<0.05$, **$p<0.01$). n=7-8 mice per time point. 232

Figure 8.10 Evaluation of T-cell subsets in adoptive transfer model of EAE. Flow cytometry at day 9 post-adoptive transfer demonstrates T-cell subsets present in IN, spinal cord, lymph nodes, and spleens. Data are presented as mean + SEM. Only Th1 (Il-17^{-}, IFN^{+}) cells in scaffolds and spinal cords were significantly increased at this time point. Statistical analysis performed by student's t-test, asterisks indicate change from control for that organ (*$p<0.05$), (n=8). 233

Figure 8.11 Gene expression from entire OpenArray Panel for immunized mice. a) Heatmap and hierarchical clustering of gene expression from entire OpenArray panel (n=8 immunized control [4 at day 7, 4 at day 13] and n= 8 diseased [at each time point]). b) Volcano plot of OpenArray data. Black lines indicate a fold change of ±2 and red line indicates $p = 0.05$. In total, 222 genes are significantly differentially expressed at the INs between healthy and diseased mice. 234

Figure 8.12 IN gene expression changes enables scoring and segmenting of diseased and healthy in an immunization model of EAE. a) Heatmap and hierarchical clustering of 25 identified genes of interest, expression levels standardized by gene (n=8 immunized control [4 at day 7, 4 at day 13] and n= 8 diseased [at each time point]). b) An unsupervised dimensionality reduction technique (singular value decomposition – SVD) was used to reduce the gene expression of the 25-gene signature to a score ($F(1,20) = 23.84$, # $p = 0.000090$). c) Gene expression data was used to train a bootstrap aggregated (bagged) decision tree ensemble to predict the probability that any given mouse was diseased ($F(1,20) = 104.70$, #$p=2.1e-9$). Two-way ANOVA was used to compare pooled OVA controls vs diseased mice. A Bonferroni-corrected post-hoc multiple comparisons test was used to compare diseased to time matched controls (*$p<0.05$, **$p<0.00005$). d) Plot of the bagged tree (BT) prediction score versus SVD indicates separation between groups. Black lines indicate 99.9% confidence intervals for pooled diseased or control mice. Filled ovals indicate mean (centroid) and standard error of the mean for each indicated group. 235

Figure 8.13 Evaluation of immune cell populations during an immunization model of EAE. Flow cytometry for immune cell surface markers demonstrates cell populations through time in IN, blood, and spleens. Data are presented as mean + SEM. Statistical analysis performed by student's t-test at individual time points, asterisks indicate change from control (*p<0.05, **p<0.005). INs at day 4 and 7: n=4 (Ctl), n=6 (EAE); at day 13: n=14 (Ctl), n=16 (EAE). Blood and spleens at day 4 and 7: n=2 (Ctl), n=3 (EAE); at day 13: n=7 (Ctl), n=8 (EAE). 236

Figure 8.14 Dynamics of EAE disease state are detectable in IN. a) SJL mice were implanted with PCL INs 14 days prior to adoptive transfer of T cells reactive to either $PLP_{139-151}$ (EAE) or $OVA_{323-339}$ (control). INs were subsequently removed at a remission (21 day - purple) or relapse (28 day - orange) time point for analysis via qPCR. A second adoptive transfer of cells reactive against another immunodominant epitope (to mimic epitope spreading in relapse) was performed on day 23 to induce relapse. b) Heatmap and hierarchical clustering of 21 identified genes of interest, expression levels standardized by gene. 237

Figure 8.15 IN enables treatment monitoring for nanoparticle induced tolerance. a) SJL mice were implanted with PCL INs 14 days prior to adoptive transfer of T cells reactive to either $PLP_{139-151}$ (EAE) or $OVA_{323-339}$ (control). Nanoparticle treatments were injected intravenously on day 2 and INs subsequently removed on day 9 for analysis via qPCR. Analysis of gene expression by the trained bagged tree ($F(2,15) = 34.2$, $p = 2.6e-06$) (b) and SVD ($F(2,15) = 15.96$, $p = 0.0002$) (c) demonstrated significantly higher scores for mice that received ineffective treatments (and developed symptoms of EAE). One-way ANOVA and a Bonferroni-corrected post-hoc multiple comparisons test was used to compare each group (**p<0.0005, different from both control and PLPp treated). d) Mean clinical scores of the mice at each time point demonstrate only the OVA loaded particle treatment demonstrating significantly increased scores from control. A Kruskal-Wallis test (Kruskal-Wallis statistic = 11.69, p=0.0002) was used to compare scores for EAE mice and a Dunn's multiple comparisons test was used to compare each group to the OVA control (**p = 0.0016). 238

Figure 8.16 INs indicate disease onset and enable pre-emptive treatment. INs were implanted subcutaneously two weeks before adoptive transfer to induce disease. Seven days post-transfer INs were explanted and gene expression analyzed to plot BT score versus SVD which indicated that mice were developing disease. This information was used to enable pre-emptive treatment with either an I.V. injection of 2.5 mg PLGA nanoparticles encapsulating $PLP_{139-151}$ or daily I.P. injections of 5 mg/kg dexamethasone. 239

Figure 8.17 ROC curves validate the signature scores from the IN as an effective diagnostic, prognostic, and treatment monitor. ROC curves were plotted for the disease onset data used to train the signature classification model (a), relapse and remission data (b), and particle treatments (c). In each case the area under each curve is > 0.8 indicating successful diagnostic efficacy. 239

Figure 8.18 Gating Scheme for innate immune panel. All samples were divided in half and half allocated to innate immune panel staining and half to adaptive. Cells were gated using forward scatter area and side scatter height before singlets were gated with forward scatter height and area. Within the singlet population CD45+, live cells (dead cell negative) stains were gated. At this point, CD11b and F480 were plotted to enable selection of CD11b+ F4/80+ cells and subsequent analysis. The CD11b+ gate was used to select Ly6C and Gr-1 to enable the selection of CD11b+ Gr-1+ Ly6C- cells. Then the F4/80 was plotted against Ly6C to enable selection of F4/80- Ly6C+ cells. Finally F4/80 was plotted with CD11c to enable selection of F4/80- CD11c+ cells. Arrows indicate flow of gating and red texts indicates final cell populations used for analysis. 240

Figure 8.19 Gating Scheme for adaptive immune panel. All samples were divided in half and half allocated to innate immune panel staining and half to adaptive. Cells were gated using forward scatter area and side scatter height before singlets were gated with forward scatter height and area. Within the singlet population CD45+, live cells (dead cell negative) stains were gated. At this point, CD4 and CD8 were plotted to enable selection of CD4+ or CD8+ cells. Next CD19 and CD49B were plotted to select the CD19+ and CD49b+ populations. Arrows indicate flow of gating and red texts indicates final cell populations used for analysis. 241

Figure 8.20 Gating scheme for Treg panel. All samples were divided in half and half allocated to Treg panel staining and half to Th panel. Cells were gated using forward scatter and side scatter height before singlets were gated with forward scatter height and area. Within the singlet population live cells (dead cell negative) stains were gated. At this point, CD3 positive cells were selected of which the CD4 positive subset were selected for further analysis. CD25+ T-cells were selected. Finally, CD127 and FoxP3 were plotted to select the CD127- and FoxP3+ population as regulatory T-cells. Arrows indicate flow of gating and red texts indicates final cell populations used for analysis. 241

Figure 8.21 Gating scheme for Th panel. All samples were divided in half and half allocated to Treg panel staining and half to Th panel. Cells were gated using forward scatter and side scatter height before singlets were gated with forward scatter height and area. Within the singlet population live cells (dead cell negative) stains were gated. At this point, CD3 positive cells were selected of which the CD4 positive subset were selected for further analysis. The CD4+ gate was used to select Il-4+ to enable the identification of Th2 cells. Finally, the CD4+ population was analyzed by plotting IFNγ stain against IL-17 to enable identification of other Th1/Th17 cell subsets. Arrows indicate flow of gating and red texts indicates final cell populations used for analysis. 242

Figure A.1 Properties and efficacy of PLG(MOG_{35-55}) treatment of PP EAE. Characterization of nanoparticle properties (A). 262

Figure A.2 Implantable scaffold gene expression changes enables scoring and segmenting of diseased and healthy during EAE onset. a) C57BL/6 mice were implanted with PCL

scaffolds 14 days prior to adoptive transfer of T cells reactive to either $MOG_{(35-55)}$ (EAE) or $OVA_{323-339}$ (control). INs were subsequently removed at early disease (7 day - yellow) or late (9 day - green) time point for analysis via high-throughput qPCR (OpenArray). b) Heatmap and hierarchical clustering of 20 identified genes of interest, expression levels standardized by gene. e) Plot of the bagged tree (BT) prediction score versus SVD indicates separation between groups. Black lines indicate 99.9% confidence intervals for pooled diseased or control mice. Filled ovals indicate mean (centroid) and standard error of the mean for each indicated group. Each point is from an individual mouse and increasing point size indicates sicker mice (as an average of the day of explant and day after). Mouse cartoon from Servier image bank, https://servier.com/Powerpoint-image-bank..... 263

Figure A.3 Treatment of PP EAE with PLG(MOG_{35-55}) provides clinical protection with disease associated with reduced cytokine secretion from plate splenic cells. a) C57BL/6 mice were implanted with PCL scaffolds 14 days prior to adoptive transfer of T cells reactive to either $MOG_{(35-55)}$ (EAE) or $OVA_{323-339}$ (control). INs were subsequently removed at various time points for analysis via Taqman PCR probes. b) Early administration of PLG(MOG_{35-55}) results in improved clinical outcomes. c) Spleens were harvested and plated in 96 well format for stimulation by exposure to $OVA_{323-339}$ or MOG_{35-55} prior to ELISA-based measurement of cytokine production. d) Spinal cords from mice were collected at the conclusion of the study, homogenized, and analyzed by ELISA for cytokine expression within tissue. Mouse cartoon from Servier image bank, https://servier.com/Powerpoint-image-bank. 264

Figure A.4 Mice were sensitized by i.p. administration of alum-adsorbed ovalbumin protein on days 0 and 14. Mice received early (Day 21 and 28) or late (Day 28 and 35) treatment with PLG(OVA) (A). Mice were challenged by 6 oral administrations of ovalbumin on days 42, 44, 46, 49, 51, and 53 and assessed for anaphylactic response. Diarrhea incidence (B) and protection from anaphylactic temperature drop (C) suggest a trend towards protection with early administration of PLG(OVA). 268

Abstract

A variety of immunological disorders are characterized by inappropriate responses to innocuous protein. This is particularly relevant in autoimmune disease, allergy, and transplant rejection. For these, the therapeutic options that exist are minimal or involve broadly immunosuppressive regimens which are often characterized by undesirable side effects. This dissertation highlights advances in the design of a biodegradable poly-lactide-co-glycolide (PLG) nanoparticle (NP) platform to provide antigen-specific tolerance in these disease models. Strategies to incorporate multiple antigens conjugated to bulk PLG were investigated in a murine model of multiple sclerosis with the observation that a minimum antigen loading of 8μg of antigen per mg of nanoparticle was sufficient to induce maximally observed efficacy. Importantly, this innovation enabled the controlled delivery of multiple antigens to simultaneously treat immunity to multiple antigens. Conjugation of Transforming Growth Factor Beta (TGF-ß) on the surface of these particles while retaining bioactivity represents an improvement to this strategy hypothesized to improve efficacy by promoting induction or expansion of regulatory T cells. Application in a murine model of multiple sclerosis demonstrated improved clinical outcomes with reduced doses, which may be critical to enable clinical translation. Insights gathered from development of these particles were critical to the design of experiments to test the hypothesis that the platform would be safe and effective in murine models of food allergy. Importantly, we demonstrate that it is possible to delivery peanut extract via nanoparticles intravenously without induction of anaphylactic response. Prophylactic and therapeutic administration of particles resulted in improved clinical outcomes and reduction

in Th2 markers, including IL-4, IL-5, and IL-13. Interestingly, administration of PLG NPs to deliver allergen did not induce skewing of immunological responses towards Th1/Th17, which is a common approach to treat allergy in pre-clinical models and certain clinical immunotherapy regimens. Studies in a murine model of allogeneic skin transplant rejection demonstrated that the method of incorporation of antigen into the PLG NP resulted in statistically significant delay in graft rejection. These studies also demonstrated shortcomings in the platform's ability to completely prevent rejection, which we hypothesize is the result of an inability to prevent direct rejection. Development of FasL-conjugated implantable polymeric discs supported the hypothesis that an immunologically privileged site on which to transplant islet cells can delay transplant rejection, which may represent an opportunity to supplement tolerogenic therapies like our PLG NPs. A similar polymeric, implantable technology was designed to enable analysis of the function of inflammatory immune cells, a novel finding which has provided a method to monitor disease progression and response to therapy in a murine model of multiple sclerosis. Collectively, this work has provided several novel strategies to improve polymeric nanoparticle therapies and an implantable, biodegradable platform that shows promise as a complementary diagnostic for therapies that impact immune function, including PLG NPs.

Chapter 1 Introduction: Nanotechnology and Biomaterials for Immune Modulation and Monitoring

Authors

Aaron H. Morris*, Kevin R. Hughes*, Lonnie D. Shea

*These authors contributed equally to this work

Preface

Nano-scale particles can be tuned to attenuate undesired immune responses without impacting healthy immune function. Delivery of antigen-loaded particle formulations has induced tolerance in models of autoimmunity, allergy, and organ transplantation. This thesis will provide an overview of recent advances related to their clinical translation and understanding of their mechanisms of action as well as an explanation of my contributions to the work presented in each chapter. In addition, an emerging opportunity for biomaterials as engineered immunological niches *in vivo* and the potential for analysis of these surrogate tissues to enable disease diagnosis, prognosis, and therapeutic monitoring will be discussed.

Background

The human immune system has evolved to exquisitely protect against an incredible variety of assaults. To accomplish this objective, specialized cell types defined by their form and function have developed to enable recognition and elimination of possible threats to the host organism. Immune responses and cells are often categorized as “innate” or “adaptive”. This thesis will use this convenient method of organization, yet please note that ongoing research repeatedly highlights the overlap between innate and adaptive immune responses and the difficulty to succinctly capture

the complexity of immunity [1, 2]. Although the ability of the immune system to identify and resolve threats is unmatched, many undesirable immune responses routinely occur, and strategies specific to the disease are needed.

While a great number of technologies can be classified as biomaterial or particulate approaches for immune modulation, we focus on polymeric technologies for which compelling evidence indicates that the delivery system plays a critical role in modulating immune function, as opposed to serving as a passive carrier for a potent pharmaceutical ingredient (e.g. chemotherapeutic). Nanoparticle technologies provide a unique ability to interface with a wide variety of immunological cells and systems to modulate immune function [3]. Much of their utility is related to the fact that an array of materials and chemistries are available and highly tunable, providing opportunities for modification of physical and immunological properties. Importantly, many polymeric nanoparticle materials have demonstrated acceptable biocompatibility and degradability, which has, in several cases, enabled translation [4, 5]. Many highly promising materials including liposomal and metallic technologies are under investigation, and excellent reviews are available [3, 6-9]. While there are many types of diseases and disorders that are characterized by an undesired aggressive immune response, many of the antigen-specific therapies under development target allergy, autoimmunity, and transplant rejection.

This thesis will focus on the recent application of nanoparticles (defined broadly within this thesis to include platforms where all dimensions are less than 1μm) to treat examples of undesired response to non-threatening peptides and proteins, including allergy, autoimmunity, and transplant rejection, with a discussion of nanoparticles that have reached human clinical trials (Figure 1). Given the relatively small number of technologies that have advanced beyond pre-clinical studies, our discussion will be expanded to include the liposomal and metallic platforms that have been

tested in humans. Finally, this thesis will discuss the need for improved methods to identify these undesired immune responses at early stages, monitor disease progression and the response to therapy.

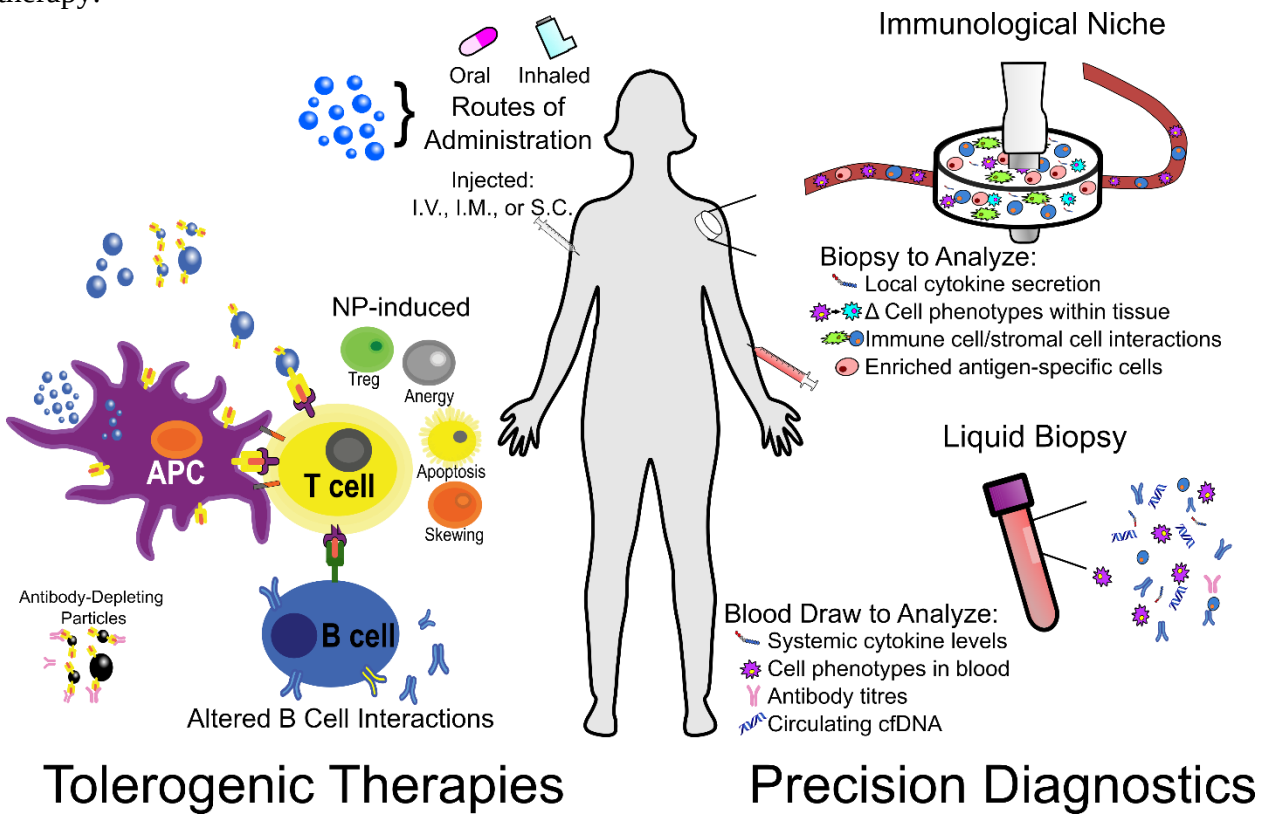


Figure 1.1 Overview of the intersection of tolerogenic therapies and precision diagnostics for monitoring patient health and response to therapies

Autoimmunity

Evolutionarily, the benefits of recognizing an incredible diversity of pathogens and toxins has resulted in immune systems with specificity for a large number of unique antigens. Both the "innate" and "adaptive" arms of the immune system possess this ability to identify foreign substances. As implied by the name, innate immunity is a naturally occurring defense system; it features genetic encoding for recognition of molecular features typically associated with toxin or infection (e.g. pathogen- or damage-associated molecular patterns). Innate immune responses are notoriously rapid due to the ability of large numbers of cells to respond vigorously upon recognition of what "appears" to be a signal of infection or toxicity. Adaptive immunity is typically

a much less rapid response to the first encounter of a new pathogen, as it involves a significant proliferation of a small subset of cells capable of recognizing the immunogenic structures. Adaptive immunity relies on specificity to certain molecular patterns with only one or a few of these patterns capable of inducing a measurable response for a particular cell. With this specificity, it is perhaps not surprising that, occasionally, a failure in the ability to discriminate between "self" and "non-self" results in an undesired amount of self-recognition and leads to negative outcomes. This undesired response is the case in autoimmune diseases, which are characterized by some degree of identification of "self" as foreign or dangerous [10]. It is estimated that there are 81 unique autoimmune diseases in humans, many of which are poorly understood [11]. Here, we will discuss recent developments in nanoparticle-based therapies for treatment of several of the more common autoimmune diseases, which are typically characterized by high incidence, impact on patient health, and cost to healthcare systems.

Standards of care for autoimmune disease vary wildly; however, they often involve some degree of broad immunosuppression [12]. Enumerating the consequences of non-specific immunosuppression remains an active area of study. Interestingly, broad ablation of B cell compartments through administration of anti-CD20 antibodies is relatively well-tolerated in adults other than in rare cases involving deadly risk of opportunistic infection [13, 14]. Other immunosuppressive regimens are considerably less-well-tolerated and are associated with increased risk of malignancy, opportunistic infection, leucopenia, and general toxicity [15]. These limitations highlight the need for the field to develop improved methods of antigen-specific therapies so that the underlying cause of the disease can be managed with reduced impact to normal immune function.

Nanoparticle-based therapies for treatment of autoimmunity has had several recent and exciting successes in pre-clinical and clinical development. Several trends are emerging, including that carrier systems in models of these diseases often behave as more than passive carriers of payloads. Recently, the effects of carrier properties on the ability to provide protection from autoimmune disease has been described [16]. Tuning of molecular weight and relative composition of lactide and glycolide units within poly(lactide-co-glycolide) nanoparticles significantly impacted the clinical scores and relative association of nanoparticle with liver-resident cells of mice with relapsing experimental autoimmune encephalomyelitis (EAE), a murine model of MS. The field is moving toward a more nuanced understanding of the variety of mechanisms contributing to the efficacy of these platforms, which often involve induction of anergy, expansion or induction of regulatory T cells (Tregs), apoptotic signaling, and promotion of regulatory APC phenotypes [4, 17-21].

Identifying disease-relevant epitopes is essential to enable the development of improved therapies. Some of this has been motivated by landmark trials using cell-based therapeutics which, while promising, often require considerable expense and complexity which will continue to limit their ability to translate [22, 23]. Identifying disease-inducing proteins and peptides will enable engineering of platforms to effectively target particular cell types and induce relevant signaling cascades for the development of cell-free therapies. Nevertheless, identifying these immunogens is likely to be challenging, as evidenced by the observation that certain autoimmune diseases involve epitope spreading following tissue damage, increasing the number of autologous proteins to which the body is reactive. Recently, groups have observed evidence of infectious tolerance with similar technologies, which, while still controversial, may provide a method to address issues of epitope spreading or poorly-defined antigens [19, 24]. Unlike in allergy and transplant rejection

where screening for antigen sensitization is relatively straightforward (via allergen testing or HLA-typing), identification of disease-relevant epitopes in autoimmune disease is more challenging. The process typically involves development of MHC tetramers which are specific to individual peptides, which are useful tools, yet a need to rapidly identify self-reactive T cells remains [25]. Despite these challenges, nanoparticle-based strategies are primed to achieve potent biological outcomes while providing shelf-life, tunability, and cost that make them more attractive than cell-based therapies.

Allergy

General allergy incidence is increasing rapidly in the global population and has a significant range in severity, and few methods exist to modify underlying allergic disease. Specific immunotherapy (SIT) is under clinical investigation by multiple routes of administration for various allergies. Oral immunotherapy (OIT) is currently FDA-approved for treatment of peanut allergy, while epicutaneous (EPIT), subcutaneous (SCIT), and sublingual (SLIT) immunotherapies are under investigation as promising methods of therapy for food or other allergies. Studies suggest that these therapies can temporarily desensitize patients, have been associated with a dampening of Th2 responses through the induction of regulatory and Th1 responses [26]. Unfortunately, administration of unmasked allergen to sensitized patients bears a risk for anaphylaxis [27], and patients with severe anaphylaxis are frequently excluded from participation in clinical trials [28]. Further, the existing SIT strategies induce skewing of responses or desensitization to allergen which do not reliably induce long-lasting immune tolerance [27, 29].

To alleviate the financial and societal impacts of allergy, a variety of biomaterial strategies are being developed. To date, these approaches are largely related to correcting the inappropriate recognition and response to allergens by inducing some degree of "desensitization", which enables

patients to better tolerate unavoidable exposure to allergen but does not provide a cure. Currently, many of the strategies learned from the field of vaccination are being applied to address allergy. These often involve the delivery of a nanoparticle system in the context of allergen to induce an immunological skewing from Th2 phenotypes to Th1 or 17 phenotypes through the use of mucosal vaccination. This type of desensitization also commonly induces production of allergen-specific immunoglobulins (generally immunoglobulin G, IgG) in pre-clinical models which is hypothesized to provide protection by occupying allergen binding sites that may otherwise be recognized by mast cell-bound IgE. Through this competition, degranulation is reduced and protection is afforded for as long as the allergen-specific IgG is present in sufficient quantity. A mounting body of evidence in humans demonstrates that high levels of IgG are associated with reduced risk for anaphylaxis and generally improved results. Ongoing studies will need to identify whether these therapies provide similar outcomes in human disease and whether there are unforeseen safety concerns associated with generating immunity to an antigen to compete with an allergic response to it.

Fewer groups are investigating methods to induce "tolerance" to allergen, which we will define as an unresponsiveness to allergen challenge without obvious skewing to cellular phenotypes associated with Th1/17 disease. These approaches are often referred to as "reverse", "inverse", or "tolerogenic" vaccines to differentiate them from more immunogenic strategies, although it is likely that ongoing studies may demonstrate that these strategies result in many overlapping biological outcomes [30]. The Miller and Shea lab collaboration recently demonstrated the ability to prevent or treat a Th2-mediated murine model of ovalbumin-induced airway inflammation without the delivery of active pharmaceutical ingredients [31]. In a similar model of airway inflammation, Liu *et al* demonstrated that PLGA delivery of ovalbumin was associated with TGF-

β, IL-4, and IL-10 production which was associated with increased targeting of the liver through decoration of particles with ApoB peptide [32].

The field of allergy is relatively young and ongoing clinical investigations are rapidly improving our understanding of the disease. The humoral response to allergen, while important in the generation of effector cells, is only a small part of the immunological makeup of allergy. Thus, targets for biomaterial-based interventions are becoming increasingly common and nanoparticle-based systems look promising. A recurring theme for this field is the need for improved ability to monitor the response to therapy to improve patient outcomes. This need is particularly relevant for allergy, as the existing methods to diagnose disease or efficacy of immunotherapy generally involve skin-prick testing or measurement of allergen-specific serum IgE. Both of these methods have high rates of false-positivity in allergy settings and are generally indicative of sensitization to an allergen which may or may not be associated with clinical symptoms of allergy [33]. A more reliable method to assess allergy or response to therapy involves a "challenge": intentional exposure to the allergen in a controlled setting. The costs and risk associated with this method are undesirable and alternative indicators of tolerance or sustained unresponsiveness are a major goal of the field.

Allergy provides a unique opportunity for nanoparticle-based antigen-specific therapies due to the ability to identify responsible epitopes using standard molecular biology techniques. This opportunity is not always the present in autoimmunity or transplant rejection where a baseline recognition of the autologous or allogeneic antigens is present. A critical step for the field will be the development of reliable strategies to identify and deliver these antigens through refinement of the extracts used to source epitopes. Unlike autoimmunity or transplant rejection, delivery of the offending antigen possesses significant risk in allergic individuals due to the inherent threat of

allergic response, regardless of route of administration. Interestingly, carrier properties may play a role in the risk associated with allergen delivery, as it was recently demonstrated that allergen-associated polystyrene, but not PLG, induced anaphylaxis in sensitized mice [31]. This has also been observed in multiple virus-like particle (VLP) formulations which are discussed elsewhere [34]. The field of biomaterials is well-positioned to lead the development of well-tolerated therapies for allergy through advanced application of concepts of controlled release, "stealthy" particle formulations, and strategies to control the tissue- and cellular-level distribution of therapies.

Transplant Rejection

The immunological pathways involved in rejection of allogeneic or xenogeneic transplants are complex and not completely understood. Elimination of cells or tissues from these sources would seem unlikely to occur before advances in modern medicine in the early 1900s. A commonly cited hypothesis for why transplant rejection occurs at such a high rate relates to the process by which central tolerance is achieved. During the development of central tolerance, only T cell repertoires that bind with intermediate strength to Major Histocompatibility Complexes (MHCs) displayed on antigen-presenting cells (APCs) are preserved. By selecting for these cells that have a baseline ability to recognize "self" MHCs (in humans, referred to as human leukocyte antigens, HLAs), similar (but not identical) MHCs present on donor cells may be statistically likely to produce undesired strong interactions and, consequentially, T cell priming. Efforts to put numbers to these mechanisms suggest that, whereas one in ten-thousand T cells in a person's body might recognize a particular antigen in the context of "self" MHC, between 1 and 10% of all T cells might bind to the 3-d structure presented by an allogeneic MHC, regardless of bound peptide[10, 35]. In addition to the complexity of T cell responses to transplantation, the involvement of innate and humoral

cells in the rejection process is increasingly being studied [36-38]. Regardless of the particular mechanisms involved, transplant rejection is a major challenge for modern medicine and several groups are investigating the use of biomaterials to address the issue.

Organ transplantation remains the preferred therapy for many end-stage diseases, and the demand for organ donation is high and significantly outpaces the supply of healthy donor tissues. Methods to induce allogeneic tolerance would theoretically increase the number of acceptable tissues for a particular recipient and, importantly, could delay or prevent the eventual rejection of the organ which would dictate transplantation of an additional organ. Induction of allogeneic tolerance is significantly complicated by the routes through which rejection can occur. Rejection generally occurs through multiple pathways which can simultaneously contribute to recognition. While a great variety of cell types are involved in transplant rejection, recognition of allografts by T cells is a critical step in allorejection. Recognition of allogeneic cells and tissues is typically thought to occur through some combination of direct, indirect, and semi-direct pathways. These pathways and their relative contributions to rejection are discussed extensively elsewhere [35, 39], but are summarized briefly in Table 1.

Table 1.1: Role of direct, indirect, and semi-direct recognition in allorejection

	Foreign molecule being recognized	**Cell displaying foreign molecule**	**Relative timing of rejection**
Direct	Intact donor MHC	Donor cell	Rapid
Semi-Direct	Intact donor MHC	Recipient APCs (via cross-dressing)	Poorly-defined. Expected to be rapid.
Indirect	Processed donor protein	Recipient APCs	Delayed; chronic

Strategies to address these pathways remain limited. Broadly immunosuppressive regimens have had considerable success in delaying the acute rejection often observed with direct recognition. However; even in severely immunosuppressed patients, long-term graft acceptance remains relatively unchanged relative to non-suppressed patients. This observation is thought to

be related to chronic recognition of minor mismatches (i.e. alterations of protein structure outside of MHC molecules) that, over time, can result in organ failure [39]. Broadly immunosuppressive regimens result in numerous complications which are reviewed more fully elsewhere [40].

Several groups have had success in pre-clinical models of transplantation by targeting the direct, semi-direct, and/or indirect pathways of allorecognition [41]. Nanoparticle-based strategies provide unique opportunities to control the cells and tissues targeted by these therapies, although several challenges exist. For example, strategies focusing on direct or semi-direct allorecognition likely require the display of intact MHC molecules to accomplish any degree of allospecificity. Many of the methods utilized to associate proteins with nanoparticles involve harsh solvents, irreversible conjugation, and general exposure to processing that may influence the 3-dimensional structure of components of the MHC. Nonetheless, multiple pre-clinical investigations have demonstrated the ability to incorporate proteins while retaining their bioactivity and highlight the promise of this approach. The Shen lab [42] recently demonstrated exciting results indicating that a relatively small number of intact MHC tethered to PLGA particles were able to delay skin graft rejection. Through incorporation of complex combinations of Fas, PD-L1, TGF-β, and CD47, the results demonstrate ability to modulate degree of apoptosis, T cell proliferation, particle retention time, and induction of Tregs, further highlighting the ability to tune particle function. Other groups have developed novel methods to incorporate intact membrane components from cells onto synthetic biomaterials, which is an attractive method to recapitulate powerful cellular signals [43, 44]. For example, Yeste, *et al* recently demonstrated the ability to promote Treg differentiation by nanoparticle delivery of a ligand of the aryl hydrocarbon receptor to improve the antigen-specific tolerance to proinsulin [45]. Relative to targeting direct and semi-direct pathways, delivery of proteins to influence indirect rejection is more easily accomplished with nanoparticle technologies.

Because this pathway requires uptake of protein by APCs, the natural tendency for nanoparticles to be phagocytosed allows for targeting of relevant cell populations with relatively low requirement to extensively modulate the biodistribution of the platforms [3, 46]. Further, once taken up by APCs, proteins delivered by these platforms are degraded for presentation on MHC and the preservation of 3-dimensional protein structure is not necessary as it is when targeting direct or semi-direct pathways of recognition. Several challenges remain, however. Control over the relative loading of MHC I (recognized by CD8 T cells) versus MHC II (recognized by CD4 T cells) is complicated by the differences in intracellular processing and cytosolic availability of nanoparticle-delivered proteins. The relative contributions of CD4 and CD8 T cell repertoires varies depending on a variety of factors and types of transplantation, but strategies to target both are desirable [45, 47]. Additionally, while groups have demonstrated that relatively small quantities of intact MHC are required to have profound biological effects, delivery of proteins to be processed and presented on APCs appears to be most effective when quantities are relatively large. A promising strategy to enhance efficacy within these models is the utilization of gene editing strategies. Zhang *et al* demonstrated the ability to significantly delay fully-mismatched skin graft rejection by delivery of Cas9 mRNA and CD40 gRNA with PEG block PLGA nanoparticles [48]. While this approach is likely to non-specifically disrupt CD40 signaling, future studies within the field will likely incorporate these methods with existing antigen-specific techniques.

Several goals related to the application of biomaterials to reduce transplant rejection have emerged. The ability to screen patients to identify the degree of HLA matching is critically important, but the relative success of immunosuppressants to prevent acute rejection of grafts currently makes it impractical to maximize HLA matching unless methods and policies to increase

the number of donor grafts become possible [39]. While strategies to target chronic rejection are of greater immediate clinical need, technologies that target the direct and semi-direct pathways of rejection will still provide considerable benefits to patients given the undesirable off-target effects of broadly immunosuppressive regimens [49]. Further, evidence indicates that the direct or semi-direct methods of recognition and severity of acute rejection may contribute to chronic rejection [35]. Among the advances related to targeting direct and semi-direct pathways, the increasing appreciation for the role of exosomes within a variety of disease states has contributed to exciting advances in generating synthetic or biomimetic particle platforms. These are expected to enable similar interaction with the direct and semi-direct pathways of allorecognition [41, 50, 51]. It is clear that improved methods to predict allorejection prior to or shortly after transplant are critical. This need is particularly true for chronic rejection, for which there are few treatment options. Predicting the impact that minor antigen mismatches on long-term survival of a graft for any given patient is challenging [39]. Nanoparticle-based therapies for the prevention of chronic rejection will require development of strategies to either identify patient-specific minor and major antigens responsible for chronic rejection or methods to deliver complex lysates and extracts that contain all likely antigens.

Clinical Trials of Tolerogenic Nanotherapies

Tolerogenic therapies have tremendous potential to revolutionize the treatment of undesired immune responses. Success inducing tolerance would mean an ablation of disease symptoms in patients and the ability to discontinue other therapies, many of which have deleterious side effects. Recently, concern has been expressed in the field of nanotherapeutics due to the relatively small percentage of technologies that have successfully translated to patients. Much of the field of nanotherapeutic drug delivery involves passive delivery of cancer therapeutics, which has proved

incredibly challenging to translate for several reasons that are summarized elsewhere [52]. Although tolerogenic nanotherapeutics similarly have an outsized number of preclinical investigations compared to success in humans, efforts to dampen immune responses using particle technologies are a more recent application of nanotechnology. Nanoparticles for tolerance in addition to targeting a more accessible and often readily-phagocytic cellular compartment, benefit significantly from the lessons learned from the translation of targeted cancer therapeutics. In light of recent successes in clinical trials detailed below, we anticipate nanotherapeutic strategies to treat diseases of immune dysfunction will emerge as a tremendous biotechnological success in the coming years.

As is the case for cancer treatments, the most common nanotherapeutics for tolerance are liposomal-based formulations, but metallic and polymeric nanotherapeutics are now in clinical trials as well. In this section, we briefly review the nanotherapeutics that have been tested or are currently in clinical trials for immunomodulation in autoimmunity, transplant, and allergy and discuss the platform technologies (Table 2). The next several years will likely transform how we care for chronic immune diseases and success with any one of these platforms may shape the field.

Liposomal

One study has examined the use of liposomal delivery of immunomodulators in allergy. Although not a tolerogenic therapy, liposomal delivery of cetirizine, an anti-histamine used to treat allergic rhinitis, has been tested in human subjects [53] (NCT00533637). In this study, liposomal delivery topically (by nasal inhalation) to the nasal passages was been compared to oral systemic delivery. The liposomal delivery had similar effects by most metrics, but outperformed oral delivery when measuring plasma exudation (quantified by α2-macroglobulin content in nasal gavage) in response to administered histamine.

Liposomal delivery of steroids has been tested in three clinical trials as a treatment for autoimmune diseases including multiple sclerosis and rheumatoid arthritis (NCT02048358, NCT00241982, NCT01039103). Nanocort, a liposomal prednisolone formulation, has been tested in human trials to treat rheumatoid arthritis, multiple sclerosis, and ulcerative colitis (NCT00241982, NCT01039103). Despite seemingly exciting results reported in conference abstracts, the authors of this chapter were not able to find any peer-reviewed publications concerning Nanocort's use in human clinical trials. In preclinical models, glutathione conjugated PEG liposomes containing methylprednisolone reduced symptoms of EAE compared to saline control, but free methylprednisolone had no effect [54]. Interestingly, glutathione conjugation to liposomes demonstrates dose-dependent endocytic uptake targeting brain tissue [55]. When the platform was tested in healthy human subjects, it resulted in prolonged delivery and a reduced lymphocyte count compared to free methylprednisolone [56]. Importantly, the formulation was determined to be safe, as only mild adverse events were reported.

Inhaled liposomal delivery of cyclosporine as an immunosuppressant to prevent bronchiolitis obliterans syndrome (BOS) after lung transplant or hematopoietic stem cell transplant is the subject of five clinical trials and basis for Breath Therapeutics (NCT03656926, NCT03657342, NCT01650545, NCT04039347, NCT04107675). The first exploratory trial examined 21 lung transplant patients with BOS, an inflammatory condition that results in obstruction of the bronchioles [57]. In the initial trial, patients treated with liposomal cyclosporine demonstrated stabilized sustained forced expiratory volume in 1 second compared to standard of care, and altered levels of cytokines as determined by bronchoalveolar lavage. Although, no significant change in BOS progression-free survival was observed, a trend toward substantial improvement was seen. This observation coupled with the significant differences in expiratory volume stabilization and

cytokine levels motivated the ongoing clinical trials with increased numbers of patients (NCT03657342, NCT01650545, NCT04039347, NCT04107675).

Table 1.2: Clinical trials harnessing nanotherapeutics to target immune dysfunction

	Company	Product Name	Platform	Diseases Targeted	Delivery Route	Trial Number
Liposomal	BBB Therapeutics	2B3-201	GSH-PEG liposomal methylprednisolone	Relapsing Remitting Multiple sclerosis (RRMS)	IV	NCT02048358
	Galapagos NV	Nanocort	PEG-liposomal prednisolone	RRMS, Rhematoid Arthritis, Ulcerative Colitis	IV	NCT01039103, NCT00241982
	Breath Therapeutics	L-CsA	Liposomal Cyclosporine A	Lung Transplant	Inhaled	NCT03656926, NCT03657342, NCT04039347, NCT04107675, NCT01650545
	Biolipox AB	NLA Nasal Spray	Liposomal Cetirizine dihydrochloride	Allergic Rhinitis	Inhaled	NCT00533637
Metallic	Cardiff University	C19-A3 GNP peptide	Proinsulin peptide conjugated to gold NP	Type 1 Diabetes	Intradermal injection	NCT02837094
	University of Zurich	-	HLA-coated magnetic nanoparticles	Kidney Transplant	*Ex Vivo*	NCT04277377
Polymeric	Selecta Biosciences	ImmTor	Rapamycin loaded PLG nanoparticles to induce tolerance to uricase	Gout	IV	NCT02648269, NCT02959918, NCT03905512
	Cour Pharmaceuticals	TIMP-GLIA	Gliadin-loaded immune modifying PLG nanoparticles	Celiac Disease	IV	NCT03486990, NCT03738475
	InnoUp Farma	INP20	Peanut protein loaded Poly(anhydride) nanoparticles for oral immunotherapy	Peanut Allergy	Oral	NCT04163562
VLPs	Cytos Biotechnology	CYT003-QbG10 / CYT005-AllQbG10	VLPs as an adjuvant for allergy vaccine	Dust mite allergy, allergic asthma, grass pollen allergy	Subcutaneous	NCT00652223, NCT00574223, NCT00575003, NCT00800332, NCT00574704, NCT00890734, NCT01673672, NCT02087644, NCT00293904

Virus-like Particles

Virus-like particles (VLPs), are created from recombinant viral capsid proteins and naturally self-assemble *in vitro.* These particles can easily be loaded with antigens and TLR agonists, and ultimately induce strong cellular and humoral immune responses [58]. These particles are rapidly produced using recombinant technology, and engineering alterations and scale production can be achieved quickly, which has made them an attractive vaccine platform. In the context of allergies, VLPs have been investigated as a tool to skew the immune system away from the Th2-type immune response classical for allergies and toward a Th1 response. This platform has been heavily investigated by Cytos Biotechnology (now Kuros Biosciences).

In the first human study for VLPs to treat allergies, a peptide from the dust mite allergen Der p 1 was conjugated to the backbone of a bacteriophage protein, Qβ [59]. This construct results in a VLP with the Der p 1 peptide displayed in a repeated fashion on the surface of the particle. When this VLP was administered to healthy subjects, a rapid, dose-dependent, IgG response was measured, but no IgE response suggesting that this immunomodulation may help treat allergies to dust mites. Follow up studies have used a similar Qβ VLP platform loaded with A-type CpG ODN, a TLR9 ligand, as an adjuvant to be co-delivered with dust mite antigen in a subcutaneous injection [60] (NCT00652223). This system was tested in patients with mild to moderate allergic asthma to dust mites and ultimately reduced allergy and asthmatic responses for 38 weeks post-treatment.

A follow-up study tested the same platform without co-administration of the allergen [61] (NCT00800332). With nearly 100 patients in each group, a dose-dependent reduction in allergy symptoms with the VLP vaccine was observed even without the administration of exogenous antigen, highlighting this strategy as a possibly broad approach to mitigating allergies. A follow-up clinical trial compared four groups of n=10 participants: VLP with antigen, VLP placebo with

antigen, VLP with antigen placebo, and placebo VLP with placebo antigen. The results of the trial have not been published in peer-reviewed publication, yet they are available online (NCT00574704). Although details are limited, each of the treatment groups produced the same median "Factor of increased allergen tolerance", and each outperformed the placebo group. Finally, in patients with allergic asthma, the same VLP platform with no antigen was able to significantly stabilize asthmatic responses compared to placebo [62] (NCT00890734). Two more clinical trials were underway for testing VLPs in asthma yet have been terminated or withdrawn (NCT01673672, NCT02087644).

Metallic

An ongoing clinical trial is harnessing gold nanoparticles coupled to a proinsulin-derived peptide for eventual tolerogenic therapies in type 1 diabetes (NCT02837094). This phase 1 uncontrolled trial is being performed to check for safety. This study is inspired by other clinical studies demonstrating safety and possibly slight improvements in patients with type 1 diabetes who received intradermal injections of the same peptide, proinsulin C19-A3 [63, 64]. The platform technology in the ongoing gold nanoparticle clinical trial involves the proinsulin peptide conjugated to 5 nm gold nanoparticles that are delivered intradermally by a microneedle device. This platform has been tested *ex vivo* on human skin and successfully delivered large numbers of particles to Langerhans cells [65]. A second clinical trial involving metallic nanoparticles to prevent transplant rejection has yet to enroll patients (NCT04277377). The aim of this project is intriguing as it aims to harness human leukocyte antigen (HLA)-coated magnetic nanoparticles to remove donor specific antibodies from blood and prevent antibody-mediated graft rejection. They plan to magnetically separate the particles *ex vivo* and thus remove the donor specific antibodies.

Polymeric

As described above, polymeric nanoparticles offer potential advantages for treating immune dysfunction *in vivo* and their recent transition to clinical trials appears promising. Currently three polymeric nanoparticle-based technologies are in clinical trials each for a different indication: i) peanut allergies, ii) anti-drug immunity, and iii) celiac disease. InnoUp Farma has an ongoing clinical trial (NCT04163562) examining orally administered nanoparticles containing peanut protein (INP20). Although the exact technology being tested in the trial is unclear, the principle investigator of the trial has been involved with research investigating polyanhydride nanoparticles encapsulating peanut antigen that have shown efficacy in several preclinical models [66-68]. The clinical trial is designed to first test a dose escalation study and then have a double-blind, placebo controlled, randomized study comparing two doses of particles and placebo in patients with peanut allergy.

Selecta Bioscience is leveraging a nanoparticle-based system to treat anti-drug immunity for treatment of gout. Recombinant uricases are used to reduce uric acid levels in chronic gout, but in many patients the formation of anti-drug antibodies may reduce treatment efficacy. Selecta discovered that PLGA nanoparticles releasing rapamycin when co-delivered with their proprietary pegylated uricase could induce tolerogenic responses to the drug and enable its long-term use [69, 70]. This drug platform has been tested in three clinical trials (NCT02648269, NCT02959918, NCT03905512). Although peer-reviewed publications have yet to be published, the data reported by Selecta suggest that they are able to avoid anti-drug antibodies and better control system uric acid levels with their nanotherapeutic platform. Although not yet in trials in humans, Selecta Bioscience has extended this platform technology to mitigating immune responses to the gene

therapy vector, adeno-associated virus (AAV) and successfully tested it in non-human primates [71]. This technology has been licensed to Spark Therapeutics for five genetic targets.

Cour Pharmaceuticals has harnessed an immune modifying PLG nanoparticle that, when loaded with antigen, is able to induce systemic tolerance. In their target indication, they use a gliadin loaded particle to induce tolerance in celiac disease. This platform has been tested in numerous preclinical models of autoimmunity, transplant rejection, and allergy [31, 72-76]. Importantly, a recent paper demonstrates that mice sensitized to gliadin exhibited unresponsiveness after being treated with TIMP-GLIA [77]. In the clinic, Cour has completed Phase 1 and 2 trials (NCT03486990, NCT03738475). Although peer-reviewed publications are not yet available, according to Cour's website, in Phase 2 trials patients treated with their platform showed decreased inflammation and a trend toward protection of their intestines after gluten exposure. As of October 2019, Cour has licensed the technology for celiac to Takeda for further development, yet has other indications in their internal pipeline.

A growing number of technology platforms are being tested in human clinical trials including liposomes, metallic nanoparticles, virus-like particles, and polymeric particles. With this array of technologies that function in different ways, there is optimism that multiple platforms will demonstrate safety and efficacy. Nevertheless, this field is nascent and the hurdles related to addressing immune dysfunction are numerous. Many trials underway are with conditions for which the immunogen is well-characterized and can be exogenously administered, such as celiac disease, peanut allergy, or anti-drug immunity. Development of translational nanotherapeutics focused on more heterogeneous diseases and antigens will be more challenging, yet are critical to address many forms of aberrant immunity. Strategies to both accelerate timelines and reduce costs associated with clinical trials of tolerogenic therapies will prove highly valuable.

Precision Diagnostics

As clinical trials of tolerogenic therapies progress, one key development will be the creation of precision diagnostics and monitoring tools for determining responses to therapy. Clinical trials can be lengthy and difficult due to challenges in disease monitoring, and novel methods to indicate disease progression or the lack thereof are critical [78]. Typically, clinical trials for inflammatory conditions measure some combination of outputs including: i) disease symptoms, ii) radiological analysis, iii) biopsy-based tissue analysis, and iv) blood-borne biomarkers.

Each metric for measuring treatment outcomes has distinct advantages and disadvantages. Effective biomarkers and diagnostics are measured by: i) analytical validity, ii) clinical validity, and iii) clinical utility. Monitoring disease symptoms provides a direct metric of clinical validity, but can be subjective and, depending on the disease, long periods of remission might complicate analysis. Radiology can provide a non-invasive quantification of inflammatory activity in many tissues, but lesions must be large enough to detect and key molecular information may be missed. Tissue biopsy is perhaps the best way to gain disease insight because it enables molecular dissection of inflamed tissue, but its invasiveness and the associated tissue damage limit the frequency of use. Finally, blood-based biomarker analysis is non-invasive and can be routine, but unfortunately has not demonstrated clinical utility for indications of aberrant immunity. The utility of blood for patient monitoring in tolerogenic therapies is hindered partly because disease-relevant cells are rarer and phenotypically dissimilar when comparing blood to tissue. Because disease-relevant cells are rare in the blood and often do not have phenotypes reflective of tissue-invading cells, the utility of blood for patient monitoring in tolerogenic therapies is limited. [79] Improvement in our ability to monitor disease in patients could lead to improved clinical trial pipelines that are segmented to the patients who are most likely to benefit. Furthermore, when

therapies make it to market, improved monitoring could enable a more personalized approach to therapy in which a patient is monitored for response to therapy such that treatment can be administered or altered based on the dynamics of the pathology rather than on a schedule. Here, we briefly discuss recent developments in approaches to diagnostics and treatment monitoring and the implications these approaches may have for tolerogenic therapies.

Liquid Biopsy

The field of cancer diagnostics and monitoring may provide a source of inspiration for therapeutic monitoring in diseases of immune dysfunction. Metastasis of cancer is what causes eventual morbidity, and unfortunately is difficult to detect due to the stochastic nature of metastatic lesion formation [80]. For monitoring cancer, many technologies are under investigation, including analysis of circulating tumor DNA or circulating tumor cells [81-83]. For a more in-depth discussion of next-generation cancer diagnostics please see [84]. Unfortunately, these strategies have limitations: in the context of breast cancer, a tumor large enough to be detected by mammography is unlikely to be detected by typical methods of circulating tumor DNA analysis [85]. Large organ transplants, on the other hand, may shed measurable levels of DNA for clinical utility. For example, CareDx has diagnostic panels for detecting cell-free donor DNA in kidney and heart transplant and has begun clinical trials into lung and pancreatic transplants (NCT04271267, NCT04318587, NCT04130685). Although, their clinical utility is somewhat limited as described above, screening for blood-borne antibodies to allergens or autoantigens is readily accessible.

Immunological Niches

Recent work in the space of cancer metastasis has demonstrated the possibility of harnessing implanted biomaterials to create synthetic immunological niches (INs) reflective of native tissues.

These INs reflect immune cell influx similar to native metastatic cites and ultimately induce cancer metastasis to a synthetic site prior to native organs [86, 87]. Architectural changes within the niche during cancer metastasis are measurable by non-invasive imaging approaches [88, 89]. Because the changes in immune infiltrate into the IN precede metastasis, a multivariate gene signature focused on immune cells within the niche enabled prediction of the likelihood of metastatic progression [90]. In addition to adequately staging early vs late disease, this approach is able to determine likelihood of response to surgical therapy. Further analysis via single-cell RNA-seq determined that the immune populations within the IN were generating immunosuppressive, pro-tumor environments. Ultimately, these synthetic immunological niches are useful for diagnosis and treatment monitoring in metastatic cancer, and reflect alterations associated with systemic disease dynamics. Moving forward, one could envision harnessing these immune-focused systemic disease monitors for monitoring a host of immune-associated pathologies.

A limited number of reports suggest that the idea of a biomaterial-based immunological niche would extend beyond the confines of cancer to autoimmune diseases. The first report examines antigen-loaded PLG scaffolds for recruitment of autoreactive T-cells [91]. First, the authors implanted scaffolds subcutaneously in mice loaded with ovalbumin and derivative peptides and determined that both ovalbumin-reactive CD4 and CD8 T-cells enriched at the scaffolds when their cognate antigen was present, compared to unloaded control scaffolds. Next, they demonstrated that scaffolds loaded with β-cell lysate enriched in autoreactive CD8 T-cells in diabetic mice and that these cells could induce diabetes when adoptively transferred into a healthy host. Interestingly, implantation of antigen-laden scaffolds resulted in no change in disease course in these mice, suggesting that proper engineering of an immunological niche can safely enrich disease-relevant cells at an easily accessible subcutaneous site in type 1 diabetes. A similar

approach employed localized delivery of GM-CSF and conjugation of $PLP_{139-151}$ to a porous collagen scaffold to reduce disease burden in the $PLP_{139-151}$ induced EAE model [92]. The authors similarly found increased cellularity in their antigen-conjugated scaffolds, but observed that the T-cells within spleens of these mice exhibited an exhausted phenotype. Together these studies suggest the ability to engineer immunological niches that enrich in particular antigen-reactive cell subsets and highlight that materials and model systems used can result in dramatically different effects.

Clearly, a precedent exists for the development of an engineered immunological niche for interrogating disease-relevant immune populations *in vivo*. These experimental technologies have proven successful in monitoring disease progression and response to therapy in metastatic cancer and may rapidly extend to other immune-mediated pathologies. Additionally, careful engineering of these sites can alter populations of cells present which could be harnessed for monitoring very specific, tolerogenic immunotherapies. We anticipate that, as this emerging area continues to develop, it will be indispensable in clinical trials to aid patient segmentation and monitor outcome measures as complementary or complementary diagnostic. If these novel monitoring platforms provide actionable information to clinicians, they will almost certainly be translated to monitor disease and treatment response in individual patients. Immunological niches will form an essential tool in the era of personalized medicine for diseases of immune aberration .

Outlook

Undesired immune response that lead to autoimmunity, allergies, and transplant rejection have been on the rise for the last 70 years [93]. Unfortunately, treatments available rely on broad immunosuppression with associated deleterious side effects or symptomatic mitigation. The development of tolerogenic therapies has long been a goal of the field, but has to date been elusive.

Biomaterials scientists and engineers have developed nanotherapeutic platforms that have demonstrated an impressive list of successes in preclinical models. Although none are clinically available, human trials have begun with a number of divergent platforms and, in the years to come, tolerogenic therapies have the potential to reshape the treatment of autoimmunity, allergies, and transplant rejection.

Thus far, clinical trials of antigen-specific nanotherapeutics for tolerance have largely focused on diseases which have well-defined immunogens. For example, Cour Pharmaceuticals is targeting celiac disease (antigen: gliadin) and Selecta Biosciences is targeting anti-drug immunity (antigen: exogenous uricase). For early trials, targeting conditions with well-defined antigens makes sense, yet as the technologies mature, technologies to rapidly identify responsible epitopes that underlie the disease are expected to emerge. One of two approaches will likely be necessary for many diseases: i) a personalized medicine approach to screen individual antigens for unique patient therapies or ii) therapies with such a low risk of adverse events that they can administer many, if not all of the identified antigens in the broader population. Ultimately, the early narrowly focused trials will provide both a proving ground for the technologies and a robust accumulation of knowledge that will inform the next generation of therapies.

In addition to novel therapeutic platforms, development of improved diagnostic capability will only grow in its importance for patient management, both for diagnosing diseases of immune dysfunction earlier and also for monitoring responses to therapy. Already, simple qPCR panels such as Oncotype DX have enabled more precise administration of therapy for cancer patients, and the technologies are rapidly improving. Patient monitoring tools for cancer have rapidly proliferated in recent years and more recently, have begun to be applied to diseases of immune dysfunction. Proof-of principle studies have demonstrated that with precisely engineered material

platforms, antigen specific cells can be enriched in isolated locations sufficiently to investigate them *ex vivo*. Moving forward, biomaterial platforms and engineered immunological niches may present new tools for monitoring patients, accelerating and improving clinical trials, and as a tool to help identify disease-relevant epitopes for novel therapeutics.

The increasing number of clinical trials of tolerogenic therapies are encouraging and we anticipate that successful strategies will be identified. To adequately address the increasing immune dysfunction in our populations will require refined strategies, and biomaterial-based systems provide a promising avenue for this development. Biomaterials designed to intricately interact with immune functions will prove essential in developing an arsenal of tolerogenic therapies and complementary diagnostics. The future of healthcare involves precision health and biomaterial systems that are exquisitely and precisely designed are well-positioned to provide the backbone for many of these strategies.

Biomaterial Interventions Discussed in This Thesis

This thesis focuses primarily on poly(lactide-co-glycolide) (PLG) NPs and PLG or poly(ε-caprolactone) (PCL) discs (scaffolds) and their application in disease models of autoimmunity, allergy, and transplant rejection.

This work was motivated by a need to refine methods of generating antigen-specific therapies like those developed by the Shea Lab and our many collaborators over the past decades. The labs of Miller (Northwestern University) and Luo (Northwestern and Duke Universities) have made tremendous advances related to cell-based delivery of antigen for induction of "tolerance" in vivo[94-98]. Their work has primarily utilized splenocytes rendered apoptotic by chemical crosslinking via carbodiimide chemistry. It was discovered that antigens (either natively present or otherwise) associated with these cells are tolerated in pre-clinical

models of autoimmunity, transplant rejection, and allergy following intravenous administration. In these models, the effects of this treatment are very robust, prompting investigation of the strategy in a Phase 1 clinical trial for patients with multiple sclerosis[23]. Despite the pre-clinical and clinical successes, the technology is hindered by the expense and complexity associated with sourcing and treatment of donor cells. To overcome some of these limitations, the Shea Lab has sought methods to generate synthetic antigen carriers that are capable of inducing similar effects *in vivo*. Currently, our platform typically consists of PLG NPs of various ratios of lactide and glycolide composition and multiple molecular weights. We have developed several strategies to incorporate antigen within or on these NPs depending on the desired properties of the particle, which is discussed thoroughly throughout this thesis. While the mechanistic similarities and differences between PLG NPs and apoptotic splenocytes are only partially understood, we have routinely demonstrated the ability to deliver relevant antigen to antigen presenting cells (primarily in the liver) which can then process the antigen and present it on major histocompatibility complexes (MHC) to impact T cell fate. Importantly, this platform has recently shown safety and efficacy in a Phase IIa clinical trial in patients with celiac disease and continues to be developed[99]. Based on the promising pre-clinical and clinical results, the Shea Lab is working very hard to improve the platform and investigate it within other models to acquire additional biological insights and to identify strategies that maximize the possibility that the technology can make broad clinical impacts. While certain underlying mechanism of various immunological disorders share similarities, the distinct mechanism of disease can vary wildly and investigation of the efficacy of our NP platform is necessary and important.

This thesis provides multiple novel contributions to the field. First, strategies to conjugate peptides and bioactive proteins to polymer systems were develop thoroughly. These were tested

in multiple disease models and showed efficacy in pre-clinical models of autoimmunity (Chapters 3, 4, and 8) and transplant rejection (Chapters 6 and 7). Second, this thesis demonstrates the ability to apply an existing NP technology for the treatment of food allergy and provides a preliminary determination of physicochemical thresholds required for safety of the therapy in murine models of food allergy (Chapter 5). Third, this thesis applies implantable polymeric scaffolds in murine models of autoimmunity and transplant rejection to complement or evaluate the effects therapeutic intervention (Chapters 7 and 8).

Contents

Chapter 1 introduces themes of this thesis and the content contained in each chapter.

Chapter 2 provides an overview of the methods available to engineer antigen-specific responses to correct aberrant immunity. Various trends associated with the development of the immune disorders of autoimmunity, allergy, and transplant rejection are introduced. Of particular interest for this thesis are the sections predominantly written by this author, which include the biological signals related to induction of natural tolerance, natural and synthetic immune privileged sites, and carrier-free therapeutics capable of antigen presenting cell (APC) reprogramming.

Chapter 3 represents a major contribution of this thesis to the field with the development of antigen-polymer conjugate nanoparticles. The technology developed in this chapter required extensive modification of existing methods to generate particles in order to provide a method to achieve controlled delivery of multiple antigens from a single NP. Previous technologies to incorporate more than one protein required extensive trial and error to identify NP formulations that would contain a desired quantity of particular antigens without sacrificing favorable physicochemical properties. Here, we conjugate peptides to PLG polymer prior to emulsion

synthesis. This strategy enables loading of targeted quantities of antigen within PLG NPs while minimizing the "burst release" of antigen observed in encapsulation-based loading methods upon reconstitution or intravenous injection. This is accomplished without significantly impacting the size, Zeta potential, or polydispersity of the NPs as is often the case when antigen is incorporated by surface conjugation. Importantly, this technology enabled the delivery of multiple antigens within a murine model of multiple sclerosis (MS) induced by two antigens. My most critical contributions to this chapter were the maximization of the reaction efficiency to enable significantly larger antigen loading, determination of co-solvent synthesis methods, and development of a nuclear magnetic resonance (NMR)-based method to non-destructively quantify antigen loading. The strategies developed in this chapter are built upon throughout this thesis.

Chapter 4 introduces a method to conjugate Transforming Growth Factor Beta (TGF-ß), a commonly used factor associated with reduced inflammation, to the surface of PLG NPs to enhance their efficacy. This chapter demonstrates that the antigen-conjugate NPs developed in Chapter 3 are amenable to modification with bioactive compounds. Therapeutic efficacy was achieved subcutaneously and with a significantly lower quantity of these particles in a murine model of multiple sclerosis. These are both major advancements for maximizing clinical translatability of the platform. My contributions to this chapter consisted of the development of the materials used throughout, methods of conjugation, and their application *in vivo*.

Chapter 5 demonstrates, for the first time, the ability to treat and prevent a murine model of food allergy with this PLG NP platform. Critically, this chapter demonstrates that allergen can be administered safely in PLG NPs, provides the field with a quantification of the amount of soluble or exposed antigen that can be delivered intravenously without generating anaphylaxis,

and provides to enable quantification of similar safety parameters in similar models. We demonstrate the ability to significantly reduce anaphylactic symptoms with minimal doses, which will be important for the refinement of the limited number of clinically-available therapeutic approaches to food allergy. In these studies, my intellectual contributions included experimental design, material synthesis and characterization, development of novel methods to assess NP safety, and generation of the manuscript.

Chapter 6 leverages the antigen-polymer conjugate nanoparticle technology to delay skin graft rejection in a transgenic murine model of transplantation. In this manuscript, peptides containing the mutations within the hypervariable region of MHC-II that result in recognition and rejection of skin allografts were delivered using a variety of NP formulations to delay rejection. Studies were conducted to determine the contribution of peptide length, method of antigen incorporation (i.e. antigen-polymer bioconjugation versus surface-conjugation), and method of conjugation to the efficacy of NP formulations. Interestingly, while the specific peptide that was utilized made a considerable difference, neither method of antigen incorporation or type of conjugation chemistry had a particularly large effect on the length of time that rejection was delayed. Further, it was found that apoptotic splenocytes from donor mice significantly outperformed the most effective NP formulation as well as apoptotic splenocytes from *recipient* mice that delivered the relevant peptides. These results suggest that intact donor MHC may be particularly important in the allogen-specific protection afforded by apoptotic splenocytes. Throughout these studies, I contributed the experimental design, material design, synthesis, and characterization, and interpretation of *in vitro* and *in vivo* results.

Chapter 7 introduces implantable polymeric scaffolds in a transplantation setting. Transplantation of islets to treat models of Type 1 Diabetes (T1D) is a common approach. This

manuscript investigated the incorporation of FasL on these scaffolds to generate an immunoprivileged site on which transplanted islets would receive additional protection from the host immune system. These studies demonstrated ability to incorporate bioactive FasL in an implantable system and improved islet function after transplantation on the construct. My contribution to this project were in generation of methods for bioconjugation of FasL on PLG polymer as well as final intellectual edits on the manuscript.

Chapter 8 builds on lessons learned from Chapter 7 and additional studies conducted in the Shea lab related to implantation of polymeric scaffolds for early diagnosis of disesae. While pharmaceutical interventions like the PLG NPs may provide an improvement for patients of autoimmune disease, development of technologies that diagnose disease at early timepoints are expected to improve patient outcomes significantly. Additionally, complementary diagnostics that can detect response to therapy are highly desirable to distinguish between patients that are responding well and those that will require further intervention. This manuscript interrogates the foreign body response to an implantable PCL scaffold in relapsing remitting experimental autoimmune encephalomyelitis (RR EAE), a murine model of the most common form of human MS, to predict disease onset, track progression, and monitor response to therapeutic intervention. Importantly, analysis of scaffolds enabled generation of a disease "score", which correlates strongly with established metrics of clinical disease and allowed for therapeutic intervention with PLG NPs. Throughout these studies, I contributed experimental design, material design, synthesis, and characterization, and *in vivo* experimentation.

Chapter 9 provides an overview of the results from this thesis and their contribution to the field. Considerable time is spent discussing future directions of the work, including

consideration of the hurdles remaining for clinical translation of PLG NPs and implantable scaffolds.

Acknowledgements

Portions of this work are under review for publishing: A.H. Morris*, K.R. Hughes*, L.D. Shea, Nanotechnology and Biomaterials for Immune Modulation and Monitoring, Elsevier, Immunomodulatory Biomaterials (anticipated 2020). We would like to thank Dr. Liam Casey for insightful discussions as related to this manuscript. We would like to thank the UM Precision Health Scholars grant for funding this work. This work was supported in part by NIH grant R01AI148076. A.H.M. is supported by a Michigan Life Science Fellows award and a NIH T32 grant DE007057-43 and would like to thank both of these funders for their support.

Chapter 2 In Vivo Rreprogramming of Immune Cells: Technologies for Induction of Antigen-Specific Tolerance

Authors

Ryan M. Pearson, Liam M. Casey, Kevin R. Hughes, Stephen D. Miller, Lonnie D. Shea

Abstract

Technologies that induce antigen-specific immune tolerance by mimicking naturally occurring mechanisms have the potential to revolutionize the treatment of many immune-mediated pathologies such as autoimmunity, allograft rejection, and allergy. The immune system intrinsically has central and peripheral tolerance pathways for eliminating or modulating antigen-specific responses, which are being exploited through emerging technologies. Antigen-specific tolerogenic responses have been achieved through the functional reprogramming of antigen-presenting cells or lymphocytes. Alternatively, immune privileged sites have been mimicked using biomaterial scaffolds to locally suppress immune responses and promote long-term allograft survival. This review describes natural mechanisms of peripheral tolerance induction and the various technologies being developed to achieve antigen-specific immune tolerance in vivo. As currently approved therapies are non-specific and carry significant associated risks, these therapies offer significant progress towards replacing systemic immune suppression with antigen-specific therapies to curb aberrant immune responses.

Introduction

Induction of antigen (Ag)-specific immune tolerance is a complex process that requires the collaboration of multiple immunological pathways. Aberrant activation of T cells *in vivo* results

in cellular damage against specific tissues and is responsible for the development of autoimmune diseases. To minimize the occurrence of undesirable immune responses to self-Ags, most self-reactive lymphocytes are eliminated in the thymus and bone marrow by a mechanism known as central tolerance. Unfortunately, this process is only 60-75% effective and potentially harmful Ag-specific cells with possible effector activity are released into the blood and tissues [100, 101]. To suppress potentially autoreactive cells that have avoided elimination by central tolerance, peripheral tolerance mechanisms exist. Intrinsic peripheral tolerance mechanisms are sometimes insufficient to curb inappropriate immune activation, necessitating therapeutic intervention to enable the body to limit responses to "self." Common therapies used to subdue abnormal immune activation are not Ag-specific and involve systemic immune suppression or immunodepletion therapies that target the T cell receptor (TCR), co-signaling molecules, cytokines, or inhibit leukocyte trafficking, among other mechanisms [102, 103]. However, administration of these non-specific treatments over a prolonged period of time is associated with numerous adverse effects, including increased patient susceptibility to opportunistic infections [104], viral reactivation [105], and neoplasia [106].

Ag-specific tolerance approaches are needed to restore immune homeostasis in the cases of autoimmune disease, as indicated above, and can be extended to establish selective Ag tolerance in the cases of allogeneic transplant and allergy. In Ag-specific tolerance, undesired immune activation is suppressed while the activity of the remaining immune system is maintained. Thus, the desirability of therapies to address these conditions has gained significant traction over several decades as the incidence of immune-mediated diseases has steadily risen [93, 107]. T cell-mediated autoimmune diseases are driven by the continued presentation of self-Ag by Ag-presenting cells (APCs) to autoreactive T cells. Conversely, allograft rejection involves a

combination of allorecognition by T cells and alloantibody production by B cells [108]. Allergic reactions involve the activation of granulocytes such as mast cells, basophils, and eosinophils by allergen binding to antibodies [109]. Important immune elements of these diseases are the development of Ag-specific effector T-helper type 1 (Th1) and Th17, or Th2 responses that are associated with the clinical features of disease progression [110]. The acquired phenotype of a T cell that differentiates from a naïve T cell is determined by its type of interaction with an APC as well as other factors that include the microenvironment, co-signaling molecule expression, type and load of Ag, and the intramolecular signals transduced [110]. A thorough discussion of the molecular mechanisms of these conditions is beyond the scope of this review and readers are directed towards several excellent reviews [108, 111-116].

Peripheral tolerance can be induced *in vivo* using a variety of technologies (Figure 2.1). For Ag-specific tolerance, the Ag is presented by APCs in the presence of low levels of co-stimulatory molecule expression and in the absence of other activating stimuli (i.e. absence of inflammation, infectious agents, and other pathologies) [102, 117]. These specific interactions aid in driving Ag-specific effector T cells towards an unreactive state (anergy or deletion) or induce regulatory T cells (Tregs) that can modify the activity of other T cells [103]. To drive immune responses towards tolerance, the Ag must be delivered to the appropriate cell types and initiate a cascade of tolerogenic signaling pathways. Other technologies, such as biomaterial scaffolds, mimic immune privileged sites in the body and can bolster tolerogenic responses through modulation of the local microenvironment. In this review, we will briefly introduce natural mechanisms of peripheral tolerance that will serve as a backdrop for an in-depth discussion of the state-of-the-art technologies available to reprogram immune cells to induce Ag-specific immune tolerance. Systematically, we will discuss technologies that promote tolerogenic responses by acting on

APCs, lymphocytes, and by the creation of immune privileged sites using examples for the treatment of autoimmune disease, allograft transplantation, and allergy as each of these therapies has unique immunological characteristics that motivate/influence the design of new technologies.

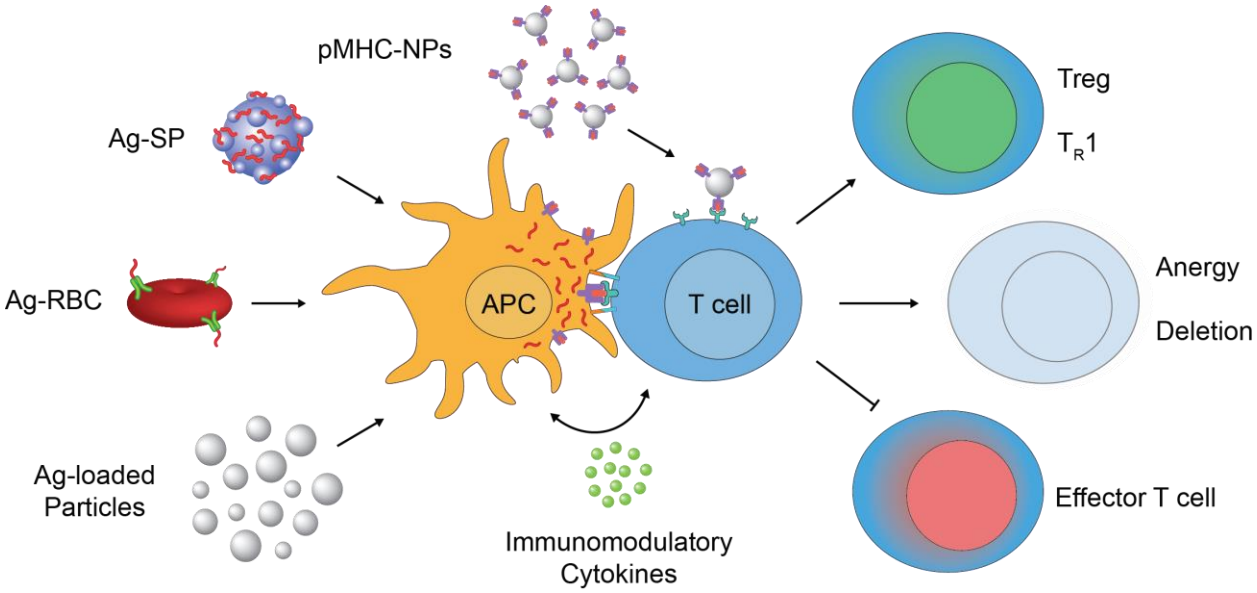


Figure 2.1: Highlighted approaches of technologies implemented for antigen-specific tolerance induction. Most antigen-specific tolerance strategies result in reprogramming lymphocytes through antigen presenting cells (APCs), however, there are platforms that target T cells and specifically recognize their autoreactive T cell receptors. Inspired by the natural clearance of apoptotic cells which results in peripheral tolerance maintenance, antigen has been delivered by various platforms including antigen-coupled splenocytes (Ag-SP), erythrocyte-targeted peptides (Ag-RBC), and antigen-loaded synthetic particles. These carriers are internalized, processed by APCs, and induce tolerogenic costimulation and soluble signaling pathways that direct T cell phenotypes away from immunogenic effector T cell activation and toward regulatory T cells (Tregs), anergy, or deletion. Direct interaction of particle-bound peptide-major histocompatibility complexes (pMHC-NPs) with antigen-experienced T cells can induce a tolerogenic regulatory-like TR1 phenotype that can mitigate immune-mediated disease progression.

Peripheral tolerance mechanisms

The development of T cell tolerance to self-Ags begins in the thymus and is refined in the periphery. As mentioned earlier, negative selection is not completely effective and autoreactive T cells that escape to the periphery are potentially harmful since they may provoke immune responses towards common Ags such as those in food or organ tissues [118]. T cells evade negative selection through multiple mechanisms that include low TCR avidity, TCR crossreactivity, and incomplete self-Ag representation by thymocytes [119]. When autoreactive T cells reach the periphery, their activity is modulated by anergy and deletion mechanisms.

However, if either of these mechanisms fails, T cells can become activated due to the presence of activating stimuli such as inflammation, infection, or other pathologies that lead to the enhanced expression of co-signaling molecules that aid in the development of effector T cell responses. This autoreactivity can propagate the development of autoimmunity, however, the body has acquired mechanisms to restrain self-Ag-reactive T cells.

Activation of naïve T helper (Th) cells has been generally assumed to be the result of 2 signals: (1) TCR stimulation (signal 1) and (2) co-signaling molecules (signal 2). However, data that has been recently accumulated provided evidence for a 3 signal model for T cell activation, where signal 3 is provided by inflammatory cytokines such as interferon-gamma and interleukin-12 [120]. To enable TCR stimulation, proteolytically processed antigenic peptides are presented on the surface of APCs on major histocompatibility (MHC) complexes and recognized by cognate TCRs on T cells [102, 116]. A diverse repertoire of co-signaling molecules exists that function as either co-stimulatory or co-inhibitory receptors that influence the outcome of TCR signaling [121, 122]. The effects of co-signaling molecules are Ag-independent and act to modify signal 1. T cell co-signaling pathways have diverse immune regulation functions that can control effector, memory, and Treg functions [123]. Furthermore, the presence of inflammatory cytokines in the microenvironment aid in Th1 polarization. This complex interplay between co-stimulatory molecules, co-inhibitory molecules, and cytokines directs downstream immunity or tolerogenic signaling pathways and is critical to understand the type and strength of immune responses generated. These findings have given rise to the concept of the tidal model of co-signaling, where changing environmental conditions can lead to dynamic cell-surface interactions and intracellular signaling [121]. Self-tolerance and immune homeostasis are naturally maintained as self-Ags are presented to T cells in the absence of inflammation through steady-state processes

such as clearance of apoptotic cells, exosomes, and by other cell death mechanisms involved in peripheral T cell tolerance.

Apoptotic cells

The clearance of apoptotic cells is a natural process that acts to maintain homeostasis and promotes the maintenance of peripheral tolerance through non-inflammatory pathways. This is unlike another cell death process, pyroptosis, which results in the activation and release of pro-inflammatory cytokines such as IL-1ß and IL-18 that may hinder tolerance induction [124, 125]. For apoptosis, a combination of signals regulate dead cell clearance (efferocytosis) and aids to ensure that immunity is not generated towards self-Ags [126]. Dysfunction of these natural clearance mechanisms has been shown to result in autoimmunity [127]. When a cell dies, phosphatidylserine normally present on the inner leaflet of the plasma membrane is externalized and serves as an apoptosis indicator [128, 129]. In one pathway, the interaction of apoptotic membrane-associated ligands (Growth arrest specific-6 and Protein S) with Tyro-3, Axl, and Mer (TAM) receptor kinases on dendritic cells (DCs) interferes with Toll-like Receptor (TLR) signaling and prevents DC maturation [130]. Evidence supports that the TAM family interactions affect other phagocytic pathways which do not necessarily depend on phosphatidylserine binding. Integrin-based systems and scavenger receptors, for example, are implicated in TAM interaction and have been targeted by tolerogenic technologies but may not necessarily involve phosphatidylserine [131].

An important co-stimulatory pathway involved in apoptosis and maintenance of peripheral tolerance involves the programmed death-1 (PD-1) receptor and the corresponding ligands PD-L1 (known also as B7-H1 or CD274) and PD-L2 (known also as B7-DC or CD273) [132]. PD-1 is part of the cluster of differentiation 28 (CD28)/cytotoxic T-lymphocyte-associated protein 4

(CTLA-4) superfamily and is expressed on a variety of cells, including T cells, B cells, monocytes, natural killer cells, and myeloid cells. PD-L1 is commonly expressed on non-activated T cells, B cells, dendritic cells, and macrophages while PD-L2 is primarily expressed by macrophages and dendritic cells [133]. The PD-1:PD-L1/2 pathway has been implicated in immune suppression in models of autoimmunity, transplantation, and allergy through a variety of mechanisms, including promotion of T cell apoptosis [132]. The complex mechanisms of PD-1-dependent immune suppression are discussed more fully in other reviews, but binding of PD-1 by PD-L1/2 typically results in cross-linkage between PD-1 and the TCR, leading to tyrosine phosphorylation of the tyrosine-based inhibitory or switch motifs (ITIM and ITSM, respectively) of PD-1 [134, 135]. The binding of Sarcoma Homology 2 domain Phosphatase 1 or 2 (SHP-1 or SHP-2) to these phosphorylated regions limits activation of the phosphoinositide 3-kinase/protein kinase B (PI3K/Akt) pathway by dephosphorylation of relevant signaling molecules, eventually resulting in increased apoptosis, decreased cell proliferation, and decreased IL-2 production, among other suppressive outcomes [134, 135].

Naturally occurring exosomes

Exosomes are 30-100 nm cell-derived extracellular vesicles that are produced during intraluminal vesicle formation of endosomal membranes [136, 137]. The mechanism of exosome formation is not entirely clear, yet likely involves the endosomal sorting complex or ceramide-dependent lipid raft formation [138]. Exosomes are frequent carriers of micro/messenger RNA (mi/mRNA), proteins/lipids, and other cellular material. Evidence suggests that Tregs can also produce exosomes and frequently utilize this mechanism of gene transfer to direct T cells towards tolerogenic phenotypes [139]. Additionally, recent studies support that Treg exosomes may target and influence cells other than T cells towards stable tolerance induction through a

variety of pathways, including antibody inhibition, cytokine modulation, or presentation of exosome-delivered Ags [138, 140].

Non-specific deletion

In peripheral tolerance, T cell deletion occurs through apoptotic cell death via apoptosis stimulating fragment (Fas)- and Bcl-2-interacting mediator of cell death (Bim)-regulated pathways. T cells express Fas (CD95) and, following Ag and IL-2 signaling, FasL (CD178). Activation of Fas by FasL or certain antibodies initiates activation-induced cell death (AICD), involving the formation of the death-inducing signaling complex (DISC) and downstream activation of apoptotic caspases. Alternatively, Bim may act as antagonist survival protein Bcl-2 to induce apoptosis through mitochondrial membrane permeabilization [118].

APC Reprogramming

APCs are skilled phagocytes that are well-adapted to process and present Ag derived from native and foreign sources. This makes them a natural target for immunotherapies. APCs efficiently scavenge and traffic to T cell compartments, so carrier-based tolerance strategies rely less on targeted delivery, and more on Ag (signal 1) and co-signaling (signal 2), and cytokine (signal 3) modulation. This section discusses strategies for the delivery of Ag to APCs to promote tolerogenic phenotypes in the context of autoimmunity, allograft transplantation, and allergy.

Cell-based therapeutics

Cell-based technologies have been developed to induce Ag-specific tolerance by exploiting naturally-occurring peripheral tolerance processes responsible for maintaining immune system homeostasis. Skewing APCs toward tolerogenic phenotypes *ex vivo* has demonstrated Ag-specific tolerance and has been extensively reviewed elsewhere [141-143]. Using cells as

tolerogenic agents typically utilizes *ex vivo* biochemical modification, however *in situ* modification has been successfully demonstrated [144-146]. Cell-based carriers have the advantage of closely recapitulating the body's natural clearance mechanisms such as apoptotic cell clearance resulting in secretion of inhibitory cytokines, increased expression of co-inhibitory molecules, and expansion of Ag-specific Tregs [147]. However, *ex vivo* manipulation of autologous patient or donor cells requires extreme care and must be conducted using good laboratory practices [148, 149]. The high costs and standards for procedural care may limit the translational potential for cell-based therapies that require *ex vivo* handling. Cell-based therapies that utilize *in situ* targeting strategies (e.g. Ag targeting to red blood cells) represent an "off-the-shelf" option for harnessing autologous cells destined for clearance by APCs [150]. Together, technologies that recapitulate the natural clearance of apoptotic cells represent promising cell-based strategies for inducing Ag-specific tolerance.

Particle-based therapeutics

Nanotechnology has demonstrated great potential to revolutionize the treatment of disorders with an underlying immunological pathogenesis. Nano/microparticles comprised of safe and widely-available biocompatible materials have gained traction as relevant surrogates for cell-based carriers to induce Ag-specific tolerance [151]. Synthetic materials offer the ability to achieve fine control over the structure, surface properties, and various interactions between particles and biological systems (i.e. nanobio interactions) [152], that is not always possible using cell-based platforms. Modulation of various physicochemical properties such as composition, size, and surface charge can direct biological responses [98, 151, 153-155].

Tolerogenic responses have been achieved *in vivo* using Ag-associated particles or particles engineered to deliver non-specific immune modulators such as small molecule immune

suppressants, anti-sense oligonucleotides, short-interfering RNA, and others [156-159]. The carrier itself has also been shown to modulate immune responses for some applications [160]. Particles are combined with disease-relevant peptides or proteins, either through surface-coupling or encapsulation-based approaches, to obtain Ag-specificity. Importantly, some particle platforms induce tolerance by delivering Ag alone [161], while others require the co-incorporation of immune modifiers such as rapamycin, (2-(1′H-indole-3′-carbonyl)-thiazole-4-carboxylic acid methyl ester) (IDO), IL-10, or others [162-164]. This requirement for an immune modifier is attributed to the many differences in particle physicochemical properties and differences in biological mechanisms that have not been directly compared.

Particles have been fabricated with a variety of natural and synthetic materials, yet the most common composition of particles developed to modulate immune responses have been comprised of biocompatible and biodegradable polymers such as poly(lactide-co-glycolide) (PLGA), polylactide (PLA), and co-polymers thereof such as PLA-poly(ethylene glycol) (PLA-PEG) [151, 162]. Particles comprised of inorganic materials such as gold [163, 165], or iron oxide and quantum dots [166] have also successfully induced tolerance. Regardless of the particle composition, to be effective, the particle must deliver its therapeutic payload at a sufficient level and distribute to the appropriate site of action in the body.

For tolerance induction, delivery of tolerogenic Ags using particles provides numerous advantages over delivery of soluble Ags. A summary of particles that have been demonstrated to promote Ag-specific immune regulation are detailed in Table 2.1: Nanoparticles investigated for antigen-specific immune regulation delivering protein or peptide antigens.. Through fine-tuning of the particle size (approximately 500 nm), the biodistribution can be tailored to target tolerogenic organs such as the liver and spleen [72, 161, 167, 168]. Furthermore, in contrast to

soluble Ag, particles deliver a bolus of Ag to APCs which may result in lower therapeutic doses and safer Ag profiles. Directing the Ag distribution in the body is especially important for antibody-mediated immune reactions such as allergy, where encapsulation of Ags within particles alleviates potentially deadly side effects such as IgE-mediated anaphylaxis (Figure 2.2) [169]. Lastly, the surface properties of particles such as charge can be modulated to mimic naturally occurring apoptotic bodies (i.e. highly negative) by coating the particle surface with synthetic (poly(ethylene-alt-maleic anhydride)) or natural materials (phosphatidylserine) to mediate uptake by cell debris-clearance pathways [44, 170].

Table 2.1: Nanoparticles investigated for antigen-specific immune regulation delivering protein or peptide antigens.

Indication	Particle type	Antigen	Important finding	Reference
EAE	Ag-coupled PLGA and PS	$PLP_{139-151}$; $PLP_{178-191}$; MBP_{35-55}	MARCO scavenger receptor mediated tolerance induction	[161]
EAE	Ag-coupled PLGA	$PLP_{139-151}$; $PLP_{178-191}$	Lower negative charge on particles resulted in improved efficacy	[170]
EAE	Ag-coupled PLGA	$OVA_{323-339}$; $PLP_{139-151}$	Increased Ag conjugation and particle concentration enhanced Ag presentation and reduced co-stimulatory expression	[171]
EAE	Ag-encapsulated PLGA	$OVA_{323-339}$; $PLP_{139-151}$; $PLP_{178-191}$	Tolerance induction was not completely dependent on the spleen	[167]
EAE	Ag-polymer conjugate PLGA	$OVA_{323-339}$; $PLP_{139-151}$; $PLP_{178-191}$	Modular Ag loading, negligible burst release, tolerance induction to multiple epitopes	[172]
EAE	Ag-encapsulated PLGA and IL-10 encapsulated PLGA	MOG_{35-55}	Subcutaneous prophylactic administration reduced clinical disease. Co-administration of IL-10 PLGA was necessary to suppress disease	[164]
EAE	Ag and rapamycin co-encapsulated PLGA/PLA-PEG	$PLP_{139-151}$	Significantly reduced clinical disease score when Ag co-encapsulated with rapamycin.	[162]
EAE	Poly(maleic anhydride-alt-1-octadecene)-coated superparamagnetic iron oxide nanocrystals	$MBP_{AC-1-9\ (4Tyr)}$; MOG_{35-55}	Ag delivery to LSECs by particles induced Ag-specific Tregs and suppressed clinical disease	[166]

EAE	Ag and ITE-loaded PEGylated gold	MOG_{35-55}; $PLP_{139-151}$; $PLP_{178-191}$	Co-encapsulation of ITE with particles expanded Tregs and suppressed clinical disease	[163]
EAE	Peptide-MHCII complex-conjugated iron oxide	N/A	Tolerance mediated by expansion of Ag-specific TR1-like cells and suppressive regulatory B cells	[7]
Diabetes	Peptide-MHCI complex-conjugated iron oxide	N/A	Expanded CD8+ T cells with regulatory potential but conventional memory-like phenotype	[173]
Diabetes	Peptide-MHCII complex-conjugated iron oxide	N/A	Tolerance mediated by expansion of Ag-specific TR1-like cells and suppressive regulatory B cells	[7]
Glomerular nephritis	Ag-coupled latex	OVA	Tolerance in the liver is dependent on KCs in a non-inflammatory microenvironment	[17]
Collagen induced arthritis	Ag-encapsulated PLGA	CII	Oral administration of particles suppressed arthritis symptoms	[174]
Collagen induced arthritis	Peptide-MHCII complex-conjugated iron oxide	N/A	Tolerance mediated by expansion of Ag-specific TR1-like cells and suppressive regulatory B cells	[7]
Proteoglycan induced arthritis	Ag-encapsulated PLGA and PLGA-TMC	Hsp 70-peptide mB29a	Intranasal delivery of particles suppressed arthritis symptoms	[175]
Islet transplant	Ag-coupled PLGA	Donor cell lysate	Full MHC-mismatched murine allogeneic transplantation was achieved in 20% of recipients and improved to 60% with short course rapamycin	[72]
Bone marrow transplant	Ag-encapsulated PLGA	Dby, Uty	Delivery of CD4 Dby epitope prevented transplant rejection and delivery of CD8 epitope Uty did not induce tolerance	[147]
Hemophilia	Ag-encapsulated PLGA/PLA-PEG	Factor VIII	Significantly reduced antibody formation when Ag co-encapsulated with rapamycin.	[162]
Hemophilia	Ag-conjugated liposomes	Factor VIII	Suppression of antibody responses and prevented bleeding when delivered with CD22 ligand	[176]
Anti-drug antibody	Ag-conjugated liposomes	OVA; MOG_{1-120}	Suppression of antibody responses when delivered with CD22 ligand	[176]

Anti-drug antibody	Soluble Ag and rapamycin-encapsulated PLGA/PLA-PEG	OVA; $OVA_{323-339}$; adalimumab; pegsiticase	Delivery of rapamycin in particles and Ag within 1 day of particle administration was necessary to suppress antibody responses	[177]
Allergy	Ag-encapsulated PLGA/PLA-PEG	OVA; $OVA_{323-339}$	Significantly reduced antibody formation when Ag co-encapsulated with rapamycin.	[162]
Allergy	Liposomes	OVA	Suppression of antibody responses when delivered with CD22 ligand	[176]
Allergy	Ag-encapsulated PLGA	Bet v 1	Subcutaneous administration of particles modulated Th2 response	[178]
Allergy	Ag-encapsulated PLGA	$OE_{109-130}$	Intranasal administration of particles suppressed IgE and IgG1 production but increased IgG2a	[179]
Allergy	Ag-encapsulated PLGA	OVA	Inhibited Th2 responses in models of allergic airway inflammation	[169]

PLGA (poly(lactide-co-glycolide)); PS (polystyrene); PLA-PEG (polylactide-poly(ethylene glycol)); TMC (trimethyl chitosan); LSEC (liver sinusoidal endothelial cell); KC (Kupffer cell); OVA (Ovalbumin); PLP (proteolipid protein); MOG (myelin oligodendrocyte protein); MBP (Myelin basic protein); CII (type II collagen); Bet v 1 (Birch pollen allergen); OE (Olive allergen); ITE (2-(1′H-indole-3′-carbonyl)-thiazole-4-carboxylic acid methyl ester)

Autoantigen delivery

There are at least 81 types of autoimmune diseases that are heterogeneously observed in humans and their estimated worldwide prevalence is 4.5% [180] .These diseases are associated with complex pathologies in which the immune cells of the body attack healthy cells and tissues resulting in a state of persistent inflammation and chronic tissue destruction. Many immunotherapies are not Ag-specific and target signaling pathways that curb pathogenic T cells in active autoimmune disease, however they are not always effective [181]. Notably, the difficulty in developing therapies for autoimmune diseases, such as multiple sclerosis (MS), is that the primary disease-specific Ags involved in occurrence and progression are numerous and not always well-defined. However, proteins found in the tissues targeted by autoimmune diseases are good starting targets when designing Ag-specific therapies. For example, in MS, known autoAgs are associated with the myelin sheath proteolipid protein (PLP), myelin basic protein

(MBP), and myelin oligodendrocyte protein (MOG). Delivery of disease-relevant Ags using cell- and particle-based carriers to APCs results in the initiation of tolerogenic signaling cascades that can reprogram autoreactive responses. In this section, we describe the various cell- and particle-based approaches to induce Ag-specific immune tolerance to treat autoimmunity.

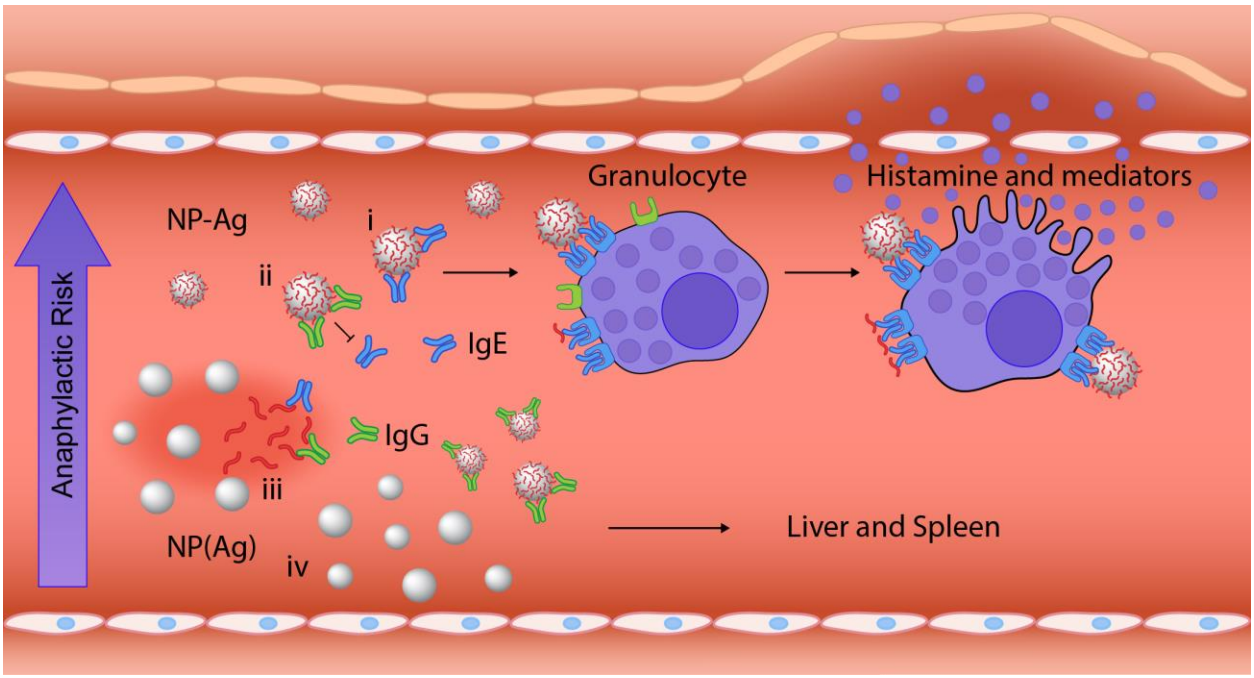


Figure 2.2: Mode of antigen-association with particles affects the risk of anaphylaxis following intravenous administration in individuals with prior antigen sensitization. Antigen is associated with particles by surface-coupling (NP-Ag) or by encapsulation (NP(Ag)) methods. *In vivo*, granulocyte activation occurs when NP-Ag or soluble antigen is recognized by circulating IgE antibodies or binds to pre-bound IgE on granulocytes. Cross-linking of IgE on granulocytes triggers degranulation and subsequent release of histamine and other inflammatory mediators that cause increased permeability, distension of blood capillaries, and anaphylaxis. (i) Binding of antigen-specific IgE to NP-Ag can trigger granulocyte activation. (ii) Binding of antigen-specific IgG to NP-Ag reduces potential granulocyte activation but can result in off-targeted biodistribution and reduce tolerance induction. (iii) Pre-mature antigen release from NP(Ag) can result in granulocyte activation but to a lesser extent than NP-Ag. (iv) NP(Ag) with negligible rate of antigen release reduces the risk of granulocyte activation and enables unaffected distribution to the liver and spleen to induce tolerogenic responses.

Cell-based approaches

For the past three decades, autoAg-coupled syngeneic splenocytes (Ag-SPs) have been investigated for their ability to induce tolerance in models of autoimmunity based on direct and indirect T cell interaction pathways (Figure 2.1) [94, 182]. These Ag carriers have demonstrated tolerance to autoAg in Th1/17-mediated autoimmune models of experimental autoimmune encephalomyelitis (EAE), a mouse model of MS, and the non-obese diabetic (NOD) model of

type 1 diabetes (T1D) [183, 184]. After intravenous infusion, Ag-SPs accumulate in the marginal zone of the spleen where they are phagocytosed by marginal zone macrophages. Ag-SP uptake is followed by IL-10 production and upregulation of PD-L1 by macrophages [185]. Tolerance was not attained in IL-10 knockout mice, or mice treated with anti-PD-L1 antibody, suggesting that IL-10 and PD-L1 are necessary for Ag-SP-mediated tolerance. Direct presentation of Ag-SPs to T cells has been demonstrated to result in unresponsiveness, but studies coupling whole protein to splenocytes or using MHC-deficient or MHC-mismatched splenocytes have shown that the indirect presentation pathway is sufficient for tolerance [183]. Furthermore, the accumulation of Ag-SPs in the spleen was necessary, as autoAg tolerance was not achieved in models of splenectomy or subcutaneous administration.

The reality of human MS is that treatment needs to be effective in individuals with pre-existing disease and that the variety of autoAgs is not well-characterized. Due to epitope spreading during chronic autoimmunity, a person may have several Ags causing the pathogenesis of their disease [186]. A study by Smith et al. evaluated the feasibility of preventing EAE using Ag-SP coupled with an array of autoAgs (i.e. $PLP_{139\text{-}151}$, $PLP_{178–191}$, $MBP_{84–104}$, and $MOG_{92–106}$) [187]. EAE clinical scores and delayed type-hypersensitivity (DTH) responses indicated that disease suppression in the therapeutic tolerance model was different than in the prophylactic model where an increase in anti-inflammatory cytokine production (IL-10 and TGF-β) was observed. This study, in addition to the years of experimental success by Ag-SPs, provided justification for a first-in-man clinical trial using Ag-coupled cells to treat MS.

In 2013, a clinical trial was published that built on the work of Miller et al. using Ag-coupled cells for the treatment of autoimmune disease. In this study, autologous peripheral blood mononuclear cells (PBMCs) were coupled with seven known myelin peptides described to be

potentially antigenic in MS. This trial demonstrated that the treatment was safe, and patients that received doses of Ag-PBMCs higher than 1 x 10^9 cells showed a decrease in Ag-specific T cell responses following therapy [149]. This study provided evidence that autologous cells could be used to induce tolerogenic responses in humans, although further studies using larger cohorts of patients will be required to demonstrate its wide-scale applicability and versatility.

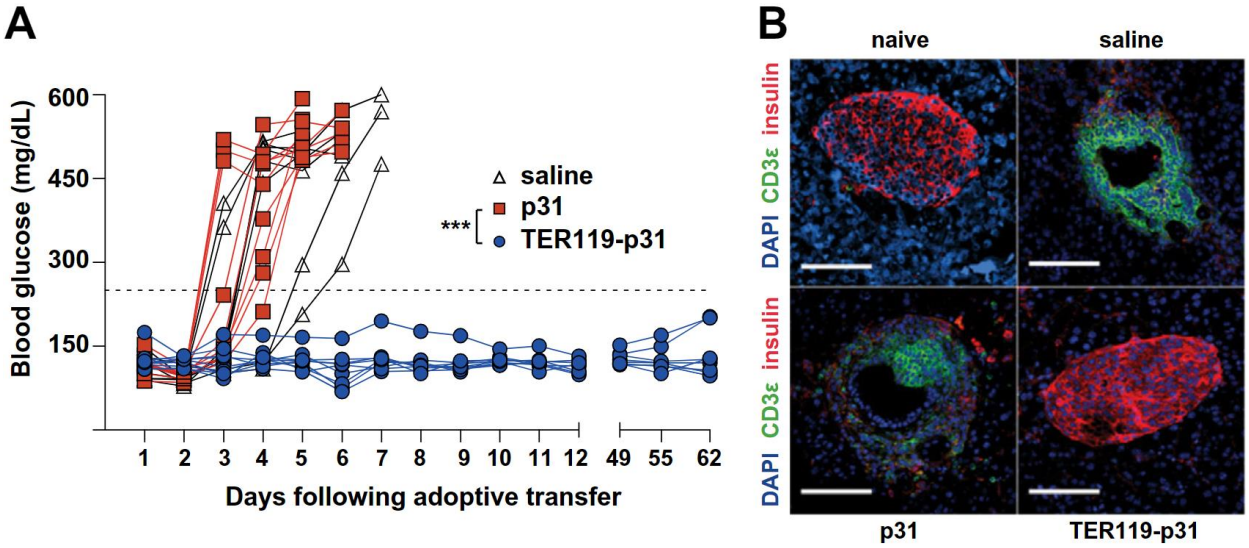


Figure 2.3: Erythrocyte-binding TER119 scFv antibodies fused with autoantigen (p31) specifically target red blood cells in situ after intravenous administration and induce antigen-specific tolerance in type 1 diabetes model. (A) TER119-p31 induces tolerance and results in normoglycemia. Normoglycemic NOD/ShiLtJ mice received adoptive transfer of diabetogenic BDC2.5 CD4+ T cells and 3 intravenous treatments of saline, p31, or TER119-p31 (n =8, n = 9, and n = 9, respectively) over the first week. ***P < 0.0001. (B) Immunohistochemistry of pancreatic islets excised 4 days after treatment and stained for CD3ε T cells (green), insulin (red), and nuclei (blue). Saline-treated and untargeted autoantigen mimetope p31 resulted in T cell infiltration and islet destruction in contrast to mice treated with red blood cell-binding autoantigen (TER119-p31) which prevented T cell infiltration and preserved insulin production. (Scale bar = 100 μm). Reproduced from [146] with permission.

Another tolerance therapy that takes advantage of the body's natural apoptotic clearance mechanisms targets autoAgs to circulating erythrocytes (Ag-RBC) (Figure 2.1). Kontos et al. have utilized Ag-conjugates that targeted murine glycophorin A-binding (TER119) on erythrocytes [146]. After intravenous infusion, the Ags become associated with erythrocytes and are cleared by naturally tolerogenic pathways. This treatment resulted in cross-presentation of Ag, and proliferation of $CD8^+$ T cells with upregulated PD-1 and annexin-V indicating potential exhaustion and deletion outcomes. In the NOD T1D model, complete prevention of

hyperglycemia was demonstrated with injections of erythrocyte targeting fusion peptides containing the diabetogenic mimetope peptide p31 (Figure 2.3). By utilizing *in situ* association to cells bound for apoptotic clearance, *ex vivo* manipulation of cells has been avoided, making this cell-based strategy a strong candidate for clinical translation.

Expanding on the work of immunoglobulin G-mediated tolerance, B cells have been retrovirally transduced to produce conjugates of the IgG heavy chain and Ags of interest (peptide-IgG) [188]. In one example of this technology, the HIV TAT protein was fused with a peptide and IgG to form TAT-Ag-IgG, with the TAT protein functioning to mediate cell entry of the relevant Ag, as shown in previous studies [189, 190]. B cells activated with LPS and reprogrammed by TAT-MOG_{35-55}-IgG displayed the ability to reduce EAE disease score when injected 10 days after immunization with MOG_{35-55}, but interestingly did not reduce EAE disease score when injected one week prior to disease induction. In NOD T1D, B cells incubated with a fusion protein incorporating islet Ag B_{9-23} (TAT-B_{9-23}-IgG) displayed a delayed onset of diabetes when administered prophylactically [188]. In each of these studies, delivery of irrelevant peptide-transduced B cells were unable to reduce or delay disease progression, suggesting Ag-specificity of the platform [188]. Preliminary mechanistic studies indicate that the tolerance induction by transduced B cells required $CD4^+CD25^+$ Tregs as well as CTLA-4/B7-dependent interaction between B and T cells [191]. Similar successes were observed using this platform in murine models of hemophilia, experimental autoimmune uveitis, and arthritis, and represent a promising method of tolerance induction [192-196].

Particle-based approaches

Peripheral tolerance induction by recapitulating natural tolerance maintenance in the hematopoietic compartment has offered insight into potential avenues to develop particulate

delivery systems that follow a similar mechanism of action. Intravenously injected 500 nm Ag-coupled carboxylated polystyrene particles or PLGA particles were found to localize in similar regions of the splenic marginal zone and liver as Ag-SPs and target specific scavenger receptors on APCs that play an active role in tolerance induction (Figure 2.1) [161]. These particles efficiently prevented the onset of EAE, prevented epitope spreading, and reversed the progression of EAE in a therapeutic disease model. Importantly, tolerance was dependent on the highly-negative charge (less than -30 mV) and size (500 nm) of the particles, which targeted their distribution to macrophages expressing macrophage receptor with collagenous structures (MARCO) in the spleen. In a follow up study, Ag-coupled PLGA particles induced tolerance in EAE as demonstrated by significantly reduced mean clinical scores, reduced DTH responses, and reduced central nervous system (CNS) immune infiltration of Th1/17 cells [170].

The previous examples have demonstrated that tolerance can be induced by particles with surface-coupled Ag. However, the covalent modification of the particle surface with Ags affects physicochemical properties of particles such as their size, charge, and solution stability [169, 170]. Therefore, encapsulation of Ag within particles represents a more advantageous method to deliver Ag *in vivo*. McCarthy et al. recently described the encapsulation of peptide Ags ($OVA_{323-339}$, $PLP_{139-151}$, and $PLP_{178-191}$) into PLGA particles (PLGA(Ag)) to treat EAE [167]. PLGA(Ag) particles significantly abrogated EAE induction *in vivo* and inhibited Th1/17 Ag recall responses (proliferation, IFN-g, and IL-17a) *in vitro*. Corroborating previous studies using peptide-coupled PLGA particles, the biodistribution of intravenously injected PLGA(Ag) particles was found primarily in liver and to a lesser extent in the spleen and lungs. Previous studies using Ag-SP demonstrated the dependence of the spleen for tolerance induction [185], however, prophylactic tolerance induction by PLGA(Ag) particles was not solely dependent on the spleen [167].

Pearson et al. developed Ag-polymer conjugate PLGA (acNP) particles that displayed modular Ag loading (up to 150 µg peptide per mg particle), low burst release, and minimally exposed surface Ag [172]. *In vitro*, acNPs were effective at inducing Tregs in a co-culture model of BMDCs, naïve OTII T cells, and TGF-ß1. Treg induction was dependent on Ag loading and particle concentration, where the highest Ag loading in acNPs enabled a 10-fold lower concentration to be used. Furthermore, acNPs were effective at treating EAE that was induced by a single administration of multiple peptides (Figure 2.4). This approach holds promise to deliver several therapeutic antigens that can tolerize to multiple disease relevant epitopes.

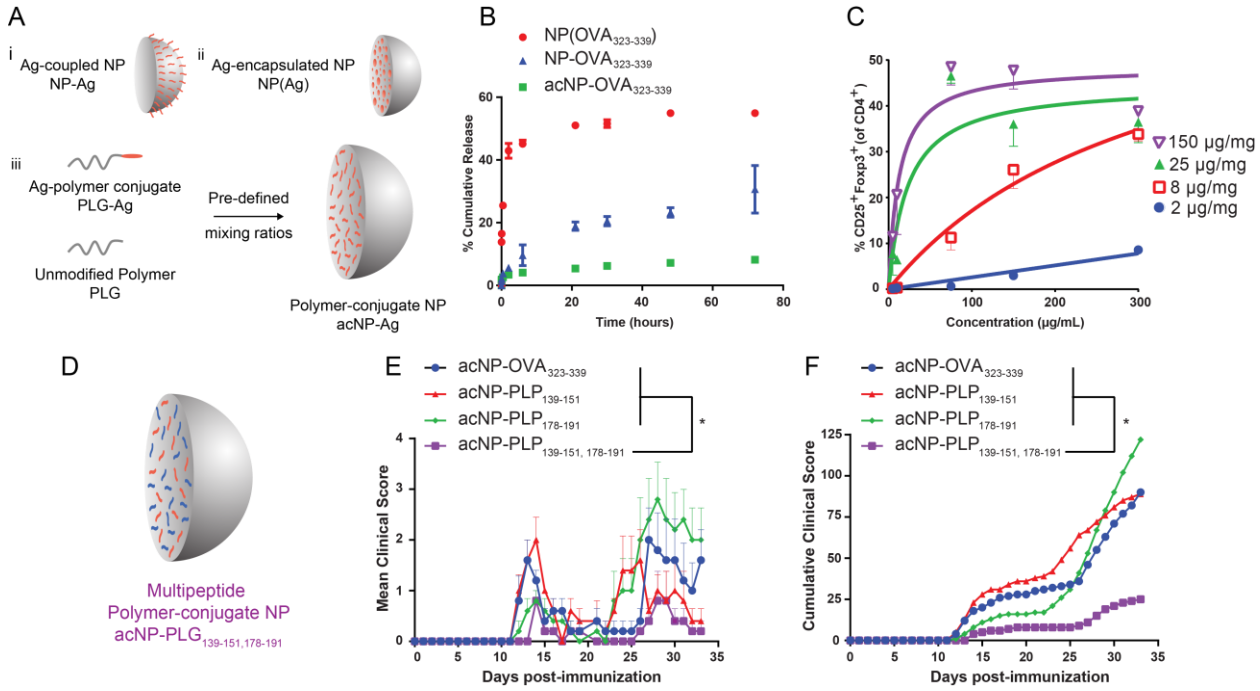


Figure 2.4: Antigen-polymer conjugate nanoparticles display favorable physicochemical and biological properties for tolerance induction. (A) Release profile of NP(OVA$_{323-339}$), NP-OVA$_{323-339}$, and acNP-OVA$_{323-339}$. (B) Regulatory T cell induction is dependent on nanoparticle concentration. BMDCs were treated for 3 h with various concentrations of 400 nm of acNP-OVA$_{323-339}$ (2, 8, 25, 150 µg/mg loading) formulation. Excess acNP-OVA$_{323-339}$ particles were subsequently washed from the cell surface prior to addition of OT-II T cells and 2 ng/mL of TGF-β1. (C) Schematic representation of antigen-polymer conjugate nanoparticles delivering multiple Ags. (D) Clinical scores of SJL/J mice treated with 1.25 mg of acNP-OVA$_{323-339}$ (8 µg/mg OVA$_{323-339}$), acNP-PLP$_{139-151}$ (8 µg/mg PLP$_{139-151}$), acNP-PLP$_{178-191}$ (8 µg/mg PLP$_{178-191}$), or acNP-PLP$_{139-151,178-191}$ (8 µg/mg PLP$_{139-151}$ and 8 µg/mg PLP$_{178-191}$) and immunized with PLP$_{139-151}$ and PLP$_{178-191}$ in CFA to induce R-EAE 7 days later. (E) Corresponding cumulative clinical score for mice treated with particles (n = 5). Differences between disease courses of different treatment groups were analyzed for statistical significance using the Kruskal-Wallis test (one-way ANOVA non-parametric test) with Dunn's multiple comparisons test ($p < 0.05$).

Additional *in vivo* tolerance mechanisms have implicated the liver as critical for tolerance induction since it is exposed to numerous self and non-self Ags regularly and therefore must balance immunity and tolerance [197]. Many APCs in the liver have a low abundance of MHC and co-stimulatory molecule expression, which can reduce immune cell activation. Kupffer cells (KCs) and liver sinusoidal endothelial cells (LSECs) internalize a majority of particles administered intravenously [198]. Heymann et al. utilized carboxylated latex particles to study the mechanism of action of tolerance induction using particle-delivered Ags. The liver was specifically identified as important for tolerance induction where Kupffer cells were demonstrated to be associated with Ag-presentation that induced $CD4^+$ T cell arrest and expansion of naturally occurring Tregs [17]. In a model of Ag-specific glomerular nephritis, particle delivery protected against kidney damage by reducing T cell infiltration, reduced glomerular damage, and reduced periglomerular infiltration. However, in models of liver injury, Kupffer cells lost expression of their tolerogenic phenotype, and tolerance was abrogated due to the redistribution of Ag to infiltrating monocyte-derived macrophages away from the hepatic phagocyte compartment. Similarly, the liver was determined to play an important role in tolerance induction by Carambia et al. [166]. Small poly(maleic anhydride-alt-1-octadecene)-coated particles induced tolerance though LSECs. Mice treated with particles displayed higher frequencies of Tregs and tolerance induction was abrogated when Tregs were inactivated using anti-CD25 antibody. These studies provided support that the liver plays an important role in tolerance induction by particles, however, it should be noted that due to distinct differences in particle physicochemical properties (size, charge, composition), the mechanism of action for each particle platform must be determined experimentally and cannot be assumed.

Co-delivery of immune modulating agents such as immune suppressants, cytokines, or other immune modifiers with Ag by particles is sometimes necessary to induce Ag-specific tolerance. One of the most commonly delivered agents for immune modulation is rapamycin, a mammalian target of rapamycin (mTOR) inhibitor. Encapsulation of rapamycin within PLGA nanoparticles induced a tolerizing phenotype *in vitro* where particles decreased the expression of maturation markers MHCII, CD86, and CD40 expression and increased levels of TGF-β using bone-marrow derived dendritic cells (BMDCs) [199]. Maldonado et al. developed tolerizing nanoparticles (tNPs) comprised of a mixture of PLGA and poly(ethylene glycol)-polylactide (PEG-PLA) that co-encapsulated Ag and rapamycin. These tNPs delivered antigenic peptides or whole proteins and could tolerize against both cellular and humoral immune responses. The co-encapsulation of rapamycin with Ag into tNPs was necessary to induce tolerance, whereas co-delivery of soluble rapamycin with Ag-encapsulated particles did not elicit tolerogenic effects but rather propagated humoral immunity [162]. In another example, immune modifying agent 2-(1-indole-3-carbonyl)-thiazole-4-carboxylic acid methyl ester (ITE), an activator of the aryl hydrocarbon receptor transcription factor (AhR), was loaded into 60 nm gold particles with MOG_{35-55} peptide [163]. In the EAE model, particle treated mice displayed expanded populations of Tregs and abrogated EAE clinical disease symptoms. In a subsequent study, the same gold particles delivering β cell proinsulin and ITE were found to induce a tolerogenic phenotype in dendritic cells by inducing *Socs2*-mediated inhibition of NF-kB and suppression of inflammatory cytokines as well as the promotion of Treg generation *in vivo* [165]. MOG_{35-55} peptide and IL-10 were separately encapsulated into 200 nm PLGA particles for the treatment of EAE by the subcutaneous route of administration. Co-administration of IL-10 containing NPs was required to significantly mitigate EAE clinical scores, while IFN-γ and IL-17 were significantly decreased [164].

Immune polyelectrolyte multilayers (iPEMs) have been built on calcium carbonate templates to promote immunological tolerance [200]. Delivery of a regulatory antagonist ligand of TLR9, GpG oligonucleotide, along with a MOG-triarginine peptide was hypothesized as able to restrain the pro-inflammatory signaling and redirect T cell differentiation from inflammatory populations and towards regulatory phenotypes such as Tregs. Interestingly, iPEMs reduced TLR9 signaling, reduced dendritic cell activation, and polarized myelin-specific T cells towards a tolerogenic phenotype and function. In an EAE model, iPEMs abrogated disease, which coincided with Treg expansion and reduced IL-17, IL-6, and IFN-γ production, with no effect on T cell proliferation.

Alloantigen Delivery

Achieving allogeneic tolerance to multiple foreign Ags represents a significant challenge to the field of transplantation. Transplantation of allogeneic or 'non-self' tissues between genetically different individuals of the same species leads to a T cell-mediated immune response resulting in rejection and graft destruction. Current methodologies for improving transplant tolerance are similar to those of treating autoimmunity (such as the chronic use of immunosuppressive agents) that are associated with numerous risks [116]. The severity of the immune response against the transplanted tissue depends on the differences in Ag between the donor and recipient as well as the intragraft expression of inflammatory cytokines following transplantation [201]. There are three pathways through which allograft recognition and rejection can occur: 1) direct, 2) indirect, and 3) semi-direct. In the direct pathway, recipient T cells recognize MHC molecules present on the surface of donor APCs. In the indirect pathway, recipient APCs internalize allogeneic proteins and present it to recipient T cells on recipient MHC molecules. It has been observed that $CD4^+$ T cells with indirect specificity can provide "unlinked" T cell help to $CD8^+$ T cells with direct specificity, which does not agree with the commonly-accepted "linked" model of immune

response in which the same APCs activate both $CD4^+$ and $CD8^+$ T cells. An explanation for this phenomenon is the acquisition of MHC molecules from donor APCs by recipient APCs and subsequent direct presentation to $CD8^+$ T cells. This is known as the semi-direct pathway and is under investigation [202].

The wide breadth of Ags necessary to tolerize against in allogeneic transplants and the multiplicity of allorejection pathways pose significant challenges to the development of new tolerance therapies. The primary Ags that influence rejection in mice are MHCs, and in humans are called human leukocyte Ags (HLAs). These HLA proteins are of two types, Class I and Class II, and are involved in Ag presentation and recognition, such as between APCs and T cells. Both major and minor mismatches in HLAs between the donor and recipient are highly deterministic of the success of a transplant. In addition to the major Ags, mismatches in numerous other proteins of the cell, which are termed minor Ags, can also mediate rejection. Tolerance induction strategies have aimed to affect the direct or indirect pathways of allograft rejection and are the focus of many Ag carrier therapies.

Cell-based approaches

Immunosuppression-free allogeneic transplant tolerance has been achieved in mice by pretreatment with ethylene carbodiimide (ECDI)-fixed splenocytes (ECDI-SP) that mimicked donor apoptotic cells. Long-term tolerance to allogeneic islets was achieved by two infusions of ECDI-SP from the donor mouse strain, 1-week prior to, and 1-day post, kidney-capsule transplant [145]. The effect was shown to be strain-specific and dependent on ECDI treatment. The durability of this tolerance was challenged with a second islet transplant 60 days after the initial treatment. Donor strain-matched islets were protected by the tolerance, whereas third party islets led to rejection as indicated by hyperglycemia. The authors attributed the allograft

tolerance induction, but not maintenance, to an increase in Tregs in the spleen as Treg ablation early (day -9), but not late (day 15), prevented engraftment. Furthermore, graft rejection dominated in PD-L1 deficient mouse suggesting a potential role for the PD-1 pathway in mediating ECDI-SP allotolerance. Since the kidney capsule is not considered a translatable transplantation site, this tolerance protocol was combined with islet transplantation on a PLGA microporous scaffolds into the mouse peritoneal fat, an analogue to human omentum [96]. Tolerance for islets transplanted on the PLGA scaffold was as effective as the kidney capsule, with both providing a site for successful long-term allogeneic islet engraftment. Combined with tolerance directed toward islet Ag $InsB_{9-23}$, allotolerance by ECDI-SP offers a potential solution for islet replacement therapy for T1D patients.

Further investigation of ECDI-SP induced allotolerance revealed contribution of both direct and indirect tolerance mechanisms [144]. *In vivo* selective depletion experiments showed that DCs, but not B cells or macrophages, were necessary for ECDI-SP induced allotolerance. Furthermore, there were T cell responses to APC-processed EDCI-SPs (indirect) as well as presentation of un-phagocytosed ECDI-SP alloAg to T cells (direct). After uptake of ECDI-SPs, $CD11c^+$ DCs upregulated co-inhibitory molecules PD-L1 and PD-L2 and caused the rapid expansion of T cells, followed by clonal deletion and hindered migration to the site of engraftment. The directly stimulated T cells experienced weak proliferation and became unresponsive to subsequent stimulatory signals. Thus, in addition to the expansion of Tregs in the spleen, graft, and graft draining lymph nodes, ECDI-SPs induced tolerance by causing clonal deletion and anergy of alloreactive T cells. In other disease models, ECDI-SPs have been used to prolong cardiac allografts (indefinitely if combined with a short course of rapamycin) [203], and

have induced long-lasting xenograft tolerance to rat islets transplanted into mouse kidney capsules when combined with transient B cell depletion [204].

Particle-based approaches

The induction of donor-specific tolerance to transplanted cells and organs remains of utmost importance to mitigate allograft rejection. The first uses of particles to improve allotransplant acceptance involved the delivery of small molecule immune suppressants such as rapamycin or calcineurin inhibitors [157]. Achieving Ag-specific suppression of anti-donor immune responses is complicated due to the wide array of major and minor Ags. PLGA particles have been used to induce donor-specific tolerance and mediate long-term acceptance of full MHC-mismatched allografts using an allogeneic islet transplant model (BALB/c to C57BL/6). Donor Ags were obtained from the lysate of BALB/c splenocytes, with the lysate Ag conjugated to the surface of 500 nm PLGA particles using ECDI chemistry. Delivery of PLGA particles with surface-coupled donor Ags to transplanted C57BL/6 mice led to tolerance in 20% of recipients. In combination with a short course of low-dose rapamycin at the time of transplant, tolerance was greatly improved to 60% (Figure 2.5) [72]. In another study, PLGA particles were used to induce tolerance in minor histocompatibility Ag sex-mismatched C57BL/6 model of bone marrow transplantation. Peptide Ags Dby and Uty are respective $CD4^+$ and $CD8^+$ T cell Ags that mediate male bone marrow transplant rejection in females. Interestingly, delivery of Dby peptide either by conjugation to the surface or encapsulation promoted transplant tolerance. However, delivery of Uty peptide using particles did not induce tolerance. In this model, depletion of Tregs using anti-CD25 antibody did not alter tolerance induction, suggesting other potential tolerance induction mechanisms [147].

Exosomes have also been used to induce tolerance in allogeneic transplant models. Exosomes derived from PBMCs have been used to prolong cardiac transplants in a C57BL/6 to BALB/c model [205]. Song et al. could extend cardiac allografts 40 days using 2 doses of exosomes from donor C57BL/6 mice. The authors attributed the tolerance to a skewing of Th2 T cells toward a regulatory phenotype. While they ruled out the possibility of direct induction of Tregs by exosomes, they concluded that MMP1 carried by the donor exosomes was necessary for Treg induction in a Th2:DC co-culture system.

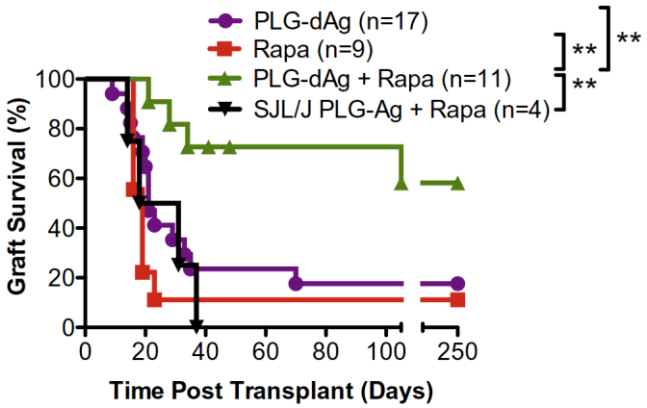


Figure 2.5: A short course of low dose rapamycin synergizes with PLG-donorAg (dAg) to enhance tolerance efficacy. Recipient mice (C57BL/6) receiving donor (BALB/c) PLG-dAg injections at days 7 and +1 in combination with a 4-day course (days 1, 0. +1, and +2) of low dose (0.1 mg/kg) rapamycin demonstrated significantly greater islet allograft survival (n=11) compared with mice treated with rapamycin alone (n=9), BALB/c PLG-dAg alone (n=17), or PLG particles coupled with lysate proteins from a third party donor SJL/J (n=4). **$p < 0.01$. Reproduced from [72] with permission from Elsevier.

In the same C57BL/6 to BALB/c cardiac transplant scheme, another group of investigators used immature dendritic cell exosomes (imDex) to prolong cardiac graft survival [206]. Cardiac allografts were extended 25 days using 3 doses of imDex from C57BL/6 donor mice. Interestingly, infusion of more or less than 10 μg resulted in minimal graft protection. When rapamycin was administered for 11 days, half of the grafts were maintained indefinitely. The tolerogenic effects were donor-specific and dependent on rapamycin. The same group also demonstrated liver transplant tolerance using imDex [207]. In a rat model, imDex from donor rats (Brown Norway) prolonged liver graft survival about 25 days in recipient Lewis rats. Instead

of administering rapamycin to extend graft survival, recipients were infused with donor-specific recipient Tregs, which resulted in an indefinite survival of 70% of liver grafts. The mechanism by which DC-derived exosomes induce tolerance is unknown. Like ECDI-SP and PLGA NPs mentioned earlier, intravenously delivered DC-derived exosomes have accumulated in liver Kupffer cells as well as marginal zone macrophages and DCs [208]. Like their immature DC source, these exosomes express low levels of MHC class I and II as well as subimmunogenic levels of co-stimulatory molecules. In the cardiac allograft model, the data suggested that splenic T cells become hyporesponsive to alloAg challenge, and there was an observed increase in $Foxp3^+$ splenic T cells following a co-treatment with imDex and rapamycin [206]. Co-administration and *in vivo* proliferation of Tregs seems to support their role in exosome induced allotolerance [207]. It is unknown whether the T cell interactions result from direct presentation of exosome Ags by fusion with host APCs, or indirect presentation of exosome Ags following APC phagocytosis [207].

Allergen Delivery

Allergic diseases such as asthma and food allergies are becoming increasingly common in developed nations. Immediate allergic reactions (Type 1), involve an overreaction of the immune system and the formation of IgE antibodies. The development of allergic responses is reliant on $CD4^+$ Th2 cells as they produce cytokines that induce immunoglobulin class switching to IgE. IgE binds with high affinity to mast cells and basophils that release pro-inflammatory mediators once they encounter the allergen [109]. At current, the most effective treatment regimen consists of avoidance or other specific immune tolerance (SIT) strategies that deliver soluble Ag at increasing dosages to mitigate symptoms. SIT is usually carried out by repetitive subcutaneous injections or sublingual delivery of increasing doses of the allergen [209]. However, SITs feature

numerous potential issues especially for treating food allergies that pose a risk of developing adverse reactions including life-threatening anaphylaxis. Additionally SIT by subcutaneous injections often requires 3-5 years of treatment, involving multiple sessions per week in the build-up phase [210]. Recent work has focused the delivery of antigen to the lymphatic system by ultrasound guided intranodal injections which show promise in decreasing the injection frequency and duration of SIT regimes. A study comparing a 3 year subcutaneous SIT regime (54 injections) to a 2 month intralymphatic regime (3 injections) demonstrated equivalent tolerance to pollen as measured by hay fever symptoms, skin reactivity, and decreased allergen-specific serum IgE [211]. A similar study of 3 intralymphatic inguinal resulted in a decrease in seasonal allergic symptoms and nasal inflammatory leukocytes compared to adjuvant delivery without pollen (aluminum hydroxide only) [212]. Other allergen-specific tolerance strategies include using Tregs, anti-IgE, or by blocking Th2 cytokines. SIT to allergens leads to a shift in Th2 and Th17 towards a Th1 response and Treg induction [213]. This results in reduced production of IgE production, IL-4, and IL-13 and an increased production of IFN-g and IgG subtypes that can act as blocking antibodies and capture the allergen before activating effector cells [214].

B cells express a variety of B cell receptor (BCR) inhibitory co-receptors that aid in setting a threshold for B cell activation. Among them are CD22 and SIGLEC-G (SIGLEC-10 in humans), and members of the SIGLEC (sialic-acid binding Ig-like lectin) immunoglobulin family that recognize sialic acid-containing glycans of glycoproteins and glycolipids and ligands [215]. Targeting Ag-specific B cells is a mechanism to induce systemic humoral tolerance. Favorable approaches to induce B cell tolerance involve taking advantage of mechanisms to suppress B cell activation.

Cell-based approaches

One of the methods currently available to induce Ag-specific immune tolerance is the use of Ag-SP. As described earlier in this review, Ag-SP have been prophylactically and therapeutically tolerogenic in models of Th1/17-mediated autoimmune disease. An early demonstration of Ag-SP to treat Th2-associated models was performed by Smarr et al. [188]. This study utilized two models of allergy: peanut hypersensitivity as well as ovalbumin (OVA)-induced allergic airway inflammation. Whole peanut extract (WPE) or whole OVA protein was coupled to splenocytes using ECDI, and the Ag-SPs were intravenously infused resulting in decreased local and systemic Th2-related disease. In the peanut hypersensitivity model, characterized by mast cell-mediated anaphylaxis, prophylactic WPE-SP administration diminished the levels of Ag-specific IgE (but not IgG), eosinophil numbers, and IL-3, IL-4, and IL-13 in recall assays that resulted in a prevention of anaphylactic symptoms in an oral WPE challenge. The authors observed anaphylactic symptoms when Tregs were inactivated by anti-CD25 antibody indicating a partial role for Tregs in the tolerance mechanism. In the OVA-induced allergic airway model, prophylactic OVA-SP treatment similarly reduced IgE, eosinophil numbers, and Th2-associated cytokines (*in vivo* and *ex vivo*). IgG levels were also reduced and the tolerogenic effects were Treg independent. Regardless of allergy model and Treg activity, treating with Ag-specific Ag-SPs decreased IgE levels indicating inactivation of B cell class switching which the authors posit is a result of previously observed decreased CD40L levels on helper T cells (previously observed) [188, 216]. Though IgE levels were decreased compared to controls, the levels were increased compared to Ag-inexperienced animals, however, this did not result in anaphylaxis. The increased use of biologics in medicine has led to the development of anti-drug antibodies (ADAs) in patients. This undesired immune recognition has hindered the effective use of

biologics and has created a demand for drug-specific tolerance. The usage of erythrocyte-targeted Ags has recently been applied to prevent development of ADAs against acute lymphoblastic leukemia (ALL) therapeutic enzyme Escherichia coli L-asparaginase (ASNase) [217]. An infusion of ASNase conjugated to glycophorin A-binding peptide (ERY1-ASNase) significantly reduced anti-ASNase IgG titers against 6 weekly challenges, compared to infusion of untargeted ASNase. This reduction in anti-ASNase titer was observed in all IgG subclasses. The treatment showed no effect on the development of humoral responses to OVA indicating that this therapy is both effective and Ag-specific in mice.

Particle-based approaches

PLG particles have been used to tolerize against OVA in a Th2-mediated allergic airway inflammation model both pre- and post-sensitization [169]. Since activation of mast cells is APC independent, avoiding Ag recognition by antibodies is desirable. Encapsulation of allergens into particles shielded their detection by IgE auto-antibodies on mast cells and basophils thus preventing any undesired side effects associated with SIT and Ag-coupled particles (Figure 2.2). Encapsulation of OVA protein within PLGA particles (PLGA(OVA)) eliminated the presence of particle surface-associated protein that could lead to deleterious biological effects such as anaphylaxis. In a prophylactic disease model, PLGA(OVA) particles inhibited the production of anti-OVA IgE and suppressed the production of Th2-mediated cytokines IL-4, IL-5, IL-13, IL-10, and IL-17. In a therapeutic model of allergic airway inflammation, PLGA(OVA) particles inhibited the Th2 responses and airway inflammation but led to increases in OVA-specific IgE (Figure 2.6) [169]. Importantly, the encapsulation of OVA into PLG particles eliminated OVA-specific IgG and IgE binding to the surface of the particle preventing anaphylaxis.

Particles loaded with rapamycin that co-delivered PEGylated uricase or adalimumab demonstrated suppression of ADAs. Interestingly, the ability to suppress ADA production was dependent on the timing of rapamycin-encapsulating particle administration. Significant suppression of anti-keyhole limpet hemocyanin (KLH) antibodies was only achieved if the protein was administered within 1 day of particle administration [177]. Macauley et al. demonstrated that SIGLEC-engaging tolerance-inducing antigenic liposomes (STALs) (liposomes that displayed Ag as well as glycan ligands for CD22) could induce Ag-specific B cell apoptosis. CD22-dependent tolerance induction was demonstrated for both T cell-independent (nitrophenol) and T cell-dependent (hen egg lysozyme) Ags as Ag-specific antibody titers were significantly reduced. Furthermore, STALs induced tolerance to FVIII using a hemophilia mouse model. STALs significantly reduced anti-FVIII titers and prevented bleeding [176].

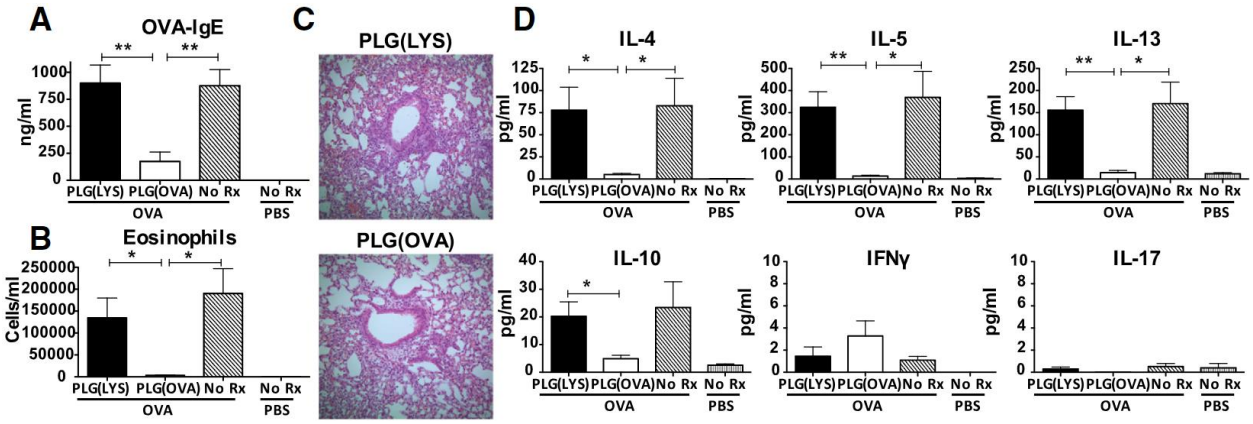


Figure 2.6: Prophylactic treatment with PLG(OVA) inhibits Th2-induced airway inflammation. Naive female BALB/c mice (n = 5) were treated i.v. with 2.5 mg PLG(OVA) or control PLG(LYS) on days −7 and +7 relative to i.p. immunization with 10 μg of OVA in 3 mg of alum or alum alone on days 0 and +14 before aerosol challenge with 10 mg/mL OVA for 20 min on days +28–30 and sample collection on day +31. LYS, lysozyme. (A) Concentration of serum OVA-IgE was determined by sandwich ELISA. (B) Lungs were flushed with BALF, total cell counts were determined, and samples were cytospun onto slides before DiffQuik staining for differential cell counts of bronchoalveolar lavage eosinophils. (C) Lungs were fixed in formalin and stained with H&E. (D) Cytokines from BALF supernatant were analyzed by Milliplex. Results are mean ± SEM and are representative of three separate experiments. *P < 0.05; **P < 0.01. Reproduced with permission from [169].

Carrier-free therapeutics

Although much recent focus has been on cell-based and particle-based technologies for bulk delivery of Ag, molecular-scale carrier-free platforms (less than 200 kDa) offer distinct advantages. The unique properties of carrier-free technologies such as their small size enable enhanced lymphatic drainage and bioavailability from the subcutaneous route of administration. For example, subcutaneously administered Ag-graft polymers (less than 100 kDa) showed improved tolerogenic properties compared to similarly functionalized particles (500 nm) due to their decreased size and increased solubility that improved interstitial drainage and bioavailability of the Ag-grafted polymer [218]. Furthermore, soluble carrier-free platforms often incorporate specific binding motifs that target specific cell types or interrupt inflammatory signaling pathways associated with cell activation. Fusion peptides comprised of Ag-antibody bioconjugates have demonstrated improved outcomes by targeting delivery of autoAg to tolerogenic APC subtypes [219]. Alternatively, polymer platforms co-grafted with autoAg and peptide inhibitors of co-stimulation have demonstrated Ag-specific tolerance that is dependent on interrupting APC:T cell interactions [218]. Soluble carrier-free systems deliver similar payloads as particle and cell-based systems, but their small scale, solubility, and engineered specificity make these systems unique.

Fusion proteins

Fusion proteins are a class of biologics that have seen remarkable success in research and clinical applications. Many design variations exist, but most are composed of a protein/peptide of interest linked to an antibody (often an IgG subclass) at the fragment crystallizable (Fc) region. Conjugation to IgG provides several benefits to therapeutics, including increased serum half-life

(through increased size and, consequently, reduced clearance) and recycling (through increased interaction with the neonatal Fc receptor, which protects IgG from degradation) [220, 221]. Multiple tolerogenic fusion proteins have demonstrated the ability to induce Ag-specific tolerance. Recently, blood clotting protein FVIII conjugated to human IgG1 (rFVIIIFc) demonstrated the ability to diminish anti-FVIII antibody responses associated with FVIII protein replacement therapy. In mice, this treatment was accompanied by development of Tregs and a general shift towards a tolerogenic phenotype, as indicated by up-regulation of IL-10, TGF-β, IL-35, and IDO-1, as well as down-regulation of IL-17 measured by real time polymerase chain reaction [222]. Importantly, mice pretreated with rFVIIIFc retained the ability to mount an antibody response to both dinitrophenol and OVA, demonstrating the Ag-specificity of the platform. The mechanisms behind these observations are being investigated, and studies support a role of the Fc□ class of Fc receptors, which are particularly important in phagocytosis, and the neonatal Fc receptor, which the authors suggests implicate B cells and dendritic cells [222]. Antibody-Ag fusion proteins combine solubility and specificity to achieve efficient delivery of autoAg to specific cell types. Coupling of autoAg to anti-DEC205 antibody resulted in *in vivo* targeting of the endocytic receptor DEC205 on tolerogenic dendritic cells and demonstrated tolerance in models of EAE, NOD T1D, and experimental autoimmune arthritis (EAA) [223-225]. In the EAE model, intraperitoneal injection of anti-DEC205 antibody linked with PLP, but not isotype fusion protein or anti-DEC205 with irrelevant peptide, ameliorated disease onset. The protective effects in this context were attributed to hindered proliferation of IL-17-producing T cells and anergy in the remaining Ag-specific T cell population [223]. In the NOD T1D mouse model, it was shown that delivery of β cell peptide mimotope on anti-DEC205 antibody results in cross-presentation of peptide to $CD8^+$ T cells and subsequent clonal deletion [224]. In EAA,

decreased disease scores were associated with lower B cell counts and IgG1 and IgG2a serum levels resulting from insufficient T follicular helper cell differentiation. Mechanistic studies showed that targeting autoAg to migratory DC subsets using anti-DEC205-Ag and anti-Langerin-Ag prevented EAE onset and caused an increase in $Foxp3^+$ T cells, whereas targeting lymphoid-resident DCs with anti-DCIR2-Ag and anti-Treml4-Ag only mitigated symptoms [219]. These outcomes demonstrate the specificity and utility of using antibodies to deliver autoAg to tolerogenic APC subsets.

Soluble Ag arrays

AutoAg are being coupled to targeting proteins and peptides to deliver Ags to specific cells and internalization pathways to dictate tolerogenic Ag presentation. Soluble Ag arrays (SAgAs) are composed of hyaluronic acid polymers with grafted Ag (e.g., $PLP_{139\text{-}151}$) and a co-stimulatory molecule inhibitor (B7 inhibiting peptide). Hyaluronic acid is employed as it is hydrophilic, and its relatively large molecular weight ($\approx 10^6$ Da) provides the opportunity to conjugate many Ags/inhibitor molecules. SAgAs that co-delivered B7-inhibiting peptides with $PLP_{139\text{-}151}$ decreased clinical disease scores in the EAE model with three subcutaneous injections. The resulting decrease in co-stimulation in the context of TCR stimulation is thought to lead to the observed tolerance, as disease was only alleviated when the inhibitor and Ag were presented on the same polymer and not when any other combination of components was administered. Specifically, it is suggested that the coincident binding of signals 1 and 2 interferes with APC interaction and dampens T and B cell clonal expansion [218, 226].

Lymphocyte Reprogramming

T cells play a central role in orchestrating adaptive immune responses and their phenotypes dictate the pathophysiology of immunity and tolerance [227]. As such, they have been the target

of many tolerogenic therapies. Specifically, strategies for treating autoimmunity have explored Ag-specific Tregs, and in the case of allogeneic transplant, polyclonal populations [228]. Tregs have been extensively studied for their ability to suppress Ag-specific effector T cells, and even dampen the inflammatory effects associated with inflammatory environments that lead to epitope spreading [186]. Reprogrammed T cells with chimeric Ag receptors (CAR T cells) have been studied extensively in the field of cancer immunotherapy, but have recently been applied to immune tolerance. These engineered cells have been used as effector cells to delete autoreactive cells, and more commonly as regulatory cells that specifically target autoAg and alloAg [229-231]. Particle-based systems, though common for implementing tolerance through APCs, have also been designed to target T cells with specific Ag-reactivity resulting in a regulatory T_R1-like phenotype [7]. These T cell-targeted approaches for Ag-specific tolerance are discussed in the following section.

Regulatory T cell induction

$CD4^+CD25^+Foxp3^+$ Tregs are a critical component of peripheral tolerance mechanisms, and deficiency of Tregs is associated with severe autoimmune diseases and chronic inflammation [232]. Regulatory T cells suppress immune responses to a broad range Ags and indirectly limit immune inflammation-mediated tissue damage through multiple mechanisms [233]. Tregs actively suppress activated T cells through the production of anti-inflammatory cytokines (IL-10, IL-35, and TGF-β), cytolysis, metabolic disruption, and by targeting the maturation or function of DCs [232]. There are three main subclasses of $Foxp3^+$ Tregs that are classified by the location of their differentiation: thymus-derived Tregs (tTregs), peripherally-derived Tregs (pTregs), and *in vitro*-induced Tregs (iTregs) [234]. tTregs are effectors of central tolerance and have been shown to permit differentiation of Th1 and Th17 cells in the lymphatic system, but prevent

circulation of these effector T cells into the tissues containing cognate antigens [235, 236]. In contrast, iTregs, which are generated *in vitro* by stimulating T cells in the presence of TGF-β, are thought to suppress APCs by local release of anti-inflammatory cytokines such as IL-10 [235, 237, 238]. As a result, the APCs become less potent primers of effector T cells. iTregs have shown adept regulatory behavior, but have a phenotype that is considered incomplete compared to *in vivo* derived tTregs and pTregs. The role of pTregs is thought to be complementary to tTregs in maintaining tolerance especially by transiently bolstering tolerance in the peripheral compartment [239]. Strategies to increase Tregs and restore a healthy T cell balance have been extensively researched and reached clinical trials.

A method to generate Ag-specific Tregs *in vivo* has been developed that was effective at treating EAE and NOD diabetes in mice. Mice were treated with a systemic sublethal irradiation or depletion of B and $CD8^+$ T cells followed by administration of autoAg peptides. The irradiation of cells induced apoptosis which triggered professional phagocytes to produce TGF-β, under which the autoAg peptides directed naïve $CD4^+$ T cells to differentiate into $Foxp3^+$ Treg cells instead of effector T cells [240].

CAR T cells

The development of chimeric Ag receptor (CAR) technology more than 25 years ago for enhanced immunity by Eshher et al., has also been employed to reverse autoimmunity [230, 241]. *In vitro* expanded $CD4^+CD25^+$ Tregs were engineered with CARs directed toward the carcinoembryonic Ag (CEA), which is overexpressed in inflamed colon tissue and colon cancer. In colitis-induced by adoptive transfer of CEA-specific effector CAR T cells, adoptive transfer of CEA-specific CAR Tregs (1:1 Treg:Teff) increased the 4-wk survival to 75% compared to 25% by non-specific CAR Tregs. Tolerance was also tested in the azoxymethane-dextran sodium

sulfate (AOM-DSS) induced model that combines the pathogenesis of colitis and colon cancer. Here, treatment by CEA-specific CAR Tregs halved the average colitis score compared to non-specific CAR Tregs. Interestingly and paradoxically, treatment with CEA-specific Tregs also significantly decreased tumor burden. Whereas the anti-inflammatory effects of Tregs are often implicated in the unchecked progression of tumors, here they acted to reduce the tumor burden. The authors postulated that the CAR Tregs acted to reduce the inflammatory mediators associated with intestinal polyps resulting in a reduction in neoplastic exacerbation.

The usage of $CD19^+$ B cell depleting CAR T cells has demonstrated effective treatment of acute lymphoblastic leukemia (ALL), and has been recently adapted to target and eliminate autoreactive B cells responsible for causing pemphigus vulgaris (PV) [229, 242-244]. PV is currently treated with systemic corticosteroids, but the off-label use of rituximab (combined with IVIG therapy) has shown effectiveness in creating long-term remission. Unfortunately, the resulting B cell depletion by anti-CD20 treatment resulted in cases of patient infection and septicemia [245]. These chimeric autoantibody receptor (CAAR) T cells were used to selectively deplete B lymphocytes that produce antibodies against keratinocyte desmosome adhesion protein desmoglein 3 (Dsg3). The CAAR-T cell strategy utilizes human T cells transduced with lentiviral vectors to express transmembrane receptors with extracellular chimeric autoAg Dsg3 with an intracellular signaling CD173-CD3ζ domain [229]. The investigators demonstrated *in vitro* that these CAAR-T cells induce lysis of hybridomas producing antibodies against the extracellular cadherin domains on Dsg3, but not control hybridomas producing irrelevant antibodies. *In vivo*, the CAAR-T cells were evaluated in NSG mice infused with B cell hybridomas secreting antibodies against Dsg3 domains or with hybridomas cloned to express antibodies that target Dsg3 in human PV. Compared to control CAR treatment, Dsg3 CAARs

depleted circulating autoAg-secreting B cells, reduced the anti-Dsg3 IgG levels in serum, and prevented mucosal blistering. Interestingly, the presence of soluble anti-Dsg3 IgG did not prohibit effectiveness of the CAAR-T cells *in vitro* or *in vivo*. This successful experimental treatment of PV shows the promise of using CAAR T cells to treat B cell-mediated autoimmune disorders in an Ag-specific manner.

In contrast to CAR T cells expressing autoAgs, others have used the chimeric receptor to home toward sites containing autoAg. Loskog et al. used a lentiviral vector system to express both a CAR single-chain variable fragment (scFv) for MOG as well as to stably express Foxp3 in $CD4^+$ T cells [246]. After intranasal administration, the MOG-specific CAR Tregs, also transduced with GFP, were histologically observed in several regions of the brain and cerebellum. In the MOG-induced EAE model, MOG-specific CAR Tregs delivered at peak of disease resulted in complete remission of disease symptoms in ten days. Importantly, this treatment resulted in astrogliosis and remyelination. However, administration of mock-transduced T cells also resulted in a decrease in symptoms (but to a lesser extent). The therapeutic effect of these non-CAR T cells may have been affected by the naturally occurring Treg population, yet questions about specificity remain.

While most uses of CAR T cells for tolerance have focused on targeting specific autoAg epitopes, Levings et al. have developed a regulatory CAR T cell for treating alloreactivity by targeting HLA-A2 (A2-CAR Tregs), a major histocompatibility complex often implicated in transplant rejection [231]. The human $CD25^{hi}CD45RA^+$ A2-CAR Tregs expressed CD25, Foxp3, LAP, GARP, CTLA-4 expression. Compared to irrelevant control CAR T cells, injection of A2-CAR T cells with HLA-$A2^+$ xenogeneic PMBCs resulted in a prolongation of survival and a 2-fold increase in the time to graft versus host disease (GVHD) onset. Additionally, the A2-CAR T

cells maintained their Foxp3 expression for twice as long. When A2-CAR Tregs were infused into HLA-$A2^+$ mice with HLA-A2- PBMCs, the mice experienced no observed tissue cytotoxicity (in contrast to infusion with $CD25^-CD45RA^+$ A2-CAR T cells).

Peptide-MHC complexes on particles

Peptide-MHC (pMHC) complexes attached to the surface of crosslinked dextran-coated or PEGylated iron oxide particles (pMHC-NPs) offer a new therapeutic strategy, targeted directly at specific T cells, to treat autoimmune diseases in a disease- and organ-specific manner. To date, pMHC-NPs have demonstrated efficacy in multiple mouse models of autoimmunity (diabetes, MS, collagen-induced arthritis) using MHC class I or II complexes (Figure 2.1) [7, 173]. Importantly, as the Ag diversity in autoimmune diseases is highly complex, it has been demonstrated that pMHC-NPs that carry subdominant disease-relevant Ags show similar biological effects towards inducing tolerogenic responses as dominant Ags. In the first study, it was initially hypothesized that the delivery of multiple Ags within MHC molecules was necessary to abrogate disease in a mouse model of diabetes [173]. However, it was found that functionalization of NPs with monospecific pMHC complexes suppressed T1D progression in pre-diabetic mice as well as restored normoglycemia in recently diagnosed diabetic mice. pMHC-NPs expanded autoAg-experienced $CD8^+$ T cells that suppressed the activation and recruitment of cells with non-cognate specificities to islets. Furthermore, in a humanized mouse model of diabetes, particles coated with disease-relevant pHLA complexes restored normoglycemia. Studies showed that cognate T cells internalize these NPs without accumulating in $CD11b^+$, $CD11c^+$, or B cells. The ability to blunt disease progression was demonstrated to be due to the expansion of subsets of $CD8^+$ T cells with regulatory potential but a conventional memory-like phenotype [7, 173].

More recently [7], Clemente-Casares et al. demonstrated that pMHC II-NPs could induce Ag-specific regulatory $CD4^+$ T cell type 1 (T_R1)-like cells in various mouse models of autoimmunity as well as in humanized mice (Figure 2.7). By using ten human or mouse autoimmune-disease-relevant pMHC-NPs, the reversion of pathology was shown to be independent of genetic background or type of disease. Note that peptide-functionalized particles in NP-Ag discussed earlier did not induce T_R1 responses suggesting significantly different mechanisms of action. To induce the Ag-specific suppressive effects, pMHC-NPs rely on previous autoAg experience in the T cell repertoire whereas without previous experience, favorable outcomes were not observed. Disease suppression was dependent on IFN-γ and IL-10 as transgenic mice deficient in IFN-γ or IL-10 abrogated disease suppression. Taken together, the data from both studies support that the attachment of a single disease-related pMHC to NP could be used to suppress autoimmunity.

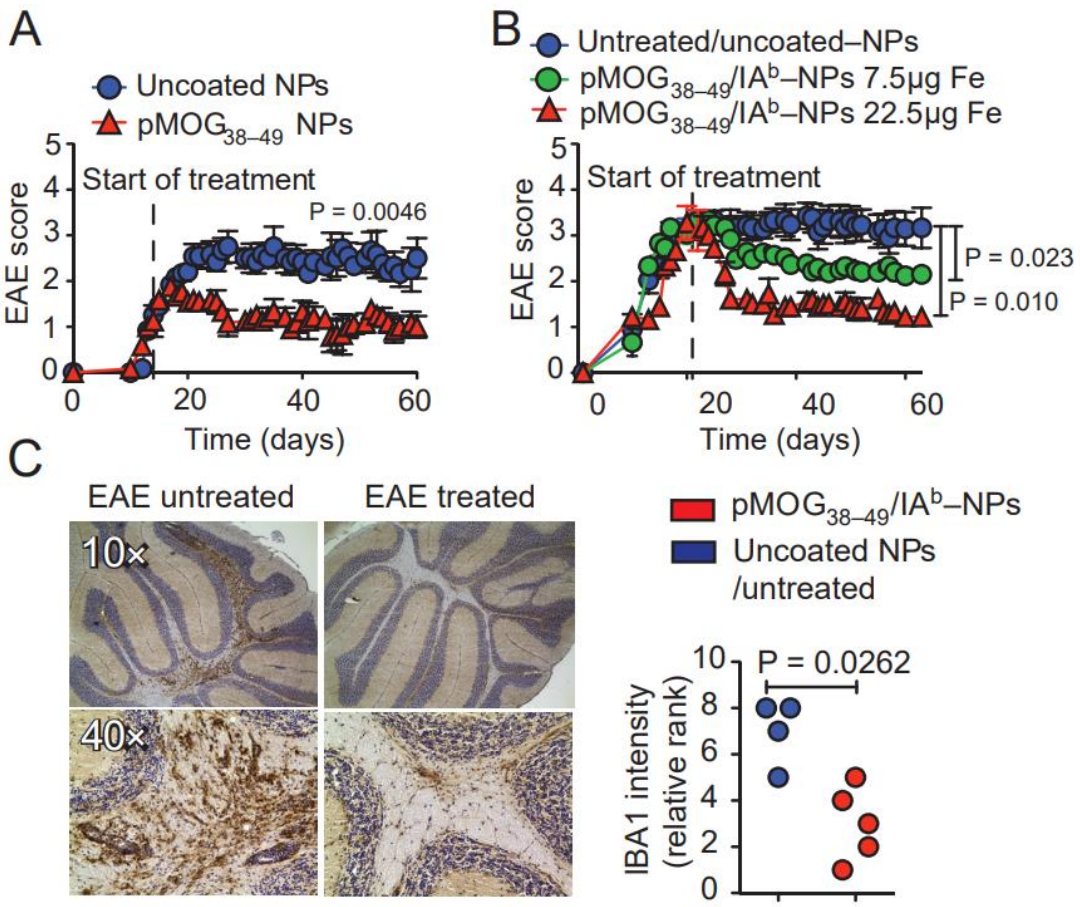


Figure 2.7: pMHC-NPs suppress MOG-induced EAE *in vivo*. C57BL/6 mice were immunized with $pMOG_{35–55}$. (A) EAE scores of mice treated from day 14 (n=4 each). (B) EAE scores of mice treated from day 21 (n=10, 7 and 3 from top). (C) Representative microglial IBA1 staining and relative rank scores in the cerebellum of mice from B (n=4–5). Reproduced with permission from [7]. ©2016 Macmillan Publishers Ltd.

Immune privileged sites

Biomaterial scaffolds have been employed for several regenerative medicine and cell transplantation applications, and more recently, these scaffolds have been designed to modulate the local environment [103, 247]. The strategy aims to mimic natural sites in the body, such as testes or eye, that intrinsically have local immunomodulation [248]. Scaffolds have been implanted that release cytokines, co-transplant cells, or locally present T-cell apoptosis inducing factor FasL [249]. While these strategies have had some efficacy in delaying rejection or promoting long-term engraftment, these strategies are not typically Ag specific, which represents an opportunity for the field.

Microporous PLG scaffolds have been used to co-transplant islets along with Tregs specific for islet Ag to enhance graft survival [250]. Islet Ag (BDC2.5)-specific Tregs were cultured in vitro and were co-incorporated with 300 NOD scid gamma (NSG) islets before implantation within the abdominal cavity. In control scaffolds lacking Tregs, no insulin-producing islet cells were detected at day 25 of implant, while islets from scaffolds containing Tregs survived significantly longer which was associated with a significant survival benefit. Interestingly, a second implant possessing islets but lacking Tregs into the kidney capsule, 97 days after the scaffold implant, did not result in rejection of those islet cells, even after removal of the original scaffold. This protection of the second islet-only transplant demonstrated a systemic tolerance. Following removal of the scaffold and kidney capsule transplant, mice became hyperglycemic, confirming that the transplanted islets were responsible for euglycemia.

Conclusion and future directions

Ag-specific therapies offer numerous advantages to improve the treatment of diseases with immune-mediated pathology. However, significant challenges remain to be addressed regarding the heterogeneity and breadth of disease-relevant Ags, understanding the molecular mechanisms of tolerance induction, the refinement of the production and characterization of therapeutics, and identifying the most favorable applications to apply Ag-specific tolerance therapies.

The wide-scale application of Ag-specific immune tolerance technologies is complex, as disease progression can be mediated by a single or many Ags and multiple immune pathways are often involved. The wide-breadth of Ags implicated in clinical disease makes it difficult to produce Ag-specific therapies especially for autoimmunity, allograft transplantation, and allergy. In diseases such as MS, additional layers of complexity exist due to processes such as epitope spreading and the relative reactivity of a patient's cells to particular autoAgs [102]. In a small

cohort of MS patients, PBMCs coupled with a library of seven relevant antigenic peptides (Ag-PBMCs) demonstrated promising results [149]. It is possible that the use of cell lysates or protein extracts containing a plethora of immunogenic epitopes may be more effective in these disorders, however, as the complexity of these Ag mixtures increases, the ease of formulation and characterization of the Ag carriers is likely to decrease. Furthermore, the low concentrations of individual Ags present in the extracts may not yield significant tolerogenic responses *in vivo* as it is likely that there is an Ag loading requirement necessary for tolerance induction. Future research targeted towards the discovery of additional epitopes will aid in the development of Ag-specific tolerogenic therapies.

Molecular mechanisms described for Ag-specific therapies are complex and not completely understood. The majority of efforts for the development of therapeutics have focused on inducing tolerogenic responses through APC or lymphocyte reprogramming (Figure 2.1). Modulation of signal 1 and signal 2 of T cell activation through APCs represents an important pathway to alter T cell activation and induce tolerance. Other mechanisms such as direct interactions of therapeutics and CAR T cells with lymphocytes to induce tolerogenic phenotypes such as Tregs and deletion represent additional methods to curb aberrant immune activation. However, as each technology is different, individual mechanisms of action need to be identified and should not be extrapolated from one to another.

Developing improved strategies to produce therapeutics that deliver peptide and protein Ags will be required to enable the large-scale progression of these technologies to the clinic. Cell-based technologies have shown promise in clinical trials, but may have limited translatability due to limited sources of cells, complicated *ex vivo* manipulations, and poor shelf-life. Particle-based therapeutics may address these issues and are expected to gain significant traction in these

applications, however, difficulties regarding scale up and controlling physicochemical properties such as size, charge, and Ag release as well as methods to characterize the presence of relevant epitopes within the particle will need to be overcome.

There is an excellent opportunity to develop novel Ag-specific therapies to improve the efficacy and long-term usability of therapeutic proteins and antibodies for which the formation of anti-drug antibodies limits their clinical applicability. ADA-specific tolerance strategies may revitalize the use of previously discovered therapies. Since the Ags are well described when tolerizing against therapeutic proteins and limiting ADAs, the use of Ag-specific tolerance therapies for this purpose is highly promising.

Acknowledgement

This work was previously published with manuscript information: R.M. Pearson, L.M. Casey, K.R. Hughes, S.D. Miller, L.D. Shea, In vivo reprogramming of immune cells: Technologies for induction of antigen-specific tolerance, Advanced Drug Delivery Reviews, (2017).

Chapter 3 Controlled Delivery of Single or Multiple Antigens in Tolerogenic Nanoparticles Using Peptide-Polymer Bioconjugates

Authors

Ryan M. Pearson[*], Liam M. Casey[*], Kevin R. Hughes, Leon Z. Wang, Madeline G. North, Daniel R. Getts, Stephen D. Miller, Lonnie D. Shea *These authors contributed equally to this work

Abstract

Polymeric nanoparticles (NPs) have demonstrated their potential to induce antigen (Ag)-specific immunological tolerance in multiple immune models and are at various stages of commercial development. Association of Ag with NPs is typically achieved through surface coupling or encapsulation methods. However, these methods have limitations that include high polydispersity, uncontrollable Ag loading and release, and possible immunogenicity. Here, using antigenic peptides conjugated to poly(lactide-co-glycolide), we developed Ag-polymer conjugate NPs (acNP) with low polydispersity, modular loading of single or multiple Ags, negligible burst release, and minimally exposed surface Ag. Tolerogenic responses of acNPs were studied *in vitro* to decouple the role of NP size, concentration, and Ag loading on regulatory T cell (Treg) induction. $CD4^+CD25^+Foxp3^+$ Treg induction was dependent on NP size, but CD25 expression of $CD4^+$ T cells was not. NP concentration and Ag loading could be modulated to achieve maximal levels of Treg induction. In relapsing-remitting experimental autoimmune encephalomyelitis (R-EAE), a murine model of multiple sclerosis, acNPs were effective in inhibiting disease induced by single or multiple peptides. The acNPs provide a simple, modular,

and well-defined platform, and the NP physicochemical properties offers potential to design and answer complex mechanistic questions surrounding NP-induced tolerance.

Introduction

T cell-mediated autoimmune diseases are major medical issues that result in a wide-range of immune dysfunctions in patients. Methods to induce antigen (Ag)-specific immune tolerance to treat T cell-mediated autoimmune diseases have the potential to attenuate aberrant activity while leaving the remainder of the immune system intact. Mechanisms to induce tolerance rely on the alteration of T cell receptor interactions with major histocompatibility complexes, reduction or inhibition of co-stimulatory molecules, engineering interactions with scavenger receptors, and the induction of tolerogenic dendritic cells (DCs) and regulatory T cells (Tregs) *in vivo* [161, 165, 177]. Initial attempts to induce tolerance employed soluble-peptides, DNA-vaccines, Ag-coupled-cells, and altered-peptide ligands [102, 103]. Of those methods, Ag-coupled cell-induced tolerance has been one of the most efficacious methods to treat autoimmune diseases and prevent transplant rejection, whereby coupling of Ags to ethylene carbodiimide-fixed splenocytes (Ag-SP) effectively induced T cell anergy and peripheral tolerance [145, 187, 251-253]. The safety and feasibility of this approach in humans was determined in a Phase 1 Clinical Trial (NCT01414634), where tolerogenic responses in both relapsing-remitting multiple sclerosis (MS) and secondary progressive MS patients were observed [149]. However, regulatory challenges, difficulty in manufacturing, and cost of producing Ag-coupled cells has driven the development of synthetic carriers to deliver the Ags for inducing tolerance.

NPs overcome many of the challenges associated with preparing Ag-SP for clinical use. Delivery of antigenic peptides or proteins associated using NPs has been reported to be efficacious in murine models of autoimmunity and cell transplantation [72, 147, 161-163, 165, 167, 169, 170].

In these studies, Ag is associated with NPs by surface coupling to pre-formed NPs (NP-Ag) or by encapsulation within NPs [NP(Ag)]. Clinical disease symptoms and progression have been substantially reduced or ameliorated with NP delivery without adverse events; however, modification of NP formulation may enhance their efficacy. Coupling of Ag to NP surfaces, as in NP-Ags, can alter the particle nanostructure resulting in increased size, polydispersity, agglomeration, and undesired immune recognition including anaphylaxis [169, 170, 254]. Encapsulation of Ag as in NP(Ag) overcomes issues related to the size and surface properties of NP-Ags. However, Ag loading by encapsulation can be variable and is dependent on Ag properties and NP synthesis conditions [255]. Furthermore, since the Ag is not covalently attached to the NP, premature/burst release of Ag can contribute to sub-optimal delivery and potentially reduced safety profiles [147, 167].

In this report, we covalently modify the carboxyl end-group of poly(lactide-co-glycolide) (PLG) with short peptide Ags and investigate their use to generate NPs (Ag-polymer conjugate NPs; acNPs) featuring precisely tunable Ag loading for immunomodulation, which has the potential to serve as a NP platform that combines the advantages of both NP-Ag and NP(Ag) while overcoming many of the inherent disadvantages of each individual system. We evaluated physicochemical properties of acNPs including particle size, zeta potential, and the release profile of Ag to determine the suitability of this bioconjugation approach for producing well-defined immune-modifying nanoparticles. $CD4^+$ T cell activation and regulatory T cell (Treg) induction were measured to determine if acNP-delivered Ag could be processed by antigen presenting cells (APCs) and efficiently presented to T cells. A functional relationship between acNP design parameters and subsequent tolerogenic responses was determined. The *in vivo* efficacy of acNP was examined using a murine model of multiple sclerosis, relapsing-remitting

experimental autoimmune encephalomyelitis (R-EAE), using particles that delivered single or multiple antigenic peptides. The potential ease of manufacturing, modular design parameters, well-defined and highly-reproducible physiochemical characteristics, tunable biological responses, and demonstrated *in vivo* efficacy may ultimately enable acNPs to provide a controlled and reproducible platform to investigate mechanisms of NP-mediated tolerance and ultimately to treat immune disorders.

Results

Synthesis of antigen-polymer conjugates and particle preparation

Encephalitogenic proteolipid peptides ($PLP_{139-151}$ or $PLP_{178-191}$) and ovalbumin peptide ($OVA_{323-339}$) were conjugated to the terminal carboxylic acid group of PLG (4200 g/mol; 0.17 dL/g) using carbodiimide chemistry (Figure 3.1A and Figure 3.7**,** Figure 3.8). Coupling efficiencies were determined by ^{1}H-NMR characterization for PLG-$OVA_{323-339}$ (73.6%), PLG-$PLP_{139-151}$ (74.1%), and PLG-$PLP_{178-191}$ (66.9%) (Figure 3.1B). Two sizes (400 nm and 80 nm) of acNP-Ags were prepared using the solvent evaporation emulsion method (S.E.) and nanoprecipitation method [256], respectively [147]. Ag loadings were controlled by admixing Ag-polymer conjugates with unmodified PLG at various ratios (Figure 3.1C) and the post-fabrication loadings of several acNP-Ags were confirmed using ^{1}H-NMR characterization (Table 3.1 and Table 3.2). Furthermore, NP-Ag and NP(Ag) were prepared as previously described (Figure 3.1C)[163, 169]. Given the coupling efficiencies of PLG-Ags, a maximum Ag loading (μg of Ag per mg of acNP-Ag) of 211 μg/mg (266 μg/mg theoretical), 218 μg/mg (274 μg/mg theoretical), and 220 μg/mg (297 μg/mg theoretical) is possible to be achieved for acNP-$PLP_{139-151}$, acNP-$PLP_{178-191}$, and acNP-$OVA_{323-339}$, respectively. The size of the acNP-Ag particles prepared by the S.E. method was minimally affected by varying the Ag loading from 0 to 25 μg/mg but increased

slightly with antigen loadings of 50 μg/mg and higher (Table 3.1). Significant aggregation was observed for NP-Ag after surface coupling of Ag to PLG particles. The sizes for acNP-Ags prepared by nanoprecipitation trended upwards with Ag loading and a maximum loading of only 2 μg/mg could be achieved as greater loadings resulted in aggregation and low recovery. The zeta potential of acNP-Ags was not impacted by the Ag loading and was highly negative (between -30 to -56 mV). Furthermore, the morphology of acNP-Ags was evaluated using SEM (Figure 3.9). acNP-Ags displayed spherical morphologies without significant structural differences between formulations. These experiments confirmed that acNP-Ags could be prepared with tunable Ag loadings and well-controlled physicochemical properties through systematic combination of PLG-Ag conjugates with unmodified PLG polymer.

Table 3.1: Size and zeta potential of the nanoparticle formulations used in this study. Ag loading (μg Ag/mg PLG) was precisely controlled by combining PLG-Ag conjugates with unmodified PLG at predetermined mixing ratios. *ac-PLG-PLP139-151, 178-191 particles contained 8 μg/mg of both PLP139-151 and PLP178-191.

Particle	Theoretical Loading (μg/mg)	Size (nm ± SD)	Zeta (mV ± SD)
NP	0	521.5 ± 23.0	-56.0 ± 0.7
NP-Cy5.5	0	454.8 ± 26.0	-39.7 ± 0.5
NP-OVA323-339	7.5	8642 ± 1300	-10.3 ± 1.8
NP(PLP139-151)	2.6	605.0 ± 12.4	-38.0 ± 0.9
acNP-OVA323-339	2	322.0 ± 4.0	-49.9 ± 4.9
acNP-OVA323-339	4	326.6 ± 5.8	-44.7 ± 1.5
acNP-OVA323-339	8	321.5 ± 8.5	-43.8 ± 1.8
acNP-OVA323-339	25	345.5 ± 5.2	-37.9 ± 0.4
acNP-OVA323-339	50	468.0 ± 6.5	-36.4 ± 0.7
acNP-OVA323-339	150	558.1 ± 5.3	-38.9 ± 0.5
acNP-PLP139-151	2.6	397.5 ± 9.8	-42.8 ± 0.6
acNP-PLP139-151	8	656.5 ± 13.7	-45.5 ± 1.4
acNP-PLP178-191	8	490.9 ± 15.0	-51.3 ± 1.0
acNP-PLP139-151, 178-191	16*	454.7 ± 17.4	-45.0 ± 0.9
NP	0	72.2 ± 1.9	-33.5 ± 1.1
NP-Cy5.5	0	79.0 ± 0.8	-31.3 ± 0.6
acNP-OVA323-339	0.1	74.8 ± 0.3	-34.5 ± 0.3
acNP-OVA323-339	0.5	85.6 ± 1.9	-31.5 ± 1.2
acNP-OVA323-339	1	103.9 ± 0.3	-32.4 ± 0.6
acNP-OVA323-339	2	112.0 ± 0.6	-32.0 ± 0.9

acNP-Ags were compared to NP-Ag and NP(Ag) for Ag-specific antibody binding to their surface using fluorescently-tagged $OVA_{323-339}$-IgG1. Encapsulation of Ag into particles has been demonstrated to reduce the potential for antibody binding to particle that could result in immune activation *in vivo* [169]. Flow cytometric analysis of antibody presence on the surface of the three particle variations demonstrated significantly less binding of IgG1 to acNP-$OVA_{323-339}$ (8 µg/mg) than NP-$OVA_{323-339}$ particles (7.5 µg/mg) (Figure 3.1D). Ag-encapsulated NP($OVA_{323-339}$) bound the least amount of IgG1, however a maximal Ag loading of only 2.6 µg/mg was achievable. The decreased IgG1 binding is suspected to result from the significantly lower Ag loading and burst release of Ag that was similarly observed for other PLG particles [147, 169]. Importantly, acNP-Ags did not display burst release of Ag compared to NP(Ag) particles and displayed less Ag release than NP-Ag, likely due to the significantly reduced surface exposed Ag (Figure 3.1E).

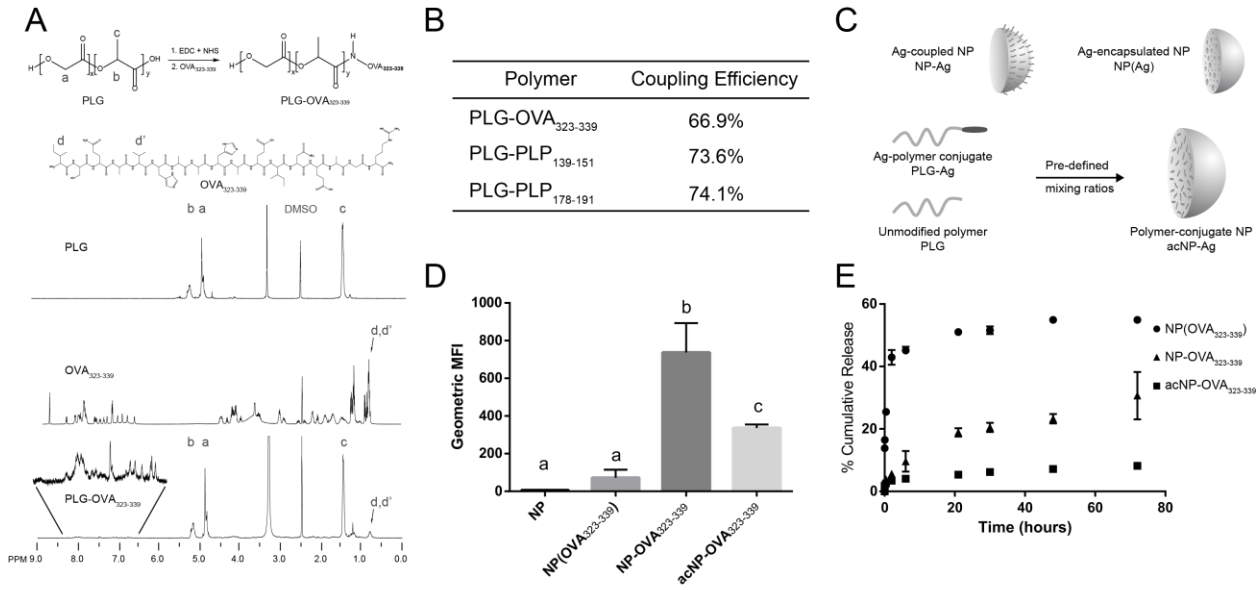


Figure 3.1: Synthesis and characterization of PLG-antigen conjugates and nanoparticle formation. (**A**) ^{1}H-NMR spectrum of PLG, $OVA_{323-339}$, and PLG-$OVA_{323-339}$ measured in DMSO-d6 (calibrated at 2.5 ppm). (**B**) The coupling efficiency of $OVA_{323-339}$ to PLG was calculated by comparing the integration values of the overlapping methyl proton peaks of leucine and isoleucine present at 1.4 ppm in $OVA_{323-339}$ (d, d') to the methylene proton peak present at 5.3 ppm in PLG (b). (C) Schematic representation of nanoparticles used in this study. (**D**) PLG, NP($OVA_{323-339}$), NP-$OVA_{323-339}$, and acNP-$OVA_{323-339}$ were incubated with FITC-labeled anti-$OVA_{323-339}$ IgG to identify the presence of peptide on the surface of the particles. Results are geometric mean fluorescence intensity. (**E**) Release profile of NP($OVA_{323-339}$), NP-$OVA_{323-339}$, and acNP-

$OVA_{323-339}$. Statistical differences between groups was determined by performing a one-way ANOVA and Tukey's Post-hoc test ($p<0.05$). Groups with similar letters indicates no statistical significance.

Regulatory T cell induction by acNP-Ags is size and antigen loading-dependent

Next, the effect of NP size and Ag loading on the ability of acNP-Ags to promote Ag presentation by dendritic cells and subsequently influence the *in vitro* activation and differentiation of naïve $CD4^+CD25^-$ T cells toward regulatory T cells (Tregs) was investigated. NPs must be internalized by APCs and the associated Ag processed for Ag presentation to T cells. Differential cellular associations (either internalization or surface association) of 80 nm and 400 nm particles were measured *in vitro*, where 80 nm particles displayed approximately 40% lower cellular interactions than 400 nm particles and a concentration of 300 µg/mL led to saturated cellular associations for both particle sizes (Figure 3.10A)**.** The size-dependent cellular associations were further confirmed by evaluating the biodistribution of particles *in vivo*. As a percentage of single cells, 80 nm particles accumulated to a relatively low extent in all organs evaluated (liver, spleen, and lungs); whereas 400 nm particles accumulated significantly in the liver and at lower levels in the spleen and lungs (Figure 3.10B).

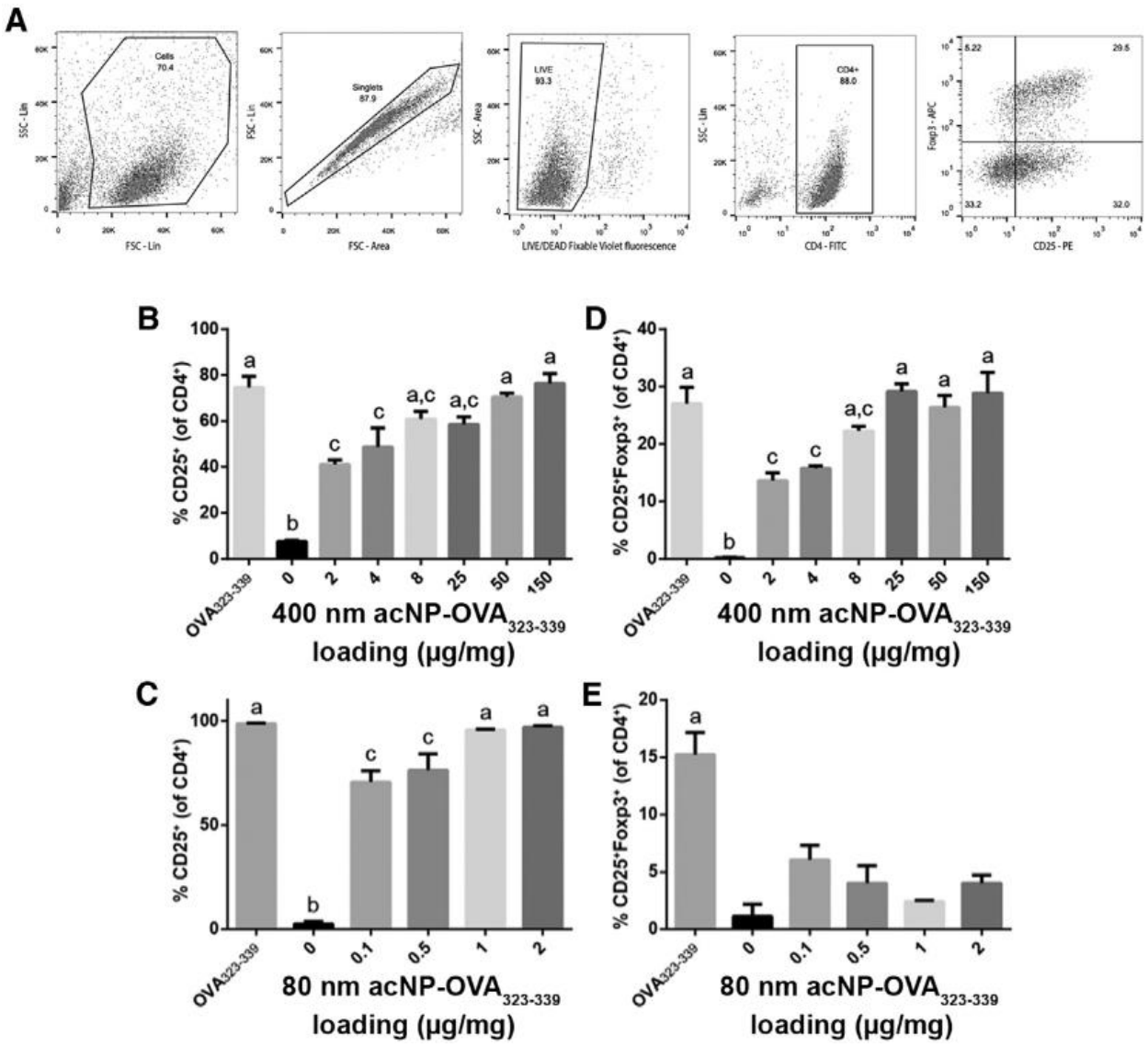


Figure 3.2 Figure 3.3: Regulatory T cell induction in vitro is dependent on nanoparticle size and Ag loading. BMDCs were treated for 3 h with 300 µg/mL of 400 nm (**B** and **D**) and 80 nm (**C** and **E**) acNP-OVA$_{323-339}$ or 100 ng/mL of soluble OVA$_{323-339}$. Excess acNP-OVA$_{323-339}$ was subsequently washed from the wells prior to addition of naïve CD4$^+$ OT-II T cells and 2 ng/mL of TGF-β1. Cells were co-cultured for 4 days prior to flow cytometric analysis. (**A**) Representative gating strategy for regulatory T cell induction. All cells, singlets, live, and CD4+ cells were examined for CD25 and Foxp3 expression. (**B** and **c**) The effect of antigen loading on CD25 and (**D** and **E**) Foxp3 expression of T cells was measured. Although both particles formulations increased CD25 expression similarly, only 400 nm acNP-OVA$_{323-339}$ particles could efficiently induce CD4$^+$CD25$^+$Foxp3$^+$ regulatory T cells. Statistical differences between groups was determined by performing a one-way ANOVA and Tukey's Post-hoc test ($p<0.05$). Groups with similar letters indicates no statistical significance.

The ability of Tregs to mediate immune tolerance *in vivo* has been previously demonstrated, supporting use of Treg induction to determine tolerogenic effects of acNP-Ags (Figure 3.2 Figure 3.3A) [237, 257, 258]. Delivery of both 80 and 400 nm acNP-OVA$_{323-339}$ to bone marrow-derived dendritic cells (BMDCs) followed by co-culture with Ag-specific naïve OTII

$CD4^+CD25^-$ T cells in the presence of TGF-β1 resulted in upregulation of CD25 on T cells, even at the lowest Ag loading conditions tested (Figure 3.2 Figure 3.3B,C). Although CD25 expression was increased in response to both acNP-$OVA_{323-339}$ particle sizes, it did not correlate with Treg induction as measured by $CD4^+$ T cells positive for both CD25 and Foxp3 expression. Tregs were induced at high levels only with the 400 nm acNP-$OVA_{323-339}$ and was dependent on Ag loading (Figure 3.2 Figure 3.3D). At an acNP-$OVA_{323-339}$ concentration of 300 μg/mL, maximal Treg induction was observed at an Ag loading of 8 μg/mg and there was no significant difference observed by increasing the loading to 150 μg/mg. acNP-$OVA_{323-339}$ with a diameter of 80 nm, regardless of Ag loading, only induced low levels of Tregs (Figure 3.2 Figure 3.3E). Taken together, the T cell expression of CD25 was particle size independent and induction of Tregs was particle size dependent. Importantly, we found that at high concentrations, acNP-$OVA_{323-339}$ up to 150 μg/mg loading were not significantly different than particles with 8 μg/mg loading for inducing Tregs *in vitro*.

Regulatory T cell induction by acNP-Ag nanoparticles is concentration-dependent

The concentration dependence of acNP-$OVA_{323-339}$ on the activation of naïve $CD4^+CD25^-$ T cells and induction of Tregs was tested using 400 nm acNP-$OVA_{323-339}$ at multiple Ag loadings (2, 8, 25, 150 μg/mg) and particle concentrations (0, 5, 10, 75, 150, and 300 μg/mL). The range of Ag delivered to the BMDCs varied from 10 to 45,000 ng/mL (Table 3.3). A minimum of 1,200 ng/mL of Ag was required to achieve CD25 expression in greater than 40% of $CD4^+$ T cells. This level of expression was achieved even at low acNP-$OVA_{323-339}$ concentrations (5-10 μg/mL) with 150 μg/mg Ag loading (Figure 3.4A). Similar CD25 expression was achieved using an acNP-$OVA_{323-339}$ concentration of 150 μg/mL and acNP-$OVA_{323-339}$ with 8 μg/mg Ag loading (1,200 ng/mL Ag delivered). CD25 expression in over 60% of $CD4^+$ T cells occurred for an Ag

concentration of 1,875 ng/mL or greater. Foxp3 expression by $CD4^+CD25^+$ T cells required a larger amount of Ag to reach the highest expression levels (Treg differentiation over 30%). Treg induction correlated to levels of CD25 expression in greater than 60% of $CD4^+$ T cells. Treg induction by acNP-$OVA_{323-339}$ was highly dependent on the total amount of Ag delivered per well. Additional Ag delivery above 1,875 ng/mL did not dramatically influence the percentage of Tregs detected *in vitro* (Figure 3.4B).

Subsequent experiments were performed using acNP-$OVA_{323-339}$ delivery to OTII splenocytes, rather than BMDCs, to assess the necessity for TGF-β1. OTII splenocytes were incubated with acNP-$OVA_{323-339}$, which were then cultured in the presence or absence of TGF-β1. Interestingly, Tregs were induced by OTII splenocytes in the absence of TGF-β1, which was not observed with BMDCs, although induction without TGF-β1 was generally to a lesser extent than conditions that included TGF-β1 (Figure 3.4C). acNP-Ags prepared with various Ag loadings enabled the determination of Ag requirements for inducing significant levels of Tregs *in vitro* and the ability to induce Tregs in the absence of TGF-β1 presents the possibility of utilizing acNP-Ags to modulate biological responses *in vivo*.

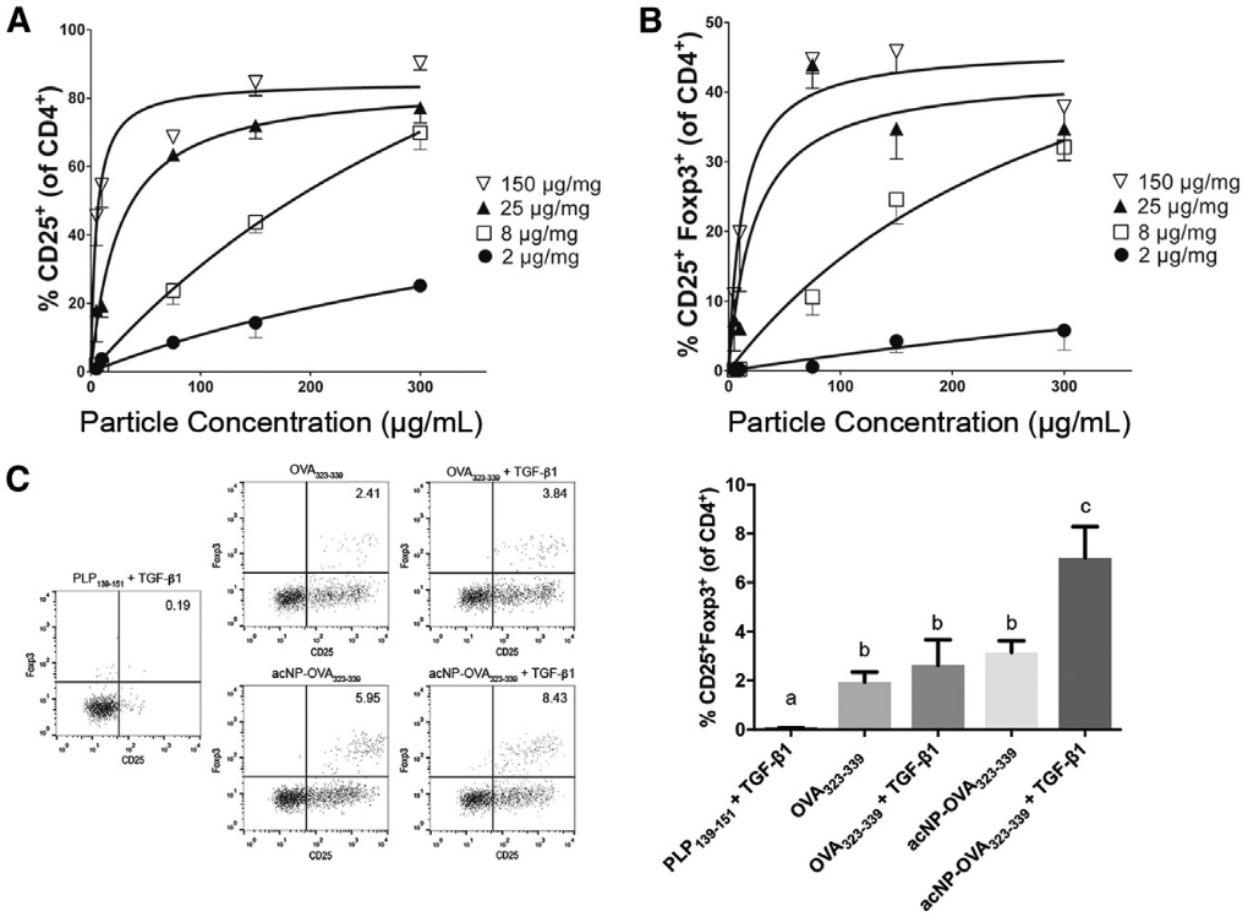


Figure 3.4: Regulatory T cell induction is dependent on nanoparticle concentration. BMDCs were treated for 3 h with various concentrations of 400 nm of acNP-OVA$_{323-339}$ (2, 8, 25, 150 μg/mg loading) formulation. Excess acNP-OVA$_{323-339}$ particles were subsequently washed from the cell surface prior to addition of OT-II T cells and 2 ng/mL of TGF-β1. The cells were co-cultured for 4 days prior to using flow cytometry to measure CD25 (**A**) and Foxp3 expression (**B**) of T cells. OT-II splenocytes were treated with soluble OVA$_{323-339}$ (100 ng/mL) or acNP-OVA$_{323-339}$ (25 μg/mg loading; 75 μg/mL) in the presence or absence of 2 ng/mL of TGF-β1. (**C**) The cells were co-cultured for 4 days prior to using flow cytometry to measure CD25 and Foxp3 expression. Statistical differences between groups was determined by performing a one-way ANOVA and Tukey's Post-hoc test ($p<0.05$). Groups with similar letters indicates no statistical significance.

acNP-Ags suppress EAE induced by PLP$_{139-151}$ immunization

The ability of acNP-Ags to induce Ag-specific immune tolerance was tested using the R-EAE disease model of MS. While the *in vitro* data support that NP internalization, Ag presentation, and Treg induction occurs, the *in vivo* study is more challenging since the NPs must reach the appropriate cell types to elicit a tolerogenic response. A previous study demonstrated tolerance induction using NP(PLP$_{139-151}$) with an Ag loading of approximately 2-3 μg/mg at a dose of 2.5 mg with two administrations, and a similar particle was prepared and used as a control [167].

Using a prophylactic disease model, particles were administered intravenously to SJL/J mice on day -7 and -1 relative to R-EAE immunization. Untreated NP($OVA_{323-339}$) control mice displayed severe clinical symptoms, whereas Ag-specific particle treated mice displayed significantly reduced disease symptoms as measured by both the mean clinical score (Figure 3.5A) and cumulative clinical score (Figure 3.4B). Importantly, acNP-$PLP_{139-151}$ were prepared with the same Ag loading (2.6 µg/mg) as NP($PLP_{139-151}$), which enabled the comparison of both particle types. acNP-$PLP_{139-151}$-treated mice displayed slight disease during the acute phase but was not significantly different ($p > 0.99$) than NP($PLP_{139-151}$). These results confirmed that acNP-Ags could effectively induce Ag-specific tolerance *in vivo*.

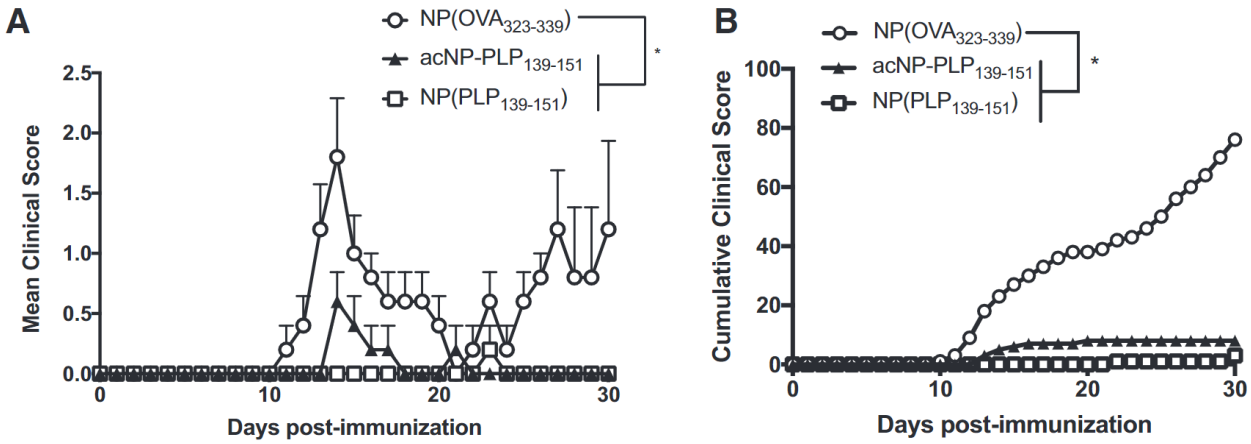


Figure 3.5: acNP-Ags prophylactically induce tolerance in R-EAE. Clinical scores for SJL/J mice treated with 2 doses of 2.5 mg of NP($OVA_{323-339}$), 2.5 mg of NP($PLP_{139-151}$) (2.6 µg/mg $PLP_{139-151}$), or 2.5 mg of acNP-$PLP_{139-151}$ (2.6 µg/mg $PLP_{139-151}$) and immunized with $PLP_{139-151}$/CFA to induce R-EAE. (**A**) Treatment of mice with nanoparticle formulations resulted in significantly abrogated clinical disease scores compared to the control. (**B**) Corresponding cumulative clinical score for mice treated with tolerogenic particles (n = 5). Differences between disease courses of different treatment groups were analyzed for statistical significance using the Kruskal-Wallis test (one-way ANOVA non-parametric test) ($p < 0.05$).

acNP-Ags suppress EAE induced with a cocktail of encephalitogenic peptides ($PLP_{139-151}$ and $PLP_{178-191}$)

Diversity in the autoreactive T cell repertoire has been well established in autoimmune diseases such as MS; therefore, tolerogenic NPs will likely need to deliver multiple epitopes to effectively treat a disease with a complex pathogenesis [259]. We tested whether multiple myelin peptide–

PLG conjugates, namely PLG-$PLP_{139-151}$ and PLG-$PLP_{178-191}$, could be incorporated into a single acNP-Ag and be used as an effective treatment for R-EAE induced by immunization with $PLP_{139-151}$/$PLP_{178-191}$/CFA (Figure 3.6A).

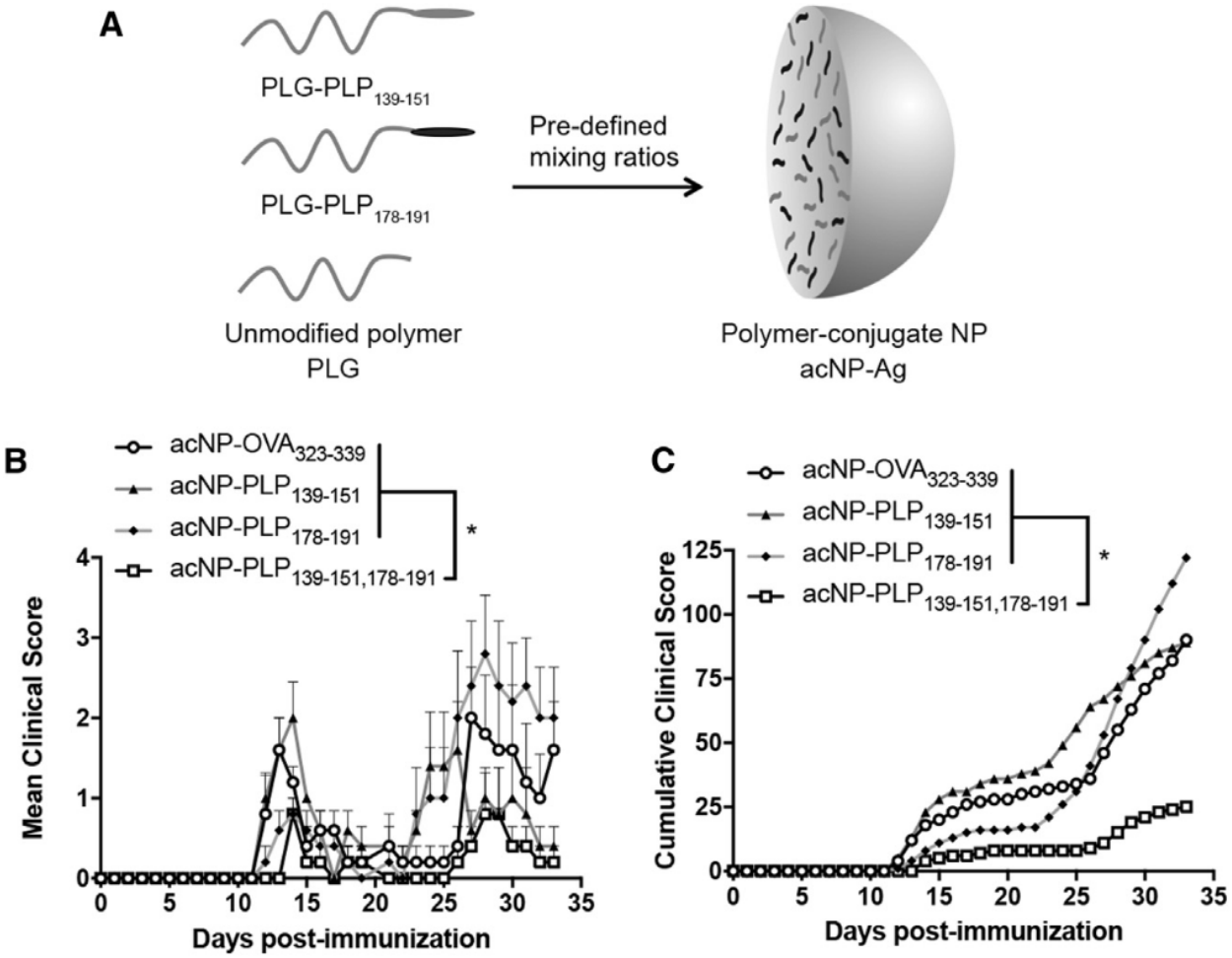


Figure 3.6: acNP-Ag particles induce protective tolerance against R-EAE induced with cocktail of autoantigens. Clinical scores of SJL/J mice treated with 1.25 mg of acNP-$OVA_{323-339}$ (8 µg/mg $OVA_{323-339}$), acNP-$PLP_{139-151}$ (8 µg/mg $PLP_{139-151}$), acNP-$PLP_{178-191}$ (8 µg/mg $PLP_{178-191}$), or acNP-$PLP_{139-151,178-191}$ (8 µg/mg $PLP_{139-151}$ and 8 µg/mg $PLP_{178-191}$) and immunized with $PLP_{139-151}$ and $PLP_{178-191}$ in CFA to induce R-EAE 7 days later. (**A**) Schematic representation of antigen-polymer conjugate nanoparticles delivering multiple Ags. (**B**) Treatment of mice with acNP-Ags formulated with both pathogenic epitopes resulted in significantly abrogated mean clinical disease scores compared to mice treated with only a single or irrelevant epitope. (**C**) Corresponding cumulative clinical score for mice treated with particles (n = 3-7). Differences between disease courses of different treatment groups were analyzed for statistical significance using the Kruskal-Wallis test (one-way ANOVA non-parametric test) ($p < 0.05$).

acNP-Ags were administered intravenously to SJL/J mice on day -7 relative to R-EAE immunization. Control mice, treated with acNP-$OVA_{323-339}$, acNP-$PLP_{139-151}$, or acNP-$PLP_{178-191}$, displayed severe clinical disease symptoms compared to acNP-$PLP_{139-151,178-191}$ as measured by

both the mean clinical score (Figure 3.6B) and cumulative clinical score (Figure 3.6C). Interestingly, it appears that mice treated with acNP-$PLP_{139-151}$ particles displayed a trend towards strong acute disease phase and a less severe relapse, in contrast to mice treated with acNP-$PLP_{178-191}$ particles, where a reduced acute disease was observed and a severe relapse occurred. However, analysis over days 11-19, 21-33, and 11-33 demonstrated no statistical differences were present between acNP-$PLP_{139-151}$ and acNP-$PLP_{178-191}$ treated animals. Mice treated with acNP-$PLP_{139-151,178-191}$ displayed significantly reduced clinical scores over the entire study period and displayed significantly less disease burden as measured by a significant diminishment in the measured cumulative scores. These results suggest the ability acNP-Ag particles to simultaneously tolerize against multiple peptides associated with the pathogenesis of disease. The modular design of acNP-Ags incorporating various Ags using a PLG-Ag conjugate "mix-and-match" approach clearly demonstrates the versatility of the acNP-Ag platform and design.

Discussion

The development of NPs for the treatment of immunological diseases holds significant promise to prevent and improve symptoms of disease and affords the opportunity to improve the efficacy with precise control over their size, Ag loading, and Ag release. NP-based formulations are typically prepared by coupling Ag to the surface of particles (i.e. NP-Ag) or encapsulation of Ag within particles (i.e. NP(Ag)) [17, 72, 147, 161-163, 165-167, 169, 170]. Here, we hypothesized that the preparation of NP from Ag-polymer conjugates would dramatically improve NP physicochemical properties to produce a more well-defined and clinically translatable platform than NP-Ag or NP(Ag). Ag-polymer conjugates were synthesized at high coupling efficiency using carbodiimide chemistry. This methodology enables acNP-Ag particles to be formed with

controlled and reproducible Ag loadings which are only limited by the polymer:Ag molecular weight ratio and the coupling efficiency of Ag to polymer. It should be noted that in our studies we have used short peptide Ags and further optimization may be required to employ this conjugation strategy to highly charged or longer length peptides or proteins. Unlike NP-Ag, acNP-Ags display consistent sizes and zeta potentials following single- or multiple-Ag incorporation. Furthermore, acNP-Ags bound less Ag-specific IgG1 at similar Ag loading than NP-Ag indicating a reduced potential for causing antibody-induced immune recognition (Figure 3.1 and Table 3.1) [169].

The studies herein have identified a relationship between Ag loading and dosing requirements for efficient BMDC processing and Ag presentation resulting in induced tolerogenic T cell responses (Figure 3.2 Figure 3.3 and Figure 3.4). CD25 expression on T cells reached high levels even at low Ag loadings and was independent of acNP-Ag size, confirming that Ag was effectively processed by BMDCs and presented to T cells. Treg induction, however, was size-dependent and required Ag loadings greater than 8 μg/mg to reach maximal levels. Interestingly, the total amount of Ag delivered to BMDCs affected the efficiency of Treg induction. Using 400 nm acNP-Ags, at least 1,875 ng/mL of Ag was required to yield the greatest percentage of Treg induction (over 30% of $CD4^+$ cells). These *in vitro* studies provide insight into the minimal Ag doses required for tolerance induction, allowing for a more rational design of future *in vivo* studies.

The feasibility of Ag-polymer conjugate incorporation into particles for tolerance induction was demonstrated *in vivo* using a prophylactic R-EAE model. Ag-encapsulated NP($PLP_{139-151}$) were used as a control due to their demonstrated tolerance induction in our previous work [167]. acNP-$PLP_{139-151}$ significantly reduced disease initiation and suppressed relapse symptoms (Figure

3.5) similarly to NP($PLP_{139-151}$). The highly negative surface charge of acNP-Ag (less than -30 mV) has been proposed to facilitate their *in vivo* uptake by marginal zone macrophages expressing the MARCO scavenger receptor [160, 161]. Notably, acNP-$PLP_{139-151}$ achieved similar tolerogenic efficacy as NP($PLP_{139-151}$) when delivered at the same dose (2.5 mg) and Ag-loading (2.6 μg/mg).

Tolerogenic acNP-Ags can be formulated to incorporate multiple Ags responsible for the pathogenesis of MS and represents a significant advancement towards achieving a comprehensive therapy. An array of autoAgs implicated in human MS could be simultaneously delivered using this platform [149]. Although not complete, several of the pathogenic autoantigens in MS have been identified from proteins within the myelin sheath such as myelin basic protein (MBP), myelin oligodendrocyte protein (MOG), and proteolipid protein (PLP), and have been well-established as drivers for the autoreactive immune response. Smith et al. employed a cocktail of four encephalitogenic peptides to induce tolerance in an R-EAE model using Ag-SP [187]. Interestingly, they demonstrated that the preventative tolerance model prevented activation of autoreactive Th1 cells and subsequent infiltration of inflammatory cells into the central nervous system. Furthermore, in the therapeutic tolerance model, treatment significantly increased the production of anti-inflammatory cytokines TGF-β and IL-10 in the peripheral and central nervous system. Recently, a phase 1 clinical trial using a cocktail of seven myelin peptides coupled to autologous peripheral blood mononuclear cells demonstrated decreases in Ag-specific T cell responses in MS patients [149]. This clinical trial found promising results, but cell-based therapies are expensive and may have difficulty reaching wide-spread implementation due to the need to manipulate patient cells *ex vivo*.

Here, we have demonstrated that two myelin peptides ($PLP_{139-151}$ and $PLP_{178-191}$) are successfully coupled to PLG forming Ag-polymer conjugates and combined in precise ratios during the particle fabrication to produce a single acNP-$PLP_{139-151,178-191}$ particle. These particles inhibited initiation of active R-EAE induced by a mixture of the two peptides (Figure 3.6). Particles that delivered only a single peptide (acNP-$PLP_{139-151}$ or acNP-$PLP_{178-191}$) had minimal effects and were not significantly more effective than acNP-$OVA_{323-339}$ particles containing irrelevant peptide. Importantly, our tolerogenic acNP-Ags are not patient-specific and offer numerous advantageous over cell-based therapies including lower cost, lower variability, greater control over physicochemical properties (size, zeta potential, Ag loading, and release), greater shelf-life, easier handling, and better scalability.

Soluble peptide, Ag-coupled cells, genetically engineered food products, and particles have been investigated as treatment options for applications including allergy, autoimmune disease, and cell transplantation [103, 151]. An advantage of acNP-Ags over current nano-based tolerance platforms is that tolerance induction by acNP-Ags is achieved without co-delivery of immunosuppressive agents that have been associated with many side effects [103]. Differences in uptake mechanism and context of Ag presentation of acNP-Ags may partially account for platforms such as soluble Ag arrays [218], tolerogenic nanoparticles (tNPs) [162], and PEGylated gold nanoparticles [163] requiring co-delivery of various immunomodulatory agents to induce tolerance. The results presented herein demonstrate a novel NP platform that achieves precise control over Ag delivery and tolerogenic responses *in vivo* to single- or multiple-disease initiating epitopes. This controllable Ag delivery platform enabled the identification of the relationship between Ag loading, concentration, and size of acNP-Ags with respect to the activation of T cells and induction of Tregs *in vitro*.

The ability to incorporate well-defined quantities of Ag into acNP-Ags using various Ag-polymer conjugates will allow for future studies to identify important characteristics of tolerogenic particle platforms. Furthermore, incorporation of one or more Ags into a single acNP-Ag will enable the clinical development of a particle platform capable of treating a variety of disorders in which aberrant immune responses underlies disease pathogenesis, such as autoimmune diseases and allergies.

Materials and Methods

Poly(lactide-co-glycolide) (50:50) (PLG) with a single carboxylic acid end-group and an inherent viscosity of 0.17 dL/g in hexafluoro-2-propanol was purchased from Lactel Absorbable Polymers (Birmingham, AL). Poly(ethylene-alt-maleic anhydride) (PEMA) was purchased from Polysciences, Inc. (Warrington, PA). Amine-terminated ovalbumin peptide (NH_2-$OVA_{323-339}$) and proteolipid peptide (NH_2-$PLP_{139-151}$ or NH_2-$PLP_{178-191}$) was purchased from Genscript (Piscataway, NJ). All other reagents were purchased from Sigma Aldrich (St. Louis, MO) unless noted otherwise.

PLG-Ag conjugation

PLG (37.8 mg, 0.009 mmol, 4200 g/mol) of was dissolved in 2 mL of N,N-dimethylformamide (DMF) in a 20 mL scintillation vial equipped with a stir bar. N-(3-Dimethylaminopropyl)-N'-ethylcarbodiimide hydrochloride (EDC) (9.0 mg, 0.047 mmol, 5X to PLG) was dissolved in 0.5 mL of DMF and added dropwise to the PLG solution. N-Hydroxysuccinimide (NHS) (5.5 mg, 0.047 mmol, 5X to PLG) was dissolved in 0.5 mL DMF and added dropwise to the solution. The reaction was allowed to stir for 15 minutes at room temperature. Antigenic peptide (1.2X to PLG) was dissolved in a solution of 1 mL dimethyl sulfoxide (DMSO) and 0.5 mL DMF and stirred at 400 RPM. Triethylamine (5X to peptide) was added to peptide solution and the mixture

was added dropwise to the stirring PLG solution. The reaction was allowed to proceed overnight at room temperature. The resulting polymer was isolated and purified by dialysis using 3,500 molecular weight cut-off membrane against four liters of distilled water over two days. Distilled water was replaced a total of six times. The dialyzed polymer was collected and washed with MilliQ water three times MilliQ water by centrifugation at 7000 x g before resuspension in 20 mL of water and lyophilization for two days. Coupling efficiency peptide to PLG was determined by ^{1}H-NMR analysis in DMSO-d6.

Mice

Female SJL/J mice (6-8 weeks) were purchased from Envigo (Indianapolis, IN). C57BL/6J mice (6-8 weeks) and OT-II mice (B6.Cg-Tg(TcraTcrb)425Cbn/J) were purchased from Jackson Laboratory (Bar Harbor, ME). All mice were housed under specific pathogen-free conditions in the University of Michigan Unit for Laboratory Animal Medicine and maintained according to protocols approved by the University of Michigan Animal Care and Use Committee.

Nanoparticle preparation

Nanoparticles (acNP-Ags) of two different sizes (80 and 400 nm) were prepared following either the nanoprecipitation or emulsion solvent evaporation (S.E.) method, respectively. To produce acNP-Ag using the S.E. method, Ag-polymer conjugates were combined with unmodified PLG at various ratios to give calculated Ag loadings in particles as described in Table 1. The method has been described in our previous publications [167, 170]. To prepare smaller, approximately 80-120 nm acNP-Ags, the nanoprecipitation method was employed [256]. Briefly, 100 mg of PLG (Ag-polymer conjugates and unmodified PLG at desired ratios) was dissolved in acetonitrile at a concentration of 1 mg/mL and poured into 300 mL of MilliQ water under rapid stirring. The solutions were stirred for 24-48 h to completely remove residual acetonitrile. The

acNP-Ags were recovered using an ultracentrifuge membrane filter 10 kDa MWCO at 4000 x g. Cryoprotectants (4% (w/v) sucrose and 3% (w/v) mannitol) were then added to the particles before lyophilization. Cy5.5-labeled NPs (NP-Cy5.5) were prepared by incorporating 1% w/w of PLG-Cy5.5 into particles as described in our previous publication [167].

Nanoparticle characterization

The size and zeta potential of the acNPs was determined by dynamic light scattering (DLS) by mixing 10 μL of a 25 mg/mL particle solution into 990 μL of MilliQ water using a Malvern Zetasizer ZSP (Westborough, MA). The release of peptide from NP($OVA_{323-339}$), NP-$OVA_{323-339}$, and acNP-$OVA_{323-339}$ particles was measured over 72 hr. Approximately 8 mg of each particle was dispersed in 1 mL of PBS and incubated at 37 °C. At pre-determined time points, the particles were centrifuged at 7000 x g for 5 min and 0.5 mL of supernatant was collected. The particles were resuspended, and 0.5 mL of fresh PBS was added to each sample. All supernatant samples were stored at -20 °C until the experiment was completed. After the final time point, the pellet of particles was dissolved in DMSO and the total amount of remaining protein was determined. Peptide content was determined using the Micro BCA assay (Pierce, Waltham, MA). The surface morphology of acNPs was examined using scanning electron microscopy (SEM, FEI/Philips XL30 FEG). Lyophilized particles were washed with MilliQ water to remove the cryoprotectant. A drop of particle suspension was placed on carbon adhesive tape, mounted onto an aluminum stub, and dried for at least 2 hr. Samples were sputter coated using gold and visualized at an accelerating voltage of 5 kV and 7 mm working distance.

$OVA_{323-339}$-IgG1 binding *in vitro*

$OVA_{323-339}$ antibody (Innovagen, Sweden) was fluorescently labeled with FITC using Abcam Easy Link FITC Conjugation Kit (Abcam, Cambridge, MA). 20 μg of $OVA_{323-339}$-associated

particles were incubated with 1 µg/mL FITC-labeled $OVA_{323-339}$ antibody for 20 min at 4 °C in DPBS containing bovine serum albumin and washed 3 times. Fluorescence was measured using a Beckman Coulter CyAn ADP Analyzer (Indianapolis, IN). Statistical differences between groups was determined by performing a one-way ANOVA and Tukey's Post-hoc test ($p<0.05$).

Cell culture

BMDC were generated from the bone marrow of C57BL/6J mice using the Lutz protocol [260]. Media consisted of RPMI containing L-glutamine (Life Technologies, Carlsbad, CA) supplemented with penicillin (100 units/mL), streptomycin (100 mg/mL), 10% heat-inactivated fetal bovine serum (FBS) (Invitrogen Corporation, Carlsbad, CA) and 50 mM β-mercaptoethanol (Sigma Aldrich). GM-CSF (Peprotech, Rocky Hill, NJ) was added at 20 ng/mL, and media was added on days 3, 6, and 8. T cell media was similar but without GM-CSF or β-mercaptoethanol and supplemented with 1 mM sodium pyruvate, and 0.1 mM non-essential amino acids (Life Technologies, Carlsbad, CA).

Antibodies and flow cytometry

FcR blocking was performed with anti-CD16/32 (Biolegend) prior to staining with various combinations of the following antibodies: anti-CD4 (RM4-5), -CD25 (PC61) (Biolegend), and -Foxp3 (FJK-16s) (eBioscience, San Diego, CA). Viability was assessed with fixable violet dead cell stain kit (Invitrogen, Carlsbad, CA). Foxp3 staining was performed with eBioscience staining kit according to the manufacturer's protocol. Flow cytometric data were collected using a Beckman Coulter CyAn ADP Analyzer. Analysis was performed using FlowJo (FlowJo, Ashland, OR).

Cell isolation and *in vitro* Treg induction assay

Treg induction assays were carried out with slight modifications as described. $CD4^+CD25^-Foxp3^-$ T cells were isolated from the spleen of OT-II mice using a naïve $CD4^+$ T cell isolation kit (Miltenyi Biotec, San Diego, CA). The assay was carried out in T cell media. BMDCs (2×10^4/well) were seeded into 96-well round-bottom cell culture plates and incubated with acNP-$OVA_{323-339}$ of various particle concentrations and Ag loadings for 3 hours. Following incubation, all wells were washed to remove excess particles that had not been internalized by cells. Cells were co-cultured with 2×10^4/well naïve T cells in the presence of 2 ng/mL TGF-β1 (Cell Signaling Technology, Danvers, MA). Groups receiving antigen in lieu of acNP-$OVA_{323-339}$ received soluble $OVA_{323-339}$ (100 ng/mL) at this time. For Treg induction experiments using splenocytes, an OTII spleen was obtained and splenocytes were isolated by lysing red blood cells using ACK lysis buffer. 2×10^5/well splenocytes were added to each well to be assayed with various combinations of acNP-$OVA_{323-339}$ particles or $OVA_{323-339}$ peptide with or without 2 ng/mL TGF-β1. For particle-treated groups, a concentration of 75 μg/mL was used. After 4 days of co-culture, the T cells were collected, stained for viability, CD4, CD25, and Foxp3, and analyzed using flow cytometry. Statistical differences between groups was determined by performing a one-way ANOVA and Tukey's Post-hoc test ($p<0.05$).

R-EAE disease induction and measurement

R-EAE was induced by immunization with encephalitogenic peptides as previously described [261]. To induce R-EAE with $PLP_{139-151}$ or both $PLP_{139-151}$ and $PLP_{178-191}$, mice were immunized by s.c. administration of 100 μL of 1 mg/mL $PLP_{139-151}$/complete Freund's adjuvant (CFA) or 0.25 mg/mL of $PLP_{139-151}$/CFA and 0.5 mg/mL of $PLP_{178-191}$/CFA, respectively, distributed over 3 spots on the nape and hind flanks of SJL/J mice. Disease severity in individual mice was

assessed using a 0 to 5 point scale: 0 = no disease, 1 = limp tail or hind limb weakness, 2 = limp tail and hind limb weakness, 3 = partial hind limb paralysis, 4 = complete hind limb paralysis, 5 = moribund. The cumulative clinical score was calculated by summing the daily EAE scores of all mice included in the studies. The cumulative clinical score was used as an indicator of overall disease burden in mice. Differences between disease courses of different treatment groups were analyzed for statistical significance using the Kruskal-Wallis test (one-way ANOVA non-parametric test).

Acknowledgements:

This work was previously published with manuscript information: R.M. Pearson, L.M. Casey, K.R. Hughes, L.Z. Wang, M.G. North, D.R. Getts, S.D. Miller, L.D. Shea, Controlled Delivery of Single or Multiple Antigens in Tolerogenic Nanoparticles using Peptide-polymer Bioconjugates, Molecular Therapy, (2017).

Supplementary Tables and Figures

Table 3.2: Determination of acNP-Ag loading using ^{1}H-NMR. Lyophilized acNP-Ag particles were dissolved in DMSO-d6 and the protein content was determined by comparing the integration values of the overlapping methyl proton peaks of leucine and isoleucine to the methylene proton peak present in PLG.

Particle	Theoretical Loading (μg/mg)	Measured Loading (μg/mg)
NP	0	0
acPLG-OVA$_{323-339}$	8	8.6
acPLG-OVA$_{323-339}$	25	24.9
acPLG-OVA$_{323-339}$	50	51.7
acPLG-OVA$_{323-339}$	150	162.6
acPLG-PLP$_{139-151}$	2.6	3.0
acPLG-PLP$_{139-151}$	8	8.9

Table 3.3: Concentration (ng/mL) of antigen delivered per well as a function of acNP-OVA$_{323-339}$ concentration and loading. Orange colored cells represent the protein loadings evaluated in Figure 3.4.

	Particle concentration (μg/mL)					
	0	5	10	75	150	300
0	0	0	0	0	0	0

Particle loading (µg/mg)	2	0	10	20	150	300	600
	4	0	20	40	300	600	1200
	8	0	40	80	600	1200	2400
	25	0	135	250	1875	3750	7500
	50	0	250	500	3750	7500	15000
	150	0	750	1500	11250	22500	45000

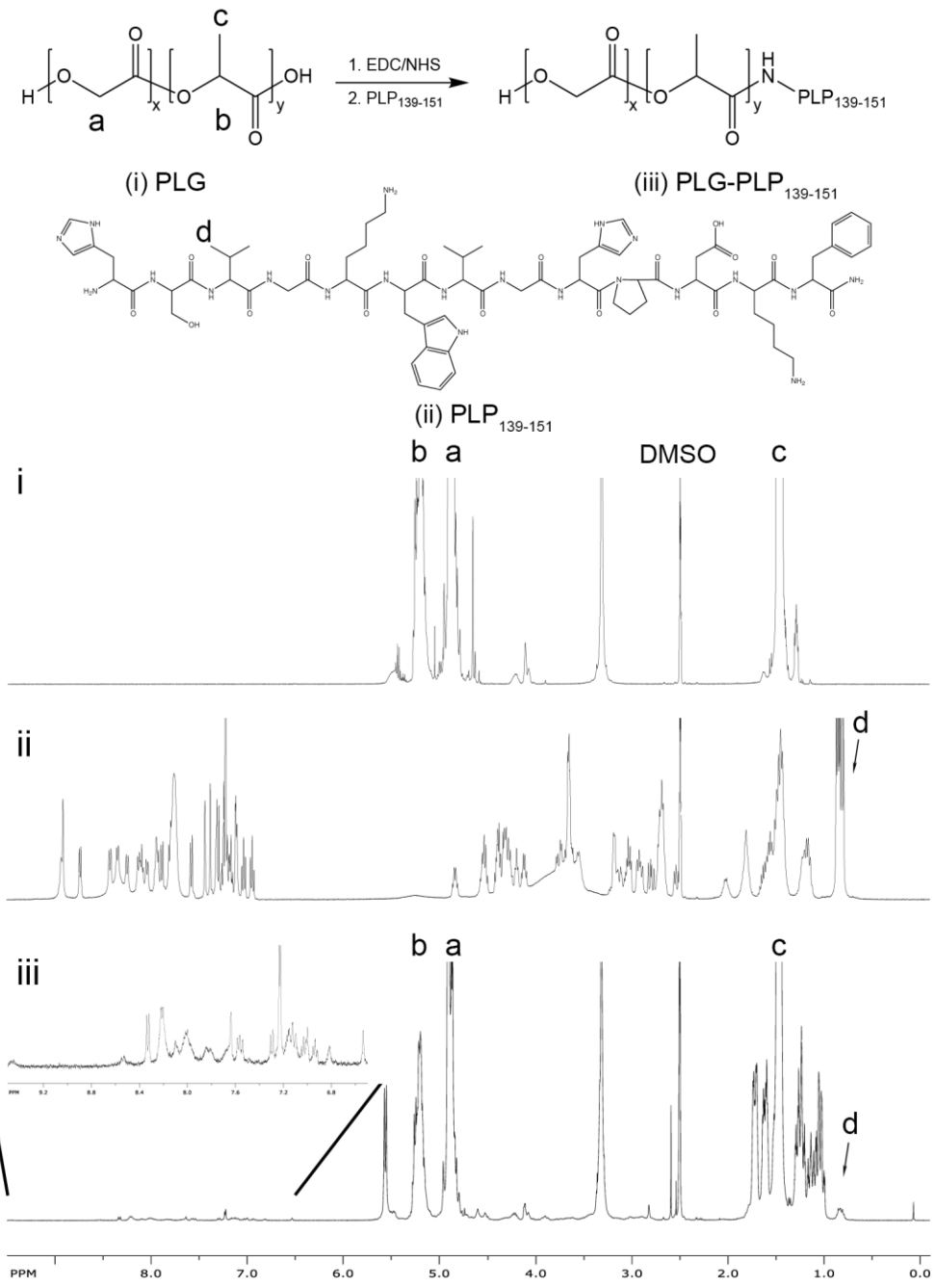


Figure 3.7: Synthesis and characterization of PLG-PLP$_{139\text{-}151}$ conjugates. ^{1}H-NMR spectrum of **(i)** PLG, **(ii)** PLP$_{139\text{-}151}$, and **(iii)** PLG-PLP$_{139\text{-}151}$ measured in DMSO-d6 (calibrated at 2.5 ppm).

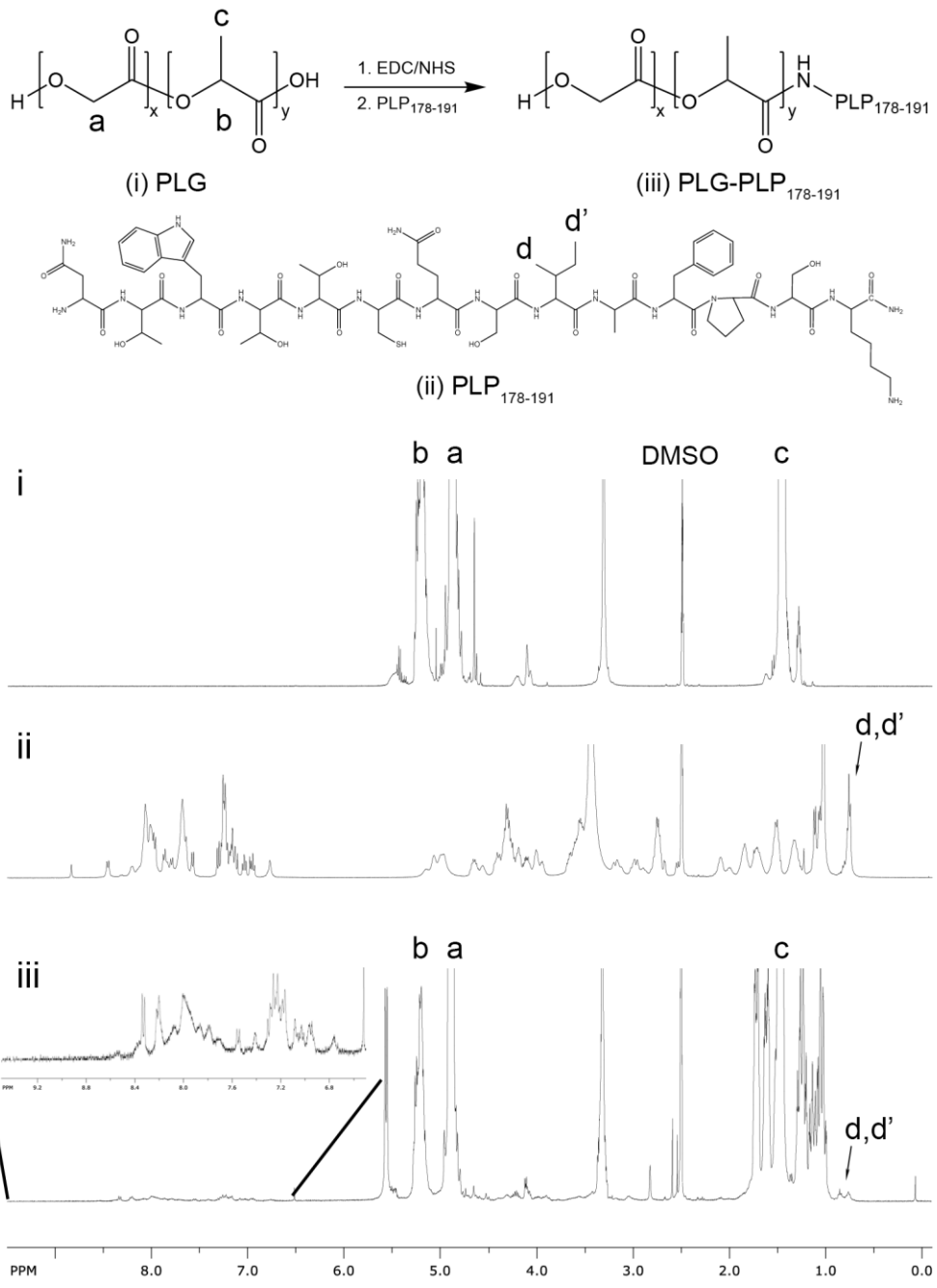


Figure 3.8: Synthesis and characterization of PLG-PLP$_{178\text{-}191}$ conjugates. ^{1}H-NMR spectrum of **(i)** PLG, **(ii)** PLP$_{178\text{-}191}$, and **(iii)** PLG-PLP$_{178\text{-}191}$ measured in DMSO-d6 (calibrated at 2.5 ppm).

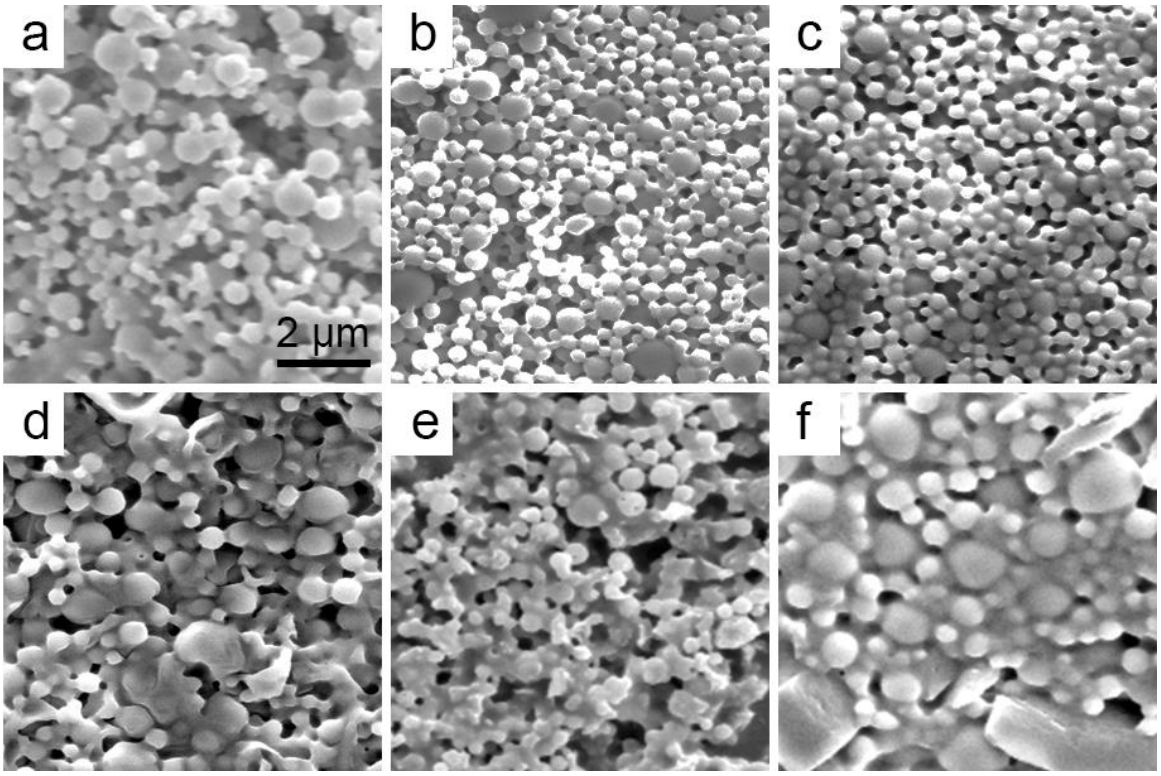


Figure 3.9: SEM images of various acNP particle formulations utilized in this study. **(a)** NP; **(b)** acNP-OVA$_{323-339}$ (8 µg/mg); **(c)** acNP-OVA$_{323-339}$ (25 µg/mg); **(d)** acNP-OVA$_{323-339}$ (50 µg/mg); **(e)** acNP-OVA$_{323-339}$ (150 µg/mg); **(f)** acNP-PLP$_{139-151,\ 178-191}$ (16 µg/mg). Scale bar: 2 µm.

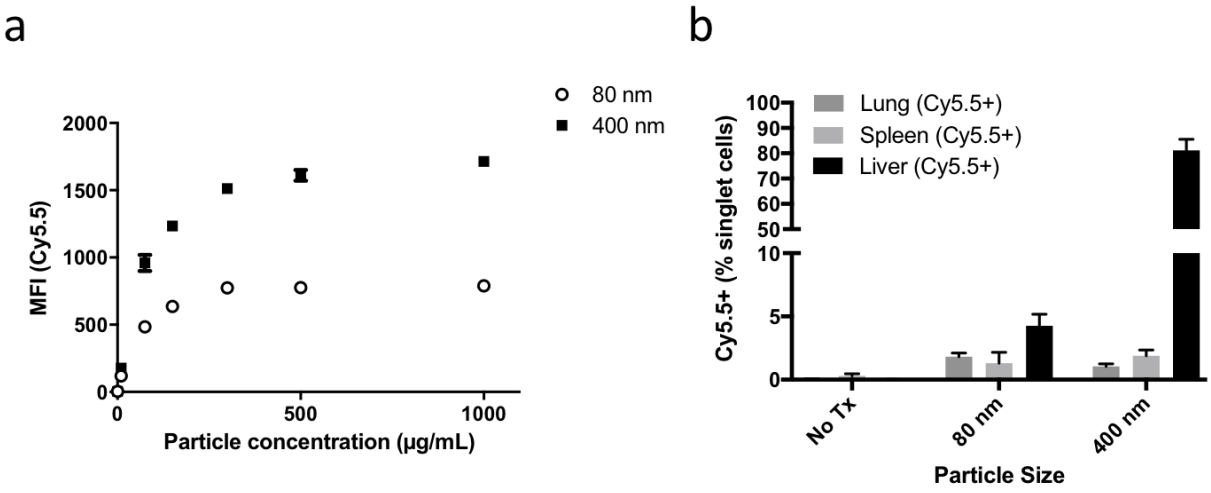


Figure 3.10: Size-dependent cellular interactions and biodistribution of Cy5.5-labelled 80 nm or 400 nm PLG particles. **(a)** Bone marrow-derived dendritic cells were treated with particles at various concentrations for 3 hr. Maximum cellular associations were observed for both particles at 300 µg/mL and were not increased when the concentration was increased to 1 mg/mL (n=3).

(b) Size-dependent biodistribution of 80 or 400 nm particles in the liver, spleen, and lungs. 1.25 mg of each particle type was intravenously administered to SJL/J mice and 24 h following particle administration, the mice were euthanized, and cellular fluorescence was analyzed. A significantly lower percentage of 80 nm particles accumulated in the organs evaluated. 400 nm particles accumulated significantly in the liver and to a much lesser extent that was comparable to the 80 nm particle in the spleen and lungs (n=3). No Tx; no treatment.

Chapter 4 Conjugation of Transforming Growth Factor Beta to Antigen-Loaded Poly(lactide-co-glycolide) Nanoparticles Enhances Efficiency of Antigen-Specific Tolerance

Authors

Liam M. Casey*, Ryan M. Pearson*, Kevin R. Hughes, Jeffrey M.H. Liu, Justin A. Rose, Madeleine G. North, Leon Z. Wang, Mei Lei, Stephen D. Miller, Lonnie D. Shea *These authors contributed equally to this work

Abstract

Current strategies for treating autoimmunity involve the administration of broad-acting immunosuppressive agents that impair healthy immunity. Intravenous (i.v.) administration of poly(lactide-co-glycolide) nanoparticles (NPs) containing disease-relevant antigens (Ag-NPs) have demonstrated antigen(Ag)-specific immune tolerance in models of autoimmunity. However, subcutaneous (s.c.) delivery of Ag-NPs has not been effective. This investigation tested the hypothesis that co-delivery of the immunomodulatory cytokine, transforming growth factor beta 1 (TGF-β), on Ag-NPs would modulate the immune response to Ag-NPs and improve the efficiency of tolerance induction. TGF-β was coupled to the surface of Ag-NPs such that the loading of Ag and TGF-β were independently tunable. The particles demonstrated bioactive delivery of Ag and TGF-β *in vitro* by reducing the inflammatory phenotype of bone marrow-derived dendritic cells and inducing regulatory T cells in a co-culture system. Using an *in vivo* mouse model for multiple sclerosis, experimental autoimmune encephalomyelitis, TGF-β co-delivery on Ag-NPs resulted in improved efficacy at lower doses by i.v. administration and significantly reduced disease severity by s.c. administration. This study demonstrates that the co-

delivery of immunomodulatory cytokines on Ag-NPs may enhance the efficacy of Ag-specific tolerance therapies by programming Ag presenting cells for more efficient tolerance induction.

Introduction

Millions of Americans are affected by an autoimmune disorder, and the currently available treatments address the clinical symptoms but are not considered curative. Autoimmunity arises from abnormal immune recognition of endogenous antigens (Ags) resulting in the self-destruction of the body's vital tissues [103, 262]. Clinically available treatment strategies attempt to mitigate symptoms using immunosuppressive molecules and biologics that non-specifically block entire immune pathways which can leave individuals susceptible to opportunistic infections and neoplastic growths [104, 106, 263]. Rather than non-specifically blocking immune responses, strategies that can block responses to specific Ag have the potential to address the pathology of disease while leaving protective immunity intact.

Peptide- and protein-loaded nanoparticles (NPs) have been developed as strategies to induce Ag-specific immune tolerance [103, 262]. NPs comprised of biodegradable polymers have been formulated with Ag encapsulated, surface-bound, or conjugated to the bulk polymer of the NP. These various Ag-NPs platforms have demonstrated transplantation tolerance and abrogation of Th1/17- and Th2-mediated hypersensitivity [72, 147, 161-163, 169, 170, 172, 264, 265]. Strategies that employ Ag-NPs are frequently administered intravenously (i.v.), where they distribute to the liver and spleen and are cleared by Ag presenting cells (APCs) in a fashion that resembles the body's natural clearance of apoptotic cells. The negative charge of the particles has been associated with increased internalization by macrophages resulting in Ag presentation and anti-inflammatory signaling by IL-10 and regulatory T cell (Treg) production [151, 161]. Although Ag-NPs have not been evaluated for toxicity, dose escalation studies have

demonstrated toxicity of similar polyester NPs at high doses, which motivates the design of Ag-NPs that induce tolerance efficiently at lower doses [266, 267]. Additionally, despite advances in i.v.-induced NP tolerance, Ag-specific tolerance by subcutaneously (s.c.)-delivered NPs has not yet been realized without the use of other anti-inflammatory mediators such as IL-10, antisense oligonucleotides, or the immunosuppressive agent rapamycin [162, 164, 268]. As a s.c. administered therapy, Ag-NP-induced tolerance could be more accessible to patients outside of the hospital setting, increasing the societal impact of this treatment. Overcoming the immunological barriers with s.c. administration motivates the use of anti-inflammatory cytokines in NP immune therapy.

Transforming growth factor beta 1 (TGF-β) is a pleiotropic cytokine that reduces inflammation, maintains peripheral tolerance, and importantly, has been shown to impart and maintain protective tolerance in models of autoimmunity [269]. Previous studies have shown that TGF-β injections can delay and prevent disease onset in relapsing-remitting experimental autoimmune encephalomyelitis (EAE), a mouse model of multiple sclerosis (MS). Repeated s.c. injections of TGF-β reduced the occurrence and severity of EAE in mice adoptively transferred with active myelin basic protein (MBP)-specific T cells [270]. When administered i.v., TGF-β decreased the severity of EAE symptoms in new and ongoing disease [271]. Mechanistically, mice lacking functional TGF-β receptor II (TGF-βRII) on their dendritic cells showed increased severity of EAE disease symptoms, and spontaneously developed EAE symptoms when crossed with mice containing only myelin oligodendrocyte glycoprotein (MOG)-specific T cell receptors [272]. Thus, TGF-β signaling plays a vital role in preventing the pathological onset of autoimmune inflammation. However, due to its pleiotropic effects, TGF-β monotherapy would have the same disadvantages as immunosuppressive agents. Therefore, the therapeutic use of TGF-β should be

in the setting of disease-relevant Ag to skew the context of Ag presentation toward one that promotes Ag-specific tolerance.

This investigation tested the hypothesis that co-delivery of surface-coupled TGF-β with encapsulated autoAg using a single poly(lactide-co-glycolide) (PLG) NP could modulate and enhance Ag-specific immune responses. An *in vitro* co-culture system of bone marrow-derived dendritic cells (BMDCs) and naïve T cells was used to evaluate the bioactivity of Ag and TGF-β co-delivered by NPs. The immunomodulatory effects of TGF-β-coupled NPs on mature and immature BMDCs were determined by analyzing surface costimulatory markers and inflammatory cytokine production. The *in vivo* Treg frequency and number were measured following injection of particles into OT-II mice that expressed $OVA_{323-339}$-restricted T cell receptors. Finally, the ability of surface-bound TGF-β to enhance the tolerogenicity of Ag-NPs was evaluated using the EAE mouse model in the context of i.v. and s.c. administration routes.

Results

Bioactivity of TGF-β-coupled PLG nanoparticles

TGF-β was chemically coupled to the surface of PLG NPs (PLG-TGF-β NPs) using carbodiimide chemistry (**Error! Reference source not found.**A) [273]. The bioactivity of NP-bound TGF-β was determined *in vitro* by its ability to differentiate naïve $CD4^+CD25^-Foxp3^-$ T cells into $CD4^+CD25^+Foxp3^+$ Tregs. In this Treg induction assay, naïve $CD4^+CD25^-$ T cells stimulated with anti-CD3, anti-CD28, and IL-2 alone resulted in an upregulated expression of CD25 but not Foxp3. The addition of soluble TGF-β resulted in a significant differentiation and expansion of $CD4^+CD25^+Foxp3^+$ T cells, and delivery of surface-bound TGF-β by PLG-TGF-β NPs achieved the same high level of Treg differentiation as soluble TGF-β (**Error! Reference source not found.**B). This result demonstrated that TGF-β can be delivered on NP surfaces with

sufficient quantity and bioactivity to elicit robust immunological and tolerance-enhancing responses.

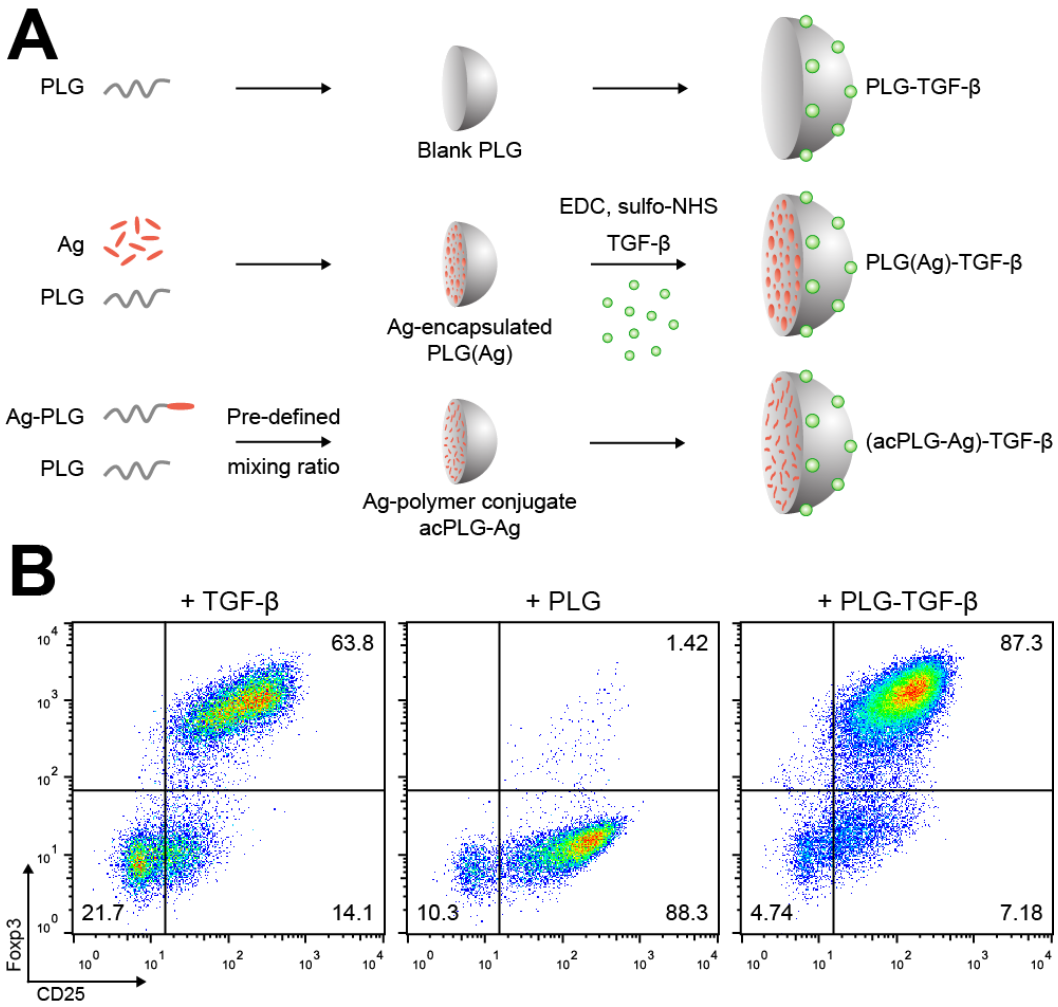


Figure 4.1 Surface-coupled TGF-β is bioactively delivered by PLG nanoparticles. (A) A schematic depiction of the NP production and TGF-β conjugation procedure used to create the NPs in this study. TGF-β was conjugated to blank PLG, Ag-encapsulated, and Ag-polymer conjugate NPs. (B) Naïve $CD4^{+}CD25^{-}$ T cells were cultured in anti-CD3-coated plates for 4 days in the presence of 2 μg/mL anti-CD28, 10 ng/mL IL-2, and 2 ng/mL of soluble TGF-β, blank PLG NPs, or 300 μg/mL of PLG-TGF-β NPs (166 ng TGF-β/mg). T cells were characterized by flow cytometry for CD25 and intracellular Foxp3.

Antigen and TGF-β bioactive co-delivery by nanoparticles

NP-coupled TGF-β and NP-associated Ag were subsequently evaluated for bioactivity in a single NP for its ability to promote tolerogenic Ag-specific responses. Two Ag-NP platforms were evaluated for TGF-β delivery: Ag-encapsulated (PLG(Ag)) NPs and Ag-polymer conjugate (acPLG) NPs (**Error! Reference source not found.**A). The PLG(Ag) particles encapsulated Ag

using a double emulsion approach, whereas the acPLG particles incorporate Ag by admixing unmodified PLG with a precise quantity of Ag-PLG polymer conjugates [172, 264]. TGF-β was conjugated to $OVA_{323-339}$ (OVA) peptide-loaded NPs and an enzyme-linked immunosorbent assay (ELISA) determined that the loading of TGF-β on PLG(OVA)-TGF-β NPs and (acPLG-OVA)-TGF-β was 166 ng TGF-β per mg of NP. Conjugation of TGF-β to the NP resulted in an increase in NP size and a decrease in the zeta potential (Figure 4.2A).

The bioactive co-delivery of Ag and TGF-β by PLG NPs was evaluated in a co-culture of BMDCs and OVA-specific OT-II T cells. In this assay, the delivery of OVA resulted in Ag presentation by BMDCs and T cell activation as measured by the expression of CD25 on nearly all T cells (Figure 4.2B). The administration of soluble TGF-β with OVA resulted in a $CD4^+CD25^+Foxp3^+$ Treg induction frequency of 25% (Figure 4.2C). Co-delivery of TGF-β and OVA by PLG(OVA)-TGF-β and (acPLG-OVA)-TGF-β particles both resulted in Treg frequencies comparable to treatment with soluble OVA and TGF-β, or soluble TGF-β administered with Ag-only NPs. Importantly, co-delivery of TGF-β with irrelevant peptide, $PLP_{139-151}$ (PLP), resulted in no T cell stimulation or Treg differentiation as indicated by the absence of CD25 and Foxp3 expression by T cells (Figure 4.2B,C).

A

Particle Type	Diameter pre-TGF-β coupling (nm ± SD)	Diameter post-TGF-β coupling (nm ± SD)	Zeta Potential pre-TGF-β coupling (mV ± SD)	Zeta Potential post-TGF-β coupling (mV ± SD)	OVA Loading (μg OVA/mg NP)	TGF-β Loading (ng TGF-β/mg NP)
PLG(OVA)-TGF-β	502 ± 7	898 ± 43	-41 ± 1	-66 ± 7	3	166.5
(acPLG-OVA)-TGF-β	485 ± 14	775 ± 112	-29 ± 1	-48 ± 6	8	166.2

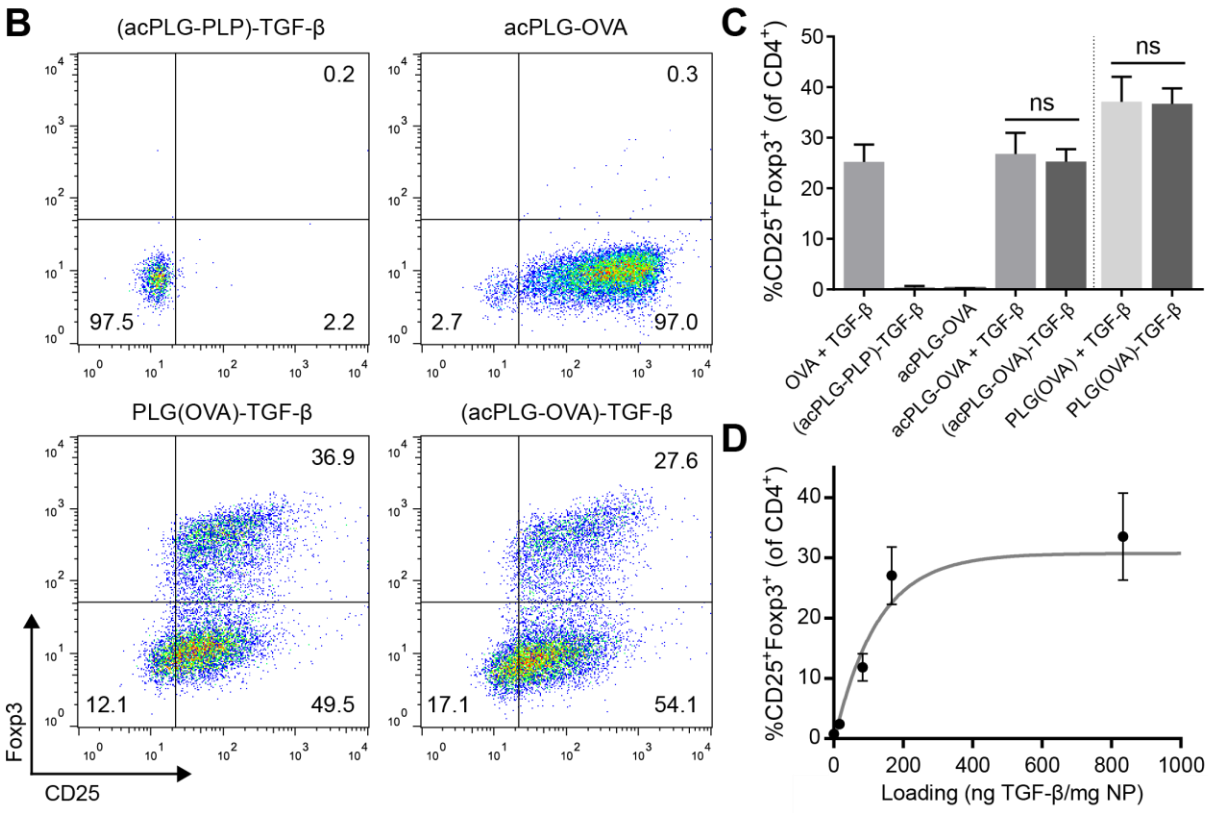


Figure 4.2: TGF-β and antigen are bioactively co-delivered by PLG particles to induce antigen-specific Tregs. (A) Characterization of Ag-NPs before and after TGF-β conjugation. Antigen-loaded NPs were prepared by encapsulating OVA peptide [PLG(OVA) NPs] or by incorporating PLG-Ag conjugates with unmodified PLG (acPLG NPs). (B-D) BMDCs were treated for 3 hours with 300 μg/mL of Ag-NPs. After 3 h, media was exchanged to remove excess particles. The BMDCs were then co-cultured for 4 days with naïve OT-II $CD4^+CD25^-$ T cells at a 1:1 ratio. Cells that were not treated with NPs received 100 ng/mL of OVA and 2 ng/mL of TGF-β. (B) Representative plots of flow cytometry data gated on live $CD4^+$ T cells. (C) Treg induction was compared between solubly derived TGF-β and NP-bound TGF-β co-delivered with PLG(OVA) NPs (3 μg OVA/mg) and acPLG-OVA NPs (2 μg OVA/mg). (D) Treg induction was evaluated with titrated amounts of TGF-β conjugated to acPLG-OVA NPs (OVA loading constant at 8 μg/mg). Statistical differences were determined using a two-tailed unpaired t-test. Error bars indicate SD.

The effective range of TGF-β loading on Ag-NPs was determined by titrating the amount of TGF-β conjugated to acPLG-OVA particles followed by measuring the degree of Treg differentiation in the BMDC:T cell co-culture assay. At a fixed loading of 8 μg OVA per mg of acPLG-OVA NP, the Treg induction efficiency of (acPLG-OVA)-TGF-β NPs increased with the

TGF-β loading, reaching a maximum Treg induction efficiency of 27% with a TGF-β coupling of 166 ng TGF-β/mg NP with no further enhancement up to 800 ng TGF-β/mg NP (Figure 4.2D). Collectively, these data demonstrate that Ag and TGF-β were bioactively co-delivered by PLG(Ag)-TGF-β and (acPLG-Ag)-TGF-β NPs and that the resulting *in vitro* Treg induction is Ag-specific.

PLG nanoparticles downregulate dendritic cell costimulatory molecules and reduce inflammatory cytokine secretion

BMDCs were used to investigate the effect of TGF-β-coupled NPs on APC phenotype, as dendritic cells (DCs) are specialized to initiate immune responses by presenting Ag and costimulatory signals to T cells. BMDC costimulatory molecules and cytokines were assessed for phenotypic changes following *in vitro* incubation with NPs. Immature BMDCs treated with NPs [PLG, acPLG-OVA, or (acPLG-OVA)-TGF-β] exhibited a downregulation of MHC II and costimulatory markers CD80 and CD86 regardless of Ag or TGF-β delivery (Figure 4.3A). NP-induced downregulation of CD80 and CD86 was also observed in BMDCs matured with interferon gamma (IFNγ) and lipopolysaccharide (LPS), but MHC II expression increased in response to NPs administered in the presence of maturation signals (Figure 4.3B). Analysis of the secreted cytokines revealed that mature BMDCs produced about 2-fold less IL-6 and IL-12 in the presence of soluble TGF-β, PLG NPs, or acPLG-OVA NPs. This effect was augmented by TGF-β delivery on NPs, which resulted in a 3- and 6-fold reduction in IL-6 and IL-12 production, respectively (Figure 4.3D). In contrast, treatment with NPs increased the production of tumor necrosis factor alpha (TNFα), and NP-associated TGF-β did not have an effect on this production (Figure 4.3C,D).

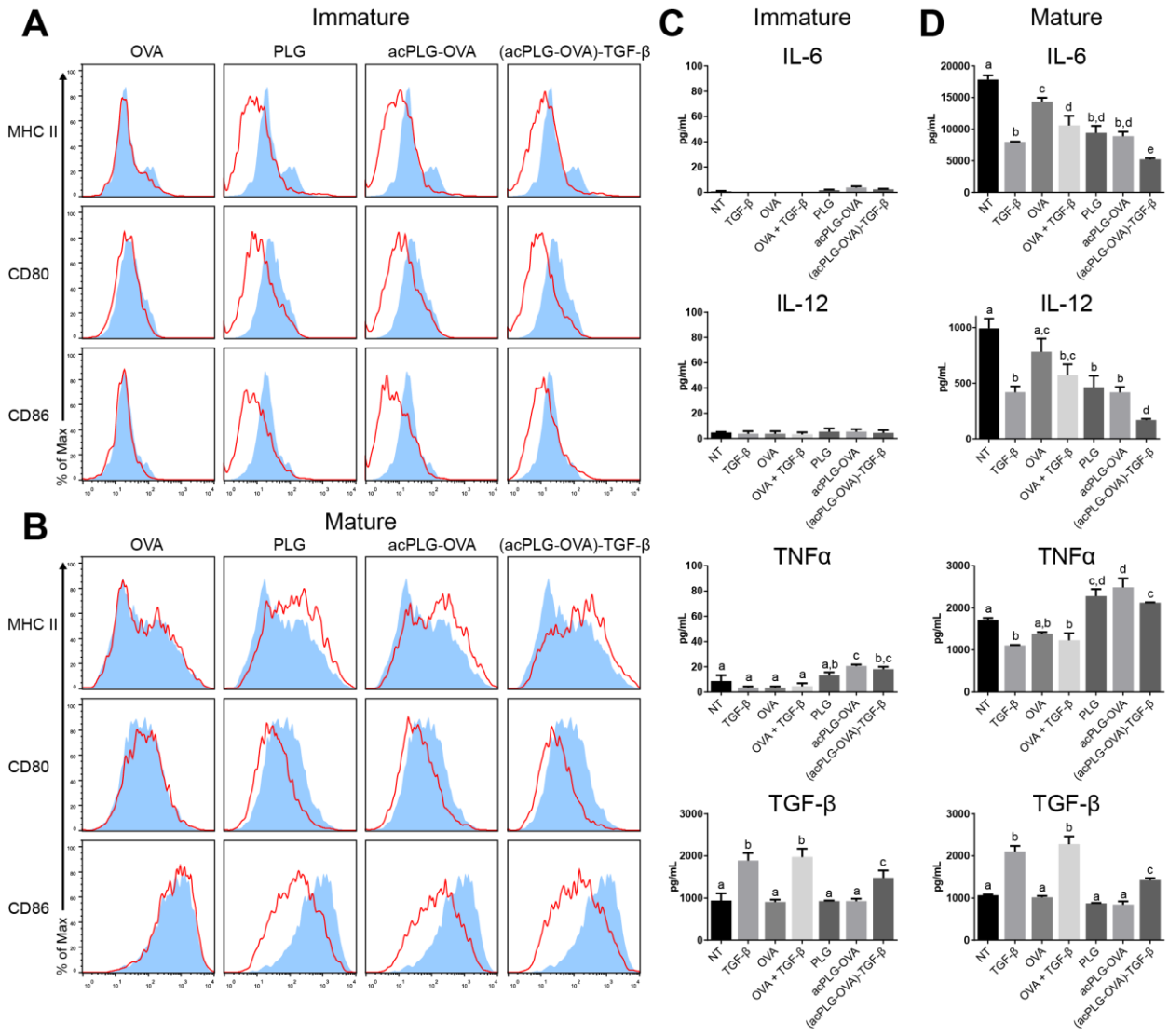


Figure 4.3: NP treatment decreases BMDC costimulatory molecule expression and cytokine secretion. BMDCs were treated with soluble OVA or with NPs for 3 h. Excess NPs were washed away, and cells were incubated for 4 days. (A and C) BMDCs were unstimulated (immature) or (B and D) stimulated (mature) with 10 ng/mL of IFNγ and 10 ng/mL LPS after 3 h NP treatment. (A and B) BMDCs were evaluated by flow cytometry on day 4. Histograms show live cell surface molecule expression with red line histograms representing the indicated treatment and blue filled histograms representing untreated BMDCs. (C and D) The cytokines present in the BMDC media on day 4 were evaluated by ELISA. Statistical differences were determined by one-way ANOVA with Tukey's multiple comparisons test. Within data subsets, no significant difference was observed between conditions labeled with matching letters ($p>0.05$). Error bars indicate SD.

Soluble TGF-β was measured to investigate whether the anti-inflammatory responses were achieved by the immobilized TGF-β, or through TGF-β that may have been released from the particle. The quantity of soluble TGF-β contributed by (acPLG-OVA)-TGF-β NPs was intermediate between TGF-β levels in the serum-supplemented media and media supplemented with 2 ng/mL of soluble TGF-β. This low level of TGF-β released from the particle is

insufficient to affect the changes observed in the BMDC response, and suggests that the reduction in inflammatory cytokines by incubation with TGF-β-coupled particles is due to particle-bound TGF-β rather than an increase in the soluble presence of TGF-β (Figure 4.3C,D). IL-10 was below the limit of detection in all conditions tested (data not shown).

Ag-NPs affect changes in the T cell compartment

The *in vivo* effect of TGF-β-coupled particles on Ag-specific T cell responses was investigated using OVA-loaded NPs in the OT-II mouse. Mice were injected with 1.25 mg of Ag-NPs (8 μg Ag/mg, 166 ng TGF-β/mg) i.v. or s.c. to evaluate Ag presentation by distinct delivery mechanisms. As expected, the NP route of administration determined the site of T cell expansion. In the spleen and liver, i.v. delivery of OVA-loaded NPs resulted in a 6-fold and 10-fold increase in the number of $CD4^+$ T cells, which included an increase in the number of Tregs (2-fold and 5-fold, respectively) (Figure 4.4A,B). However, this increase in T cell and Treg number corresponded to a decrease in the frequency of Tregs in the spleen and liver when treated with acPLG-OVA without TGF-β (Figure 4.4C). No changes in the liver and spleen T cell populations were observed following s.c. NP administration (Figure 4.4D-F).

In the pooled axillary, brachial, and inguinal lymph nodes (LNs), the number of $CD4^+$ T cells increased 30-fold after s.c. injection of particles containing OVA. The expansion of T cells was not associated with a change in Treg proportion, which was maintained at 2% (Figure 4.4F). Interestingly, the percentage of LN Tregs increased 4-fold after i.v. administration of OVA-loaded particles (Figure 4.4C). In general, OVA-loaded NPs caused increases in OT-II T cell and Treg numbers in the liver and spleen following i.v. administration and in the lymph nodes following s.c. administration. The T cell expansion was Ag-specific, and there was not an increase in Treg number or frequency attributed to TGF-β co-delivery on the particles.

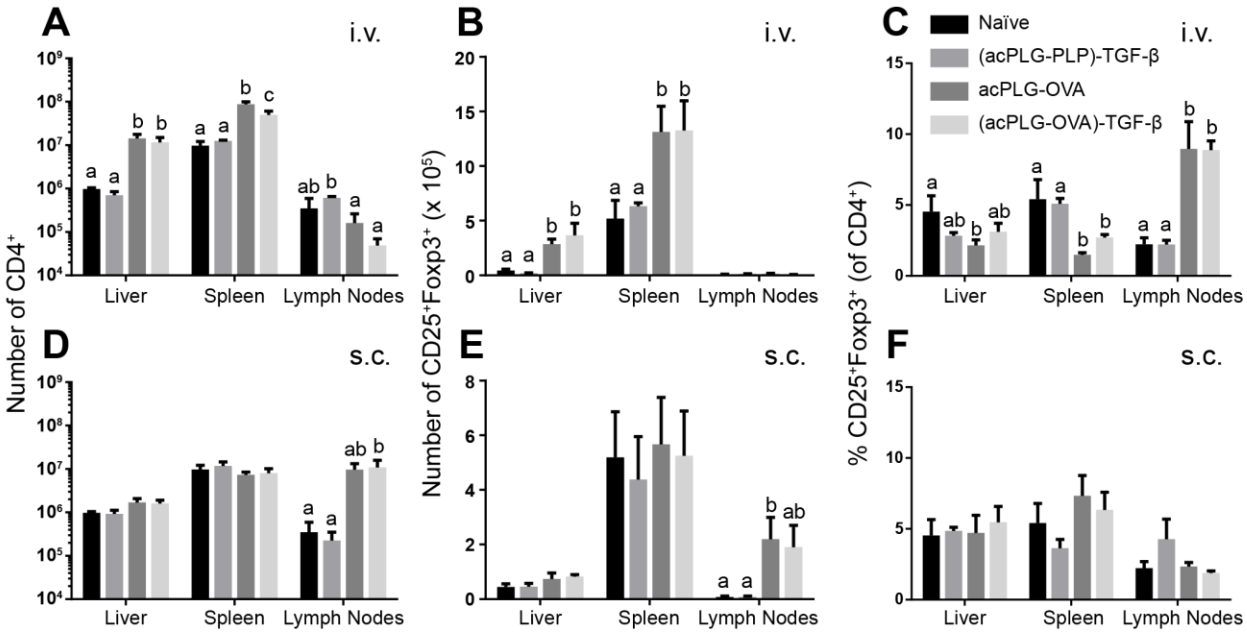


Figure 4.4: Ag-NPs cause Ag-specific changes in T cell populations *in vivo.* OT-II mice were untreated or injected with 1.25 mg of NPs (8 μg Ag/mg, 166 ng TGF-β/mg). (A-C) Mice treated i.v. received a single tail vein injection. (D-F) Mice treated s.c. received 4 injections distributed over the shoulders and hind limbs. After 7 days, the livers, spleens, and pooled brachial, axillary, and inguinal lymph nodes were excised and analyzed by flow cytometry for $CD4^+$ T cells and $CD25^+Foxp3^+$ Tregs. Statistical differences were determined by Fisher's Least Significant Difference (LSD) test. Within data subsets, no significant difference was observed between conditions labeled with matching letters ($p>0.05$). Error bars indicate SEM.

Surface conjugation of TGF-β improves the tolerogenic effect of Ag-NPs

The hypothesis that functionalizing Ag-loaded NPs with TGF-β would improve the efficiency of tolerance induction was tested in the EAE model by comparing the clinical disease scores of mice treated by Ag-NPs, with and without surface-coupled TGF-β. PLG NPs loaded with only disease-relevant peptides have demonstrated robust tolerance in previous studies; therefore, TGF-β-coupled NPs were investigated in the EAE model at sub-therapeutic doses to identify therapeutic contributions of the TGF-β modification [161, 170, 172, 264]. A single i.v. dose of 2.5 mg of acPLG-PLP (8 μg PLP/mg) was determined as the minimum requirement for suppression of EAE disease symptoms and was used as the standard for dose reduction comparisons (Figure 4.7). Mice were injected once with either an intermediate dose (1.25 mg, 2-fold lower) or a low dose (0.0625 mg, 40-fold lower) of Ag-NPs (8 μg Ag/mg, 166 ng TGF-

β/mg) compared to the noted therapeutic dose of 2.5 mg. At the intermediate dose of 1.25 mg NPs, surface-bound TGF-β did not reduce disease scores between days 10 – 14 (acute disease), yet was able to mitigate relapse disease scores (days 21 – 30) compared to acPLG-PLP and (acPLG-OVA)-TGF-β NPs (Figure 4.5A). This result suggests that surface-modification with TGF-β enhances tolerance in an Ag-specific context and does not broadly suppress the immune response to non-relevant epitopes, respectively. No significant difference was observed between the clinical disease courses of the acPLG-PLP and (acPLG-OVA)-TGF-β conditions during this period. At the low dose of 0.0625 mg NPs, (acPLG-PLP)-TGF-β NPs significantly reduced the severity of the mean clinical score over the acute and relapse disease course compared to acPLG-PLP NPs (Figure 4.5B). Subsequently, mice were treated therapeutically with 1.25 mg of NPs (day 13, third day after disease onset), to identify whether the particles can attenuate the autoimmune response in a pathogenic population of activated T cells. Both TGF-β-coupled and non-coupled acPLG-PLP NPs resulted in abrogated clinical scores from days 19 – 33 (relapse disease) (Figure 4.5C). On day-19 post-immunization (6 days after NP injection), mice from each cohort (n=3) were euthanized and the number of Tregs in their livers, spleens, and pooled lymph nodes were quantified. The number of Tregs increased in the livers of mice treated with acPLG-PLP and (acPLG-PLP)-TGF-β NPs (Figure 4.5D), with no change in the spleen and lymph nodes (data not shown).

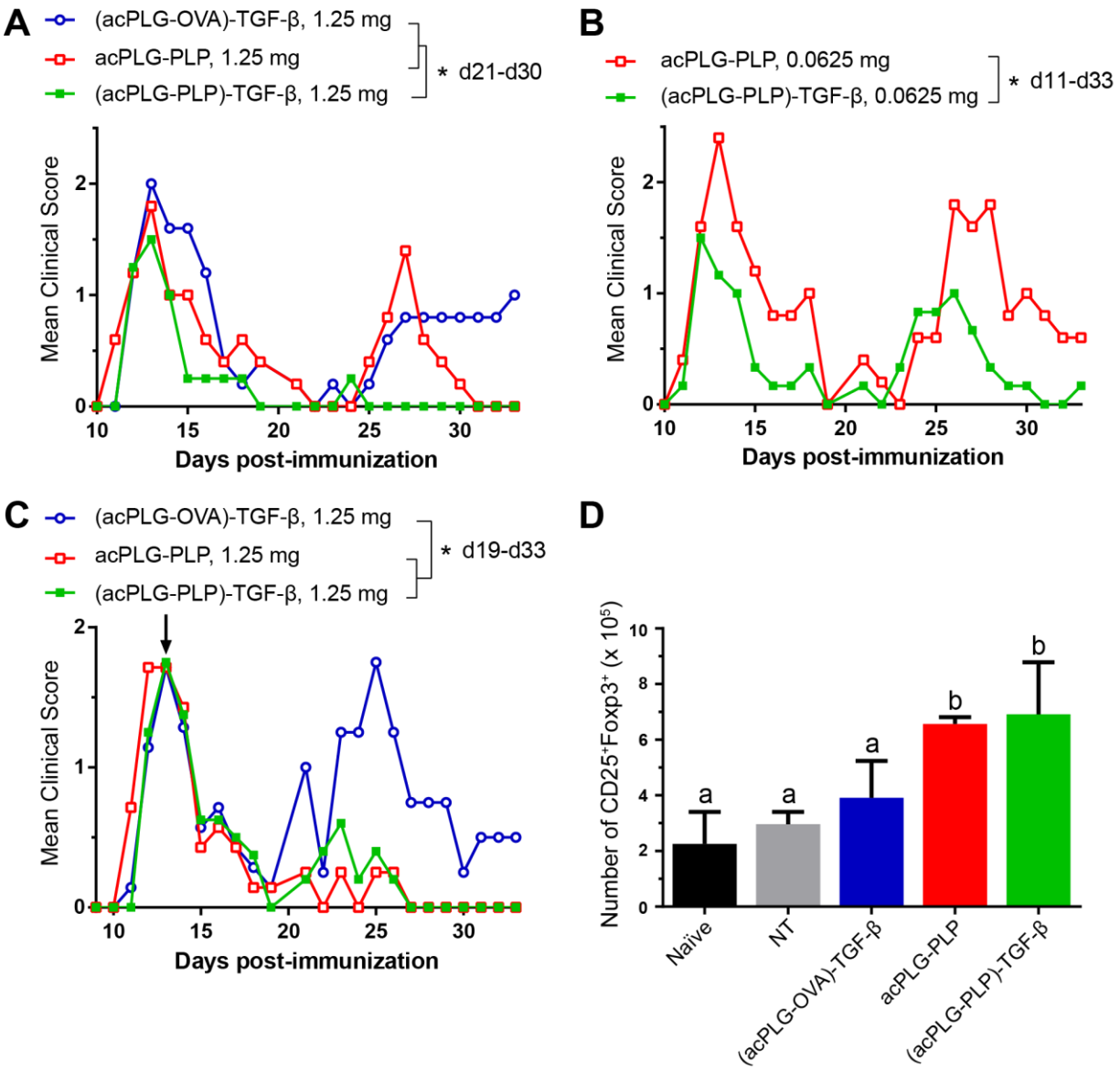


Figure 4.5: TGF-β co-delivery improves the tolerogenic efficiency of Ag-loaded NPs in EAE model. (A,B) SJL mice were prophylactically injected i.v. with sub-therapeutic doses of Ag-NPs (A, 1.25 mg or B, 0.0625 mg at 8 μg Ag/mg and 166 TGF-β/mg). After 7 days, mice were immunized with PLP/CFA on day 0 to induce EAE (n=5). (C,D) SJL mice (n=7) were immunized (day 0) and injected with 1.25 mg of Ag-NPs (8 μg Ag/mg, 166 ng TGF-β/mg) on day 13 (the third day of disease presentation). 6 days after injection, 3 mice per cohort were euthanized and (D) the number of liver CD25+Foxp3+ Tregs was quantified using flow cytometry. Statistical differences between treatments for the indicated time periods were determined by (A and C) the Kruskal-Wallis test (one-way ANOVA non-parametric test) with Dunn's multiple comparisons test ($p < 0.05$) or (B) the Mann-Whitney (two-tailed non-parametric) test ($p<0.05$). Statistical differences between cell numbers (D) were determined using Fisher's Least Significant Difference (LSD) test. Within data subsets, no significant difference was observed between conditions labeled with matching letters ($p>0.05$). Error bars indicate SD.

Subcutaneous delivery of TGF-β conjugated Ag-NPs reduces relapse scores in EAE

The local co-delivery of Ag and TGF-β by NPs in the s.c. space and draining LNs was hypothesized to program a tolerogenic phenotype in the APCs thereby skewing the context of Ag

presentation toward one that favors a tolerogenic outcome. Mice were injected s.c. with 1.25 mg Ag-NPs (8 μg Ag/mg) and presented similar mean clinical scores in the acute disease phase from days 11 – 21 post-immunization (Figure 4.6). In the relapsing phase of disease, from days 23 – 33, no difference in the clinical scores was observed between the acPLG-OVA- and acPLG-PLP-treated mice. However, mice treated s.c. with (acPLG-PLP)-TGF-β NPs (166 ng TGF-β/mg) experienced a maximum relapse score that was approximately half of the other NP groups and exhibited a significant reduction in the severity of relapsing clinical scores from days 23 – 33. This decrease in EAE clinical scores resulting from TGF-β co-delivery on PLP-loaded NPs suggests an immunomodulatory role for TGF-β and supports further investigation into the co-delivery of exogenous cytokines on NPs for modulating Ag-specific immune responses.

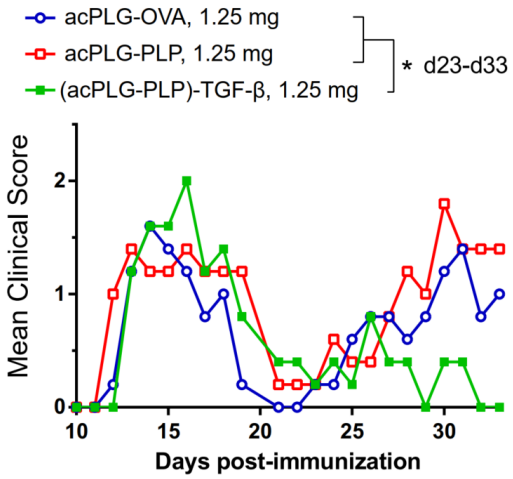


Figure 4.6: Subcutaneous delivery of TGF-β-coupled Ag-NPs reduces the severity of relapse symptoms in EAE. SJL mice were injected s.c. with 1.25 mg of Ag-NPs (8 μg Ag/mg, 166 ng TGF-β/mg) 7 days before immunization with PLP/CFA to induce EAE (n=5). Statistical differences between treatments for the indicated time periods were determined by the Kruskal-Wallis test (one-way ANOVA non-parametric test) with Dunn's multiple comparisons test ($p < 0.05$).

Discussion

Delivery of autoAgs using NPs is a promising strategy to induce Ag-specific tolerance to disease-relevant Ags without suppressing the diverse repertoire of immune cells required for maintaining protective immunity [161, 169-172, 262]. The efficacy of Ag-NPs has previously been shown to be dependent on dose and route of administration (i.v.) [170]. While Ag-NPs have

demonstrated the primary endpoint of immune tolerance, others have demonstrated toxicity by similar NPs at high doses [266, 267]. Therefore, to reduce the dose of Ag-NPs required to induce tolerance and to enable the use of a simpler and more clinically accessible route of administration (s.c.), this report investigated the effect of the co-delivery of TGF-β, a pleiotropic immunomodulator, on Ag-loaded PLG NPs. Co-delivery of surface-bound TGF-β on Ag-loaded PLG NPs enhanced the tolerogenic efficiency (reduced dose) and provided an enabling solution to induce tolerance through a previously unproven route of administration (s.c.) using PLG Ag-NPs.

PLG-based particles were produced with Ag and modified with TGF-β in a co-delivery platform that achieves precise Ag loading and maintains bioactivity of both immune-modulating factors (Figure 4.2). Water-soluble cytokines, growth factors, and short peptides are commonly encapsulated using a double emulsion protocol [164, 264, 274]. Controlling the co-encapsulation of multiple factors is complicated by differences in the molecule size, pKa, and solubility of each component. These molecular variables can thermodynamically limit the control over encapsulation efficiency, loading, and desired release profile [255]. Therefore, many particle systems deliver Ag and immune-modifiers in separate NPs [164, 177, 274]. Herein, Ag was covalently attached to the polymer, particles were formed with this Ag-PLG bioconjugate, and the resulting Ag-NPs were subsequently modified with TGF-β. This approach ensures that the NP has both Ag and TGF-β, which can provide signals to program APCs toward tolerogenic phenotypes (Figure 4.2). Unlike encapsulation, the covalent and stepwise attachment of the Ag and TGF-β to the NP avoids uncontrolled release and minimizes off-target effects while allowing the loading of each factor to be independently tuned [172]. Taken together, these NPs provide a

platform for flexible, precise, and bioactive co-delivery of disease-relevant peptides and immune-modifying proteins.

TGF-β-coupled Ag-NPs downregulated costimulatory molecules and secretion of Th1/Th17-associated inflammatory cytokines *in vitro*, using LPS and IFNγ stimulated mature BMDCs, which may reduce their potential for differentiating naïve T cells toward effector lineages (Figure 4.3). The decrease in the expression of surface proteins MHC II, CD80, and CD86 observed with TGF-β-coupled Ag-NPs is phenotypically similar to other strategies for inducing tolerogenic DCs such as *in vitro* incubation with cytokines, siRNA knock down of CD80/CD86, and genetic modification for endogenous cytokine production [268, 275, 276]. The decrease in CD80 and CD86 was also observed in mature BMDCs treated with Ag-NPs, however an upregulation of MHC II was observed. Cytokine secretion also contributes to APC phenotype, with IL-12 and IL-6 being well characterized for their role in the differentiation of Th1 and Th17 T helper cells. Further, these cytokines are implicated in the pathogenesis of EAE and human MS [277, 278]. IL-12 signals the differentiation of IFNγ-secreting Th1 cells, and IL-6 works together with TGF-β to signal the differentiation of IL-17 secreting Th17 cells that are associated with immune-mediated demyelination in the central nervous system (CNS) of individuals with MS. As a co-delivery platform, TGF-β-coupled Ag-NPs synergistically decreased both IL-12 and IL-6 production to levels significantly lower than Ag-NPs or TGF-β separately. The reduction of DC-secreted IL-12 by TGF-β-coupled NPs is in agreement with a similar result using microparticles to locally deliver soluble TGF-β [274]. Collectively, the *in vitro* data presented suggests that BMDCs respond to (acPLG-Ag)-TGF-β NPs by providing tolerogenic signals in the three-signal hypothesis of T cell activation: 1) peptide delivery for Ag-specific TCR

recognition, 2) decreased costimulatory molecules, and 3) suppressed secretion of cytokines responsible for Th1 and Th17 differentiation [120].

Injection of TGF-β-coupled particles i.v. and s.c. resulted in similar attenuation of EAE disease scores (Figure 4.5 and Figure 4.6) despite the differential organ and immune cell distribution associated with these administration routes. In both contexts, TGF-β may program a tolerogenic phenotype in the local APCs. Following i.v. administration, PLG NPs associate with APCs of the liver and spleen [264]. In the liver, Kupffer cells and liver sinusoidal endothelial cells are commonly associated with PLG NP uptake and each are natural producers of TGF-β [198, 279-281]. In the spleen, PLG NPs have been reported to be scavenged by macrophages in the marginal zones where they present Ag to T cells. This context of presentation has been implicated in tolerance induction through T cell anergy and Treg production [161]. The same NPs, injected s.c., will interact with immune cells in a different context. NPs with diameters greater than 100 nm do not passively flow to the lymph nodes, but instead are internalized by APCs and infiltrating mononuclear cells that traffic to the lymph nodes [282, 283]. Implanted PLG microporous scaffolds cause a similar recruitment of monocytes, macrophages, and DCs [284]. Experiments delivering soluble TGF-β from the scaffolds demonstrated a significant decrease in the number of infiltrating leukocytes, chemoattractants, and activating cytokines [285]. Thus, delivery of TGF-β with Ag-NPs may be acting to reduce the inflammatory context of Ag presentation in the draining lymph node. Together, i.v. and s.c. administration of TGF-β-coupled NPs result in similar patterns of disease abrogation yet may affect tolerance by different cell types due to differences in their biodistribution.

Ag-NP administration resulted in Ag-specific changes to the T cell compartment. EAE and MS are T cell-mediated diseases [277]. As such, a single infusion of myelin-specific $CD4^+$ T cells is

sufficient for inducing relapsing and remitting EAE [170]. Therefore, many Ag-specific therapies attempt to reprogram the context of MHC class II presentation to $CD4^+$ T cells to induce T cell unresponsiveness and expansion of Tregs. Tolerance induction by Ag-NPs is partly dependent on $CD4^+CD25^+Foxp3^+$ Treg production, and inactivating Tregs with anti-CD25 antibodies reduced the effectiveness of NP-induced tolerance [161]. TGF-β is required for the differentiation of Tregs *in vitro*, so NP-treated mice were investigated for *in vivo*-expanded $CD4^+CD25^+Foxp3^+$ Tregs. Indeed, mice treated with Ag-NPs did experience an expansion of $CD4^+$ T cells and Tregs; however, the presence of TGF-β on the NPs did not further augment the $Foxp3^+$ Treg numbers (Figure 4.4). This observation is consistent with others who have enhanced tolerogenic outcomes without expanding $Foxp3^+$ Tregs [164, 286, 287]. $Foxp3^+$ Tregs were investigated due to their close association with TGF-β, but future studies would benefit from studying $Foxp3^-$ T cells with regulatory potential.

TGF-β-coupled Ag-NPs administered i.v. and s.c. at intermediate doses attenuated relapse symptoms, yet not the initial EAE disease onset. Previously, Ag-coupled PLG NPs demonstrated that EAE disease abrogation was proportional to NP dose, and the severity of the acute disease symptoms was correlated with the severity of the relapse symptoms [170]. These data were consistent with the theory of epitope spreading in which the severity of relapse symptoms is directly related to the extent of myelin destruction in the acute phase [186]. This proportionality between acute and relapse scores was also observed in this investigation in the control mice treated with NPs containing irrelevant Ag or disease-relevant Ag without TGF-β. However, mice treated i.v. or s.c. with TGF-β-coupled particles experienced relapse symptoms that were disproportionately less severe than the symptoms of the acute phase (Figure 4.5 and Figure 4.6), which may indicate that TGF-β causes a reduction in the degree of acute phase tissue destruction

that leads to epitope spreading. This role for TGF-β is supported by others who observed limited extravasation of inflammatory cells into the CNS following injections of soluble TGF-β [271]. Others have demonstrated tolerance induction by s.c. administration of particles by delivering other immunomodulators such as antisense RNA (anti-CD80, anti-CD86, and anti-CD40), IL-10, or immunosuppressive agents such as rapamycin [162, 164, 268]. The current platform is an advance relative to our previous strategies because it incorporates Ag and TGF-β into a single NP ensuring the immunosuppressive effects are in the context of Ag presentation. Additionally, TGF-β is endogenously present in mice and humans, so the delivery of TGF-β as an immunomodulator takes advantage of natural peripheral tolerance pathways [280, 281]. Together, for TGF-β-coupled Ag-NPs, a critical particle dose may be required for abrogating acute EAE symptoms, and the co-delivery of TGF-β may limit the severity of relapse symptoms by reducing the degree of CNS destruction in the acute phase of disease.

In conclusion, TGF-β was conjugated to the surface of PLG NPs produced with precise Ag-loadings. The resulting (acPLG-Ag)-TGF-β NPs incorporate Ag and TGF-β in a fashion that maintains independent tunability and bioactivity. *In vitro*, BMDCs treated with (acPLG-Ag)-TGF-β NPs provided Ag-specific T cell stimulation, decreased costimulatory molecule presentation, and suppressed inflammatory cytokine secretions. In EAE, prophylactic i.v. treatment with (acPLG-PLP)-TGF-β NPs reduced clinical scores in low dose regimes, and (acPLG-PLP)-TGF-β NPs delivered s.c. reduced clinical disease scores without the use of broad-acting immunosuppressive drugs. Importantly, the tolerogenic effects of TGF-β in this NP co-delivery platform were Ag-specific. Together, this study supports the use of immunomodulatory cytokines to enhance the efficacy of Ag-specific tolerance therapies.

Materials and Methods

Poly(lactide-co-glycolide) (50:50) (PLG) with a single carboxylic acid end-group and an inherent viscosity of 0.17 dL/g in hexafluoro-2-propanol was purchased from Lactel Absorbable Polymers (Birmingham, AL). Poly(ethylene-alt-maleic anhydride) (PEMA) was purchased from Polyscience, Inc. (Warrington, PA). Amine-terminated ovalbumin peptide (NH_2-$OVA_{323-339}$) and proteolipid peptide (NH_2-$PLP_{139-151}$) was purchased from Genscript (Piscataway, NJ). N-hydroxysulfosuccinimide (sulfo-NHS) was purchased from Thermo Fisher Scientific (Waltham, MA). Recombinant mouse transforming growth factor beta 1 (TGF-β) was purchased from Cell Signaling Technology (Danvers, MA). All other reagents were purchased from Sigma Aldrich (St. Louis, MO) unless noted otherwise.

Ag-PLG conjugation

Peptide-polymer conjugates (Ag-PLG) were made as previously described [172]. Briefly, PLG (37.8 mg, 0.009 mmol, 4200 g/mol) of was dissolved in 2 mL of N,N-dimethylformamide (DMF). N-(3-Dimethylaminopropyl)-N'-ethylcarbodiimide hydrochloride (EDC) (9.0 mg, 0.047 mmol, 5X to PLG) was dissolved in 0.5 mL of DMF and added dropwise to the PLG solution. N-Hydroxysuccinimide (NHS) (5.5 mg, 0.047 mmol, 5X to PLG) was dissolved in 0.5 mL DMF and added dropwise to the solution. The reaction was stirred for 15 minutes at room temperature. Antigenic peptide (1.2X to PLG) was dissolved in a solution of 1 mL dimethyl sulfoxide (DMSO) and 0.5 mL DMF and stirred at 400 RPM. Triethylamine (5X to peptide) was added to peptide solution and the mixture was added dropwise to the stirring PLG solution. The reaction was allowed to proceed overnight at room temperature. The resulting polymer was isolated and purified by dialysis using 3,500 molecular weight cut-off membrane against distilled water. The dialyzed polymer was collected and washed with MilliQ water three times by centrifugation at

7000 x g before lyophilization. The coupling efficiency of peptide to PLG was determined by ^{1}H-NMR analysis in DMSO-d6.

Mice

Female SJL/J mice (6-8 weeks) were purchased from Envigo (Indianapolis, IN). C57BL/6J mice (6-8 weeks) and OT-II mice (B6.Cg-Tg(TcraTcrb)425Cbn/J) were purchased from Jackson Laboratory (Bar Harbor, ME). All mice were housed under specific pathogen-free conditions in the University of Michigan Unit for Laboratory Animal Medicine and maintained according to protocols approved by the University of Michigan Animal Care and Use Committee.

Nanoparticle preparation and TGF-β conjugation

Ag-polymer conjugate PLG (acPLG) NPs and Ag-encapsulated PLG [PLG(Ag)] NPs were prepared using a single and double emulsion solvent evaporation (S.E.) method, respectively. These S.E. methods have been described in our previous publications [170, 172, 264]. Briefly, acPLG NPs were produced using the S.E. method with Ag-PLG conjugates combined with unmodified PLG at various ratios to produce acPLG NPs with pre-defined Ag loadings. PLG(Ag) NPs were produced by encapsulating peptides in a two-step S.E. method [264]. Cryoprotectants (4% (w/v) sucrose and 3% (w/v) mannitol) were then added to the particles before lyophilization. Prior to TGF-β conjugation, NPs were washed and resuspended with Dulbecco's phosphate buffered saline (PBS) (Gibco, Waltham, MA) to 5 mg/mL. EDC (128 ng, 0.668 nmol, 100X to TGF-β) and sulfo-NHS (14.5 ng, 0.067, 10X to TGF-β) were dissolved in PBS, added to the NPs, and allowed to react for 15 minutes at room temperature and mixed at 700 RPM (Eppendorf Thermomixer, Hamburg, Germany). TGF-β was suspended in PBS and added dropwise to the ester-activated NPs. After a reaction time of 1 hour, NPs were washed 3 times with PBS. TGF-β loading was determined by quantification of uncoupled TGF-β recovered

during the NP wash steps. TGF-β was measured using an enzyme-linked immunosorbent assay (ELISA) (coupling efficiency 99.5%). NPs with titrated quantities of TGF-β were produced by proportionally scaling the quantities of TGF-β, EDC, and sulfo-NHS while keeping the quantity of NP constant. The size and zeta potential of the acPLG NPs were determined by dynamic light scattering (DLS) by mixing 10 μL of a 25 mg/mL particle solution into 990 μL of MilliQ water using a Malvern Zetasizer ZSP (Westborough, MA).

Cell culture

BMDC were generated from the bone marrow of C57BL/6J mice using the Lutz protocol [260]. Media consisted of RPMI containing L-glutamine (Life Technologies, Carlsbad, CA) supplemented with penicillin (100 units/mL), streptomycin (100 mg/mL), 10% heat-inactivated fetal bovine serum (FBS) (Invitrogen Corporation, Carlsbad, CA) and 50 mM β-mercaptoethanol (Sigma Aldrich). Granulocyte-macrophage colony-stimulating factor (GM-CSF) (Peprotech, Rocky Hill, NJ) was added at 20 ng/mL, and media was added/changed on days 3, 6, and 8. Day 10 BMDCs were treated with NPs at 300 μg/mL. Following incubation, all wells were washed to remove excess particles and BMDCs were incubated in media alone or supplemented with 10 ng/mL IFNγ (Peprotech) and 10 ng/mL LPS (Sigma). After 4 days of co-culture, the BMDCs were collected, stained for viability, MHC II, CD80, and CD86, and analyzed using flow cytometry. Cell culture supernatants were analyzed by ELISA for IL-6, IL-10, IL-12, TNFα, and TGF-β (University of Michigan Cancer Center Immunology Core).

Antibodies and flow cytometry

All antibodies were purchased from Biolegend (San Diego, CA) unless noted otherwise. FcR blocking was performed with anti-CD16/32 antibody prior to staining with various combinations of the following antibodies: anti-CD4 (RM4-5), -CD25 (PC61), -Foxp3 (FJK-16s) (eBioscience,

San Diego, CA) -CD80 (16-10A1) -CD86 (GL-1), -I-A/I-E (M5/114.15.2). Viability was assessed with fixable violet dead cell stain kit (Invitrogen, Carlsbad, CA) or 4',6-Diamidino-2-Phenylindole, Dilactate (DAPI) (Biolegend). Foxp3 staining was performed with the Foxp3 Staining Buffer Set according to the manufacturer's protocol (eBioscience). Flow cytometric data were collected using a Beckman Coulter CyAn ADP Analyzer. Analysis was performed using FlowJo software (FlowJo, Ashland, OR).

Cell isolation and *in vitro* Treg induction assay

Treg induction assays were carried out as previously described [172]. $CD4^+CD25^-Foxp3^-$ T cells were isolated from the spleen of OT-II mice using a naïve $CD4^+$ T cell isolation kit (Miltenyi Biotec, San Diego, CA). The assay was carried out in T cell media. T cell media was prepared similar to DC media but without GM-CSF or β-mercaptoethanol and supplemented with 1 mM sodium pyruvate and 0.1 mM non-essential amino acids (Life Technologies, Carlsbad, CA). BMDCs (2×10^4/well) were seeded into 96-well round-bottom cell culture plates and incubated for 3 hours with NPs at 300 μg/mL. Following incubation, all wells were washed to remove excess particles. Naïve T cells were added at 1:1 to the BMDCs. If OVA and TGF-β were not delivered by NPs, they were supplied in soluble form at 100 ng/mL OVA and 2 ng/mL TGF-β. After 4 days of co-culture, the T cells were collected, stained for viability, CD4, CD25, and Foxp3, and analyzed using flow cytometry. Statistical differences between conditions were determined by one-way ANOVA with Tukey's multiple comparisons test ($p<0.05$).

***Ex vivo* T cell analysis**

OT-II mice were injected i.v. (tail vein) or s.c. (4 sites over shoulders and hind limbs) with 1.25 mg of NPs or 200 μL of PBS. After 7 days, the mice were euthanized, and the liver, spleen, and pooled inguinal, brachial, and axillary LN cells were stained for viability, CD4, CD25, and

Foxp3. The cells were analyzed using flow cytometry. Statistical differences between conditions within the same organ were determined by Fisher's LSD test ($p<0.05$).

EAE disease induction and measurement

EAE was induced by immunization with encephalitogenic peptides as previously described [261]. To induce R-EAE with $PLP_{139-151}$, mice were immunized by s.c. administration of 100 µL of 1 mg/mL $PLP_{139-151}$/complete Freund's adjuvant (CFA) (Difco, Detroit, MI) distributed over 3 spots on the nape and hind flanks of SJL/J mice. Disease severity in individual mice was assessed by blinded observers using a 0 to 5 point scale: 0 = no disease, 1 = limp tail or hind limb weakness, 2 = limp tail and hind limb weakness, 3 = partial hind limb paralysis, 4 = complete hind limb paralysis, 5 = moribund. Differences between disease courses of more than two treatment groups were analyzed for statistical significance using the Kruskal-Wallis test (one-way ANOVA non-parametric test) ($p<0.05$). Statistical differences between two treatment groups were determined by the Mann-Whitney (two-tailed non-parametric) test ($p<0.05$).

Acknowledgements

This work was previously published with manuscript information: L.M. Casey, R.M. Pearson, K.R. Hughes, J.M.H. Liu, J.A. Rose, M.G. North, L.Z. Wang, M. Lei, S.D. Miller, L.D. Shea, Conjugation of Transforming Growth Factor Beta to Antigen-Loaded Poly(lactide- co-glycolide) Nanoparticles Enhances Efficiency of Antigen-Specific Tolerance, Bioconjug Chem, 29 (2018) 813-823.

Supplementary Figures

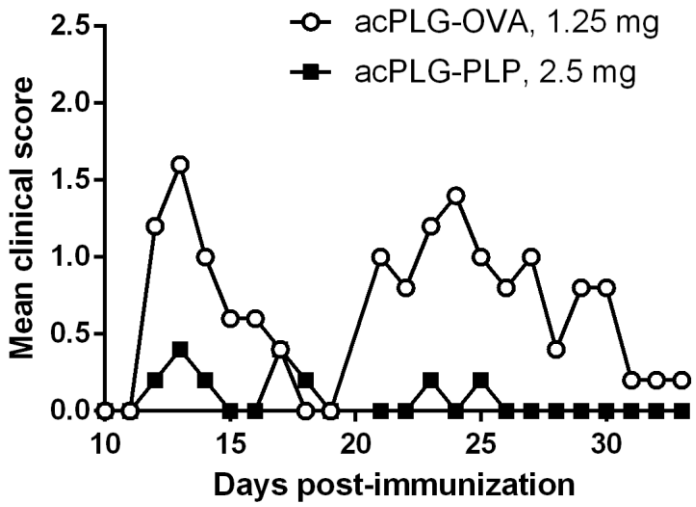


Figure 4.7: In the EAE model, symptoms are suppressed with a dose of 2.5 mg Ag-relevant NPs. SJL mice were prophylactically injected i.v. with Ag-NPs (8 μg Ag/mg NP). After 7 days, mice were immunized with PLP/CFA on (day 0) to induce EAE (n=5).

Chapter 5 Nanoparticle Delivery of Antigen Attenuates Anaphylactic Response in a Murine Model of Peanut Allergy.

Authors:

Kevin Hughes[1], Jeffrey Landers[2], Michael Saunders[1], Katarzyna Janczak[2], Hamza Turkistani[1], Lonnie Shea[1,3,*], Jessica O'Konek[2*]

Abstract:

Food allergy is a growing health concern worldwide. While specific immunotherapies (SIT) are in development clinically, these approaches are not well understood, are not effective for all patients, require many doses, may cause anaphylaxis, and lack evidence of long-term efficacy. Previously, we have demonstrated the ability to apply poly(lactide-co-glycolide) (PLG) nanoscale particles in Th1/17 skewed models of autoimmunity and transplant rejection. Here, we describe application of PLG nanoparticles (NP) for delivery of allergen to relevant antigen presenting cells for reduction of Th2-associated immunity. Importantly, intravenous delivery of allergen encapsulated with PLG NP provides a well-tolerated approach to induce allergen-specific reduction in mast cell degranulation and clinical symptoms . With few doses, we demonstrate the ability to both prevent the development of and abrogate established Th2 disease, therapeutically reduce post-challenge serum MCPT-1, and decrease inflammatory cytokines, including IFN-g, IL-2, IL-4, and IL-5. These safety and biological results are a promising preliminary step in development of improved immunotherapies for food allergy.

Introduction:

The incidence of food allergy is increasing worldwide and currently affects 30 million patients in the US[288, 289]; approximately 10% of the population. Allergic disease is associated with Type 2 helper T cells (Th2) inducing production of a variety of cytokines, including IL-4, IL-5 and IL-13, which act directly and indirectly on B cells, eosinophils, basophils, mast cells and epithelial cells[114, 290]. Allergic disease requires some amount of IgE production by B cells following help from T cell subsets and class-switch recombination. Ultimately, accumulation of effector cells including mast cells with IgE-bound FcεRI which contribute to acute allergic reactions through degranulation, releasing histamine and a variety of other mediators. The mechanisms by which these orchestrate the allergic inflammatory cascade are not completely understood; however murine models and human response to therapy suggest that there is some degree of plasticity of allergic response which may be manipulated by various immunotherapies [291]. Currently, clinical recommendations for food allergy consist of antigen (Ag) avoidance and interventional targeting of inflammatory mediators using antihistamines, leukotriene inhibitors or glucocorticoids which do not address the Th2 skewing which drives allergic inflammation[292-294]. Specific immunotherapy (SIT) has been investigated clinically for the treatment of food allergies by multiple routes of administration. Oral immunotherapy (OIT) is now approved by the FDA for the treatment of peanut allergy and epicutaneous (EPIT) and sublingual (SLIT) immunotherapies are under active investigation as other promising methods of therapy. Studies suggest that these therapies can temporarily desensitize patients, and in some instances may suppress Th2 responses through the induction of regulatory and Th1 responses[295]. However, OIT and current SIT strategies function by either skewing a response or desensitizing to the antigen, which is transient and does not induce long-lasting immune tolerance[27, 29, 296, 297]. Further, administration of

unmasked Ag to sensitized patients bears a considerable risk of adverse reactions, necessitating gradual dose escalation and/or investigation of co-administration of therapies that minimize anaphylaxis[23, 298], and patients with severe anaphylaxis are frequently excluded from participation in clinical trials[28]. Non-specific biologics have been approved for application in atopic disease and are currently in various stages of investigation for application in food allergy, though their efficacy, specificity, and safety in these diseases are poorly defined. Given the paucity of treatment options available, improved methods to safely, rapidly, and effectively induce allergen-specific Th2 tolerance remain a critical clinical need.

Here we describe development a stable, well-tolerated, off-the-shelf platform for induction of allergen-specific tolerance using poly(lactide-co-glycolide) (PLG) nano-scale particles (NPs). Previously we have demonstrated the ability of NPs to induce anti-inflammatory cytokine profiles and antigen-specific immune tolerance in multiple models of Th1/17 disease. In these models, therapeutic treatment results in significantly reduced Th1 (IFN-γ) and Th17 (IL-17a/GM-CSF) cells as well as inflammatory monocytes/macrophages[9, 299, 300]. Tolerance is most effectively induced by i.v. infusion of Ag-associated NP [301, 302], which leads to their internalization by APCs in the liver and spleen that present the antigen on MHC for recognition by T cells with minimal costimulatory signaling[303]. The specific mechanisms of these NPs have not been fully elucidated, but in Th1- and Th17-driven disease lead to combination of cell-intrinsic anergy and the activation of Ag-specific iTregs[302], similar to certain cell-based therapies and reminiscent of high zone tolerance [31, 304]. Excitingly, a similar PLG nanoparticle platform is currently under development for commercial application for celiac disease and has shown promise in Phase I and Phase IIa clinical trials for celiac disease, an autoimmune disease triggered by gluten consumption[99]. However, Th2 immune responses are distinct from Th1, featuring unique

effector cells which have proved difficult to modulate as evidenced by the lack of clinical therapies to induce the long-term suppression of allergen-specific Th2 cells [305]. Previous groups have demonstrated ability to skew immune responses which can result in unresponsiveness to allergen, but to date, no therapeutics have demonstrated the induction of long-term tolerance [306-308]. These studies investigate the ability of this PLG nanoparticle platform to safely reduce reactivity in a murine model of peanut allergy via intravenous administration.

A critical consideration for any allergen-specific treatment for allergy is the risk of anaphylaxis. Clinical administration of antigen via intravenous routes is known to confer some degree of antigen-specific tolerance and is most commonly utilized for treatment of hemophilia A or B by infusion of factor VIII (FVIII) or Factor IX (FIX) concentrate[309, 310]. Other groups are investigating intravenous infusion of peptides or peptide-loaded carriers in a variety of immune disorders[23, 311-314]. This strategy has not been investigated for treatment of food allergy, likely due to a relatively high risk of anaphylaxis associated with that route of delivery over oral adminsitrations[315-317]. The field of drug delivery has developed numerous strategies to facilitate the uptake of peptides and proteins by relevant immune cells while masking their availability to off-target cells and compartments[299, 318-320]. We hypothesize that, through application and refinement of these strategies, a well-tolerated therapeutic window may exist, providing a novel method to treat food allergy with minimal doses. Such a therapy would provide additional patient treatment options, improved access to therapy, reduced burden to patients and healthcare systems, and potential for improved duration of efficacy. Here, we provide initial determination of acceptable safety parameters of a PLG NP platform to deliver peanut allergy in pre-sensitized mice, demonstrate ability to significantly abrogate biological outcomes associated

with Th2-mediated food allergy, and provide significant protection from anaphylactic outcomes with minimal therapeutic doses.

Materials and Methods:

Peanut extract (Greer Laboratories, Lenoir, NC) was used for all intraperitoneal and intranasal immunizations. For intragastric sensitization and challenge, peanut flour (Byrd Mill 12% fat, light roast) was solubilized in PBS and concentrated using a 40,000 MWCO centricon filter unit. Aluminum hydroxide (alum; alhydrogel) was purchased from InvivoGen (San Diego, Calif). Cholera toxin (CTx) from Vibrio cholera was purchased from List Biological Laboratories (Campbell, Calif). PLG (50:50) with a single carboxylic acid end group and an inherent viscosity of 0.17 dL/g in hexafluoro-2-propanol was purchased from Lactel Absorbable Polymers. Poly(ethylene-alt-maleic anhydride) (PEMA) was purchased from Polyscience. Chromogenic LAL endotoxin quantitation kit was purchased from Thermofisher Scientific**.** All other reagents were purchased from Sigma Aldrich unless noted otherwise.

Synthesis of PLG(Greer) nanoparticles:

Greer extract was encapsulated with 50:50 PLG polymer following protocols previously described [299]. Briefly, 150µL of 50mg/mL of protein (ovalbumin or Greer Peanut Extract) was encapsulated in 20% w/v PLG in dichloromethane with PEMA surfactant and allowed to evaporate. Particles were washed three times by centrifugation (5,000xg, 5 minutes, 4°C) prior to freezing and lyophilization with 4% w/v sucrose and 3% w/v mannitol. Carbodiimide chemistry was utilized for conjugation of peanut extract as previously described[321]. Briefly, solvent evaporation particles were synthesized without incorporation of antigen as described above and were similarly washed and lyophilized. Particles were washed three times with MilliQ water prior to incubation of particles and EDC at 50mg/mL and 20mg/mL, respectively. To achieve varied

loadings of surface-exposed antigen, peanut extract was incubated after activation of PLG with EDC at concentrations of 1mg/mL, 2 mg/mL, or 4mg/mL in PBS.

Nanoparticle Characterization

The size, polydispersity, and zeta potential of the NPs were determined by dynamic light scattering (DLS) by mixing 10 mL of a 25 mg/mL particle solution into 990 mL of MilliQ water using a Malvern Zetasizer ZSP. The release of encapsulated antigen from particles was measured over 72 hr as previously described[299]. Briefly, 8 mg of particle was dispersed in PBS and incubated at 37°C. At various timepoints particles were centrifuged at 7000g and 4°C for 5 min and supernatant was collected and stored at 20°C for measurement using the Micro BCA assay (Pierce). Lyophilized particles were washed by centrifugation with MilliQ water to remove cryoprotectant.

Mice and immunizations

Pathogen-free C3H/HeJ mice (female mice, 6-8 weeks old) were purchased from Jackson Laboratory (Bar Harbor, Me). Schedules of immunizations are shown in the figures. Allergic sensitization was induced with intraperitoneal immunization of 20 m g of peanut adsorbed on 2 mg alum or intragastric administration of 1 mg of peanut and 10 μg of CTx. Peanut mixed with PBS alone served as a control in preliminary experiments. Mice were challenged intragastrically with 20 mg of peanut on 7 alternating days during the final 2 weeks of the studies. All animal procedures were performed according to the University of Michigan Institutional Animal Care and Use Committee and the National Institutes of Health ‘‘Guide for the care and use of laboratory animals.’’

Measurement of serum antibodies

Sera were obtained by means of saphenous vein bleeding. Peanut-specific IgE antibody levels were determined in serially diluted serum using peanut-coated 96-well plates and alkaline phosphatase–conjugated detection antibodies, as described previously.[322]

Analysis of cytokine expression recall assays

Spleens and mesenteric lymph nodes (mLNs) were dissected and manually disrupted to generate single-cell suspensions. Red blood cells were depleted from splenocytes with ACK lysing buffer. Lymphocytes were resuspended in culture medium and plated at 800,000 cells per well in 96-well flat-bottom plates. Cells were cultured ex vivo with or without peanut (5 μg/mL). After 72 hours, cytokine secretion was measured in cell-culture supernatants by using a Luminex Multiplex detection system (Millipore, Billerica, Mass) or by ELISA (University of Michigan Cancer Center Immunology Core). For each sample, data were determined as follows:

[Peanut stimulated] – [Unstimulated] = Total (pg/mL) for each cytokine (Mean of duplicate determinations)

Assessment of hypersensitivity reactions.

Reactions were evaluated for at least 1 hour after challenge by using the following scoring system (modified from Li et al[323] and Rodriguez et al[324]): 0, no symptoms; 0.5, transient rubbing and scratching; 1, prolonged rubbing and scratching around the nose, eyes, or head; 2, puffiness around the eyes or mouth, diarrhea, piloerection, and/or decreased activity with increased respiratory rate; 3, labored respiration, wheezing, stridor, and/or cyanosis around the mouth and tail; 4, tremor, convulsion, no activity after prodding, and/or moribund; and 5, death. Rectal temperature was monitored for at least 60 minutes after challenge. Mice were bled 30 to 90 minutes after challenge,

and serum mouse mast cell protease 1 (MCPT-1) levels were determined by using an ELISA (eBioscience).

Statistics

Statistical comparisons were assessed by using the Mann-Whitney test with GraphPad Prism software (version 6; GraphPad Software, La Jolla, Calif). A P value of less than 0.05 was considered significant.

Results:

Definition of safety parameters

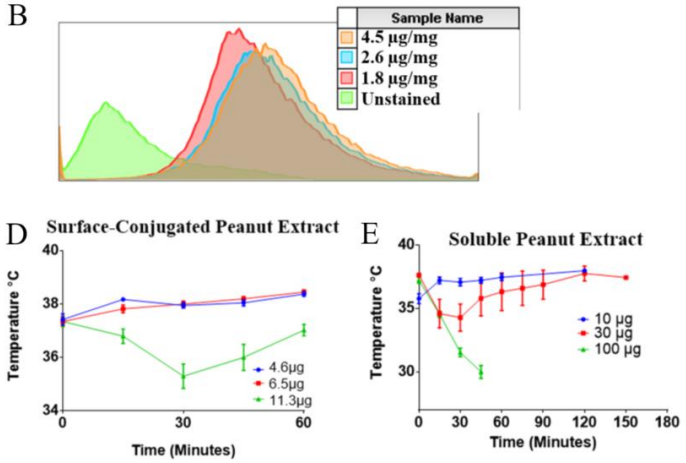
To determine whether antigen could be delivered with NP within a safe therapeutic window in these models, several studies were performed. Mice were sensitized with peanut extract and alum as previously described[322] and treated with NPs with various amounts of peanut extract conjugated via carbodiimide chemistry to their surface (Fig 1A). Mice receiving less than 11.3µg of total surface-exposed allergen did not exhibit symptoms of anaphylaxis as evidenced by temperature drop, defining an important parameter for future NP design. The amount of chicken FITC anti-peanut antibody (source) increased (Fig 1B) with increasing antigen loading as measured by µBCA assay (Fig 1A), confirming an increasing amount of surface-exposed

A

	Size (nm)	Zeta (mV)	PDI	Antigen Loading (µg/mg)
PLG-PE$_{low}$	511.4±20.3	-40.1±1.1	0.13	1.8
PLG-PE$_{med}$	654.7±37.4	-42.6±0.67	0.44	2.6
PLG-PE$_{high}$	588.3±10.0	-44.6±1.3	0.37	4.5

C

2.5mg Dose	Exposed Ag (µg)	Soluble Ag (ug)	Anaphylaxis
PLG-PE$_{low}$	4.6	N/A	Not Observed
PLG-PE$_{med}$	6.5	N/A	Not Observed
PLG-PE$_{high}$	11.3	N/A	Mild



allergen. As with surface-exposed proteins, allergen released from NPs via burst release may similarly induce anaphylactic response through

Figure 5.1 Determination of safety parameters related to delivery of peanut extract via NP. Surface-conjugated NP (PLG-PE) were generated with relatively low, medium, or high loadings of peanut extract. Physicochemical properties are listed (A). Increased surface loading of peanut extract correlates with increased FITC anti-peanut antibody as measured by flow cytometric analysis (B). Relative amounts of surface or soluble peanut extract delivered intravenously and corresponding observation of anaphylactic response (C). C3H/HeJ mice were sensitized with i.p. injection of peanut and alum at Days -14 and -0 as described. Mice received injection of surface-conjugated PLG-PE or soluble peanut extract on Day +7 and were assessed for anaphylaxis as measured by core temperature (D and E).

intravenous bolus dose of the allergen. To determine the maximum amount of tolerable allergen that can be burst release in this model, increasing doses of Greer Peanut Extract in PBS were delivered intravenously. As shown in Fig 1E, a bolus dose of 30μg results in mild temperature drop and represents the maximum amount of antigen that may be permissible from burst release. While these safety parameters are likely to vary in humans and in various pre-clinical models, these studies provide a key design parameter for particle synthesis.

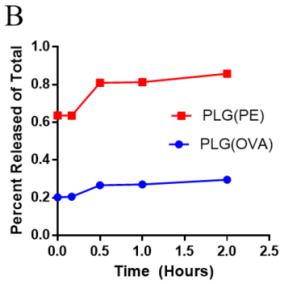
Synthesis and characterization of nanoparticles

Greer peanut extract (PE) and ovalbumin protein (OVA) were encapsulated within PLG (4200 g/mol; 0.17 dL/g) using w/o/w solvent evaporation emulsion method. Antigen loading (μg protein per mg nanoparticle) was determined by μBCA assay for the formulations **Fig 2A**. Selection of protein did not drastically impact nanoparticle size, zeta potential, or morphology and all formulations were designed to be within a range of previously-investigated values which have shown efficacy in other models[9, 299]. Antigen release over 2 hours demonstrates a relatively

large burst release of peanut extract from PLG(PE),**Fig 2B.** Endotoxin was confirmed to be below acceptable limits for each formulation [325] (Fig 2C).

A

	Size (nm)	Zeta (mV)	PDI	Antigen Loading (µg/mg)
PLG(PBS)	502.2±32.4	-42.5±0.95	0.38	-
PLG(PE)	563.5±5.7	-61.9±2.2	0.20	10.3
PLG(OVA)	633.7±9.7	-44.3±1.0	0.434	35.1



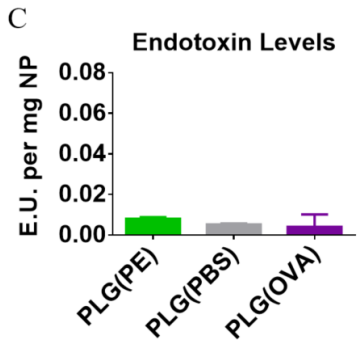
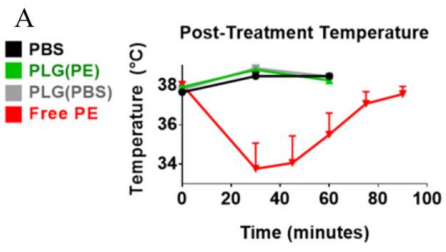
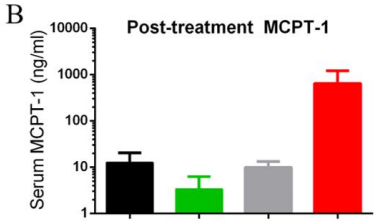


Figure 5.2 Characterization of PLG NP used for *in vivo* studies. NP Size, Zeta, Polysdispersity (PDI), and antigen loading (µg antigen per mg NP) are characterized (A). Antigen release was measured over 2 hours (B). LAL Endotoxin testing indicates acceptable levels for all formulations utilized (C).

PLG(PE) administration is well-tolerated in pre-sensitized mice

While data from previous models suggest that PLG NPs encapsulating proteins have relatively low surface antigen expression[299], it was not known whether i.v. administration of this formulation would be well-tolerated in mice with established food allergy. C3H/HeJ mice were sensitized by i.p. administration of peanut extract adsorbed on alum as previously described[322]. 7 days after sensitization, mice were administered PBS, Blank nanoparticles, PLG(PE) containing 25.75µg of total peanut extract, or an equivalent dose of PE in soluble form (**Fig 3A)**. NPs were synthesized to have sufficiently low surface expression of allergen and burst release to ensure their safety, as





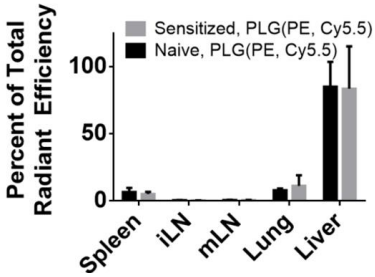


Figure 5.3 PLG(PE) is well-tolerized in pre-sensitized mice. C3H/HeJ mice were sensitized by i.p. injection of alum and Greer peanut extract on Day -7. Mice were treated on Day 0 with PLG(PE) or controls and assessed for anaphylactic response to therapy. Intravenous injection of PLG(PE), PBS, or PLG(PBS) were well tolerated, while injection of an equivalent total dose (25.75µg) of soluble Greer peanut extract resulted in anaphylactic temperature drop (A) and serum release of MCPT-1 (B) (n=5). Cyan 5.5-labeled, peanut extract-loaded NPs (PLG(PE, Cy5.5)) were injected intravenously. 24 hours post-injection, spleens, inguinal lymph nodes, mesenteric lymph nodes, lungs, and livers were collected and imaged by IVIS to determine relative organ distribution in naïve and pre-sensitized mice, presented as percent of total radiant efficiency (C). Statistical significance: * = P<0.05, ** = P <0.01

previously determined in Fig 1. Mice treated with PBS, Blank, or PLG(PE) did not show evidence of anaphylaxis as measured by rectal measurements of body temperature (**Fig 3A**) or MCPT-1 release in serum (**Fig 3B**), however an equivalent dose of total soluble Greer extract was not well-tolerated, indicating the importance of masking allergen pre-sensitized individuals. These results confirmed that PLG(PE) was well tolerated in an i.v. formulation. While surface levels of allergen in these formulations are low, it is expected that serum antibodies will bind these particles upon administration. It is unknown whether allergen-specific binding can significantly alter the distribution of nanoparticles of this size at an organ level. To investigate this, PLG(PE) was fluorescently tagged with Cy5.5 as previously described[299]. C3H/HeJ were sensitized by i.p. administration of PE adsorbed on alum and particles were administered to sensitized or naïve mice. 24 hours later, spleens, livers, inguinal lymph nodes, and mesenteric lymph nodes were collected. Organ-level biodistribution was measured by fluorescence imaging using In Vivo Imaging Systems (IVIS) and quantifying the percent of total radiant efficiency contributed by each organ **(Fig 3C)**.

Prophylactic administration of PLG(PE) prevents sensitization

Based on our results in previous models, we expected that prophylactic administration of PLG(PE) would have significant effects on disease induction. Given the complexity of response in models of food allergy and the biological discrepancies between Th2- and Th1/17-mediated diseases, we tested whether this would be true in two widely-used mouse models of peanut allergy. Development of a well-tolerated NP particle is an important step to clinical translation; however, biological efficacy is an obvious prerequisite to adoption and has not been investigated in food allergy models.

PLG(PE) or controls were administered to C3H/HeJ mice i.v. on Days 0 and 14. Mice were sensitized by i.p. administration of PE adsorbed to alum at Days 7 and 21. Mice were challenged orally with PE on days 28, 30, 32, 35, 37, 39, 42 to determine reactivity. Control mice that were treated with blank particles or PBS displayed severe disease symptoms compared to PLG(PE) as

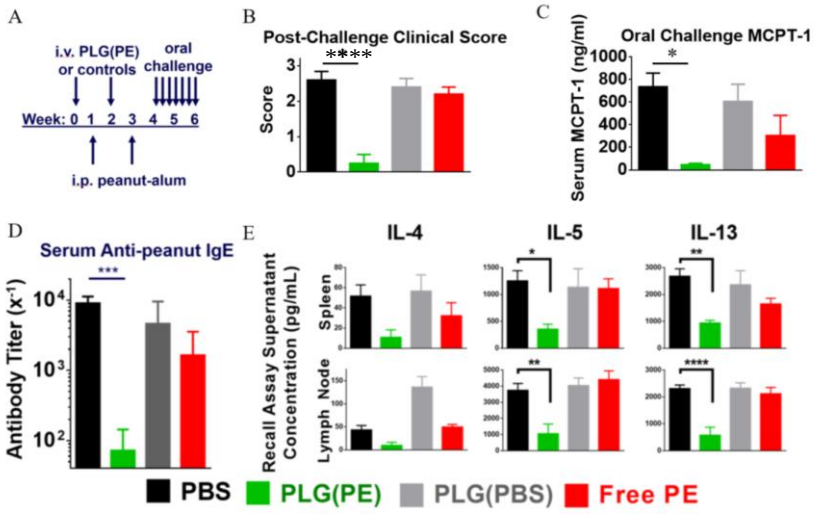


Figure 5.4 PLG(PE) provides prophylactic protection from peanut allergy. C3H/HeJ mice were sensitized by i.p. injection of alum and peanut extract on Day 0 and 14 and received treatment or controls on days 7 and 21. Data represent 7th and final oral challenge. Schematic of experimental timeline (A). Clinical anaphylaxis score was characterized (B) and serum MCPT-1 levels determined by ELISA (C). Serum peanut-specific IgE levels were characterized (D) and cytokine secretion in culture supernatants of recall assays were measured by Luminex multiplex (E). n=5 per group. Statistical significance: * = P<0.05, ** = P <0.01 **** = P <0.001

measured by Clinical Score **(Fig 4A)** and serum MCPT-1 after oral challenge **(Fig 4B).** Administration of soluble PE was not well tolerated, but did result in a trend towards protection from oral challenge as measured by serum MCPT-1, a protease released by degranulating mast cells. To determine contributions to the mechanism of sensitization prevention, serum anti-peanut IgE and allergic cytokine production by mesenteric lymph node and splenic cells were assessed following stimulation with peanut. PLG(PE) significantly reduced serum anti-peanut IgE, with expression below detectable threshold in 80% of mice **(Fig 4C).** Analysis of response to peanut in recall assays of splenic and mesenteric lymph node cells indicated significant reduction in cytokine secretion, indicating inhibition of stimulation consistent with allergenic tolerance **(Fig 4D)**. These

results demonstrate that PLG(PE) is able to robustly prevent disease induction in Th2-mediated models of food allergy.

Therapeutic administration of PLG(PE) provides benefit to clinical symptoms

The development of a well-tolerated, intravenously delivered NP platform for allergy treatment is a critical development. Further, prophylactic administration of PLG(PE) promoted tolerance to peanut and prevention of sensitization, representing an important biological outcome. Regardless, application in an established allergic disease will likely be a necessity for broad clinical translation and studies were conducted to investigate their efficacy in these settings. We next investigated whether therapeutic administration of formulations would confer protection in these models of disease. The majority of these studies utilized the alum-induced murine model of food allergy in which sensitization is achieved through i.p. administration of peanut with alum. Murine models of food allergy can also be achieved through oral administration of peanut in the presence of cholera toxin (CTx), another commonly-used model which was used here to demonstrate ability to safely treat disease with this formulation [323, 326].

Importantly, administration of three doses PLG(PE) was sufficient to significantly abrogate MCPT-1 and anaphylactic temperature (Fig 5A, B). Cytokine secretion of splenic or mesenteric lymph node cells following exposure to peanut demonstrate a significant reduction in several

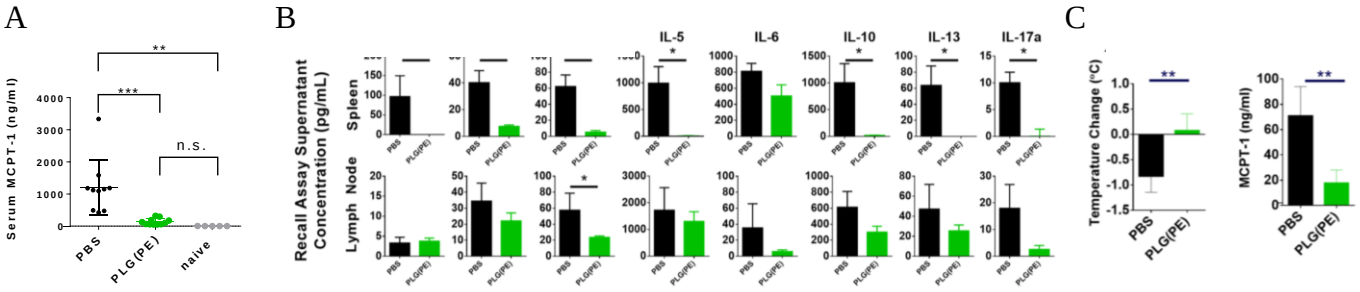


Figure 5.5. Attenuation of anaphylactic response with PLG(PE). Mice were sensitized with alum beginning on Day 0 and treated with PLG(PE) on Days 21, 28, and 35 (A) or 21 and 28 (B). Therapeutic efficacy in CTx-induced disease were tested by CTx sensitization on Day 0 and treatment on days 42, 49, and 65 (C and D). PLG(PE) provided protection from alum-induced serum MCPT-1 production (A). Serum cytokine recall assays of spleen and mesenteric lymph node cells by Luminex multiplex assay demonstrate significant reduction in allergic and inflammatory cytokines (B) in alum-induced disease. PLG(PE) provided protection from CTx-induced allergy as measured by post-challenge temperature drop (C) and serum MCPT-1 release (D). Statistical significance: * = P<0.05, ** = P <0.01

markers, including IL-2, IL-4, and IL-5 in splenic cultures and IL-4 in lymph node culture (Fig 5C). Similarly, therapeutic administration of PLG(PE) was sufficient to significantly reduce serum MCPT-1 in an alum-induced model of peanut allergy. These results are inconsistent with a mechanism of skewing toward Th1 and IL-10 dominated phenotypes, which is a commonly utilized method to abrogate Th2 disease. This may suggest a more complete tolerance to specific allergen than other therapies.

Discussion:

Food allergy is a life-threatening disease that represents a considerable quality of life reduction for patients and economic burden for society[296, 322]. While SIT is available for some patients, this treatment option carries high risk of anaphylactic response, requires months or years of treatment, and has not demonstrated long-term efficacy in most patients[27, 214]. This manuscript introduces the use of a PLG nanoparticle platform similar to those currently in clinical trials for celiac disease for the treatment of peanut allergy in a murine model[99]. While food allergy and celiac disease share certain symptoms, celiac disease involves recognition of gluten proteins by CD4+ T cells in the small intestine and lacks many of the IgE-mediated hypersensitivity responses observed in allergic disease[327]. As the effector cells and chemical mediators involved are largely disparate, it is unclear whether therapies that are effective in celiac disease would also have efficacy in food allergy. Delivery of allergen by NP would provide multiple benefits over SIT, including targeted delivery to relevant antigen presenting cells, limitation of epitope exposure for undesired immune recognition, and the potential to achieve efficacy with relatively few doses as has been previously shown in murine models of autoimmune disease[9, 167]. Intravenous delivery of allergens for treatment of food allergy is not attempted due to this risk of anaphylaxis, although there is a significant body of literature

suggesting that this route may be an effective method to induce tolerance through one of several pathways, including possible contributions from high-zone tolerance[304, 328, 329]. Regardless of the route of administration of allergen for immunotherapy protocols, there is risk of anaphylaxis which is a major shortcoming of current therapies.

In previous studies, incorporation of antigen within 500nm NP facilitates delivery of allergen to relevant liver- and spleen-resident antigen presenting cells and presentation to T cells, which is expected to afford improved efficiency over injection of soluble allergen alone[299, 307, 330]. Additionally, by encapsulating allergen or interfering with epitope availability via surface conjugation, risk of anaphylaxis is expected to be lower than for delivery of soluble allergen alone. Two commonly-used methods of antigen incorporation in polymeric NP formulations involve encapsulation or surface-conjugation. Encapsulation may reduce the risk of surface-exposed allergen triggering degranulation of effector mast cells in pre-sensitized individuals; however, there is risk of anaphylaxis related to the burst release of contents upon reconstitution or injection. This manuscript quantifies the thresholds above which anaphylaxis occurs with surface-bound or soluble allergen in order to determine appropriate methods to deliver allergen efficiently to relevant antigen presenting cells of the liver (primarily Kupffer cells) and spleen. To our knowledge, this is the first instance of quantification of the amount of surface-bound and soluble allergen that is well-tolerated intravenously within these models, which are design criteria that are critical to ensure the clinical translation of any platform. We demonstrate that 11.3μg of surface-bound allergen or 30μg of soluble peanut extract triggers anaphylaxis in this model of peanut allergy. The PLG(PE) tested exhibited burst release of 64% of its contents upon reconstitution in PBS, which is not unexpected given the low molecular weight of the PLG utilized and the heterogeneity of the peanut extract. Thus it is expected that a total dose of

approximately 47µg of peanut extract could be delivered without further optimization of this encapsulated formulation without reaching these thresholds and without impacting organ-level biodistribution. Importantly, masking of allergen by encapsulation within PLG NPs enabled delivery of 25.75µg of peanut extract without inducing measurable anaphylactic responses observed with 30µg of soluble peanut extract or 11.3µg of surface-conjugated peanut extract. While intravenous administration has historically been associated with induction of tolerance or immunological unresponsiveness, it was unclear whether a therapeutic window exists below these safety parameters and is primarily utilized in treatment of hemophilia [304, 331] [309, 310]. This manuscript details the first application of this particle platform in models of food allergy and demonstrates robust prophylactic tolerance. Interestingly, the PLG NPs used in these studies demonstrated antigen-specific suppression of T cell responses generally and was not associated with skewing of T cell phenotypes towards Th1/17, as is often the case in similar therapies under development[29, 66, 322, 332]. Interestingly, while other investigational therapies for food allergy promote a skewing toward Treg phenotypes and while this platform has demonstrated ability to increase Tregs and IL-10 production in other models of disease, here IL-10 was also reduced[26, 302]. Other observed results are consistent with previous studies performed with this NP platform in models of autoimmunity driven by Th1/17-polarized immune responses[8, 299]. Importantly, investigation of the ability of this well-tolerated platform to provide therapeutic efficacy demonstrated ability to significantly reduce quantitative measurements of anaphylactic response and provides rationale for further investigation of the technology and methods to improve it.

Future studies will investigate whether the relative contributions observed in models of autoimmunity are similar within these models of Th2-mediated food allergy. It is unclear

whether immunological skewing would be desirable in a clinical setting, though there is reason to believe that, by avoiding immune skewing, clinical outcomes may be more reflective of a non-allergic individual which may be preferable clinically[333, 334]. Ultimately any therapy capable of addressing the previously discussed shortcomings of existing OIT regimens are highly desirable. While definition of safety parameters and demonstration of prophylactic efficacy are important milestones, they do not represent a clinically-relevant result. To investigate this, we applied PLG(PE) in a murine model of peanut allergy that is thought to be more clinically relevant[326, 335]. Importantly, PLG(PE) was well-tolerated and resulted in a significant reduction in MCPT-1 and clinical score which was not observed after administration of NP lacking relevant antigen.

Conclusion:

Here, we demonstrate the ability to induce tolerance to peanut extract by administration of PLG NPs after sensitization. Current immunotherapies under clinical evaluation for food allergy therapy require months or years of administration with considerable risk of anaphylaxis and limited evidence of long-term clinical unresponsiveness[27, 322, 336, 337]. These results represent an important step in the development of food allergy therapeutics that require less arduous therapy and appear to induce immunological tolerance rather than the desensitiztion that has been observed by other polymeric or nanoparticulate technologies still under investigation or by SIT, which is often associated with reduction of Th2 phenotypes and IgE as well as other [29, 322, 334, 338]. The particles described have been developed clinically and have demonstrated efficacy in Phase I and Phase IIa trials in celiac disease and, though their efficacy in human Th2-mediated diseases remain unclear, these studies represent critical steps towards investigation of their efficacy in food allergy[99]. Future studies should investigate other strategies to limit adverse reaction to particle-

based delivery of allergen without impacting therapeutic efficacy. Such strategies will enable increased allergen loading within formulations, which has been demonstrated to be therapeutically beneficial in other models of immune disorders and are expected to similarly improve efficacy in Th2-mediated models of allergy[29, 72, 330, 339, 340].

Acknowledgements:

Funding:

This work was supported by NIH EB-013198

Chapter 6 Optimizing PLG Nanoparticle-Peptide Delivery Platforms for Transplantation Tolerance Using an Allogeneic Skin Transplant Model

Authors

Sahil Shah[*], Saeed Daneshmandi[*], Kevin R Hughes, Shuangjin Yu, Angela M. Bedoya, Lonnie D. Shea, Xunrong Luo *These authors contributed equally to this work.

Abstract

A robust regimen for inducing allogeneic transplantation tolerance involves pre-emptive recipient treatment with donor splenocytes (SP) rendered apoptotic by 1-ethyl-3-(3′-dimethylaminopropyl)-carbodiimide(ECDI) treatment. However, such a regimen is limited by availability of donor cells, cost of cell procurement, and regulatory hurdles associated with cell-based therapies. Nanoparticles (NP) delivering donor antigens are a promising alternative for promoting transplantation tolerance. Here, we used a B6.C-H-2bm12(bm12) to C57BL/6(B6) skin transplant model involving a defined major histocompatibility antigen mismatch to investigate design parameters of poly(lactide-co-glycolide) (PLG) NPs delivering peptides containing the donor antigen for optimizing skin allograft survival. We showed that an epitope-containing short peptide (P1) was more effective than a longer peptide (P2) at providing graft protection. Importantly, the NP and P1 complex (NP-ECDI-P1) resulted in a significant expansion of graft-infiltrating Tregs. Interestingly, in comparison to donor ECDI-SP that provided indefinite graft protection, NP-ECDI-P1 targeted different splenic phagocytes and skin allografts in these recipients harbored significantly more graft-infiltrating CD8+IFN-γ+ cells. Collectively, the current study provides initial engineering parameters for a cell-free and

biocompatible NP-peptide platform for transplant immunoregulation. Moreover, it also provides guidance to future NP engineering endeavors to recapitulate the effects of donor ECDI-SP as a goal for maximizing tolerance efficacy of NP formulations.

Introduction

Organ transplantation is currently the most effective treatment for end-stage organ diseases and is often the only available therapeutic option[341-343]. Allogeneic organs (i.e., from another person) are commonly used for transplantation, yet the number of individuals awaiting transplantation in the United States is over 121,000, and is growing annually at a rate far greater than the donor growing rate[344]. Confounding this unmet need, transplantation generally requires the recipient to take immunosuppressive drugs indefinitely to prevent acute graft rejection, but such a requirement often comes with an increased risk of subsequent neoplasia and infections[345-347]. Ideally, antigen-specific tolerance therapies would replace broad-scale immunosuppressants and eliminate their undesirable side effects [262, 348].

One promising antigen-specific therapy developed by us involves intravenous infusion of 1-ethyl-3-(3′-dimethylaminopropyl)-carbodiimide(ECDI) fixed apoptotic donor splenocytes (ECDI-SP) to induce donor-specific tolerance[95, 349]. This approach takes advantage of the body's natural ability to maintain self-tolerance through daily non-inflammatory clearance of billions of self apoptotic cells generated by physiological turnover and applies it to the clearance of donor apoptotic cells, thereby inducing tolerance to donor [349, 350]. This approach has proven to be highly effective in full major histocompatibility complex (MHC) mismatched transplantation models [349, 351], including in non-human primates[352]. Mechanistic studies reveal that when delivered *in vivo*, ECDI-SP mediate anergy and deletion of alloreactive T cells via PD-L1/PD-1 signaling, production of immunosuppressive cytokines, and induction of

regulatory T cells (Tregs), which collectively facilitate indefinite graft survival [95, 349, 352]. Leveraging the concept of apoptotic cell clearance as a tolerogenic process, ECDI-fixed apoptotic *syngeneic* splenocytes coupled to *donor* cell lysate also resulted in comparable allogeneic islet cell survival in comparison to apoptotic donor splenocytes themselves [351]. While powerful, these cell-based therapies are limited by the high cost of cell harvesting, processing, administration, and an increased regulatory hurdle to clinical translation [353]. A non-cell-based delivery platform that is more easily sourced and that leverages the tolerogenic features of apoptotic cell clearance would be a desirable alternative to cell-based therapies. One such promising alternative is nanoscale polymeric particles composed of poly(lactide-co-glycolide) (PLG) which is FDA-approved in several biodegradable drug delivery applications [354]. PLG has non-toxic degradation byproducts and allows precise control of characteristics such as surface charge, size, and degradation time[355, 356]. PLG nanoparticles (PLG-NPs) covalently coupled to antigenic peptides have been shown to have promising tolerance efficacies in pre-clinical models of autoimmune and allergic diseases. This platform exploits tolerogenic pathways similar to apoptotic donor cell treatment[72, 307, 308]. In models of allergy and autoimmunity such as experimental autoimmune encephalomyelitis (EAE), it has been shown that factors including nanoparticle surface charge, size, shape, and route of administration are key parameters of this platform for achieving peripheral tolerance[8, 167, 330, 339, 357-359]. Translating to allogeneic transplantation tolerance, MHCs of donor origin are the primary donor antigens recognized as “non-self”, and therefore can elicit anti-donor immune responses after being processed and presented as donor antigenic MHC peptides by recipient MHCs to activate recipient T cells [108]. Consequently, immune tolerance to such appropriately selected donor antigenic MHC peptides that encompass the entire spectrum of donor-recipient MHC

mismatches would allow donor-specific tolerance to be established in the recipient. Based on the above-mentioned published data in autoimmunity and allergy, this could be accomplished by NPs coupled to such donor antigenic MHC peptides. However, additional engineering parameters including antigenic peptide length for MHC presentation, chemical method of covalent conjugation, and location of antigen within the polymeric carrier will likely require further characterization in their contributions to transplantation tolerance induction.

Here, we investigate these engineering parameters and their contribution to inducing transplantation tolerance in a bm12 to B6 skin transplant model using PLG NPs. In this model, three point mutations in the MHC class II molecule IA^b of the bm12 donor in comparison to the IA^b of the B6 recipient is sufficient to induce T cell-mediated immunity in the recipient and to prompt acute rejection of the skin allograft within two to three weeks [360, 361]. The current study aims to use the bm12 to B6 skin transplant model to identify key engineering parameters regarding antigen selection and method of conjugation to polymeric particles, and to investigate their efficacy in enhancing skin allograft survival. Our study uncovers the effective NP formulations for *partial* graft protection in this model and their preponderance for inducing intragraft $CD4^+Foxp3^+$ Treg accumulation. However, in comparison to donor ECDI-SP that provide *indefinite* graft protection, the NP formulations target different splenic phagocyte populations, and are suboptimal in suppressing intragraft $CD8^+IFN\gamma^+$ effector cell accumulation. A broader goal is to investigate the potential of PLG-NPs coupled with either donor antigenic peptides or donor cell lysate derived antigens as a replacement for donor ECDI-SP cell therapy for transplantation tolerance. Our results thus not only form the basis from which investigators can now examine the cellular mechanisms of NP-based transplant tolerance, but will also direct future rational design of polymeric platforms eventually to be used in human transplantation.

Materials and Methods

Mice

8-10-week-old male bm12 (H-2bm12) and C57BL/6 (B6, H-2b) mice were purchased from the Jackson Laboratory and Harlan. ABM (H2b) mice (T cell receptor transgenic mice with CD4 T cells reactive to the I-A^b bm12 epitope) were provided by Dr. Mohammed Javeed I Ansari from the Northwestern University (NU). All mice were housed under specific pathogen free conditions at NU. All protocols were approved by NU IACUC.

Skin transplantation

The bm12 tail skin grafts were transplanted onto the dorsum of B6 mice on day 0. Following engraftment, rejection was determined when 80% of the graft area was necrotic.

Donor antigen preparations

Antigenic peptides KSQPEFLEQKRAEL (P1), KLGRPDAEYWNSQPEFLEQKRAELDTVCR (P2) and CSQPEFLEQKRAEL (P3), and P1-Fluorescein isothiocyanate (FITC) were synthesized by Peptide 2.0 (Chantilly, VA). To prepare donor cell lysate, bm12 splenocytes were processed into single cell suspensions and erythrocytes were lysed. Up to 1×10^9 cells were sonicated in PBS at an amplitude of 60% for 10s, followed by 10s on ice for a total of 6 cycles (Cole–Parmer). Total protein was quantified by Coomassie Plus (Bradford) Protein assay (Thermo Fisher Scientific Inc.) prior to coupling to PLG particles.

PLG particle synthesis

Single emulsion, antigen-free (blank) poly(lactide-co-glycolide) (PLG) particles to be used in surface-coupling experiments were synthesized with poly(ethylene-alt-maleic acid) (PEMA) as a surfactant as previously described[31] . Briefly, acid terminated PLG (50% D,l-lactide/50%

glycolide) (Sigma Aldrich) was dissolved in dichloromethane (DCM) to make a 20% (w/v) solution. This solution was sonicated (Cole–Parmer) at an amplitude of 100% in 1% w/v PEMA (Polysciences, Inc.) for 30s to create particles. After overnight stirring, particles were collected by centrifugation, washed 3 times with distilled water, and lyophilized overnight.

Antigenic peptide encapsulation in PLG nanoparticles

Antigen-polymer nanoparticles encapsulating the bm12 peptide were synthesized as described previously with minor modifications[299]. Briefly, PLG polymer was dissolved at 2% w/v in dimethylformamide (DMF). ECDI (5x to PLG, mole ratio) was dissolved at 2% w/v in DMF and added dropwise to the PLG solution. N-Hydroxysuccinimide (NHS, 5x to PLG, mole ratio) was dissolved at 1% w/v in DMF and added dropwise to the solution. The reaction was stirred for 15 min at room temperature. Antigenic peptide (1.2x to PLG, mole ratio) was dissolved at 2% w/v in DMF and stirred at 400 RPM. Triethylamine (5x to peptide, mole ratio) was added to peptide solution and the mixture was added dropwise to the stirring PLG solution. The reaction was allowed to proceed overnight at room temperature. The resulting polymer was purified by dialysis using 3,500 molecular weight cut-off membrane against distilled water. The dialyzed polymer was collected and washed with MilliQ water three times, and centrifuged at 7000×g before lyophilization. Coupling efficiency of peptide to PLG was determined by 1H NMR analysis in DMSO-d_6 (Supplementary Fig. 1). The NMR endgroup analysis suggested a coupling efficiency of 66.9%.

Antigenic peptide conjugation to PLG nanoparticles

For carbodiimide conjugation, 10 mg of blank single-emulsion PLG nanoparticles (NPs) were incubated with 30.75 mg of 1-ethyl-3-(3′ dimethylaminopropyl) carbodiimide (ECDI, Calbiochem) and 1 mg of P1, 2 mg of P2 or 1 mg of bm12 lysate in 1 ml of PBS (Life

Technologies Inc.) on ice for 1 h while shaking (Labline Instruments Inc., Melrose Park, IL). For maleimide conjugation, 10 mg of PLG NPs were incubated with 2.74 mg of ECDI and 6.58 mg of N-hydroxysulfosuccinimide (NHS, Sigma-Aldrich) in 1 ml of 2-(N-Morpholino) ethanesulfonic acid (Sigma Aldrich) for 15 min, followed by washing. The NPs were then incubated with 1.70 mg of N-β-maleimidopropionic acid hydrazide (BMPH, Sigma Aldrich) in 3 ml of PBS for 2 h at room temperature followed by a PBS wash and incubation with 1 mg of P3 in 1 ml of PBS for 5 min. To prepare B6 splenocytes coupled with peptides, 3.2×10^8 B6 cells were incubated with 30.75 mg ECDI and 1 mg of P1, 2 mg of P2 or 1 mg of bm12 lysate in 1 ml of PBS on ice for 1 h on a shaker followed by washing. To prepare donor bm12 ECDI-SP, 3.2×10^8 bm12 splenocytes were incubated with 30.75 mg ECDI in 1 ml PBS on ice for 1 h on a shaker followed by washing.

Particle characterization

Particles were imaged with a scanning transmission electron microscope (LEO Gemini 1525) operating at 200 kV. Z-average diameter and surface ζ-potential were obtained using a Zetasizer Nano ZSP (Malvern Instruments Ltd). The release of P1 from NPs was measured over 196 h. Briefly, 3 mg of NPs were dispersed in 1 mL of PBS with 10% FBS on a rocker at 37 °C. At predetermined time points, the NPs were centrifuged at 7000 RPM for 6 min and 0.5 mL of supernatant collected. Each time the particles were resuspended, replenished with 0.5 mL PBS with 10% FBS and further incubated until 196 h were reached. All supernatant samples were stored at −20 °C until the end of the experiment. Upon experiment completion, a CBQCA protein quantification assay (Molecular Probes) was used to determine the remaining peptide amount for each supernatant sample. 3 mgs of lyophilized NP formulations were dissolved in DMSO and a CBQCA assay was used to determine the initial amount of loaded peptide before release. Peptide

released at each time point was calculated as cumulative peptide release at that time point over the initial peptide loading amount before release ("Percent of Initial Loading"). For fluorescent imaging of NPs with surface conjugated peptide versus encapsulated peptide, P1-FITC was conjugated using the protocol in 2.6 or encapsulated using the protocol in 2.5. Rhodamine dye was encapsulated in NPs to label the NPs. Images were taken at 60× magnification on a confocal microscope and fluorescent channel intensity profiles were calculated (Nikon A1C, Nikon Elements).

In vivo biodistribution study

Donor bm12 ECDI-SPs were labeled with 2 μM PKH67 (Sigma–Aldrich). Briefly, 2×10^7 cells were suspended in 1 ml of diluent C mixed with 1 ml of diluent C containing 4 μM of PKH67 for 5 min before washing with RPMI 1640 (Gibco) supplemented with 10% FBS (Gibco). Rhodamine B conjugated nanoparticles were fabricated following the single emulsion protocol described in 2.4, with the only modification being that per 100 mg of PLG polymers, 0.5 mg of rhodamine B was dissolved simultaneously in DCM. 1×10^8 PKH67 labeled bm12 ECDI-SPs, 3 mg of blank rhodamine-labeled PLG NPs, or 3 mg of P1-coupled rhodamine-labeled PLG NPs were injected intravenously into B6 mice. At 24 and 96 h post injection, mice were sacrificed and organs collected, processed into single cell suspensions, and PKH67/rhodamine fluorescence analyzed by flow cytometry (BD FACSCantoII).

Recipient treatment schemes

PLG NPs coupled with peptides or bm12 cell lysate (3.0 mg per dose), blank PLG NPs (3.0 mg per dose), B6 SPs coupled with peptides (1×10^8 per dose) or bm12 ECDI-SP (1×10^8 per dose) were injected *i.v.* into recipient B6 mice on day −7 and day +1 with day 0 being the day of skin transplant.

Generation of bone marrow derived macrophages (BMDMs)

The femur and tibia of B6 mice were isolated. Marrow was flushed out with PBS using a 21G needle and subsequently centrifuged. Erythrocytes were lysed and remaining cells were resuspended into single cell suspensions. Bone marrow derived cells were plated in 100 mm petri dishes (Sigma Aldrich) in RPMI-1640 (Gibco) supplemented with 10% fetal bovine serum (Gibco) and 20 ng/ml recombinant mouse macrophage colony-stimulating factor (M-CSF, R&D Systems) for 7 days with a media change on day 3.

ABM T cell proliferation *in vitro*

96 well U-shape plates (Fisher Scientific) were pre-coated with 5 μg/ml hamster anti-mouse CD3e (clone 145-2C1) and 2 μg/ml hamster anti-mouse CD28 (clone 37.51) from BD Biosciences. T cell receptor transgenic (TCR Tg) ABM $CD4^+$ T cells were purified from the spleen of ABM mice using $CD4^+$ cell negative isolation kit (Miltenyi). ABM $CD4^+$ T cells were labeled with 1 μM violet proliferation dye (BD Biosciences). 4×10^4 B6 BMDMs and 4×10^4 ABM $CD4^+$ T cells were plated in the precoated plates with the addition of either 30 μg of indicated NP preparations or 1.2×10^5 indicated SP preparations in RPMI-1640 supplemented with 10% FCS for 3 days. The rationale for using 30 μg NP preparations or 1.2×10^5 SP preparations in this assay was that according to the CBQCA quantification in Fig. 1D, these doses would provide approximately the same amount of peptide antigen to the co-cultured BMDMs. Cells were then harvested for determination of ABM $CD4^+$ T cell proliferation by dilution of the violet proliferation dye.

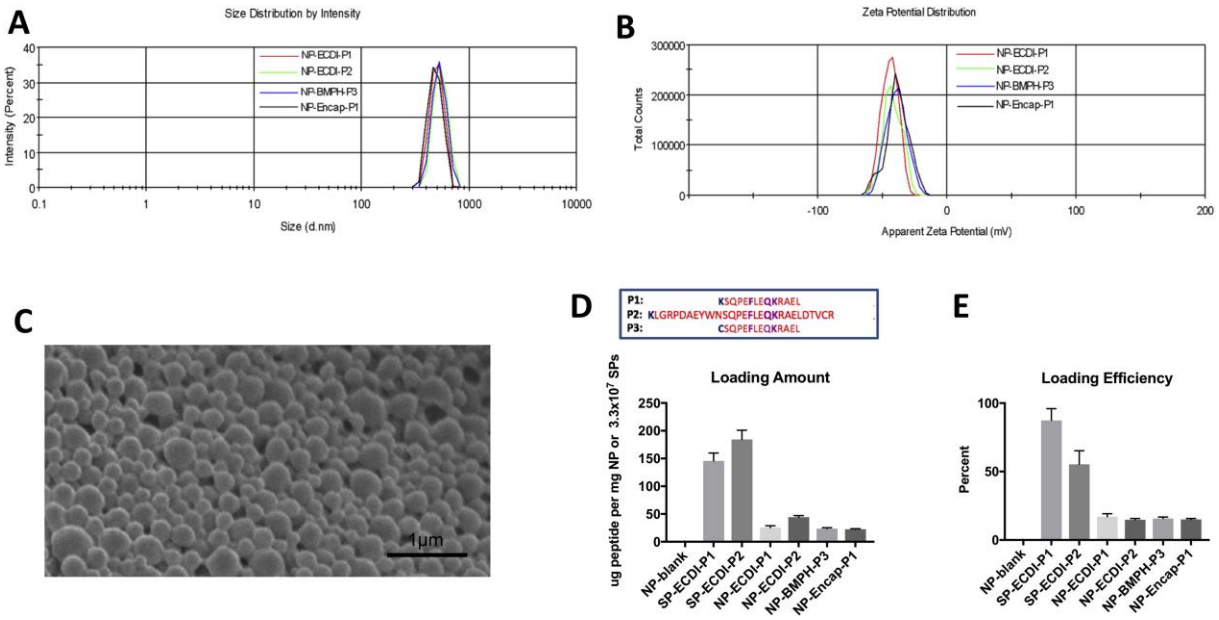


Figure 6.1 **PLG NP characterization and quantification of antigen coupling**. **(A)** Nanoparticles size (486.5 ± 26.4 nm) and **(B)** surface Zeta Potential distribution (−40.95 ± 2.66 mV) were obtained using dynamic light scattering (n = 3). **(C)** Representative scanning Electron Micrograph (SEM) image of PLG NPs used for antigen coupling. **(D)** Loading amount. After peptide coupling by different methods, the amount of peptide loaded on each platform was determined by CBQCA assay. Measurements were standardized to 1 mg of PLG NPs or 3.3×10^7 splenocytes (n = 5), as 3 mg of PLG NPs or 1×10^8 antigen-coupled splenocytes per dose were injected for subsequent *in vivo* experiments. **(E)** Loading efficiency. Calculated as the percentage of bound peptide following the conjugation/encapsulation reaction over the input peptide at the beginning of the conjugation/encapsulation reaction. For **(A)**–**(C)**, data are representative of 3 independent experiments. For **(D)** and **(E)**, data shown are average from 3 independent experiments.

Analysis of skin graft infiltrating cells and draining lymph node (DLNs) cells

PLG NPs coupled with P1 (3.0 mg per dose), blank PLG NPs (3.0 mg per dose), or bm12 ECDI-SP (1×10^8 per dose) were injected *i.v.* into recipient B6 mice on day −7 and day +1 with day 0 being the day of bm12 skin transplant. At day 8 post-transplant, mice were sacrificed, skin grafts and DLNs were collected, processed into single cell suspensions using collagenase IV (Worthington), and stained for analysis by flow cytometry (BD FACSCantoII). At the time of sacrifice, whole blood was also collected for measurement of levels of critical blood electrolytes on the Bioanalyzer system (Agilent Technologies).

Luminex liquichip microplate cytokine assays

We measured levels of IFN-ɣ, IL-12p70, IL-1β, and IL-5, GM-CSF, IL-2, IL-6, and TNF-α using a Luminex LiquiChip (BioSource International Inc.) platform, which is a solid phase bead-based immunoassay platform. Cell culture supernatants from the 3-day MLR reactions of various particle and cell formulations and known standards were incubated with cytokine specific beads in a microplate for 90 min. The excess beads were then washed away and a biotinylated detection antibody specific for the cytokine analyte was added and incubated for 30 min followed by washing. A streptavidin fluorophore specific for the detection antibody was then added and incubated for 30 min prior to determining cytokine levels on the Luminex 100™ system.

Antibodies and flow analysis

Flow cytometry was utilized to determine cell phenotype and cell proliferation. Cells were stained for surface markers using fluorochrome conjugated antibodies for 30 min on ice, washed, acquired using FACSCantoII (BD Biosciences) and analyzed using FlowJo v10.4.2 (Tree Star LLC). Antibodies and their specific clones used were: CD3-FITC (17A2, eBioscience), CD3-PerCPCy5.5 (145-2C11, Tonbo Biosciences), CD4-Pacific Blue (RM4-5, eBioscience), CD4-PerCPCy5.5 (RM4-5, Tonbo Biosciences), CD8α-APC-Cy7 (53-6.7, eBioscience), CD8α-eFluor450 (53-6.7, eBioscience), CD11b-PercpCy5.5 (M1/70, Tonbo Biosciences), CD11c-APC-eFluor780 (N418, eBioscience), B220-PECy7 (RA3-6B2, eBioscience), CD44-PECy7(IM7, eBioscience), Foxp3-FITC (FJK-16s, eBioscience), I-A^{b}-APC(AF6-120.1, eBioscience), interferon-γ-APC (XMG1.2, eBioscience), violet proliferation dye (VPD450, BD Biosciences), and aqua live/dead dye (Molecular Probes).

Statistics

Statistical analyses were performed using Graphpad Prism (Graphpad, La Jolla, CA). One-way ANOVA with Sidak's test for multiple comparisons and Student *t*-test were used to determine significance among data subsets. Log-rank (Mantel-Cox) statistic was used for comparison of skin graft survival in Kaplan Meier curves. All results were displayed as a mean with standard error of the mean, with significance determined by a p-value less than 0.05.

Results

Characterization of NPs conjugated or encapsulated with bm12 peptides

Three peptides spanning the bm12 IA^b region containing the three point mutations of bm12 were conjugated to PLG NP or B6 SP carriers. The exact amino acid sequences of the peptides are detailed in Materials and Methods. Surface carboxyl groups of PLG NPs or SPs served as the functional site for peptide binding. Peptide 1 (P1) is a 14-amino acid (AA) peptide containing the bm12/B6 mismatched epitopes and a lysine at the N-terminus which was used as the functional group to bind to surface carboxyl groups of NPs (NP-ECDI-P1) or SPs (SP-ECDI-P1) via ECDI coupling. Peptide 2 (P2) is a longer 29-AA peptide also containing the bm12/B6 mismatched epitopes and a lysine at the N-terminus for ECDI-mediated coupling to NPs (NP-ECDI-P2) or SPs (SP-ECDI-P2). Peptide 3 (P3) is a 14-AA peptide similar to P1 with the exception of a cysteine residue at the N-terminus substituting the lysine residue in P1. The cysteine thiol side chain of P3 now allows BMPH crosslinking of the peptide to NPs (NP-BMPH-P3). P1 and P2 allowed comparison of peptide length on graft survival. P1 and P3 allowed comparison of lysine-derived amine-mediated conjugation versus cysteine-derived thiol-mediated conjugation on graft survival. We further manufactured NPs “encapsulating” P1. The encapsulation method we used was based on a novel bioconjugation process previously described by us, with first conjugating

P1 peptide to PLG in the solution followed by subsequently formulation of NPs, enabling controllable loadings with reduced surface display of the antigen relative to other formulations [299]. Specifically, this method of encapsulation has been shown to reduce antigen burst release in comparison to traditional oil-in-water encapsulation techniques while limiting surface exposure of the antigen which may alter particle physicochemical properties [299]. From here onward, we referred to this NP formulation as "NP-Encap-P1". This formulation allowed comparison between such encapsulated peptide ("NP-Encap-P1") and surface-conjugated peptide (NP-ECDI-P1) on graft survival.

Size (Fig. 1A) and surface zeta potential (Fig. 1B) of all four NP formulations (NP-ECDI-P1, NP-ECDI-P2, NP-BMPH-P3 and NP-Encap-P1) were measured by dynamic light scattering and zetasizer, respectively. All NP formulations followed a tight size distribution with an average diameter of 486.5 ± 26.4 nm and highly negative zeta potential of −40.95 ± 2.66 mV. Highly anionic NPs with diameters of approximately 500 nm have been previously suggested to be important for immune tolerance[339]. Size and morphology of the PLG NPs were confirmed by scanning electron microscopy (SEM) displaying a homogenous distribution (representative image is shown in Fig. 1C, and detailed images of all four formulations are provided in Supplementary Fig. 2). Stability of nanoparticle preparations was demonstrated by minimal-to-no aggregation in PBS in the time between resuspension of the formulations and their subsequent i.v. injection (Supplementary Fig. 3). A CBQCA assay was used to quantify the peptide coupled/loaded on various formulations of NPs, and compared to that coupled to SPs. As shown in Fig. 1D, on a per dose bases rationalized and used in our studies below (i.e., 3 mg of NP preparations and 1×10^8 cells of SP preparations), NPs carried a significantly lower amount of peptides than their SP counterparts (∼75–150 μg/3 mg NP vs. ∼450 μg/10^8 SP). Similarly, the

loading efficiency (calculated as the percentage of bound peptide following the conjugation/encapsulation reaction over the input peptide at the beginning of the conjugation/encapsulation reaction) was also significantly lower for NP than SP carriers (Fig. 1E).

Peptide length and skin allograft survival

We first examined the effect of length of peptide conjugated to the NPs on skin allograft survival. Peptides P1 and P2 were conjugated to NPs (NP-ECDI-P1, NP-ECDI-P2) using ECDI chemistry, and injected to B6 recipients on day −7 and +1 at 3 mg per dose, with day 0 being the date of bm12 skin transplantation. For comparison, the same peptides were similarly conjugated to B6 splenocytes (SP-ECDI-P1, SP-ECDI-P2), injected on day −7 and +1 at 1×10^8 cells per dose, and transplanted with bm12 skin allografts on day 0. The doses chosen for our studies (3 mg NP or 1×10^8 cells per dose) were based on safety profile and efficacy of tolerance from our previous studies of PLG NP and SP administrations [95, 356]. Skin allograft survival was assessed over a period of 90 days. Images of skin allografts at different stages of rejection are provided in Supplementary Fig. 4, with rejection defined as greater than or equal to 80% graft area being necrotic. It is reported in the literature that while peptide processing for MHC class II presentation may vary, they are usually loaded at a length of 13–17 AAs [362, 363]. Our synthesized peptides represent both the common peptide presentation length (i.e. the 14-AA P1), as well as a much longer peptide (i.e. the 29-AA P2). Treatment with blank NP (NP-blank) was used as a negative control. Treatment with the "gold-standard" donor ECDI-SP (i.e. bm12 ECDI-SP) according to our published data [72, 349] was used as a positive control. As expected, bm12 ECDI-SP provided indefinite skin allograft protection in 100% of the recipients (Fig. 2). Remarkably, regardless of the carrier (NPs or SPs), preemptive P1 treatment (NP-ECDI-P1 or

SP-ECDI-P1) partially recapitulated the graft protective effect of bm12 ECDI-SP, resulting in a significantly delayed graft rejection kinetics and a prolonged graft survival in comparison to the negative control ($p < 0.001$). Furthermore, 20–35% of the grafts in both groups survived beyond 90 days post transplantation (Fig. 2). Interestingly, the graft survival was not significantly different between the SP-ECDI-P1 and the NP-ECDI-P1 groups (Fig. 2) despite that 1×10^8 SP-ECDI-P1 carried a significantly higher amount of the P1 peptide than 3 mg of NP-ECDI-P1 (Fig. 1D). These findings suggest that at the doses chosen, the amount of the peptide antigen delivered was no longer a determining factor for the degree of graft protective effect evoked by the two different delivery platforms. In contrast, regardless of the carrier, preemptive P2 treatment (NP-ECDI-P2 or SP-ECDI-P2) did not have any demonstrable graft protective effect in comparison to the negative control (median graft survival was 12 days and 13 days for NP-ECDI-P2 and SP-ECDI-P2, respectively; median graft survival was 10 days for NP-blank), and all grafts were rejected by 20 days post transplantation (Fig. 2).

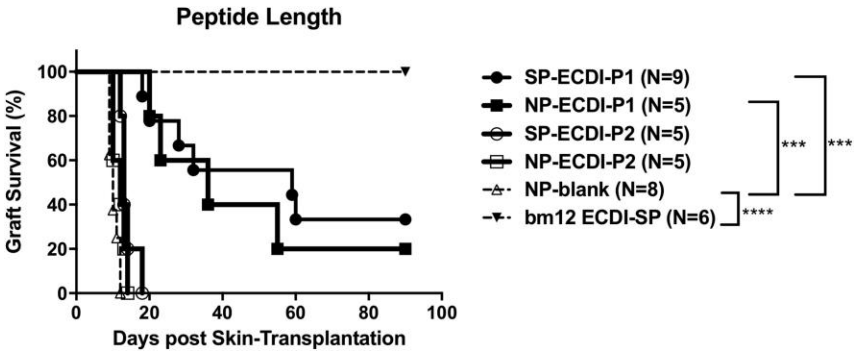


Figure 6.2 **The effect of peptide length on skin allograft survival.** Indicated preparations of NPs (3mg/dose) or SPs (1×10^8/dose) were injected (i.v.) on day −7 and +1 to mice receiving tail to back bm12 to B6 skin transplantation on day 0. Skin grafts were monitored and rejection was determined when 80% of the graft area was necrotic. Statistical significance was determined by Log-rank (Mantel-Cox) tests. ***$p < 0.001$, ****$p < 0.0001$.

Collectively, our *in vivo* studies demonstrate that the shorter P1 peptide provides better graft protection than the longer P2 peptide. Furthermore, we demonstrate that despite a significant

difference in the amount of peptide delivered, NP and SP carriers provide comparable graft protections.

Biodistribution of NP-ECDI-P1

We next examined the biodistribution pattern of NP-ECDI-P1 that demonstrated superior graft protecting efficacy in the study described above. Rhodamine-labeled NP-ECDI-P1 were injected i.v. to B6 mice. 24 or 96 h later, mice were sacrificed and the spleen, peripheral lymph nodes (LNs), and the lungs were collected and examined. As shown in Supplementary Fig. 5, at 24 h post injection, the injected NP-ECDI-P1 (marked by rhodamine positivity) were most prominently visualized in the spleen, followed by the lungs and peripheral LNs. At 96 h post injection, rhodamine positivity significantly diminished in all organs examined, demonstrating efficient NP clearance at this later time point.

As the spleen has been shown to be an important organ for tolerance[364, 365] and was the predominant site of NP entrapment in our study (Supplementary Fig. 5), we next examined the splenic cell populations that interacted with NP-ECDI-P1. For comparisons, rhodamine-labeled blank NPs ("NP-blank") and PKH67-labeled bm12 ECDI-SP were similarly injected and examined [95]. We focused on splenic phagocytes that have engulfed the NP-ECDI-P1 (i.e. cells double positive for the recipient (B6) MHC class II molecule I-A^b and rhodamine, namely I-A^{b+}rhodamine$^+$ cells)[364, 366], and compared to those engulfing NP-blank (I-A^{b+}rhodamine$^+$ cells) or bm12 ECDI-SP (I-A^{b+}PKH67$^+$ cells). As shown in Fig. 3A (representative dot plots) and 3B (summary bar graphs), we found that in comparison to bm12 ECDI-SP, NP-blank and NP-ECDI-P1 were up-taken by a significantly smaller percentage of $CD11c^+CD8\alpha^+$ and $CD11c^+B220^+$ dendritic cells (DCs). The NP formulations also showed a trend of being up-taken by a smaller percentage of $CD11c^+CD11b^+$ conventional DCs compared to bm12 ECDI-SPs.

$CD11c^+CD8\alpha^+$ DCs have been shown to be the predominant antigen presenting cells (APCs) implicated in antigen cross presentation, while $CD11c^+B220^+$ DCs have been implicated in mediating oral tolerance and inducing T cell anergy[367, 368]. In contrast to DCs, a comparable percentage of macrophages in the spleen (enumerated as $CD11c^-CD11b^+$ cells in Fig. 3A) phagocyted NP-blank, NP-ECDI-P1 or bm12 ECDI-SP (Fig. 3B). Consequently, NP formulations were relatively more avidly internalized by splenic macrophages, whereas bm12 ECDI-SP were relatively more avidly internalized by splenic DC subpopulations. When the total number of cells of various splenic DC and macrophage populations uptaking NP vs. bm12 ECDI-SP were compared, we again observed a predominance of splenic macrophages uptaking NPs but not bm12 ECDI-SP (Supplementary Fig. 6). Of note, our studies also revealed that splenic B cells ($B220^+CD11c^-$ cells) were a predominant splenic cell population uptaking both NPs and bm12 ECDI-SP, although no discernible differences between the groups could be observed (data not shown).

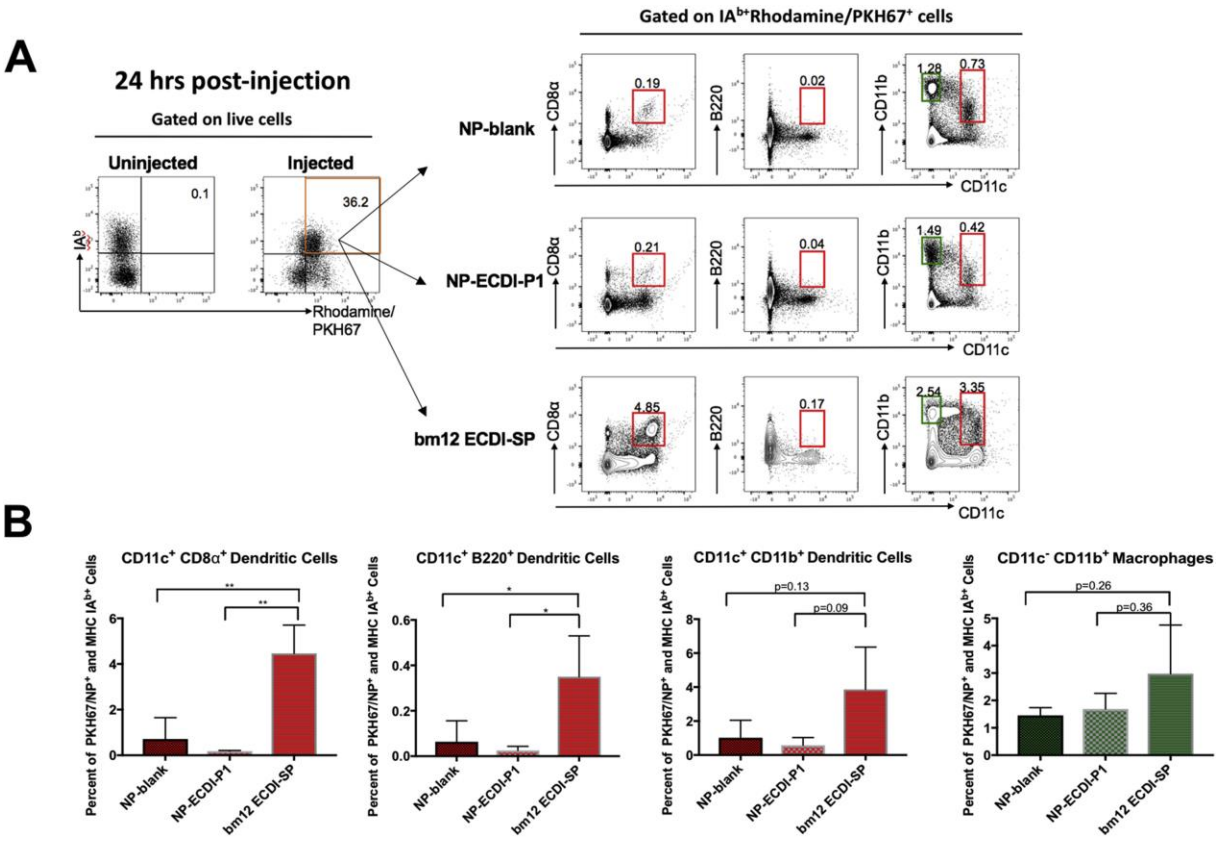


Figure 6.3 **Biodistribution of NP-blank, NP-ECDI-P1, or bm12 ECDI-SP in the spleen 24 h post i.v. injection. (A)** MHC I-A^b and Rhodamine/PKH67 double positive cells in the spleen of injected mice were gated out using the spleen from un-injected mice as a negative control (left dot plots). IA^{b+}Rhodamine/$PKH67^+$ cells were further analyzed for CD11c, CD8α, B220 and CD11b expressions (right dot plots). Plots shown are representative of 3 mice in each group. **(B)** Percentages of each splenic cell population uptaking NP-blank, NP-ECDI-P1 or bm12 ECDI-SP of total IA^{b+}Rhodamine/$PKH67^+$ cells. Statistical significance was determined by one-way ANOVA with Sidak's multiple comparisons test. *$p < 0.05$, **$p < 0.01$. Data shown were averaged from 3 mice in each group.

Collectively, our data demonstrate that NPs were predominantly phagocytosed by splenic macrophages, whereas bm12 ECDI-SP were preferentially phagocytosed by splenic DCs, particularly DC subpopulations implicated in mediating immune tolerance. Such differences between the biodistribution of NP-ECDI-P1 and bm12 ECDI-SP may partially contribute to the difference in their efficacy in graft protection observed in Fig. 2.

Graft-infiltrating cells in NP-ECDI-P1 treated recipients

We next examined graft-infiltrating cells in skin allografts from NP-ECDI-P1 treated recipients. For comparison, grafts from NP-blank or bm12 ECDI-SP treated recipients were also analyzed.

Skin grafts were harvested on day 8 post-transplant, digested with collagenase and examined by flow cytometry for antigen-experienced ($CD44^+$) regulatory or effector T cell infiltrations. As shown in Fig. 4A, compared to grafts from the other two groups, grafts from NP-ECDI-P1 treated recipients harbored a significantly higher total number of antigen-experienced $CD4^+CD44^+Foxp3^+$ regulatory T cells (Tregs). Such antigen-experienced $CD44^+$ Tregs have been shown to possess greater suppressive function than antigen-inexperienced $CD44^-$ Tregs [369]. Interestingly, when graft-infiltrating $CD8^+CD44^+IFN\text{-}\gamma^+$ effector T cells were examined, a different pattern emerged: grafts from both NP-ECDI-P1 and NP-blank treated recipients harbored a significantly higher percentage of $CD8^+CD44^+IFN\text{-}\gamma^+$ cells compared to those from bm12 ECDI-SP treated recipients (Fig. 4B), although the difference in total number of such graft-infiltrating $CD8^+CD44^+IFN\text{-}\gamma^+$ cells did not reach statistical significance. Of note, there were no significant differences in $CD4^+CD44^+Foxp3^+$ Tregs or $CD8^+CD44^+IFN\text{-}\gamma^+$ cells in the draining lymph nodes (DLNs) across the three groups (Supplementary Fig. 7). Collectively, these data demonstrate that NP-ECDI-P1 treatment results in an increase of graft-infiltrating $CD4^+CD44^+Foxp3^+$ Tregs, but is not able to effectively suppress graft-infiltrating $CD8^+CD44^+IFN\text{-}\gamma^+$ effector T cells. These changes combined ultimately result in only a moderate partial graft protection conferred by NP-ECDI-P1 treatment.

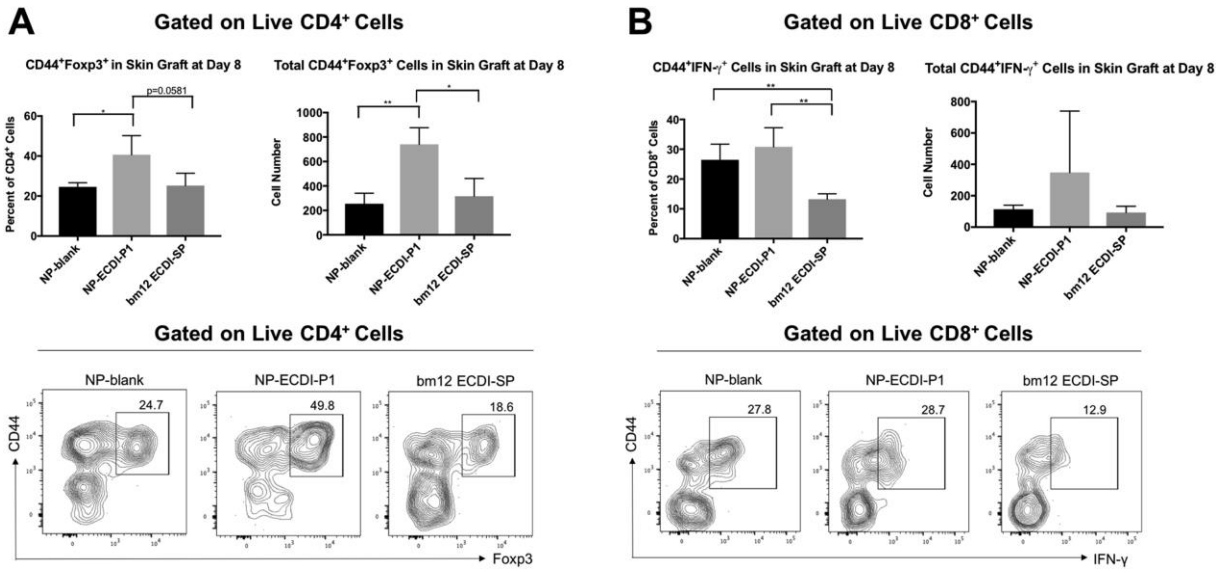


Figure 6.4 **Graft-infiltrating CD4$^+$CD44$^+$Foxp3$^+$ and CD8$^+$CD44$^+$IFN-γ$^+$ cells in skin allografts from recipient mice treated with NP-blank, NP-ECDI-P1 or bm12 ECDI-SP. (A)** Left bar graph: Percentage of graft-infiltrating CD44$^+$Foxp3$^+$ cells among graft-infiltrating CD4$^+$ cells; Right bar graph: Total number of CD4$^+$CD44$^+$Foxp3$^+$ cells in skin allografts. Representative contour plots show gating for CD44$^+$Foxp3$^+$ cells in skin allografts from recipients of each treatment group. **(B)** Left bar graph: Percentage of graft-infiltrating CD44$^+$IFN-γ$^+$ cells among graft-infiltrating CD8$^+$ cells; Right bar graph: Total number of CD8$^+$ CD44$^+$IFN-γ$^+$ cells in skin allografts. Representative contour plots show gating for CD44$^+$IFN-γ$^+$ cells in skin allografts from recipients of each treatment group. For **(A)** and **(B)**, skin allografts were harvested and examined on day 8 post transplantation. Statistical significance was determined by one-way ANOVA with Sidak's multiple comparisons test. *$p < 0.05$, **$p < 0.01$. Data is representative or averaged from 3 mice per group.

To rule out obvious chemical toxicities from NP injections, Bioanalyzer testing of whole blood for common electrolytes was performed at the time of recipient sacrifice, and showed normal values across all three treatment groups (Supplementary Fig. 8).

Bm12-specific T cell proliferation and cytokine production

The varied efficacy between P1 and P2 formulations observed in Fig. 2 may be due to disparities in their ability to deliver bm12 antigen to APCs for processing and presentation to stimulate bm12-specific T cell proliferation. To investigate this possibility, we took advantage of the CD4$^+$ T cells from ABM mice which carry a transgenically-expressed T cell receptor (TCR) that responds to the mutated bm12 IA^b and set up *in vitro* T cell proliferation assay. In this *in vitro* assay, we used B6 bone marrow derived macrophages (BMDMs) as APCs, rather than bone marrow derived dendritic cells (BMDCs), because our biodistribution data from Fig. 3 showed

that NPs were significantly more proficiently phagocytosed by splenic macrophages than by splenic DCs. We co-cultured VPD450-labeled ABM $CD4^+$ T cells with B6 BMDMs pulsed with various NP and SP formulations of P1 and P2 as the source of bm12 antigen as detailed in Materials and Methods. After 3 days of co-cultures, we measured ABM $CD4^+$ T cell proliferation by VPD450 dilution. As shown in Fig. 5A, both P1 formulations (NP-ECDI-P1 and SP-ECDI-P1) elicited a more robust ABM $CD4^+$ T cell proliferative response in comparison to the P2 formulations (NP-ECDI-P2 and SP-ECDI-P2), consistent with P1 treatment providing superior graft protection than P2 treatments (Fig. 2). However, bm12 ECDI-SP elicited an ABM $CD4^+$ T cell proliferative response here intermediate to those seen with the P1 or P2 formulations (Fig. 5A), and yet provided the best bm12 skin allograft protection (Fig. 2), suggesting that other aspects of tolerogenic delivery (for instance, the type of phagocytes engaged as demonstrated in Fig. 3) in addition to antigen processing and presentation by macrophages also play a role in the ultimate tolerance efficacy of these formulations. Indeed, as shown in Supplementary Fig. 9, when BMDCs pulsed with for bm12 ECDI-SP were used as APCs, a more rigorous ABM T cell proliferation was observed in comparison to when BMDMs were used as APCs. In contrast, for NP-ECDI-P1, BMDMs as APCs stimulated more rigorous ABM T cell proliferation than BMDCs as APCs. These findings are therefore consistent with the observed differences in bm12 ECDI-SP and NP-ECDI-P1 biodistribution in splenic phagocytes in Fig. 3.

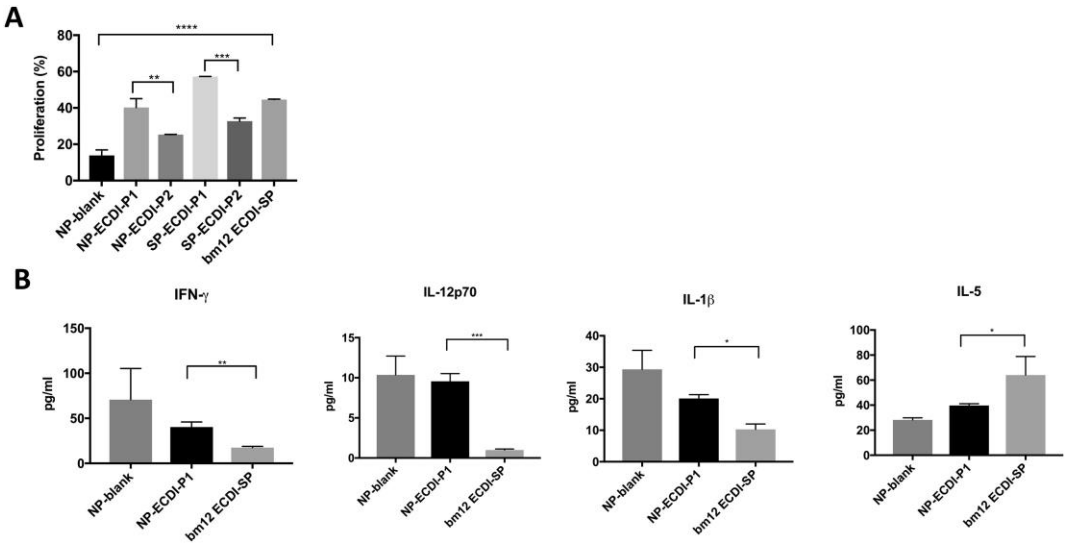


Figure 6.5 ***In vitro*** **bm12-specific CD4 T cell proliferation and cytokine production in response to stimulation by APCs pulsed with different bm12 antigen sources. (A)** ABM $CD4^+$ T cell proliferation. ABM $CD4^+$ T cells were co-cultured with B6 BMDMs pulsed with various NP and SP formulations of P1 and P2 as the source of bm12 antigen. % proliferation of ABM $CD4^+$ T cells was determined by % of ABM $CD4^+$ T cells with VPD450 fluorescence lower than that of undivided ABM $CD4^+$ T cells. **(B)** Cytokine production from ABM $CD4^+$ T cells co-cultured with B6 BMDMs pulsed with NP-blank, NP-ECDI-P1 or bm12 ECDI-SP. IFN-γ**,** IL-12p70, IL-1β, and IL-5 levels were determined by Luminex liquichip microplate reader. For both **(A)** and **(B)**, statistical significance was determined by one-way ANOVA with Sidak's multiple comparisons test or student's *t*-test. *p < 0.05, **p < 0.01, ***p < 0.001, ****p < 0.0001. Data is representative of n = 2 biological replicates per group.

We next determined cytokine release of ABM $CD4^+$ T cells in the above co-cultures. We focused on conditions in which B6 BMDMs were pulsed with either NP-ECDI-P1 or bm12 ECDI-SP, and compared to the NP-blank pulsed condition. Culture media following the 3-day ABM $CD4^+$ T cell proliferation assays shown in Fig. 5A was collected and examined for cytokine production by Luminex liquichip microplate reader. As shown in Fig. 5B, NP-ECDI-P1 and bm12 ECDI-SP conditions exhibited distinct cytokine production patterns: in comparison to co-culturing with bm12 ECDI-SP, co-culturing with NP-ECDI-P1 resulted in significantly higher levels of IFN-γ, IL-12p70, and IL-1β; but a decreased level of IL-5. Additional cytokines tested included GM-CSF, IL-2, IL-6 and TFN-α, where no difference was observed among different groups (data not shown). These differences in *in vitro* cytokine production (Fig. 5B), together with differences in *in vivo* targeting of splenic phagocytes (Fig. 3) as well as graft-infiltrating cells (Fig. 4), are

consistent with only a partial graft protection by NP-ECDI-P1 in comparison to that by bm12 ECDI-SP (Fig. 2). More importantly, these findings will now guide future NP engineering endeavors to recapitulate similar patterns seen with bm12 ECDI-SP as a goal for further enhancing the tolerance efficacy of NP formulations.

Peptide conjugation method and skin allograft survival

Following determination that a shorter peptide afforded better graft protection, we next examined the efficacy of two commonly used peptide-NP conjugation schemes on graft protection. Scheme 1 utilized ECDI to conjugate the carboxyl groups on PLG NPs to the primary amine of the N-terminus lysine residue of peptide P1 (NP-ECDI-P1). Scheme 2 utilized BMPH as a linker to form a thioether bond between PLG NPs and the N-terminus cysteine residue of peptide P3 (NP-BMPH-P3). Except for a lysine residue at the N-terminus of P1 compared to a cysteine residue at the N-terminus of P3, these two peptides were otherwise identical (Fig. 1D). Our rationale for antigen conjugation was that it has been previously demonstrated that antigens conjugated to particles exhibit significantly slower release relative to antigens absorbed to particles. We therefore used antigen conjugation to ensure that our antigen payload was not released prematurely prior to their successful delivery to the intended target organ (e.g, the spleen as shown in Fig. 3).

Following the same treatment schedule for NP-ECDI-P1, NP-BMPH-P3 was injected to B6 recipients on day −7 and +1 (relative to day 0 of bm12 skin transplantation), and skin graft survival was monitored over a period of 90 days. As shown in Fig. 6A, NP-BMPH-P3 treatment showed a trend towards a slightly worse graft outcome than NP-ECDI-P1 treatment, with a median graft survival of 23 days for NP-BMPH-P3 and 36 days for NP-ECDI-P1, although this difference did not reach statistical significance ($p = 0.169$). We next performed a similar T cell

proliferation assay using ABM CD4$^+$ T cells and B6 BMDMs pulsed with NP-ECDI-P1 or NP-BMPH-P3 as the source of bm12 antigen. As shown in Fig. 6B, ABM CD4$^+$ T cells demonstrated a significantly lower degree of T cell proliferation when incubated with NP-BMPH-P3 compared to NP-ECDI-P1. Collectively, our data demonstrate that compared to lysine-based ECDI conjugation of bm12 peptide to NPs, cysteine-based BMPH conjugation is associated with less efficient antigenic peptide processing and presentation by the interacting APCs, and has a trend towards an inferior skin allograft protective effect.

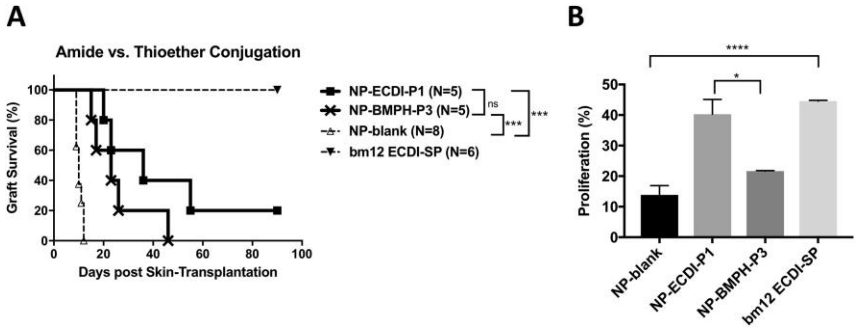


Figure 6.6 **The effect of peptide conjugation chemistry on skin allograft survival. (A)** Indicated preparations of NPs (3mg/dose) were injected (i.v.) on day −7 and +1 to mice receiving tail to back bm12 to B6 skin transplantation on day 0. Skin grafts were monitored and rejection was determined as in Fig. 2. Similarly, the bm12 ECDI-SP treated group served as a positive control whereas the NP-blank treated group served as a negative control. Statistical significance was determined by Log-rank (Mantel-Cox) tests. **(B)** ABM CD4$^+$ T cell proliferation. ABM CD4$^+$ T cells were co-cultured with B6 BMDMs pulsed with either NP-ECDI-P1 or NP-BMPH-P3 as the source of bm12 antigen. % proliferation of ABM CD4$^+$ T cells was similarly determined as in Fig. 5. Statistical significance was determined by one-way ANOVA with Sidak's multiple comparisons tests. Data is representative of n = 2 biological replicates per group. For both **(A)** and **(B)**, *p < 0.05, ***p < 0.001, ****p < 0.0001, ns = no significance.

Antigen incorporation method and skin allograft survival

We next examined whether antigenic peptide incorporation into NPs by surface conjugation or by encapsulation would influence skin allograft survival. Surface conjugation allows a covalent linkage between the antigenic peptide and the carrier particle, therefore reduces peptide disassociation from its carrier, but may increase risks of particle agglomeration and undesired immune responses. On the other hand, peptide encapsulation reduces these risks, and our novel bioconjugate encapsulation approach further serves to avoid a burst release of the peptide cargo

typically observed with encapsulated peptides [299]. The most effective surface-conjugated NP formulation, NP-ECDI-P1, was compared with NPs encapsulating the same peptide (NP-Encap-P1). Although a similar peptide loading was achieved on both NP-ECDI-P1 and NP-Encap-P1 (Fig. 1D,E), our peptide release study showed that NP-Encap-P1 exhibited a slightly decreased peptide release over time in comparison to NP-ECDI-P1 (Fig. 7A). Confocal microscopy of rhodamine-labeled NPs either surface-conjugated or encapsulated with FITC-labeled P1 peptide confirmed their respective peptide localization, namely surface peptide localization on NP-ECDI-P1 versus internal peptide localization within NP-Encap-P1 (Fig. 7B). Consistent with confocal images, a representative fluorescence intensity profile across a singular NP-ECDP-P1 showed two FITC peaks at the edges of a broader rhodamine peak demonstrating surface location of the peptide; whereas a representative fluorescence intensity profile across a singular NP-Encap-P1 showed a single FITC peak within the bounds of rhodamine demonstrating internal location of the peptide (Fig. 7C).

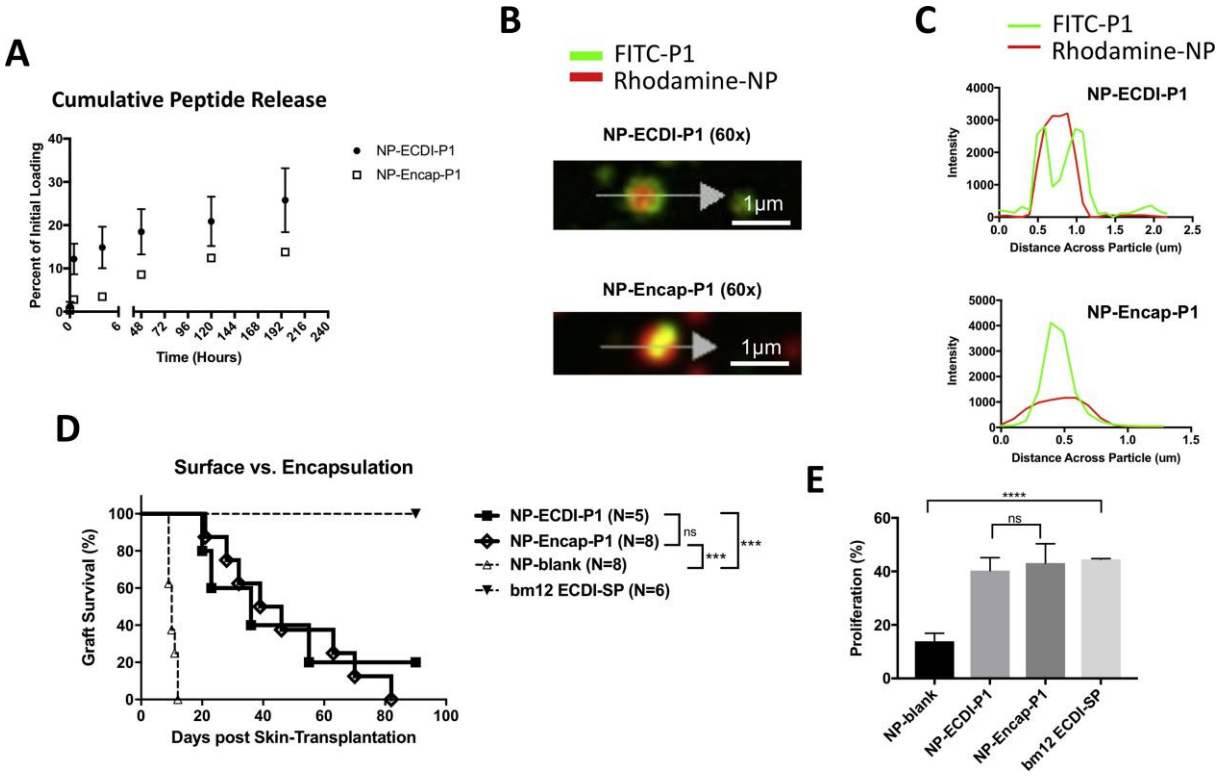


Figure 6.7 **Surface conjugation or encapsulation of P1 peptide provides equivalent skin allograft survival. (A)** Percent of peptide release over 196 h of NP-ECDI-P1 and NP-Encap-P1, as described in Materials and Methods. Note that the error bars are smaller than the size of symbols for the NP-Encap-P1 data points. **(B)** Confocal images of a single representative NP-ECDI-P1 particle and a single representative NP-Encap-P1 particle. Magnification: ×60. **(C)** Fluorescence intensity profiles calculated across the gray arrow in **(B)** of a single representative NP-ECDI-P1 particle and a single representative NP-Encap-P1 particle. **(D)** Indicated preparations of NPs (3mg/dose) were injected (i.v.) on day −7 and +1 to mice receiving tail to back bm12 to B6 skin transplantation on day 0. Skin graft monitoring, determination of rejection, positive and negative controls were similar to Fig. 2. Statistical significance was determined by Log-rank (Mantel-Cox) tests. **(E)** ABM $CD4^+$ T cell proliferation. ABM $CD4^+$ T cells were co-cultured with B6 BMDMs pulsed with either NP-ECDI-P1 or NP-Encap-P1 as the source of bm12 antigen. % proliferation of ABM $CD4^+$ T cells was similarly determined as in Fig. 5. Statistical significance was determined by one-way ANOVA with Sidak's multiple comparisons tests. Data is representative of n = 2 biological replicates per group. For both **(D)** and **(E)**, ***p < 0.001, ****p < 0.0001, ns = no significance.

Next, NP-Encap-P1 was injected on day −7 and +1, relative to day 0 of bm12 skin transplantation. As shown in Fig. 7D, NP-Encap-P1 and NP-ECDI-P1 demonstrated completely overlapping skin allograft survival, with a median graft survival time of 42.5 days for NP-Encap-P1 and 36 days for NP-ECDI-P1. We next performed a similar T cell proliferation assay using ABM $CD4^+$ T cells and B6 BMDMs pulsed with NP-ECDI-P1 or NP-Encap-P1 as the source of bm12 antigen. As shown in Fig. 7E, ABM $CD4^+$ T cells demonstrated equivalent T cell proliferation when incubated with either NP-ECDI-P1 or NP-Encap-P1. Collectively, our data

demonstrate that there is no significant difference between surface conjugation (NP-ECDI-P1) and internal encapsulation (NP-Encap-P1) as the delivery method for the antigenic bm12 peptide in terms of skin allograft protection or stimulating AMB $CD4^+$ T cell proliferation.

Whole donor cell lysate containing antigenic epitopes for tolerance delivery

In the bm12 to B6 skin transplant model, the antigenic epitope is well defined as described above. Therefore, both bm12 whole donor cell lysate as well as bm12 peptides used in our experiments above should contain the bm12 antigen necessary for antigen-specific tolerance. To test if the lysate and peptide can function similarly or if additional proteins or molecules in the whole donor cell lysate other than the bm12 antigen also contribute to skin allograft protection, we compared the skin allograft protection provided by bm12 whole donor cell lysate to that by P1. Bm12 splenocyte lysate was generated by sonication of bm12 splenocytes, and coupled to NPs or B6 SPs via ECDI (NP-ECDI-lysate or SP-ECDI-lysate) as described in Materials and Methods. NP-ECDI-lysate or SP-ECDI-lysate were injected on day −7 and +1 relative to day 0 of bm12 skin transplantation. Comparison was made to recipients treated with NP-ECDI-P1. As shown in Fig. 8A, no significant difference in skin allograft survival was observed between either of the lysate formulations and NP-ECDI-P1. Similarly, co-culture of ABM $CD4^+$ T cells and B6 BMDMs pulsed with either lysate formulations or NP-ECDI-P1 yielded similar proliferation rates (Fig. 8B). Collectively, these data suggest that when the donor antigenic epitopes are clearly defined, peptides containing the epitope(s) can provide equal donor graft protection as whole donor cell lysate in this skin transplant model. Moreover, together with data shown in Fig. 2, these results again support the notion that NP carriers are equally efficacious at providing graft protection as SP carriers, thus further validating the use of NPs as a more clinically translatable tolerogenic platform.

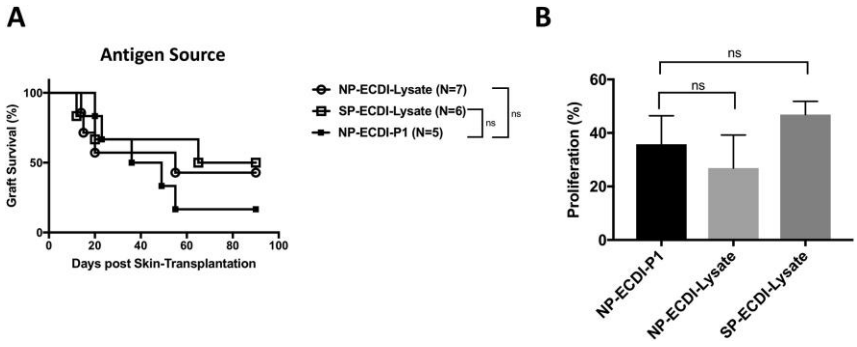


Figure 6.8 **The antigenic peptide P1 provides comparable skin allograft protection as donor cell lysate. (A)** Indicated preparations of NPs (3mg/dose) or SPs (1×10^8/dose) were injected (i.v.) on day −7 and +1 to mice receiving tail to back bm12 to B6 skin transplantation on day 0. Skin grafts were monitored and rejection was determined as in Fig. 2. Statistical significance was determined by Log-rank (Mantel-Cox) tests. **(B)** ABM $CD4^+$ T cell proliferation. ABM $CD4^+$ T cells were co-cultured with B6 BMDMs pulsed with either NP-ECDI-lysate or SP-ECDI-lysate as the source of bm12 antigen. % proliferation of ABM $CD4^+$ T cells was similarly determined as in Fig. 5. Statistical significance was determined by one-way ANOVA with Sidak's multiple comparisons tests. Data is representative of n = 3 biological replicates per group. For **(A)** and **(B)**, ns = no significance.

Discussion

Our results demonstrate that polymeric PLG NPs engineered to deliver relevant donor antigens can significantly delay allograft rejection in a murine model of skin transplantation. The significant protection afforded by donor antigen-coupled PLG NPs in this transplant model advances the notion that highly anionic PLG NPs with approximately 500 nm diameter in size indeed provide a robust platform for immune engineering for transplantation tolerance as previously demonstrated for autoimmunity and allergy[147, 162]. This platform is particularly promising and clinically translatable given the well-accepted safety profile of PLG[355]. Importantly, in the current study we have interrogated several commonly modifiable engineering parameters relevant to immune tolerance, including antigenic peptide length, chemistry of surface peptide conjugation, and antigen encapsulation versus surface conjugation. A shorter peptide length (P1) resulted in enhanced graft protection despite delivering an equimolar quantity of the relevant antigen as the longer peptide (P2) (Fig. 2). This result is consistent with previous work demonstrating that the usual length of peptides loaded and presented by MHC class II is between 13 and 17 amino acids[363]. We hypothesize that this size preference exhibited in MHC

II loading of peptides may be a major contributing factor to the improved efficacy of P1 over P2 as it is possible that P1 is capable of successful loading with fewer requisite processing steps[370, 371]. It is important to note, however, that numerous other factors including proteolytic susceptibility of the peptide, degree of peptide folding, and MHC groove geometry play critical roles in the presentation of peptides and were likely also contributing to the relative efficacy of each peptide [370, 372].

To address if antigen accessibility could contribute to graft protection, both amide and thioether conjugation were attempted to represent relatively labile and non-labile conjugations [373]. Interestingly, amide conjugation resulted in a slightly enhanced median graft survival (Fig. 6), suggesting that peptide clipping and subsequent MHC loading may be affected by the nature of the peptide bond to the polymer. This trend may merit consideration in studies that utilize full length proteins for tolerance, as the amine group of lysine residues within a protein are likely more readily available to participate in conjugation reactions compared with the thiol group of cysteine residues which often form disulfide bonds and are less-readily accessible for reactions[374]. In addition, numerous follow-up studies are currently being conducted to [1]: interrogate the specific intracellular fate of these particles and [2] tease out the more subtle differences in the efficacies of P1 and P3 formulations in order to identify mechanisms by which these particles differentially exert their graft-protective effects.

Antigen surface conjugation can result in increased agglomeration, antigen denaturation, and increased particle size; whereas traditional antigen encapsulation can result in antigen loss due to PLG bulk hydrolysis and antigen burst release [299, 375]. For our study, we utilized a novel bioconjugate encapsulation method of pre-conjugating the peptide to PLG prior to formation of nanospheres to eliminate the problem of antigen burst release[299]. Our comparison of surface

conjugation and encapsulation revealed similar graft protection (Fig. 7), suggesting that neither surface conjugation nor encapsulation significantly impair antigen processing or presentation for the purpose of tolerizing T cells. Our study further demonstrated a similar initial peptide loading for NP-ECDI-P1 and NP-Encap-P1 (Fig. 1D, E), but a slightly delayed peptide release over time from NP-Encap-P1 compared to NP-ECDI-P1 (Fig. 7A). However, equivalent graft survival was observed in recipients treated with either NP-Encap-P1 or NP-ECDI-P1 (Fig. 7D), suggests that the slightly greater peptide release from NP-ECDI-P1 did not impact graft protection by PLG-NP carriers.

In order to investigate whether the nature of the carrier platform affected tolerance efficacy, we compared NPs with SPs as carriers for antigens. We found that there was not a significant difference in graft protection provided by NP-ECDI-P1 and SP-ECDI-P1 (Fig. 2), or by NP-ECDI-lysate and SP-ECDI-lysate (Fig. 8). These findings indicate that carrier platforms for tolerance induction can be versatile. Therefore, it is feasible to replace cell-based carriers with the more clinically translatable polymeric carriers for delivering tolerogenic antigens.

Donor cell lysate is an attractive antigen source since it contains the entire repertoire of donor MHC class I and II proteins relevant to allogeneic immune responses[351]. However, preparation of donor cell lysate requires donor cell procurement and processing, which can be cumbersome. On the other hand, epitope-containing peptides can be easily manufactured, although their processing and presentation by recipient APCs may differ from that of natural proteins present in the lysate. Our previous work utilizing donor cell lysate coupled to PLG NPs in a full MHC-mismatched allogeneic islet transplantation model demonstrated a partial islet allograft protection via modulating indirect allo-specific T cell responses [72]. Here, the use of bm12 cell lysate in this skin transplant model did not result in superior graft protection compared

to that conferred by the epitope-containing peptide P1 (Fig. 8. This result is likely due to bm12 epitope being well-defined and entirely encompassed within P1. One important set of subsequent studies is to thoroughly compare dose responses of donor lysate and P1, since an equal weight of lysate undoubtedly contains a much lower dose of immunologically-relevant antigen compared to the same weight of purified, epitope-containing peptide P1. Nonetheless, these data suggest that when antigenic epitopes are known, it is possible to replace total donor cell lysate with a high dose of epitope-containing peptides. Translating this concept to clinical transplantation will require consideration of the diverse disparities between donor and recipients MHCs and their often less well-defined epitopes [376, 377]. However, it is also possible that only certain selective dominant epitopes will need to tolerized to sufficiently establish transplantation tolerance [378, 379]. Our current study has provided support for continued development of this novel technology for application in transplantation tolerance as our understanding of relevant immunodominant epitopes in donor/recipient pairings improves.

One potential cellular mechanism contributing to the partial protection seen by NP-ECDI-P1 treatment is the expansion and/or accumulation of antigen experienced Tregs at the graft site (Fig. 4A). Tregs are well known to play a crucial role in the induction and maintenance of immune tolerance, and increased intragraft Foxp3 expression has been correlated with better graft outcomes [380, 381]. Previous studies in islet transplant models have demonstrated an ability of donor ECDI-SP to expand Tregs both in secondary lymphoid organs and at the graft site, which serves as one crucial mechanism for promoting long-term graft tolerance [95]. Importantly, antigen conjugated PLG-NPs have also been shown to induce and activate Tregs in murine models of EAE and allergy [72, 340]. More specifically, it has been reported that antigen-experienced $CD44^+$ Tregs, in comparison to antigen-naïve $CD44^-$ Tregs, are more

proliferative, produce a higher amount of IL-10 and are more potent suppressors of effector T cell populations [369]. Our data in the current study suggest that antigen-experienced $CD44^+$ Treg expansion and/or accumulation at the graft site is an important mechanism in mediating graft protection provided by antigen conjugated NPs, thus identifying a subset of regulatory T cells to target for future NP engineering for enhancing antigen-specific tolerance. It has been reported in the literature that regulatory T cells employ diverse mechanisms of suppression [234], including production of soluble factors such as IL-10 [301] and TGF-β [349], conversion of extracellular ATP to adenosine via CD39 and CD73, IL-2 consumption via CD25, and downregulation of CD80 and CD86 via CTLA-4, among others. Elucidating the mechanism(s) of action by Tregs by NP-ECDI-P1 will be beyond the scope of our current study.

However, despite delivery of a high dose of epitope-containing peptides, the best performing NP formulation, namely NP-ECDI-P1, did not recapitulate the complete tolerance efficacy seen with bm12 ECDI-SPs (Fig. 2). Therefore, in the current study we focused on comparing and contrasting NP-ECDI-P1 and bm12 ECDI-SPs, with an intended goal of providing a platform for future rational design of NP formulations for transplantation tolerance. To this end, our data revealed that skin allografts from NP-ECDI-P1 treated recipients harbored an increased percentage of $CD8^+CD44^+IFN\text{-}\gamma^+$ cells compared to those from bm12 ECDI-SP treated recipients (Fig. 4B). This suggests that antigen conjugated NPs are less capable of effectively attenuating IFN-γ-producing effector CD8 T cells crucial to both acute and chronic rejection [108, 382]. A local interferon-rich environment may further increase $CD8^+$ T cell trafficking to promote graft rejection[383]. Consistent with this *in vivo* observation, we also detected a dramatically different cytokine production pattern *in vitro* by ABM T cells co-cultured with APCs pulsed with either NP-ECDI-P1 or bm12 ECDI-SP. Bm12 ECDI-SP promoted Th2 cytokine IL-5 but exhibited a

significantly lower production of proinflammatory cytokines IFN-γ, IL-12p70 and IL-1β; on the other hand, NP-ECDI-P1 promoted the production of such proinflammatory cytokines (Fig. 5). It has been reported that PLG platforms can induce proinflammatory cytokines IL-12, IL-1β and TNF-α [384, 385], which in turn impair Treg function and promote allograft rejection [386, 387]. The observed cytokine response by NP-ECDI-P1 could be one contributing factor to the suboptimal graft outcome by NP-ECDI-P1 treatment in comparison to bm12 ECDI-SP treatment. Furthermore, our *in vivo* biodistribution experiment also demonstrated that bm12 ECDI-SP were more preferentially phagocytosed by splenic DC subsets, whereas NP-ECDI-P1 were predominantly phagocytosed by splenic macrophages (Fig. 3). Splenic $CD8\alpha^+$ DCs are a crucial cell population for cross-presentation that can modulate allo-specific cytotoxic T cells, whereas $CD11c^+B220^+$ DCs have been implicated in mediating oral tolerance and inducing T cell anergy [388]. The ability of bm12 ECDI-SPs to preferentially target these DC populations could be a possible tolerogenic event not recapitulated by NP-ECDI-P1. Thus, mirroring the bm12 ECDI-SP cytokine response and biodistribution may be used in the future as a screening and validating tool for further developing and optimizing antigen conjugated NP formulations for immune tolerance.

Peptide conjugated NP formulations exclusively target T cells with indirect allo-specificities where donor MHC peptides are presented by recipient APCs to stimulate recipient T cells [72]. We have previously shown that in addition to depleting recipient T cells of *indirect* allo-specificities such as seen with NP formulations [72], donor ECDI-SP further retain the ability to anergize recipient T cells of *direct* allo-specificities [95], likely rendering them more effective in abrogating rejection. It has been reported that polymorphic residues on allogeneic MHC can be recognized by recipient allo-specific T cells regardless of the bound peptide [108]. Similarly,

acid washing of peptides bound to foreign MHC does not diminish their ability to trigger allo-specific T cell reactivities. On the other hand, mutations in HLA-DR or HLA-B27 have been associated with loss of allo-specific T cell reactivities [389-391]. These data suggest that sites within intact donor allo-MHC molecules themselves can be crucial for donor recognition and consequently for tolerance induction. Taken together, the presence of intact allo-MHC molecules within donor ECDI-SP may serve to tolerize T cells with direct allo-specificities that would otherwise engage passenger leukocytes via the direct allo-recognition pathway immediately following transplantation. Thus, the ability to modulate T cells with direct allo-specificities will be an intriguing additional target for future NP engineering, with an ultimate goal of enhancing their tolerogenic capacity to that comparable to donor ECDI-SP.

Conclusions

The present study highlights the utility of PLG NPs as a viable platform for donor antigen delivery for transplant tolerance induction in a bm12 to B6 allogeneic skin transplant model. Different engineering parameters were examined including peptide design, antigen selection, and method of antigen conjugation to NPs. We have demonstrated that selection of appropriate peptide length was critical to the success of this platform, and that one possible mechanism of protection by donor peptide conjugated NPs was promotion of accumulation of antigen-experienced Treg at the graft site. Conjugation of the peptide to NPs by amide versus thioether chemistry was found to be equivalent in providing graft protection, as was peptide surface conjugation versus internal encapsulation. We have also demonstrated that delivery of epitope-containing peptides provided equivalent graft protection compared to delivery of whole donor cell lysate. Importantly, throughout our studies, NP carriers performed comparably to SP carriers when delivering the same form of antigen. As donor ECDI-SP treatment remains the most

effective and superior modality for transplant tolerance induction, in the current study we revealed that in comparison to donor peptide conjugated NPs, donor ECDI-SP targeted different splenic phagocytes and more effectively inhibited $CD8^+CD44^+IFN\text{-}\gamma^+$ effector T cell accumulation at the graft site. These differences not only explain the superior graft protection by bm12 ECDI-SP in comparison to NP-ECDI-SP, but also provide guidance for future engineering of cell-free, biocompatible and "off-the-shelf" NP platforms with a goal of maximizing tolerance efficacy for transplantation.

Author contributions

S.S., S.D., and X.L. designed the study. S.S., S.D., K.H., and A.B. performed relevant experiments. S.S., K.H., and X.L. wrote the manuscript. L.S. provided advice on experimental design and revised the manuscript. X.L. and L.S. supervised the study.

Conflicts of interest

The authors have no competing interests to disclose.

Data availability

The raw and processed data required to reproduce these findings are available to download from: https://northwestern-box-com.proxy.lib.umich.edu/s/ovw6z0n06x333adlg2pzabaw75w6fizf.

Acknowledgments

This work was previously published with manuscript information: Sahil Shah*, Saeed Daneshmandi*, Kevin R Hughes, Shuangjin Yu, Angela M. Bedoya, Lonnie D. Shea, Xunrong Luo *These authors contributed equally to this work. Optimizing PLG Nanoparticle-Peptide Delivery Platforms for Transplantation Tolerance Using an Allogeneic Skin Transplant Model. Biomaterials, 210 (2019) 70-82

Chapter 7 Localized Immune Tolerance from FasL-Functionalized PLG Scaffolds

Authors

Skoumal M, Woodward KB, Zhao H, Wang F, Yolcu ES, Pearson RM, Hughes KR, Garcia AJ, Shea LD, Shirwan H.

Abstract

Intraportal allogeneic islet transplantation has been demonstrated as a potential therapy for type 1 diabetes (T1D). The placement of islets into the liver and chronic immunosuppression to control rejection are two major limitations of islet transplantation. We hypothesize that localized immunomodulation with a novel form of FasL chimeric with streptavidin, SA-FasL, can provide protection and long-term function of islets at an extrahepatic site in the absence of chronic immunosuppression. Allogeneic islets modified with biotin and engineered to transiently display SA-FasL on their surface showed sustained survival following transplantation on microporous scaffolds into the peritoneal fat in combination with a short course (15 days) of rapamycin treatment. The challenges with modifying islets for clinical translation motivated the modification of scaffolds with SA-FasL as an off-the-shelf product. Poly(lactide-co-glycolide) (PLG) was conjugated with biotin and fabricated into particles and subsequently formed into microporous scaffolds to allow for rapid and efficient conjugation with SA-FasL. Biotinylated particles and scaffolds efficiently bound SA-FasL and induced apoptosis in cells expressing Fas receptor (FasR). Scaffolds functionalized with SA-FasL were subsequently seeded with allogeneic islets and transplanted into the peritoneal fat under the short-course of rapamycin treatment. Scaffolds modified with SA-FasL had robust engraftment of the transplanted islets

that restored normoglycemia for 200 days. Transplantation without rapamycin or without SA-FasL did not support long-term survival and function. This work demonstrates that scaffolds functionalized with SA-FasL support allogeneic islet engraftment and long-term survival and function in an extrahepatic site in the absence of chronic immunosuppression with significant potential for clinical translation.

Introduction

Exogenous insulin treatment is the standard of care for type 1 diabetic (T1D) patients. However, daily insulin treatment negatively affects the quality of life and is often ineffective in preventing recurrent hyperglycemic episodes with consequent development of micro- and macro-angiopathic lesions and the development and progression of chronic complications[392]. Allogeneic islet transplantation has proven effective in improving metabolic control/quality of life and in preventing severe hypoglycemia in patients with T1D [393-397]. However, broad application of clinical allogeneic islet transplantation is limited by the chronic use of immunosuppression to control immune rejection and its sequelae [396], and transplantation into the liver, which compromises immediate post-graft islet engraftment as well as long-term survival [398].

T cells are the major culprit of both T1D and allogeneic islet graft rejection by recognizing and responding to beta cell autoantigens and allogeneic major and minor histocompatibility antigens [399-403]. T cells upregulate Fas receptor and become sensitive to FasL-mediated apoptosis [404]. Apoptosis induced by FasL interaction with Fas on immune cells plays an important role in immune homeostasis and tolerance to self-antigens [405-408], and can be applied to address allogeneic rejection [409]. FasL may also play an active role in the generation of immunoregulatory cells [410] and their function [411-414]. Several subsets of

immunoregulatory cells were shown to be more resistant to Fas/FasL-mediated apoptosis, and some of which use FasL as a death molecule to eliminate antigen-reactive T cells [411-416]. We have recently demonstrated localized tolerance achieved by the direct display of SA-FasL on allogeneic islets transplanted under the kidney capsule was mediated by the elimination of alloreactive T effector cells and induction/expansion of $CD4^+CD25^+FoxP3^+$ Treg cells that maintained tolerance [417]. The critical role apoptosis plays in immune tolerance (central and peripheral) combined with the potential of SA-FasL in apoptosis and generation/function of immunoregulatory cells make this an attractive molecule to modulate alloreactive immune responses for tolerance induction to allogeneic islet grafts.

The development of an extrahepatic site lacking the short and long-term complications of intraportal transplantation will significantly contribute to wide-spread application of clinical islet transplantation. For intraportal islet transplantation, islets are infused into the portal vein allowing immediate exposure of the graft to the blood, which initiates instant blood-mediated inflammatory reactions (IBMIR [418]). IBMIR is responsible for 50-80% of early loss of transplanted islets and involves the binding of tissue factor expressed on islets with platelets, resulting in their activation [398, 418]. Activated platelets trigger coagulation and complement cascades, leading to granulocyte and monocyte infiltration into the islet graft and their ultimate destruction [398, 418, 419]. Intraportal transplantation also suffers from long-term complications, including hepatic steatosis and β-cell apoptosis/non-function due to the inherent hyperglycemic environment and relatively higher concentrations of drug metabolites in the liver [420]. Porous scaffolds have demonstrated the capacity to modulate the local environment in order to promote engraftment and long-term function [421-425]. Islets can readily be seeded into the pores, while the porosity supports rapid cell infiltration for integration with the host tissue.

Microporous scaffolds composed of the biocompatible, biodegradable, FDA approved copolymer of lactide and glycolide (poly(lactide-co-glycolide) (PLG), creates and maintains a space for transplanted islets while enabling control of their distribution and density within the scaffold [426, 427]. The high porosity enables nutrient diffusion, rapid host tissue infiltration and islet revascularization. These scaffolds have been decorated with extracellular matrix proteins from the basement membrane (e.g., collagen IV), which results in a significant increase in islet function post transplantation [426, 428].

In this report, we describe the attachment of SA-FasL to microporous PLG scaffolds to achieve chronic immunosuppression-free, long-term survival of allogeneic pancreatic islets transplanted into an extrahepatic site, i.e. the epididymal fat pad. The omentum has emerged as a leading candidate in human clinical trials due to its thin, highly vascularized membrane and portal draining that recreates the physiological effects of insulin in the liver [429, 430]. In mice, the epididymal fat pad has many similar features to the omentum, and we have developed scaffolds to support engraftment of transplanted islets at this site. Initial studies employed an established model in which islets are modified with SA-FasL, with subsequent transplantation onto a microporous scaffold. Subsequently, we developed procedures for modifying microporous PLG scaffolds with biotin for subsequent immobilization of SA-FasL, and characterized the binding and functionality of the immobilized protein. These studies employed islets isolated from BALB/c mice and transplanted into the epididymal fat pad of C57BL/6 mice, a fully mismatched transplantation model. The function of the transplanted islets was monitored by blood glucose levels as well as an intraperitoneal glucose tolerance test. Collectively, these studies address two major issues with clinical islet transplantation; development of an extrahepatic site for islet

engraftment, and overcoming immune rejection without of the use of chronic immunosuppression.

Materials and methods

Materials

Poly(lactide-co-glycolide) (75:25) (PLG) (approx. 80,000 g/mol) with a single carboxylic acid end-group and an inherent viscosity of 0.76 dL/g was purchased from Lakeshore Biomaterials (Birmingham, AL). Poly(ethylene-alt-maleic anhydride) (PEMA) was purchased from Polyscience, Inc. (Warrington, PA). EZ link Amine-PEG2-Biotin was purchased from Fisher Scientific. 1-ethyl-3-(3-dimethylaminopropyl)carbodiimide hydrochloride (EDC), N-hydroxysuccinimide (NHS), dichloromethane (DCM), dimethylsulfoxide (DMSO), and all other reagents were purchased from Sigma Aldrich (St. Louis, MO) unless noted otherwise.

Biotinylation of PLG and characterization

PLG (890 mg, 0.011 mmol) was added to a 20 mL glass scintillation vial and dissolved in 10 mL DMSO. The carboxyl end group of PLG was activated by first adding EDC (10.6 mg, 0.056 mmol) dissolved in 1 mL DMSO followed by NHS (6.4 mg, 0.056 mmol) dissolved in 1 mL DMSO, and the reaction was allowed to stir for 15 min. Amine-PEG2-Biotin (5 mg, 0.056 mmol) was dissolved in 1 mL DMSO and added dropwise to the stirring solution of PLG-NHS and the reaction was allowed to stir overnight. Excess biotinylation reagent was removed by extraction. The reaction mixture was diluted into 200 mL of DCM and washed 4 times with 150 mL of a saturated salt solution (brine). The organic layer was dried over anhydrous sodium sulfate, filtered, concentrated by rotary evaporation, precipitated into ice cold methanol, and

stored in vacuo overnight to remove residual solvents. Functionalization was confirmed with ^{1}H-NMR (DMSO-d6).

Particle and scaffold fabrication

PLG microparticles were formed for scaffold fabrication as previously described [431]. Briefly, PLG was dissolved in 2.04 mL of DCM (6 wt%) and sonicated in 10 mL of a 1% solution of PEMA at 100% amplitude (Cole-Parmer, 130 W, 3 mm stepped tip). The emulsion was poured into 200 mL of 0.5% PEMA and the organic solvent was evaporated by stirring the emulsion overnight. The particles were recovered by washing four times with deionized water by centrifugation at 7000 x g for 15 min at 4 deg C. Particles were lyophilized for 48 hours and stored under vacuum. Biotin-PLG microparticles were similarly fabricated, however biotin-PLG conjugates were combined with unmodified PLG at a mass ratio of 3:1 (biotin-PLG:PLG) for a final concentration of 6 wt% in DCM.

Porous scaffolds were formed by mixing PLG particles with NaCl (250 μm< d < 425 μm) at a 1:30 ratio (PLG:NaCl). The mixture was pressed in a 5 mm KBr die using a Carver press at 1500 psi and foamed in CO_2 at 750 psi for 16 hours. Scaffolds were leached in water for 1 hour followed by a second wash for 30 minutes. Scaffolds were disinfected by soaking them in 70% ethanol and washed with deionized water.

Particle characterization

The size and zeta potential of the particles was determined by dynamic light scattering (DLS) by mixing 10 μL of a 25 mg/mL particle solution into 990 μL of MilliQ water using a Malvern Zetasizer ZSP (Westborough, MA).

Protein loading and quantification

Particles were incubated with various concentrations of fluorophore-labeled streptavidin at 1 mg particles/mL for 20 minutes at various concentrations. Unbound streptavidin was removed by washing the particles with PBS by centrifugation (7000 x g, 5 min, 4 deg. C). To quantify the amount of fluorophore binding to the particles, particles were dissolved in DMSO and fluorescence was quantified using a plate reader (Synergy 2 (BioTek)) at 578 nm excitation and 605 nm emission.

Scaffolds were incubated with fluorescent streptavidin by applying 10 µL of the SA solution (0-40 ng/µL) to both sides of the disc (a total of 20 µL) for 20 minutes. Unbound streptavidin was removed by washing the scaffold three times with 1.5 mL of PBS. Scaffolds were dissolved in DMSO and fluorescence was quantified as described above.

Apoptosis assay

Particles (1 mg) and scaffolds were incubated with SA-FasL (Particles: 1 mL, 400 ng/µL, scaffold: 20 µL, 0-50 ng/µL) and washed as described above. To assess the ability for FasL particles or scaffolds to induce apoptosis in vitro, 1 mg/mL particles or a single scaffold was added to a 96 well plate containing A20 cells (mouse B lymphoma) at a concentration of $1.5x10^6$ cells/mL and incubated for 18 hours. Cells were removed from the plate, stained with annexin V and propidium iodide (Life Technologies), and analyzed via flow cytometry.

Mice and recombinant proteins

C57BL/6 (*H-2*^{b}) and BALB/c (*H-2*^{d}) mice were purchased from Jackson Laboratory and bred in our specific pathogen-free animal facility at the University of Louisville using protocols approved by the Institutional Animal Care and Use Committee. Recombinant SA and SA-FasL

proteins were made with the *Drosophila* DES expression system (Invitrogen) following standard protocols [409].

Islet isolation and engineering with SA-FasL protein

BALB/c islets were harvested from 8 to 12-week-old donors under anesthesia. Donor pancreata were perfused with 3 mL of cold Liberase TL (Roche Diagnostics) then removed and incubated for 20 minutes at 37^{o}C. Islets were isolated using a Ficoll gradient (Sigma-Aldrich). Islets were kept overnight in RPMI-1640 medium supplemented with penicillin/streptomycin (100 U/mL and 100 µg/mL) and 10% fetal bovine serum in an incubator at 37^{o}C with 5% CO_2. Islets were transferred to a 14-mL round bottom tube and washed in PBS. Islets were then incubated in 5 µM EZ-Link™ Sulfo-NHS-LC-Biotin solution (Thermo Scientific) at 20^{o}C for 30 minutes. After incubation, islets were washed twice in PBS to remove any unbound biotin. Then, islets were incubated in PBS containing SA-FasL protein (~200 ng SA-FasL/500-550 islets/200 µl PBS) at 20^{o}C for 30 minutes. Islets were washed twice in PBS to remove any unbound protein before transplantation. Select biotin-PLG scaffolds were engineered by placing scaffolds to a round bottom tube and adding SA-FasL (0.5 or 2.5 µg /scaffold) diluted in PBS and incubating at 20^{o}C for 30 minutes while rotating and shaking the tube every 10 minutes. Scaffolds were washed twice before being loaded with islets.

Islet transplantation

C57BL/6 mice were chemically induced with diabetes by intravenous (i.v.) injection of streptozotocin (200 mg/kg). Mice were monitored by reading blood glucose where ≥ 250 mg/dL for two consecutive days was considered diabetic. Islets were loaded onto PLG scaffolds (2/mouse). Diabetic mice were given anesthesia and a small incision was made on the abdomen to allow scaffolds to be placed on epididymal fat pads. Adipose tissue was wrapped around

scaffolds before being returned to the abdomen. Mice were then sutured. Select mice were administered with rapamycin through i.p. injection of 0.2 mg/kg daily for 15 days starting the day of transplant. Mice were monitored for diabetes and those with ≥ 250 mg/dL blood glucose level for two consecutive days considered rejecting the islet graft.

Intraperitoneal Glucose Tolerance Test

Mice were put in clean cages without food and allowed to fast for 6 hours. Mice were then injected with 25% glucose solution (2 g/kg body weight) and monitored for blood glucose levels before injection and at 10, 20, 30, 60, 90, and 120 minutes post glucose injection.

Mixed Lymphocyte Reaction

Spleen and draining lymph nodes were harvested from mice after rejection of graft or at experimental end point (> 200 days) if mice remained euglycemic up to that point. Organs were processed into single cell suspensions using frosted slides. ACK lysis buffer (ThermoFisher Scientific) was added to spleen to lyse red blood cells. Splenocytes were panned, labelled with (5(6)-Carboxyfluorescein N-hydroxysuccinimidyl ester) (CFSE), and used as responders in a standard mixed lymphocyte reaction assay [432]. Stimulator cells were prepared from either naïve BALB/c (donor) or C3H (3^{rd} party) mice, irradiated with 200 cGy, and cocultured with equal numbers of responder cells in 96-well plates ($0.1x10^6$ cells/well). Cells were cultured in 200 µL DMEM supplemented with HEPES buffer, sodium pyruvate, penicillin/streptomycin, L-Glutamine (ThermoFisher Scientific), FBS, L-Arginine HCL, folic acid, L-Asparagine, 2-Mercaptoethanol (Sigma), and responder serum. Cells were harvested after four days of culture at 37°C and stained with Alexa 700-CD4 Ab, APC-Cy7-CD8 Ab, and 7AAD to separate dead cells (BD Pharmingen). Cells were collected using BD LSR II and analyzed using Diva software.

Statistical analysis

Flow data was tested for significance using a two tailed Welch's t-test. Graft survival was tested for significance using the log-rank test. P values less than 0.05 were considered significant. Survival curves, IPGTT, and flow graphs were created and analyzed using GraphPad Prism software.

Results

Transplantation of SA-FasL-engineered islets on microporous scaffolds

We investigated the transplantation of SA-FasL-engineered islets on microporous scaffolds implanted into the epididymal fat pad (Fig 1A). Initial studies employed syngeneic islets transplanted into streptozotocin-induced diabetic mice to determine the impact of the scaffolds and short-term rapamycin on the engraftment and function of the islets. Transplantation of the syngeneic islets led to the establishment of euglycemia within 10 days for all animals, and blood glucose levels fell below 200 mg/dL, which was used to define graft survival (Fig 1B). All animals with syngeneic islets engineered with SA-FasL had graft survival for the duration of the study (100 days). Subsequently, allogeneic islets engineered with SA-FasL were transplanted on microporous scaffolds. Unmodified islets transplanted on scaffolds with transient rapamycin underwent rejection, as indicated by increased blood glucose levels, by day 40 (Supplementary Fig. 1). Mice transplanted with allogeneic islets modified with SA-FasL and receiving transient rapamycin had graft survival that was sustained for 200 days (Fig 1C), similar to the results with syngeneic islets. Rapamycin has been previously reported to synergize with SA-FasL presentation to prolong allograft survival [417], as either factor alone results in only short-term graft function. An intraperitoneal glucose tolerance test (IPGTT) study demonstrated that the normalization of blood glucose levels by the transplanted islets was similar to that observed with

naïve mice (i.e., non-diabetic) (Fig 1D, E), which is consistent with previous reports of islets transplanted on scaffolds [427, 433].

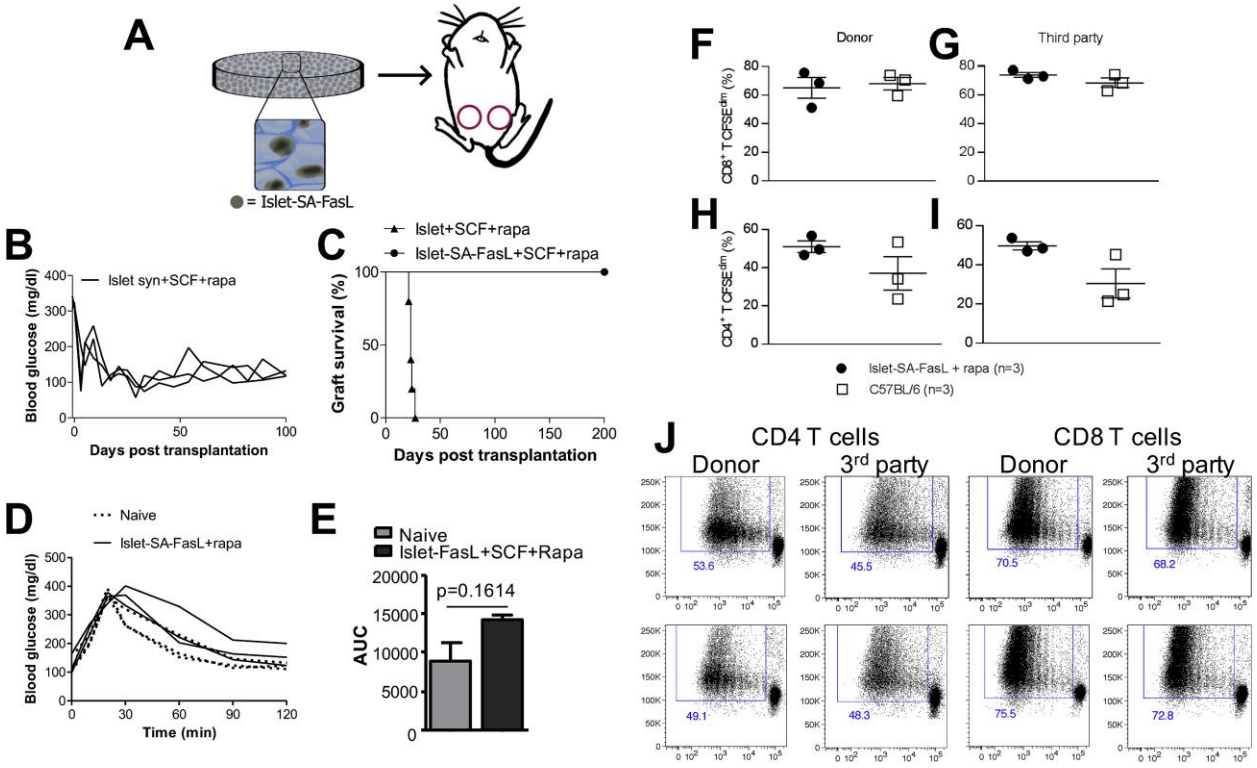


Figure 7.1 SA-FasL engineered islets establish allogeneic tolerance when transplanted on PLG scaffolds. **(A)** Schematic showing biotinylated islets functionalized with SA-FasL are loaded on microporous PLG scaffolds and implanted in the epididymal fat pad of mice. **(B)** Individual tracing of blood glucose levels for syngeneic islets modified with SA-FasL and transplanted on scaffolds (SCF), with mice receiving a short course of rapamycin (n = 3, mean survival time > 100 days). **(C)** Kaplan Meier analysis of allogeneic BALB/c islets transplanted under the short cover of rapamycin on unmodified PLG scaffolds in C57BL/6 recipients. Conditions include SA-FasL-engineered islets on scaffolds with rapamycin (n = 5, mean survival time >200 days), naïve islets on scaffolds with rapamycin (n = 5, mean survival time = 23 ± 2.19 days). **(D)** Intraperitoneal glucose tolerance test of long-term islet grafts compared to naïve C57BL/6 mice after fasting for 6 h, followed by i. p. glucose injection. Blood glucose of mice was taken starting just before injection and at the indicated time points. **(E)** Area under curve for the intraperitoneal glucose tolerance test. The area for naïve mice compared to the transplanted mice is not significantly different (p = 0.16). **(F–I)** T cell proliferative response from recipients of long-term (>200 days) BALB/c SA-FasL-engineered islets mounted on unmodified PLG scaffolds plus rapamycin (n = 3) and naïve C57BL/6 as controls (n = 3). Responders were labeled with CFSE and used against BALB/c donor (F,H) and third party C3H (G,I) stimulators in a standard *ex vivo* mixed lymphocyte reaction. After 4 days of culture, cells were stained with antibodies against CD8 (F,G) and CD4 (H,I) molecules and incubated with 7AAD to gate out dead cells before flow cytometry analysis. (J) Representative dot plots of data presented in F, G, H and I. Bars represent mean and SEM. Asterisks represent level of significance (*p < 0.05, **p < 0.01) found by using a two-tailed Welch's *t*-test.

We next assessed the immune competency of long-term islet graft recipients and if the observed graft survival is associated with systemic immune non-responsiveness against the donor alloantigens. T cell proliferative responses were analyzed from the spleens and draining lymph

nodes of the long-term allogeneic islet graft survivors. The collected cells were labeled with CFSE and used against BALB/c donor and third party C3H stimulators in a standard ex vivo mixed lymphocyte reaction [432]. After 4 days of culture, the responses from $CD8^+$ T cells indicated similar proliferative responses for the SA-FasL-engineered islets and an age-matched C57BL/6 control, with responses similar to both the donor and third-party stimulators (Fig 1F). Interestingly, $CD4^+$ T cell responses were greater for the SA-FasL-engineered islets relative to age-matched control. This response was similar for both the donor and third-party stimulators. These results demonstrate that recipients of long-surviving islet allografts are immunocompetent and show lack of systemic unresponsiveness to donor antigens, demonstrating localized nature of graft protection. Collectively, these studies demonstrate that the microporous scaffolds for transplantation of SA-FasL-engineered islets to an extrahepatic, extra-renal site provides for engraftment of the islets and protection from the immune response similar to previous reports performed with transplantation under the kidney capsule [417].

Synthesis and characterization of biotin-PLG conjugates and particle formation

We subsequently investigated the modification of scaffolds with biotin to allow for immobilization of SA-FasL as a potential off-the-self product for immunomodulation. PLG was conjugated with a biotin linker and the biotin-PLG conjugates were subsequently formed into microspheres that were assembled into scaffolds. The carboxyl-terminal group of PLG was conjugated to the heterobifunctional linker NH_2-PEG_2-Biotin using carbodiimide chemistry and confirmed using ^{1}H-NMR (Figs 2A, B). Biotin-PLG particles were prepared with a single emulsion-solvent evaporation procedure using the biotin-PLG conjugates. The particles displayed an average size of 860 ± 40 nm and a zeta potential of –16 ± 5.0 mV (Supplementary Fig 2).

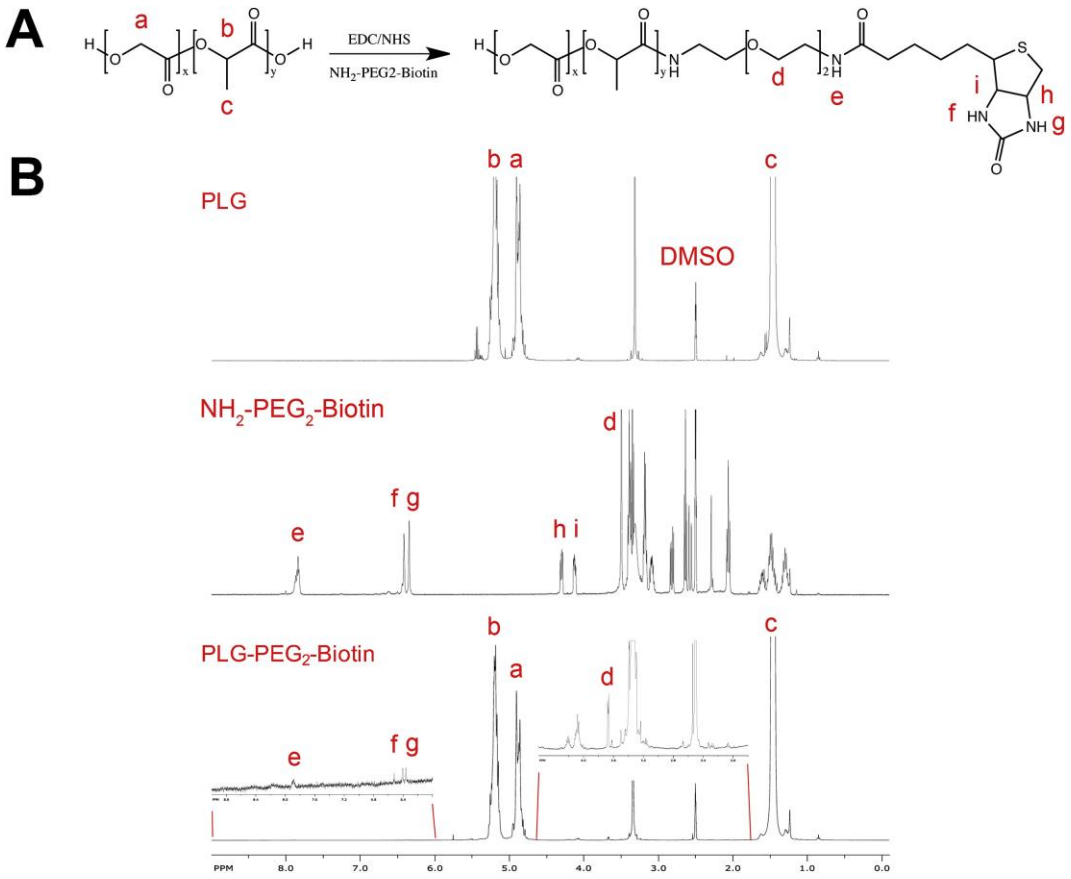


Figure 7.2 Characterization of biotin-PLG polymer. (A) Conjugation of NH_2-PEG_2-biotin to PLG via carbodiimide chemistry, resulting in biotin-PLG. (B) ^1H NMR in $(D_3C)_2SO$ of PLG (top), biotin linker (middle), and biotin-PLG (bottom).

The ability of biotin-PLG particles to bind streptavidin was quantified through the maximum loading and efficiency of fluorescently-tagged streptavidin (AF568-SA) (Fig 3A). The unmodified particles non-specifically bound a small amount of AF568-SA, however the presence of biotin significantly increased the amount of bound protein. The concentration of AF568-SA incubated with particles was varied from 100 to 800 ng AF568-SA per mg of particle, which resulted in loadings of 75 to 280 ng AF568-SA per mg of particle (Fig 3B). A dose of 40,000 ng AF568-SA per mg of particle was used as a saturating dose, which produced a loading in excess of 8,000 ng AF568-SA per mg of particle. Although the amount loaded on the particle increased with greater concentration of AF568-SA (Fig 3C), the loading did not increase linearly. The

loading efficiency (defined as the amount of protein bound divided by the amount incubated) decreased from 75% to 35% as the concentration was increased from 100 to 800 ng AF568-SA per mg of particle. At the maximal dose of 40,000 ng AF568-SA per mg of particle, the loading efficiency was 20% for the biotinylated particles and approached 0% for the non-biotinylated particles.

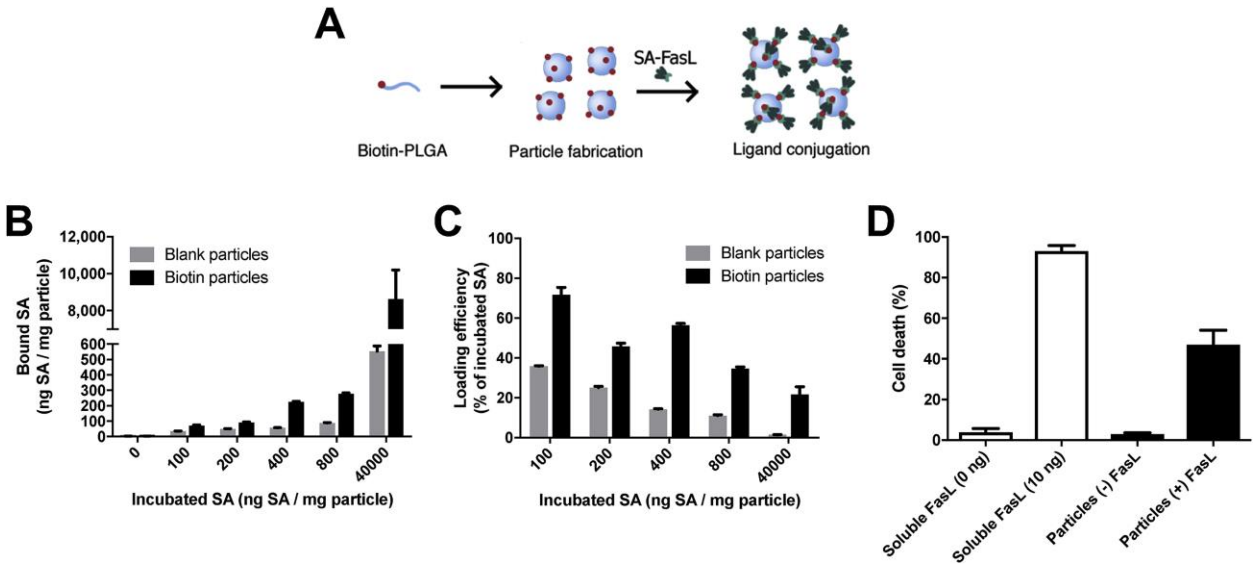


Figure 7.3 Biotin-PLG particles can be efficiently conjugated with SA-FasL and induce apoptosis in mouse B lymphoma cell line. (A) Schematic of biotin-PLG particles being functionalized with SA-FasL. (B) The amount of fluorescently tagged SA bound to the particles was investigated by varying the protein concentration (0, 100, 200, 400, 800, and 40,000 ng SA/mL in 1 mL) incubated with 1 mg of biotin-PLG particles ("biotin particles"). As a control, 1 mg of unmodified PLG particles was incubated with the same SA concentrations ("blank particles"). After two spins and washes, particles were dissolved in DMSO and fluorescence was measured, n = 3. (C) The loading efficiency was calculated by dividing the bound SA by the incubated SA, n = 3. (D) Biotin-PLG particles functionalized with SA-FasL induce cell death in A20 cells. Particles were incubated with 400 ng/mL of SA-FasL in 1 mL with 1 mg of particles. After washing to remove unbound SA-FasL, particles were incubated with 1.5×10^5 A20 cells for 18 h and cell death was analyzed via propidium iodide stain and flow cytometry (n = 3). For comparison, soluble FasL was added to cells (0, 10 ng) and demonstrated the ability to induce cell death at low concentrations (n = 3).

The bioactivity of immobilized SA-FasL was investigated next through their ability to induce apoptosis in the mouse B lymphoma cell line A20. Particles were incubated with 400 ng SA-FasL, which was selected based on the substantial difference in the binding to biotinylated and non-biotinylated particles (Fig 3B). The addition of particles modified with SA-FasL induced apoptosis in approximately 50% of the cells (Fig 3D). Biotinylated particles without SA-FasL did induce apoptosis at levels consistent with the negative control, which was approximately 1% of the cell population. The level of apoptosis induced by the particles was less than that obtained

with soluble SA-FasL, which induced apoptosis in more than 90% of the cells for a dose of 10 ng.

SA-FasL loading on biotin-PLG scaffolds

SA-FasL modified scaffolds were subsequently prepared by fabricating scaffolds from the biotinylated polymer with subsequent incubation with a solution containing SA-FasL (Fig 4A). Incubation of SA-AF568 at concentrations ranging from 100 to 800 ng SA-AF568 per mg of scaffold resulted in loadings that ranged from 70 to 620 ng SA per mg of scaffold, which was similar to particles at low concentrations (Fig 4B). The efficiency of loading was relatively constant across the range of concentrations (≈70%), which differed from what was observed with the particles that had a declining efficiency with increased concentration of SA-AF568 (Fig 4C). The increased efficiency may result from an increased surface area of the porous scaffold compared to the spherical particles. Unmodified scaffolds were used as a control, and showed similar concentrations of non-specific binding as unmodified particles at higher protein concentrations.

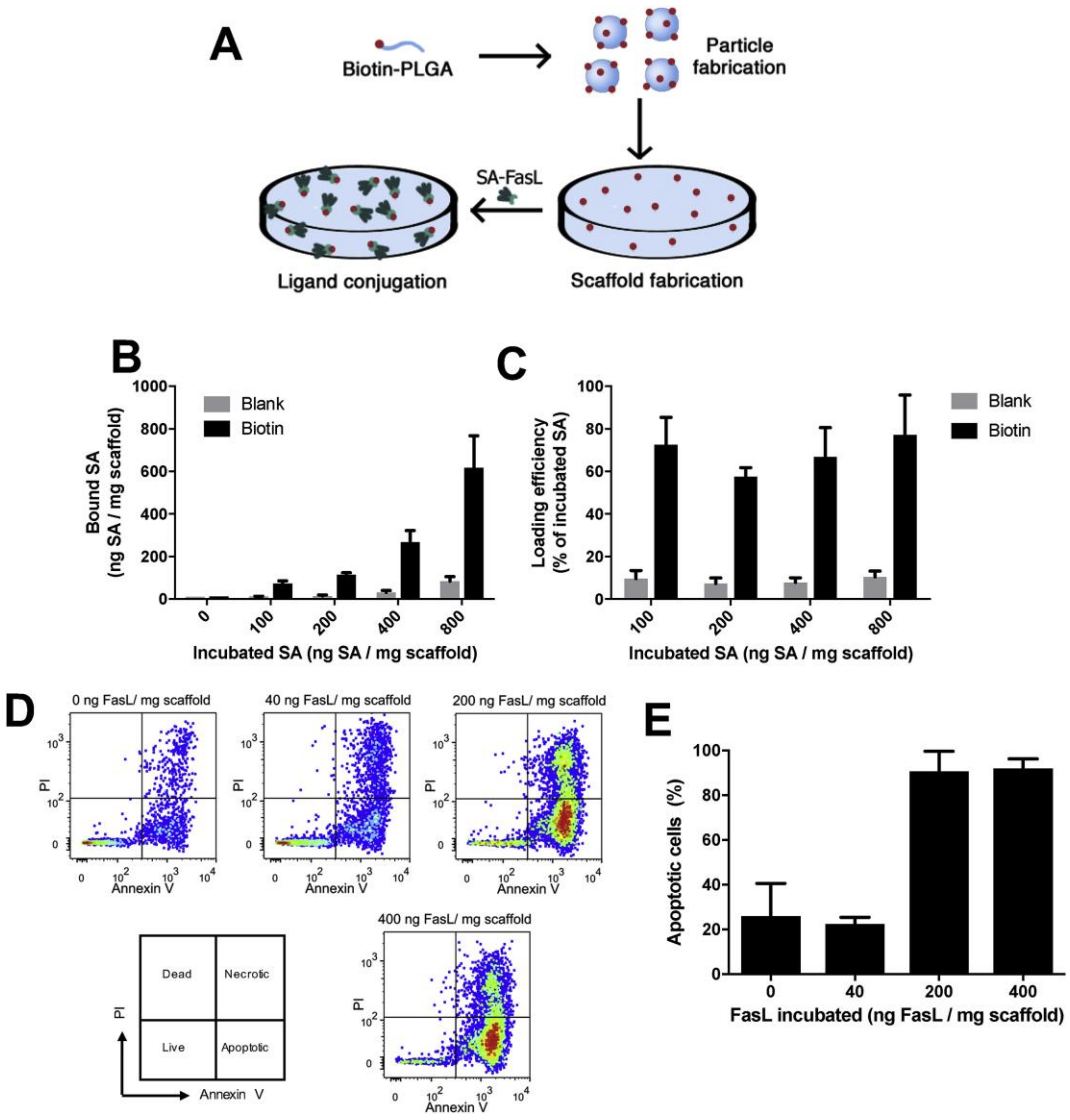


Figure 7.4 Biotin-PLG scaffolds can be efficiently conjugated with SA-FasL and induce apoptosis in mouse B lymphoma cell line. (A) Schematic of biotin-PLG particles functionalization with SA-FasL. (B) The amount of fluorescently tagged SA bound to scaffolds was investigated by varying the protein concentration (0, 100, 200, 400, and 800 ng SA/20 µL) incubated with 2.5 mg biotin-PLG scaffolds ("biotin"). As a control, unmodified PLG scaffolds were incubated with the same SA concentrations ("blank"). After two washes, scaffolds were dissolved in DMSO and fluorescence was measured, n = 3. (C) The loading efficiency was calculated by dividing the bound SA by the incubated SA, n = 3. (D) Scaffolds were incubated with SA-FasL (0, 40, 200, and 400 ng/20 µL). After washing to remove unbound SA-FasL, scaffolds were incubated with 1.5×10^5 A20 cells for 18 h. Apoptotic and dead cells were analyzed via propidium iodide and Annexin V staining and flow cytometry (n = 3). For comparison, 2.5 mg of soluble FasL was added to cells and induced apoptosis in the 98% of the cells (n = 3). (E) Scaffolds required a minimum loading of 200 ng FasL/mg scaffold to induce apoptosis in the majority of A20 cells.

SA-FasL-loaded scaffolds had a greater efficiency for inducing apoptosis of A20 cells relative to the particles (Fig 4D, E). The induction of apoptosis was concentration-dependent as 40 ng SA-FasL/mg scaffold was not significantly different than the control but 200 ng/mg and 400 ng/mg

increased apoptosis (Annexin V^+) in more than 90% of the cells. These results demonstrate that SA-FasL could be functionalized to the surface of PLG scaffolds and effectively induce apoptosis in A20 cells.

SA-FasL scaffolds support allogeneic graft function without chronic immunosuppression

We subsequently investigated whether SA-FasL modified scaffolds could prevent allogeneic islet rejection similar to the SA-FasL-engineered islets, while also supporting engraftment and long-term function to maintain normoglycemia. Scaffolds engineered with SA-FasL were loaded with islets from BALB/c donors and transplanted into the peritoneal fat of diabetic C57BL/6 mice. Naïve islets mounted on SA-FasL-engineered PLG scaffolds along with transient rapamycin demonstrated graft survival for more than 200 days in more than 80% of the animals (Fig 5A), with one animal rejecting at day 30. Rapamycin without SA-FasL had a mean graft survival time of 23 ± 2 days (Fig 5A, B). Interestingly, when both islets and scaffolds were engineered with SA-FasL but did not receive the short course rapamycin treatment, one third of the mice established long-term tolerance while the rest rejected by day 50. For the transplantation of islets on SA-FasL modified scaffolds, normoglycemia was established within days of transplantation (Fig 5B). The blood glucose dynamics were similar between the SA-FasL-modified scaffolds and the unmodified scaffolds (with rapamycin) through day 20, at which point, the blood glucose levels began to rise for the unmodified scaffolds likely due to rejection of the islets. An IPGTT performed at day 200 demonstrated restoration of normoglycemia at a rate that was similar to naïve animals (Fig 5C, D).

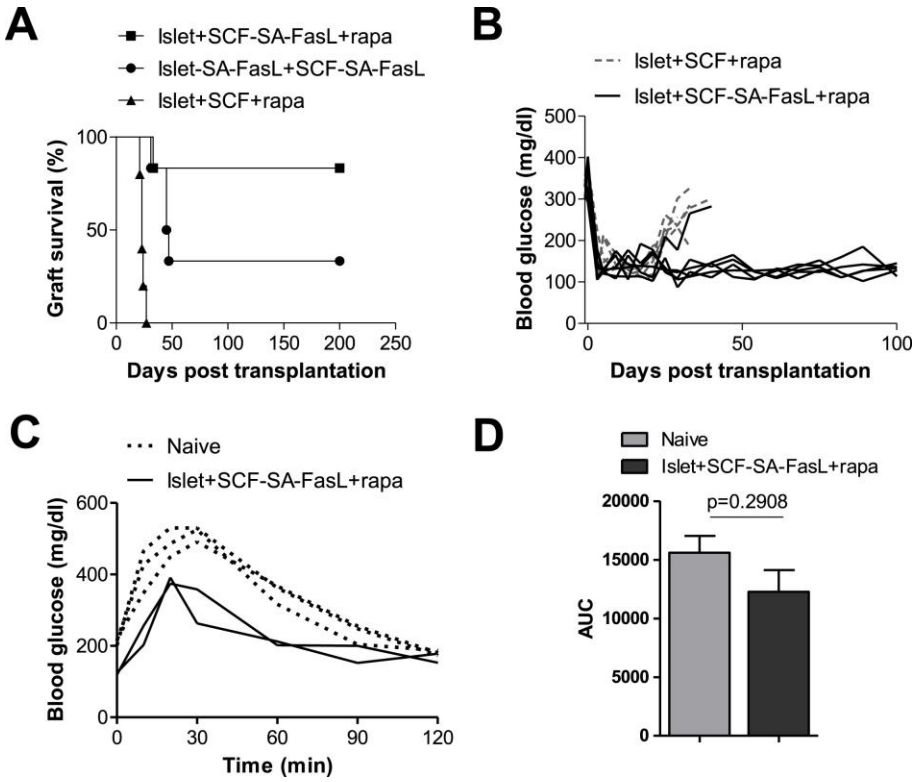


Figure 7.5 Islets on scaffolds conjugated with SA-FasL demonstrate robust long-term tolerance. (A) Survival of allogeneic BALB/c islets mounted on PLG scaffolds and transplanted in the epididymal fat pad of chemically diabetic C57BL/6 recipients. Groups included naïve islets mounted on SA-FasL-engineered PLG scaffolds plus rapamycin (n = 6, MST > 200 days, P = 0.0007 vs rapamycin alone), SA-FasL-engineered islets mounted on SA-FasL-engineered PLG scaffolds (n = 6, MST = 46 days, P = 0.0007 vs rapamycin alone), and naïve islets transplanted under a short cover of rapamycin (n = 5, MST = 23 ± 2.19 days). All mice received islets loaded on 2 PLG scaffolds. PLG scaffolds were engineered with 2.5 μg/scaffold, except 3 mice in the islet-FasL + PLG-SA-FasL that were transplanted with PLG scaffolds engineered with 0.5μg/scaffold and all 3 animals rejected their grafts. Rapamycin was given to the indicated groups through i. p. injection at 0.2 mg/kg daily for 15 days starting on the day of transplantation. Mice were monitored twice weekly for blood glucose levels. Those with >250 mg/dL for two consecutive readings 24 h apart were considered diabetic and rejecting the graft. Statistical analysis was performed using log-rank test, **P < 0.01, ***P < 0.001. (B) Blood glucose readings of two groups of mice from (A). (C) Intraperitoneal glucose tolerance test (IPGTT) of long-term islet grafts compared to naïve C57BL/6 mice after fasting for 6 h, followed by i. p. glucose injection. Blood glucose of mice was taken starting just before injection and at the indicated time points. (D) Area under the curve for (C).

Discussion

This report investigated the combination of SA-FasL and biomaterial scaffolds as a means to create a translatable site that supported the engraftment and long-term function of allogeneic islets at an extrahepatic and extrarenal site. Immunoprivileged sites, such as the testes, anterior chamber of the eye, brain, and tumors, have the ability to suppress destructive immune responses by various mechanisms [75, 434-436]. Importantly, FasL was initially discovered as one of the

molecules that plays a critical role in immunoprivileged sites [405, 406]. Indeed, we have recently reported that SA-FasL-engineered allogeneic islets induced localized immune privilege when transplanted under the kidney capsule [417]. Therefore, FasL not only contributes to the regulatory mechanisms in naturally occurring immunoprivileged sites in the body, yet also can be used to create "induced" immunoprivileged sites [417]. Herein, we demonstrated that allogeneic SA-FasL-engineered islets engrafted and normalized blood glucose levels for more than 200 days under a short course of rapamycin treatment (0.2 mg/kg daily starting the day of transplantation for a total of 15 doses) with transplantation on PLG scaffold into an extrahepatic site, one that has translational potential [437].

Given that localized presentation of SA-FasL on islets supported long-term function on the scaffold, we subsequently investigated the immobilization of SA-FasL to the scaffold as a means to minimize the cellular manipulation prior to transplantation. Biotin decorated PLG particles have been reported for targeted drug delivery to cancer cells [438]. Manipulating the scaffold to present SA-FasL would eliminate the steps needed for direct islet engineering, and as such save time and overcome potential undesired effects associated with engineering process, such as cell fragmentation. Moreover, scaffolds engineered with SA-FasL can be manufactured as a potential off-the-shelf immunomodulatory product for islet transplantation, expediting clinical translation. Importantly, the presentation of SA-FasL from surfaces has previously been reported not to interfere with its apoptotic function [417, 439]. To create scaffolds modified with SA-FasL, we chemically modified the polymer in solution [330, 438, 440, 441], which was subsequently formed in to particles and then into scaffolds. Initial attempts to functionalize scaffolds involved conjugation of biotin to the surface of a pre-formed scaffold, which produced inconsistent modification with SA-FasL and thus the direct modification of the polymer was pursued based

on prior reports indicating enhanced target binding [442]. Stable spherical particles could only be formed from mixtures of the biotinylated and non-biotinylated polymer, as particles formed from only biotinylated polymer were unstable due to aggregation. The microspheres were employed to construct the scaffold using a gas foaming and particulate leaching process [443-445]. The scaffolds can readily be stored prior to islet seeding for transplantation; however, as a potential off-the-shelf product, further studies will be needed to test long-term storage of SA-FasL pre-engineered scaffolds for downstream applications.

The microporous structure of the scaffold enhanced protein loading and bioactivity relative to the particles. This observation likely results from the higher surface area of the scaffolds. Protein loading and efficiency were similar to other techniques like carbodiimide coupling to PLG particles [321, 431]. The presentation of SA-FasL from particles or scaffolds maintained the ability to induce apoptosis, although it was not as efficient as soluble SA-FasL, which may reflect the nature of ex vivo culture setting favoring better access of soluble SA-FasL to the Fas receptor on A20 cells. Further optimization of the PEG-biotin linker length may enable enhanced binding of SA-FasL to Fas by increasing the mobility of SA-FasL [446]. Interestingly, for concentrations between 40 and 400 ng/mg, the extent of binding was highly consistent within experiments, yet considerable variation in apoptosis was observed between experiments, suggesting a sensitivity to the protein loading or presentation within this range. Previous reports of surface modified apoptosis systems utilized surface anchored polymer chains with covalently linked anti-Fas antibodies but were only able to achieve up to 34% apoptosis in cells expressing Fas, whereas the method presented here achieved 92% apoptosis and *in vivo* protection of allogeneic islets [447]. This result may be due to the far greater surface density of protein (up to 150 ng/cm^2 vs 1.6 ng/cm^2), the reported robust apoptotic function of SA-FasL [448], and the

positional display of this molecule on biotinylated scaffolds, preserving its function. These findings are consistent with our recent publication with polyethylene glycol (PEG) microparticles where we demonstrated a dose-dependent binding of SA-FasL to biotin presenting microparticles [449].

Importantly, microporous scaffolds functionalized with SA-FasL supported engraftment and function of the transplanted allogeneic islets that maintained normoglycemia for more than 200 days in the absence of chronic immunosuppression. Islets transplanted on unmodified PLG scaffolds were promptly rejected within 6-12 days after the rapamycin treatment ended, consistent with our previous results [417, 449]. The observed sustained survival and function of allogeneic islets without immunosuppression is consistent with our previously published data with islet directly engineered to transiently display SA-FasL on their surface [432]. Importantly, this data also consistent with our most recent study reporting sustained survival of allogeneic islets co-transplanted with biotinylated PEG microparticles presenting SA-Fas on their surface [449]. SA-FasL alone without rapamycin was able to delay rejection of all grafts with ~40% surviving for the 200-day observation period. This observation demonstrated that SA-FasL has the potential as monotherapy to achieve permanent graft survival, but complete efficacy may require further refinement of the protocol by increasing the dose of SA-FasL or duration of persistence. Our approach of functionalizing SA-FasL onto the surface of biotin-PLG scaffolds is an effective method to induce long-term function without chronic immunosuppression.

Long-term graft recipients generated T cell responses to both donor and third-party antigens at a similar magnitude to those of naïve mice. These findings demonstrate that immunomodulation with SA-FasL in context of PLG scaffolds does not result in immune incompetence of the graft recipients nor systemic tolerance to donor antigens. Lack of systemic unresponsiveness is

expected given the localized nature of immunomodulation by SA-FasL and the demonstrated role of this molecule in physiological immune privilege [450]. These findings are further consistent with our published studies demonstrating that SA-FasL-engineered islets or PEG microgels presenting SA-FasL transplanted under the kidney capsule establish localized tolerance, which is maintained by $CD4^+CD25^+FoxP3^+$ T regulatory cells [432, 449].

In conclusion, our studies demonstrate that PLG scaffolds support the engraftment and sustained survival of allogeneic islets directly engineered to transiently display SA-FasL on their surface in an extrahepatic and translational site in the absence of chronic immunosuppression. Importantly, scaffolds directly engineered with SA-FasL achieves a similar outcome as SA-FasL-engineered islets, demonstrating that immunoregulation induced in this setting does not require T cells establishing simultaneous physical interaction with both the alloantigen and SA-FasL on the target tissue, consistent with our recent study with PEG microgels presenting SA-FasL [449]. This observation suggests that T cells activated in response to alloantigens are eliminated within graft microenvironment upon encounter with SA-FasL attached to the scaffold. Importantly, the modification of biomaterial with SA-FasL avoids the complications associated with direct engineering of islet grafts and provides a potential off-the-shelf immunomodulatory product that may have applicability to a multitude of applications involving cell transplantation.

Data availability

The raw/processed data required to reproduce these findings cannot be shared at this time due to technical or time limitations. However, they can be provided upon request.

Conflicts of interest

H.S., E.S.Y., A.J.G., and H.Z. are inventors on a pending patent on PEG engineered with SA-FasL and H.S. and E.S.Y. hold equity in FasCure Therapeutics, which has an option to license the SA-FasL technology from the University of Louisville.

Acknowledgments

This work was previously published with manuscript information Skoumal M, Woodward KB, Zhao H, Wang F, Yolcu ES, Pearson RM, Hughes KR, Garcia AJ, Shea LD, Shirwan H. Localized Immune Tolerance from FasL-Functionalized PLG Scaffolds. Biomaterials, 192 (2019) 271-281

Chapter 8 Engineered Immunological Niches to Monitor Disease Activity and Treatment Efficacy in Relapsing Multiple Sclerosis

Authors:

Aaron H. Morris, Kevin R. Hughes, Robert S. Oakes, Michelle M. Cai, Stephen Miller, David N. Irani, Lonnie D. Shea

Abstract

Relapses in multiple sclerosis can result in irreversible nervous system tissue injury. If these events could be detected early, targeted immunotherapy could potentially slow disease progression. We describe the use of engineered biomaterial-based immunological niches amenable to biopsy to provide insights into the phenotype of innate immune cells that control disease activity in a mouse model of multiple sclerosis. Differential gene expression in cells from these niches allowed us to monitor disease dynamics and to gauge the effectiveness of treatment. A proactive treatment regimen given in response to signal within the niche but before symptoms appeared substantially reduced disease. This technology offers a new approach to monitor organ-specific autoimmunity, and it represents a platform to analyze immune dysfunction within otherwise inaccessible target tissues.

Introduction

Autoimmunity can affect nearly every organ, and these diseases collectively have a prevalence of 15-24 million patients in the United States.[451] Treatment of autoimmune disease before irreversible damage occurs represents a substantial clinical opportunity, yet requires improvements in detecting disease activity and in understanding pathogenic mechanisms. For patients already

diagnosed with an organ-specific autoimmune disease, the ability to reliably identify an immunological relapse could fundamentally change treatment approaches. Strategically administered pulses of treatment could obviate the need for lifelong immune suppression. The goal of this investigation was to develop a tool to monitor immune dysregulation occurring within target tissues in order to identify relapse onset and to predict its response to therapy.

Relapsing remitting multiple sclerosis (RRMS) causes accumulating disability due to autoimmune demyelination in the central nervous system (CNS). Sixty percent of patients with RRMS are unable to walk unassisted within 15 years of diagnosis[452]. While a growing arsenal of therapies have been shown to slow relapse rate, new lesion formation on magnetic resonance imaging (MRI) scans of CNS tissues, and disability progression in people with RRMS, an individual's response to one of these therapies can be highly variable.[3] Furthermore, such therapies have to be administered continuously over the long-term and frequently cause adverse effects. Finally, while the MRI shows areas of demyelination, it provides no information regarding the underlying immunopathology. Prior studies have shown divergent patterns of immune cell infiltration within MS lesions, implying that different immunotherapies could exert variable effects in different patients[453, 454]. Clearly, a full characterization of the pathogenic local immune response within the CNS is the goal, yet remains impossible with current technologies.

We investigated the application of tissue engineering to create easily accessible, subcutaneous immunological niches that reflect aspects of immune status of CNS tissues using the mouse experimental autoimmune encephalomyelitis (EAE) model of MS. Porous materials implanted subcutaneously induced cell ingrowth and vascularization, with persistent extravasation of immune cells into the newly forming tissue. We hypothesized that these forming immunological tissues with chronic inflammation can serve as a niche with similar cell infiltrates and phenotypes

to other inflammatory sites within the host. Moreover, we hypothesized that biopsy of these engineered immunological niches (IN) could detect changes associated with disease activity and could be used to monitor the response to therapy with high reproducibility.

For the bulk of the work we leveraged the passive adoptive transfer model of EAE by intraperitoneal injection of encephalitogenic T-cells. Although the actively induced immunization model is more common, we hypothesized that the adoptive transfer model would be better for proof-of-principle studies for three reasons: i) the passive transfer model avoids the complicating factor of granuloma formation in the subcutaneous space (the same space in which the niches are implanted), ii) passive transfer results in a more synchronized and consistent disease, and iii) immunization has dramatic effects on the haemopoietic system including exapansion of immature myeloid cells[455]. Nevertheless, we replicated some aspects of the study in the active immunization model as well.

Results

EAE alters gene expression at implantable immunological niche

Microporous poly(ε-caprolactone) (PCL) scaffolds were implanted in the subcutaneous space of SJL mice 2 weeks before adoptively transferring either autoreactive or control T-cells (reactive to $PLP_{139-151}$ or $OVA_{323-339}$, respectively). Through day 7, no mice had symptoms of disease, yet by day 9, all EAE mice became symptomatic (Fig 8.1b). INs were harvested and gene expression analyzed via the OpenArray high-throughput gene expression platform on days 7 and 9 (Fig 8.1a). Analysis revealed that of the 632 genes analyzed, 130 were differentially expressed between control and diseased mice (time points pooled, $n=8$, $p<0.05$) (Fig. 8.4). Of genes that were differentially expressed, a combination of fold change (FC), expression stability, and elastic net regularization were used to identify 21 genes, one of which, TREM1, was previously unreported

with regards to EAE or MS (Fig. 8.5). A radar plot of the log_2FC for each of the 21 genes indicated similar patterns of expression between INs isolated from pre-symptomatic (d7, yellow) and symptomatic (d9, green) EAE mice that differ from those isolated from control mice (pooled t.p., dashed) (Fig 8.1e). Additionally, unsupervised hierarchical clustering demonstrated that control mice and diseased mice cluster separately (Fig 8.1d). Collectively, EAE is associated with numerous changes in gene expression at the immunological niches and these changes are detectable before disease symptoms occur.

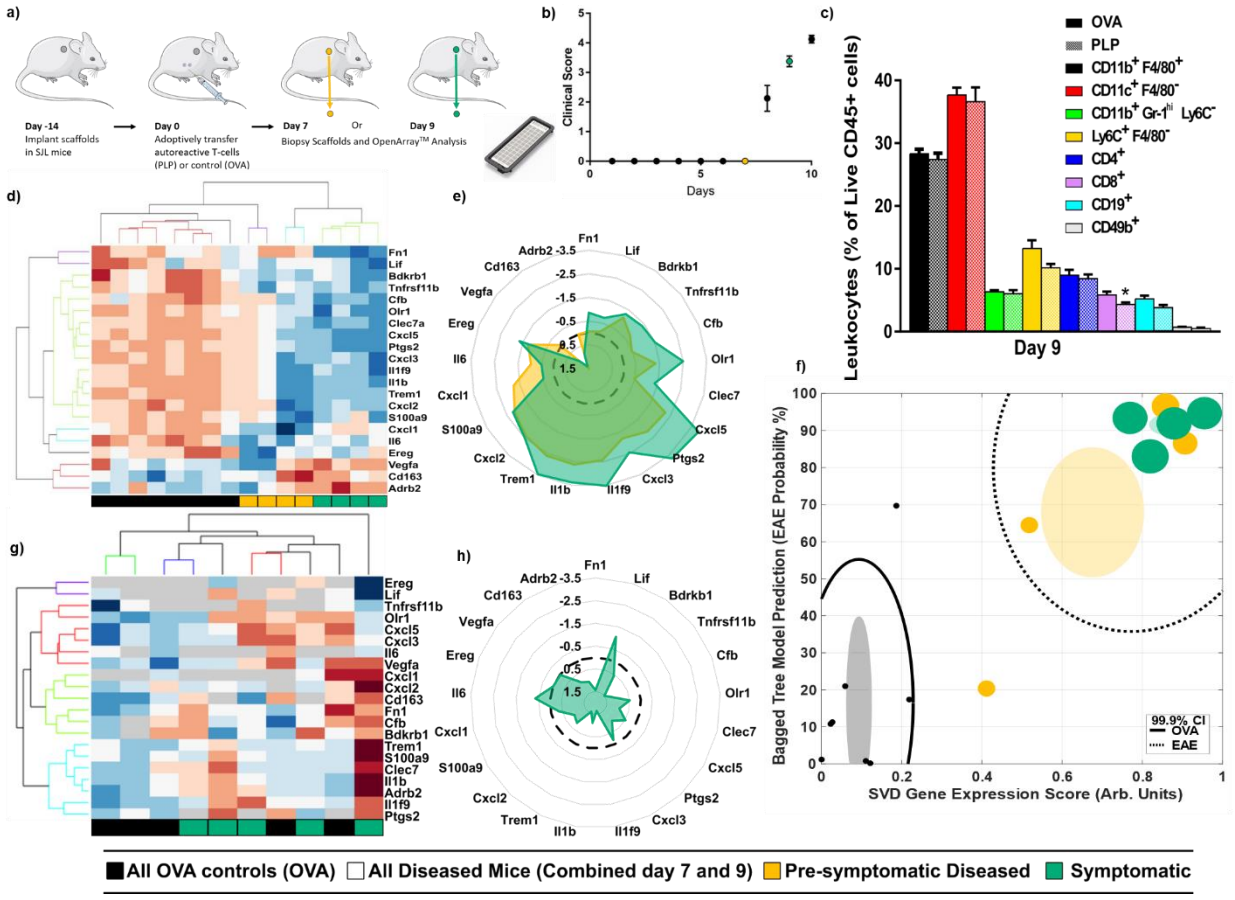


Figure 8.1 **IN gene expression changes enables scoring and segmenting of diseased and healthy during EAE onset.** a) SJL mice were implanted with PCL scaffolds 14 days prior to adoptive transfer of T cells reactive to either $PLP_{139-151}$ (EAE) or $OVA_{323-339}$ (control). INs were subsequently removed at an asymptomatic (7 day - yellow) or symptomatic (9 day - green) time point for analysis via high-throughput qPCR (OpenArray). b) Clinical scores of the mice at each time point demonstrate that no mice displayed symptoms of EAE at day 7 post-implantation, but mice were symptomatic by day 9. c) Flow cytometry for immune cell surface markers demonstrates minor differences between OVA and PLP at day 9. Data are presented as mean + SEM. Statistical analysis performed by student's t-test, asterisk indicates change from control (*p=0.038). n=7 (PLP) or 8 (OVA) mice. d) Heatmap and hierarchical clustering of 21 identified genes of interest, expression levels standardized by gene (n=8 per condition, 4 at day 7, 4 at day 9). e) Radar plot demonstrates altered gene expression (as log_2FC) for signature genes in pre-symptomatic (yellow) and symptomatic (green) when compared to time-

matched OVA controls (black), with a similar pattern at both time points. f) Plot of the bagged tree (BT) prediction score versus SVD indicates separation between groups. Black lines indicate 99.9% confidence intervals for pooled diseased or control mice. Filled ovals indicate mean (centroid) and standard error of the mean for each indicated group. Each point is from an individual mouse and increasing point size indicates sicker mice (as an average of the day of explant and day after). g) Heatmap and hierarchical clustering signature genes from blood (expression levels standardized by gene) indicate no clear clustering of controls from diseased samples, n=5 per condition. h) A radar plot of gene expression signature (as log_2FC) from blood during symptomatic onset clearly does not show the same patterns as that of the IN. Mouse cartoon from Servier image bank, https://servier.com/Powerpoint-image-bank.

.

We next applied computational approaches to develop a scoring system from the 21 gene signature that could distinguish healthy from diseased mice. Two approaches were employed: an unsupervised dimensionality reduction approach, singular value decomposition (SVD); and a supervised machine learning algorithm, bootstrap aggregated decision tree ensemble (Bagged Tree or BT).[456, 457] Results of the SVD and BT were similar and in both cases showed significant differences between control and EAE mice, regardless of time point (Fig 8.6). These data formed the basis for our trained model for disease classification used throughout the study. A clear separation was observed between INs isolated from diseased and healthy mice by plotting the two scores, (Fig 8.1f). The signature scores are predictive of disease onset, as the animals at day 7 had no symptoms, yet a high signature score. The score also predicts disease severity, as indicated by the area of each data point in Fig 8.1e. Subsequent studies confirmed that healthy mice receiving no adoptive transfers of T-cells, cluster with the OVA controls (Fig. 8.7). An in-house qPCR panel confirmed the OpenArray results and was employed throughout the study (Fig. 8.8).

Follow-up experiments utilized the active immunization model of EAE in SJL mice to demonstrate broader utility of the approach. When compared to mice receiving control immunizations (lacking the $PLP_{139-151}$ peptide) immunized EAE mice demonstrated 222 differentially expressed genes in INs (Fig. 8.11). Time points used for active disease induction were altered to match the slower disease course. The asymptomatic time point was still collected at day 7, but the symptomatic was shifted to day 13 to ensure disease development. Similarly, to

the passive disease induction, a signature of 25 genes was identified that clustered healthy (immunized with no exogenous peptide) control mice together (Fig. 8.12a). Interestingly, four genes overlapped between the signature for the passive and active disease induction, namely: CD163, Il1b, Il1f9, and S100a9. A similar computational scoring system was employed in the immunization model and demonstrated significant differences between control and EAE mice regardless of time point (Fig 8.12). Again a clear separation was observed between INs isolated from diseased and healthy mice by plotting the two scores, (Fig 8.12d).

Characterization of populations within immunological niches and blood

Cell populations within the INs were subsequently investigated using a panel of eight immune (CD45+) cells commonly involved in EAE[458]. Cells as a percentage of live CD45+ cells were measured, with substantial similarity between healthy and diseased mice, and only minor differences in CD4+ T cells at day 7 and 21 and CD8+ T cells at day 9 (Fig. 8.1c and 8.9). A similar experiment in the active immunization model of EAE examined cells in INs, blood, and spleens at day 4, 7, and 13 post-immunization. INs demonstrated substantial similarity between healthy and diseased mice at each time point, with the only significant difference a slight increase in $CD11b^{+}$ $F4/80^{+}$ cells at 4-days post-immunization (Fig. 8.13). Interestingly, the blood and spleen demonstrated increased $Ly6C^{+}$ $F4/80^{-}$ inflammatory monocytes in disease at day 13, but the INs do not. Collectively, the large changes in gene expression observed at the IN with disease were likely due to alterations in cell phenotypes within inflammatory microenvironments, rather than cell trafficking. The preponderance of CD45+ cells within the INs are innate immune cells, which are recruited to the CNS during EAE initiation and progression and contribute to damaging the tissue[459-462]. The IN may be sampling the phenotypic alterations of innate immune cells that extravasate into inflammatory environments during disease.

Because EAE and MS are CD4 T-cell driven diseases, we sought to examine T-cell subsets within the INs and compare that to those in spinal cords, inguinal lymph nodes, and spleens. At day 9 after adoptive transfer, we measured five t-cell subsets in each organ: Treg ($CD25^+$ $FoxP3^+$ $CD127^-$); Th2 ($IL\text{-}4^+$); Th1 (IL-17-, IFNγ+); Th1/17 (IL-17+, IFNγ+); and Th17 (IL-17+, IFNγ-). INs and spinal cords had similar numbers of T-cells whereas lymph nodes and spleens had an order of magnitude more. Interestingly, the only significant differences observed in these experiments were elevated levels of Th1 cells in INs and spinal cords of EAE mice when compared to OVA controls (Fig. 8.10). Clearly, implanted INs reflect immunological changes in diseased organs that are not reflected in lymphoid tissues.

Next, we tested the hypothesis that the phenotypic alterations captured by analysis of the engineered tissue represent local responses within a tissue that are not captured by analysis of blood. Over the last two decades, numerous studies have examined differential gene expression in the blood of patients with MS and healthy controls[463-467]. Although blood is a rich source of cells, most of these cells are not relevant to the immune responses occurring within the CNS, which may explain why the overall changes between diseased and healthy are modest and why at least half of differentially expressed genes have few ties to MS pathophysiology. The analysis of blood harvested from symptomatic EAE mice or OVA controls (d10) indicated that the mean expression of signature genes in the blood does not mirror that from the IN, suggesting that INs and blood provide distinct information (Fig 8.1h). Unsupervised hierarchical clustering was unable to cluster diseased from healthy mice based on blood data (Fig 8.1g); in fact, approximately 18% of samples did not have a valid reading from the blood, with some, such as Ereg, undetectable in most samples.

Immunological niches are dynamic with disease state and reflect effectiveness of therapy

We next investigated the capacity of the IN to monitor disease dynamics that are associated with remission and relapse. Disease was induced by adoptive transfer (cells reactive to $PLP_{139-151}$ or $OVA_{323-339}$) and allowed to progress towards symptomatic remission before IN biopsy at day 21, and relapse was initiated by a second adoptive transfer of cells on day 23 reactive to another immunodominant epitope that simulates epitope spreading during relapse[186] (either $PLP_{178-191}$ or $OVA_{257-264}$). The second IN was biopsied at day 28 (relapse) (schematic and clustergram, Fig 8.14). Samples isolated during remission exhibit INs with similar gene expression to those of control, illustrated by radar plots (Fig 8.2a). Interestingly, the cellular makeup of the niches during remission of disease is very similar to that during disease onset further implicating cell phenotypes as responsible for observed alterations in gene expression (Fig. 8.9 and Figure 8.1). During disease relapse, the genes exhibited similar expression to disease onset, suggesting a return to cell phenotypes associated with disease(Fig 8.2b). When analyzed via the trained model, INs from relapsing mice demonstrated high BT and SVD scores, whereas those from animals in remission were similar to control mice (data normalized to time matched controls) (Fig 8.2c-f). Importantly, the INs isolated from remitting mice demonstrated significantly reduced scores than mice experiencing symptomatic onset, but INs from relapsing mice did not. Gene expression at the IN changes during disease onset, reverts toward healthy during remission and indicates disease again during relapse. These findings demonstrate that alterations in disease and signature scores of the INs are dynamic and able to predict disease state.

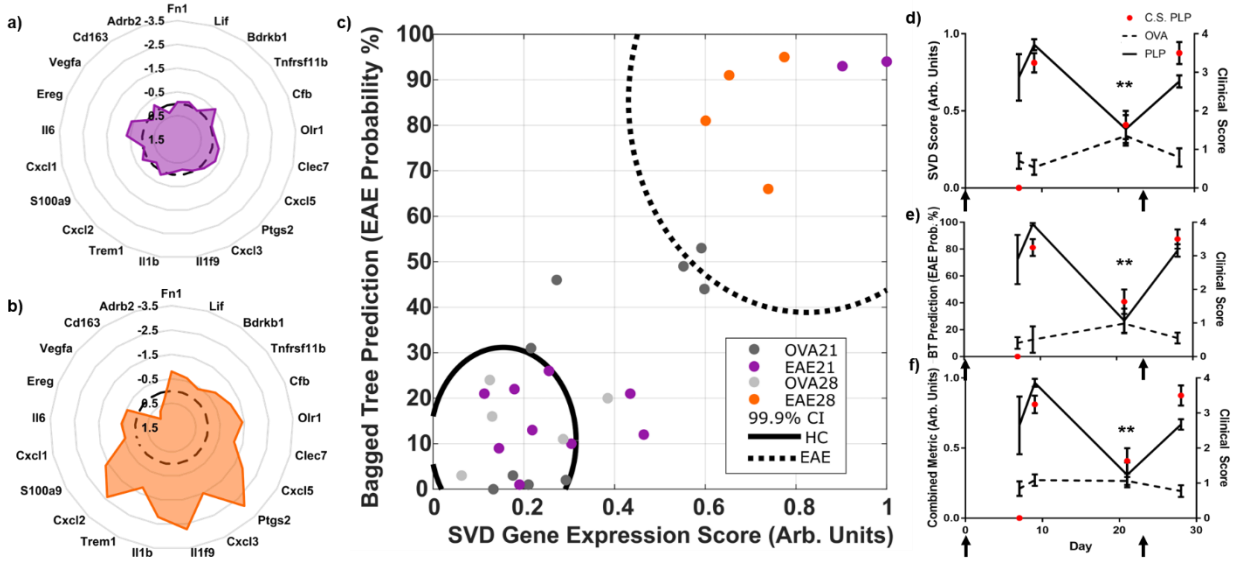


Figure 8.2 **Gene signature in IN effectively monitors disease dynamics and indicates relapse.** For relapse studies, INs were implanted subcutaneously two weeks before disease induction by adoptive transfer. INs were isolated at day 21 (remission) and day 28 (relapse). Mice received a second adoptive transfer of T cells (either $PLP_{178-191}$ or SIINFEKL) on day 23 to induce relapse (indicated on graphs with black arrows). a-b) Radar plots demonstrate similar gene expression (as log_2FC) for signature genes in remission (purple) when compared to time-matched controls (black) (a), but altered expression in relapse (orange) (b). c) Plot of BT score versus SVD indicates no separation between healthy and remitting mice, but separation between relapse and healthy. Black lines indicate historic (from disease onset data) 99.9% confidence intervals for pooled diseased or control mice. Each point indicates a single mouse. d-f) SVD score ($F(3,19) = 5.391$, $p=0.0074$) (d), BT score ($F(3,19) = 9.421$, $p=0.0005$) (e), and a combined metric ($F(3,19) = 6.504$, $p=0.0033$) (f) plotted versus time (left y-axis, black lines) and corresponding clinical scores at each time point (right axis, red points) indicates only the remission t.p. (d21) is significantly different from peak disease (d9). Data are presented as mean ± SEM. A one-way ANOVA was used to compare scores over time for EAE mice. A Bonferroni-corrected post-hoc multiple comparisons test was used to compare each time point to symptomatic disease onset (d9). (n=9 OVA at d21, n=5 OVA at d28, n= 11 PLP at d21, n=4 PLP at d28).

ROC curves were plotted to determine the diagnostic ability of the system (Fig. 8.17) and demonstrated an AUC of 0.98-1 (depending on metric: SVD, BT, or combined) (95% CI 0.94-1.03) for the training set, and an AUC of 0.81-0.90 95% CI 0.59-1.06) for distinguishing remission and relapse samples, validating the diagnostic efficacy of the signature score derived from INs in diagnosing and prognosing EAE. Collectively, this system offers the opportunity for a patient to be alerted of impending relapse, which would enable pharmacologic intervention to prevent or reduce severity of relapses.

We sought to test the ability of the implantable INs to monitor the response to therapy. We have previously reported nanoparticles to induce tolerance in these and similar models, which were

employed here as a model treatment[307, 308, 330]. Similarly to previous studies, IN-implanted mice received an adoptive transfer of T cells, yet were also injected intravenously with 2.5 mg of antigen encapsulating PLG nanoparticles 2 days post-transfer. Three groups were used: a control group (OVA reactive T-cells and PLP particles), an effective treatment group (PLP reactive T-cells with PLP particles), and an ineffective treatment group (PLP reactive T-cells and OVA particles). INs were biopsied on day 9 and analyzed for the gene signature, which indicated that the effective treatment group had similar signature score and clinical score as the control group. However, the ineffective treatment group had significantly higher signature and clinical scores relative to the control (Fig 8.3a,b and 8.15). The pattern of gene expression in the mice receiving ineffective treatment was similar to the untreated mice during disease onset. To estimate the diagnostic efficacy for treatment monitoring, ROC curves of SVD, BT, and a combined metric were created with AUC values of 0.97-1 (95% CI 0.89-1.06), suggesting a highly effective treatment monitoring tool (Fig. 8.17).

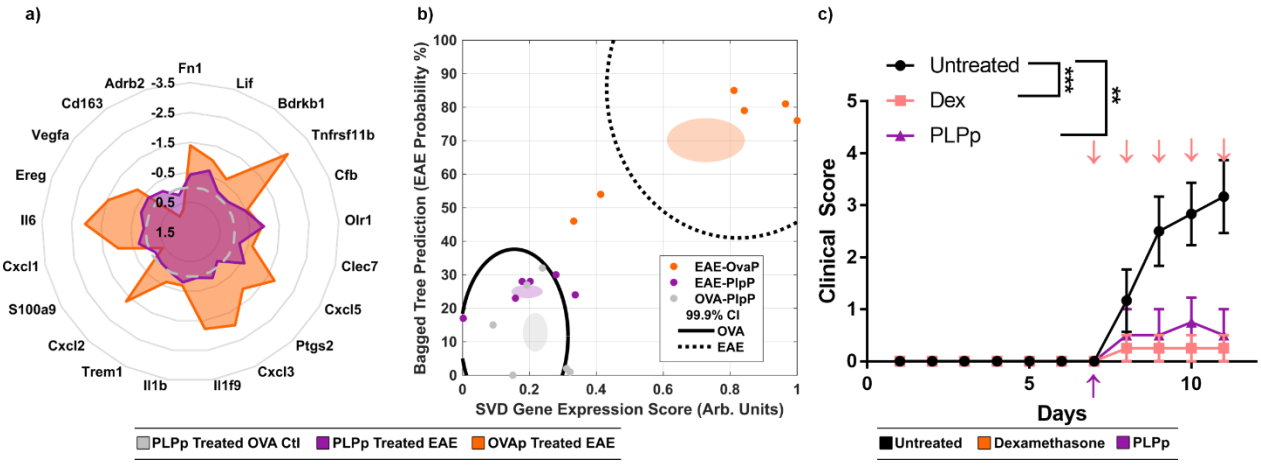


Figure 8.3 **Gene signatures indicate response to therapy and enable proactive treatment to prevent disease.** To test the ability of the IN to indicate response to therapy, 2.5 mg PLG nanoparticles encapsulating either PLP or OVA peptides were administered I.V. two days after adoptive transfer and INs were isolated on day 9 (disease onset). a) Radar plot demonstrating similar gene expression (as log_2FC) for signature genes in EAE mice treated with PLP loaded particles (purple) when compared to time-matched controls treated with particles (grey), but altered expression in EAE mice treated with control (OVA) particles (orange). b) Plot of BT score versus SVD indicates no separation between healthy mice treated with control particles and EAE mice treated with PLP particles (responders to treatment), but a clear separation in EAE mice treated with OVA particles (nonresponders / control treatment). Black lines indicate historic (from disease onset data) 99.9% confidence intervals for pooled diseased or control mice. Each point indicates a single mouse. Another experiment

was designed to test if early detection of disease by INs could enable proactive treatment to prevent the development of EAE. Seven days post-transfer INs were explanted and mice proactively treated with either an I.V. injection of 2.5 mg PLG nanoparticles encapsulating $PLP_{139-151}$ or daily I.P. injections of 5 mg/kg dexamethasone. c) Mean clinical scores of the mice at each time point demonstrate that both pre-emptive treatments reduce disease severity when compared to an untreated control. A two-way ANOVA was used to compare scores ($F(2, 11) = 5.422$, $p=0.0230$). A Dunnett's multiple comparisons test was used to compare each treatment to the untreated control at each time point. (n=6 untreated and 4 treated, $^{**}p\leq0.0012$ and $^{***}p\leq0.0002$ on days 9-11). Pink arrows indicate dexamethasone administration and purple indicate particle administration.

Preemptive intervention enabled by early detection abrogates disease.

Finally, we sought to test the hypothesis that pre-emptive intervention enabled by the INs ability to predict disease onset prior to clinical symptoms would improve outcomes. We induced EAE and biopsied INs for analysis seven days post-transfer, before delivering therapies: either a single i.v. dose of 2.5 mg of antigen encapsulating PLG nanoparticles (described below) or a daily i.p. injection of 5 mg/kg dexamethasone. In either case, the IN alerted to immune dysfunction that differed from healthy and enabled pre-emptive interventions to reduce clinical symptoms and prevent disease onset (Fig 8.3c and 8.16).

Discussion

Autoimmune disease prevalence is on the rise, and although numerous therapies targeting autoimmune conditions have been developed, autoimmunity presents a challenge, because it is typically not diagnosed until substantial damage occurs. We developed an implantable IN that forms a vascularized inflammatory tissue that is dynamic with the status of the immune system. This finding is well supported by reports demonstrating that inflammation surrounding implants is altered by systemic changes associated with various physiological and pathological states, including diabetes, obesity, cancer, and advanced age[468-471]. This implantable biopsy site thus harnesses the host immune system to identify immunological changes within innate immune cells of tissues, which contribute to disease initiation and progression.

Because the INs are predominantly composed of innate immune cells as opposed to lymphoid tissues which are predominantly adaptive immune cells, the INs favor investigations into innate

immune aberrations within tissues during disease. Innate immune cells exhibit tremendous alterations during EAE and MS and further investigations into these mechanisms may be fruitful in both understanding the basic science and identifying therapeutic targets. For example, inflammatory monocytes are known to expand before disease onset and prior to relapse, and CNS-resident myeloid dendritic cells play a large role in epitope spreading[461, 472]. The IN contains large numbers of both inflammatory monocytes and DCs and could possibly be used as a tool to better understand the roles of these cell subsets in EAE and MS pathophysiology. Nevertheless, one must acknowledge the limitation that tissue-resident cells of the CNS, are absent from the IN and thus, interesting findings should be confirmed in the CNS.

We identified 21 molecular targets that are differentially expressed at the IN in diseased animals that represent onset or relapse of EAE or MS, enabling interventions to prevent disease development before damage occurs. One of these 21 targets, Trem1, has not previously been associated with EAE or MS, demonstrating the feasibility of harnessing the IN as a tool for preclinical investigations into the mechanisms of disease. A recent conference proceeding supports Trem1 as a biomarker and suggests that Trem1 expression in the CNS indicates development of EAE before symptomatic onset. Furthermore, the site of the IN is readily accessible and easy to biopsy for analysis. In both human and preclinical models it could provide an attainable site that can be accessed without detrimental effect to native tissue structures, enabling longitudinal investigations in a single host. Interestingly, studies investigating T-cell phenotyping in the IN, spinal cord, lymph nodes, and spleen demonstrated that only the IN faithfully recapitulated upregulation of Th1 cells in the spinal cord during EAE onset, highlighting the potential utility of the IN over endogenous lymphoid tissues. Future work may examine engineering these sites to more closely mirror CNS tissues both in architecture and in molecular content. Because these sites

are synthetic, materials engineering approaches would enable facile modifications to study the role of various factors in disease initiation.

Molecular details gleaned from biopsy of the IN enables pre-emptive treatment, a strategy which could be transformative in treating RRMS patients before relapses occur, with the potential to prevent disease altogether. Furthermore, these molecular insights can help determine response to therapy. At present, MS treatment is typically staged and iterative, involving changing treatments until a patient responds. The IN could be a tool to help stratify effective vs ineffective therapies before a patient relapses (the typical indicator on non-response to therapy). In addition to aiding in patient monitoring, the IN is a tool that can provide molecular information on the dysfunctional immune cells within inflamed tissues, and may enable a precision medicine approach for improved subtyping of MS and provide indicators for factors associated with progression[473]. Multiple pathological features can underpin MS in different patients, yet, at present, identifying the sub-types can only occur post-mortem. With this IN, molecular information about responses within the tissue could be used to screen individual patients and correlate responses to disease outcomes in addition to therapeutic responses, to enhance prognosis. In contrast to blood glucose monitors for Type 1 Diabetes that monitor treatment of established disease, this immunological niche sets the stage for an implantable molecular sensor that continuously reports on the functional status of the immune system to inform disease onset, prognosis, and treatment monitoring.

Methods

Scaffold Fabrication and Subcutaneous implantation

Microporous scaffolds were prepared in the same manner as previously described.[458, 474] All procedures were performed in accordance with the regulations approved by the Animal Care and

Use Committee of the University of Michigan. Female SJL/J mice were purchased from Envigo at an age of six weeks. Mice were anesthetized with isofluorane, before subcutaneous implantation as previous described[475, 476]. Mice received subcutaneous injections of carprofen (5 mg/kg) immediately before surgery and 24 hours after surgery.

Disease Induction

Mice were immunized as described previously.[474, 477] Briefly, an emulsion was prepared containing 1:1 complete Freund's adjuvant (incomplete Freund's adjuvant [Fisher] with 4 mg/mL heat killed M. tuberculosis H37 Ra [Fisher]) : PBS with 2 mg/mL peptide ($PLP_{139-151}$ or $OVA_{323-339}$ [Genscript]). A total volume of 100 µL CFA with peptide was injected subcutaneously at three sites within each mouse. For studies using active induction of EAE the day of immunization was considered as day 0 and mice were monitored for disease symptoms after this point.

For passive, adoptive transfer disease induction, donor mice were immunized and 10 days later, donor mice were euthanized and spleens and lymph nodes (inguinal, axiallary, and brachial) were harvested before processing into a single cell suspension. Cells were cultured in RPMI with 10% FBS, 2 mM L-glutamine, 100 IU/mL penicillin, 0.1 mg/mL streptomycin, 1x non-essential amino acids solution, 1 mM sodium pyruvate, 10 mM HEPES, and 20 µg/mL peptide antigen. After three days of culture non-adherent cells were harvested, counted, and injected i.p. into recipient mice. For most studies, 30 million cells were injected per mouse, but this inevitably led to some mice becoming moribund, so for remission studies, only 15 million cells were injected. To induce relapse, the same procedure was followed for preparation of cells reactive to either $PLP_{178-191}$ or SIINFEKL, and 25 million cells were injected i.p. After induction of disease, severity was monitored on a 0-5 scale as previously described[330]: 0 = no disease, 1 = hindlimb weakness or

limp tail, 2 = hindlimb weakness and limp tail, 3 = partial hindlimb paralysis, 4 = total hindlimb paralysis, 5 = moribund.

Tissue isolation

To harvest biopsies of PCL implants for analysis, mice were anesthetized with isoflurane before an incision was made over the surface of the implant. The implant and any adherent encapsulating tissue were pulled through the incision and excised and the incision was closed with sutures. Tissues for RNA were flash frozen in isopentane on dry ice and stored at -80 °C until analysis. Tissues for flow cytometry were placed into PBS and stored on ice, and tissues for histology were immediately placed in 4% paraformaldehyde. For blood isolation, mice were anesthetized before intracardiac blood draw with EDTA. RBCs were lysed in an ACK solution (Gibco) before washing in PBS. Pellets were resuspended in Trizol and stored at -80 °C until analysis.

RNA isolation and cDNA synthesis

RNA was isolated with the Directzol RNA Miniprep kit (Zymo Research) following manufacturer's instructions. Samples to be used for OpenArray analysis were also assessed for RNA integrity (RIN) with an RNA fragment analysis with an RNA 6000 Nano Kit (Agilent Technologies), and all samples had a RIN>8.

cDNA synthesis was performed with the SuperScript™ VILO™ cDNA Synthesis Kit (ThermoFisher Scientific) according to manufacturers instructions. RT was performed with RNA concentrations of 200 ng/µL. Because RNA isolates from blood typically did not achieve this concentration, an RNA clean-up kit was used to increase concentration and purity according to manufacturer instructions (RNA Clean & Concentrator-5, Zymo Research).

OpenArray High-Throughput RT-qPCR

For high-throughput gene expression analysis, OpenArray panels focused on mouse inflammatory pathways were used. Panels and accompanying reagents were purchased from ThermoFisher (Applied Biosystems™ TaqMan™ OA Mouse Inflammation Panel, Cat. No. 4475393). The panels contained 632 validated genes that have known roles in inflammation as well as 16 endogenous controls (housekeeping genes). cDNA was prepared as described above and OA analysis and quality control was performed on a fee-for-service basis by the UM DNA Sequencing core. The core uses a robotic OA AccuFill system and the QuantStudio 12k Flex RT-PCR system (ThermoFisher Scientific). Analysis was performed as previously described using this system.[26] For OpenArray of adoptive transfer samples a total of n=8 samples per condition (diseased or healthy) were analyzed with 4 from each time point (day 7 or 9). Each sample was from an independent mouse and samples alternated between healthy and diseased in their placement on the chip to minimize spatial bias. For immunization studies, two time points were used for OpenArray, day 7 or 13. A total of n=8 immunized control (4 from each time point) and n=16 diseased (8 from each time point) were used.

Selection of Genes of Interest

Samples were analyzed first to remove genes that did not have readable data in more than one of the four mice in each condition. Next, any samples that were missing data were filled with the median for the overall dataset. This was required because downstream analysis requires complete matrices. Ultimately, 500 genes of the 648 were used for this study. Each of the 16 reference genes were analyzed via the NormFinder algorithm to select the three most stable reference genes: Hmbs, Polr2a, and Ubc. ΔC_q values were calculated for each gene from the average of the reference genes for that sample. Next, fold change (FC), p-values, and prediction scores derived from elastic net

regularization (MATLAB's lasso function, $\alpha = 0.01$, leave one out cross-validation) were calculated for each gene using time-matched controls.[33] Box-plots show $\log_2$FC, centered on the median of the time matched healthy controls. All identified 21 genes of interest were identified as predictors (elastic net scores>0), had FC>1.5, and $p<0.05$. Additionally, we attempted to include genes that increased and decreased during disease to make the model more robust and ease the eventual construction of a sensor.

Once these genes of interest were identified, all other studies were conducted via RT-qPCR analysis in 384 well plates. The same TaqMan probes used in the OpenArray chips were ordered from ThermoFisher Scientific and samples were alternated between healthy and diseased in their placement on the plate. TaqMan Gene Expression Mastermix was used and a final volume of 9 µL was used for each well of the 384 well plate. RT-qPCR was performed on the QuantStudio ViiA 7 system and C_q values determined by the accompanying software. Non-detects were left blank for any statistical analyses, but were filled with the median of all samples for SVD (because it requires complete matrices). Samples from the original OpenArray data were run on every 384 well plate to allow for a correction factor to be applied to account for variability.

Gene Signature Scores and analysis

Firstly, unsupervised hierarchical clustering analysis was performed using MATLAB's clustergram tool which plots dendrograms to indicate samples and genes that cluster together. Ultimately, genes of interest were identified, and computational approaches were used to create two metrics for evaluating whether mice were sick or healthy. Singular value decomposition (SVD) using MATLAB's svds function was applied to create a gene signature score using an unsupervised technique. Next, a supervised machine learning approach bootstrap aggregated

decision tree ensemble (Bagged Tree) was trained to classify samples as healthy or diseased. We employed MATLAB's fitcensemble function with the Bag method.

Histology

For histological analysis, samples were excised and stored immediately in 4%PFA overnight to fix the tissue before being bisected and transferred to the University of Michigan *In Vivo* Animal Core for sectioning and staining with hematoxylin and eosin using standard protocols. Images were taken at 20x within the thickness of the IN.

Flow cytometry

INs from adoptively transferred animals were prepared for flow cytometry using previously described protocols.[9,34] Briefly, samples were minced with a scalpel and incubated for 20 minutes in Liberase TL (Roche) at 37 °C. INs were then mashed through a 70 μm filter which was washed extensively with FACS buffer: PBS (Life Technologies) with 0.5% Bovine Serum Albumin (Sigma Aldrich) and 2 mM EDTA (Gibco). Cells were equally split into two tubes to enable staining and analysis of innate and adaptive immune cells from the same IN and then blocked with anti-CD16/32 (1:50, clone 93, eBioscience). Each tube was stained with Live/Dead Fixable Red (Life Technologies) and Alexa Fluor® 700 anti-CD45 (1:125, clone 30-F11, Biolegend). The adaptive immune panel was also stained with: FITC anti-CD8 (1:25, clone 53-6.7, Biolegend), Pacific Blue™ anti-CD19 (1:100, clone 6D5, Biolegend), PE-Cy7 anti-CD49b (1:30, clone DX5, Biolegend), and V500 anti-CD4 (1:100, clone RM4-5, Biolegend). The innate immune panel was also stained with: APC anti-CD11c (1:80, clone N418, Biolegend), FITC anti-Ly6C (1:100, clone HK.14, Biolegend), Pacific Blue™ anti- Ly-6G/Ly-6C (Gr-1) (1:70, clone RB6-8C5, Biolegend), PE-Cy7 anti-F4/80 (1:80, clone BM8, Biolegend), and V500 anti-CD11b (1:100, clone M1/70,

BD Biosciences). Samples were analyzed on a Cytoflex Cell Analyzer, and all single-color controls and FMOs were used to aid with gating and compensation (Fig 8.18-8.19)

INs, blood, and spleens from immunized mice were analyzed similarly to above. Blood was collected via cardiac puncture, and a single cell splenocyte homogenate was obtained by mashing through a 70 µm filter which was washed extensively with FACS buffer. Red blood cells were then lysed with ACK lysis buffer (Gibco). The panel above was used for analysis, except no anti-CD49b antibody was used.

For analysis of T-cell subsets, spinal cords and INs were harvested and processed by mincing and liberase digestion as described above. Lymph nodes and spleens were mashed through a 70 µm filter. Samples were divided for analysis with two staining panels: Treg and Th panels. Both panels were stained with Live/Dead Fixable Violet (Life Technologies), BV510 anti-CD3 (1:80, clone 17A2, Biolegend), and FITC anti-CD4 (1:125, clone RM4-5, Biolegend). The Treg panel added PE anti-CD25 (1:80, clone PC61, Biolegend), APC anti-FoxP3 (1:8, FJK-16s , eBioscience), and PE-Cy7 anti-CD127 (1:80, clone A7R34, Biolegend). The Th panel added PE anti-IL-17a (1:16, clone TC11-18H10.1, Biolegend), APC anti-IL-4 (1:16, clone 11B11, Biolegend), and PE-Cy7 anti-IFNγ (1:16, clone XMG1.2 , Biolegend). After processing and staining for surface markers as described above, cells were fixed and permeabilized using the eBioscience Foxp3 / Transcription Factor Staining Buffer Set according to manufacturer instructions, before intracellular stains. For gating scheme see Fig 8.20-8.21.

Nanoparticle Fabrication and Administration

Peptide encapsulating nanoparticles were fabricated with the double emulsion method as previously described.[167]. Briefly, 150 µL of antigen dissolved in PBS (50 mg/mL $PLP_{139-151}$ or $OVA_{323-339}$ [Genscript]) was added to 2 mL of 20% w/v poly(lactide-co-glycolide) (inherent

viscosity: 0.17dL/g, Lactel). This solution was sonicated for 30 seconds before the addition of 10 mL of 1% w/v poly(ethylene-alt-maleic anhydride) in water. This was again sonicated to form the double emulsion which was poured into 200 mL of 0.5% w/v poly(ethylene-alt-maleic anhydride) and stirred overnight. Particles were washed extensively before lyophilization in cryoprotectant. The size and zeta potential of the acNPs were determined by dynamic light scattering (DLS) by mixing 10 mL of a 25 mg/mL particle solution into 990 mL of MilliQ water using a Malvern Zetasizer ZSP.

For treatment studies, mice were implanted with INs and 14 days later adoptively transferred with 30 million T cells. Two days, post-transfer, mice received a single bolus i.v. injection of 2.5 mg $PLP_{139-151}$ or $OVA_{323-339}$ loaded nanoparticles. Mice were monitored daily for symptoms of EAE, and INs were removed on day 9.

Statistics

All statistics were calculated with MATLAB or GraphPad Prism software. When comparing pooled control vs diseased mice, two-way ANOVA was used to determine significance. A post-hoc multiple comparisons with a Bonferroni correction was then used to compare each time point to its time-matched control. When comparing the scores of EAE mice over time a one-way ANOVA with a Bonferroni corrected post-hoc multiple comparisons test was used. Additionally, the same method was used to compare the three particle treated groups at a single time point. Student's t-tests were used to analyze flow cytometry data as comparisons were made between healthy and diseases within each time point (no comparisons over time). ROC curves were plotted and analyzed in GraphPad. Box plots show the median, 25th-75th percentiles and most extreme data points not considered outliers (outliers are indicated by red +).

Data Availability:

Data supporting the findings presented here are available within the paper and in the Supporting Information.

Supplemental Figures

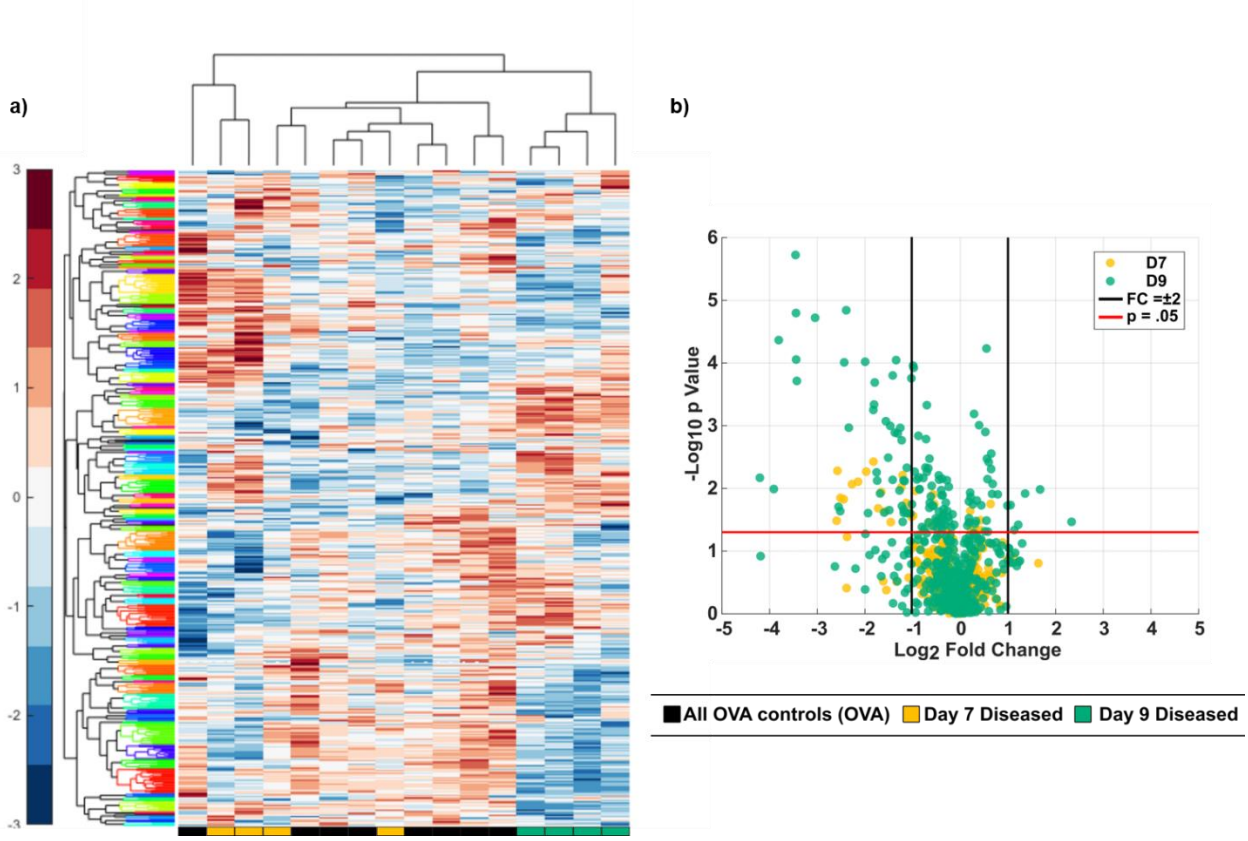


Figure 8.4 Gene expression from entire OpenArray Panel. a) Heatmap and hierarchical clustering of gene expression from entire OpenArray panel (n=8 per condition, 4 at day 7, 4 at day 9). b) Volcano plot of OpenArray data. Black lines indicate a fold change of ±2 and red line indicates p = 0.05. In total, 130 genes are significantly differentially expressed at the INs between healthy and diseased mice.

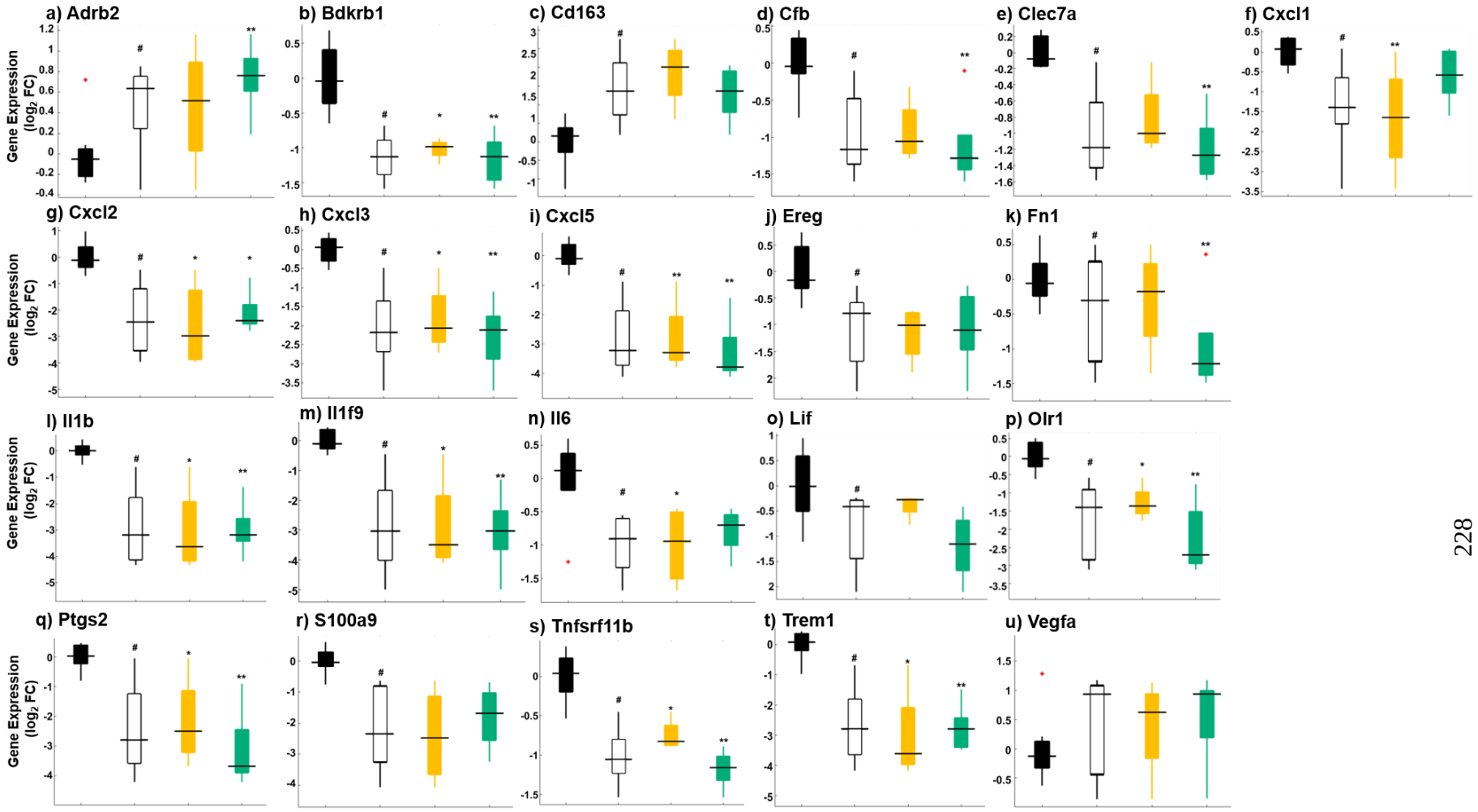


Figure 8.5 Gene expression from OpenArray for 21 genes in gene signature. Log_2 FC is displayed in boxplots with 25-75th percentiles and range of data for each group displayed (outliers indicated with red +). Black and white boxes demonstrate pooled OVA controls and diseased mice, while yellow and green boxes represent the log_2 (fold change) at days 7 and 9, respectively. Two-way ANOVA was used to compare pooled OVA controls vs diseased mice (# $p<0.05$). A Bonferroni-corrected post-hoc multiple comparisons test was used to compare diseased to time matched controls (*$p<0.05$, **$p<0.005$).

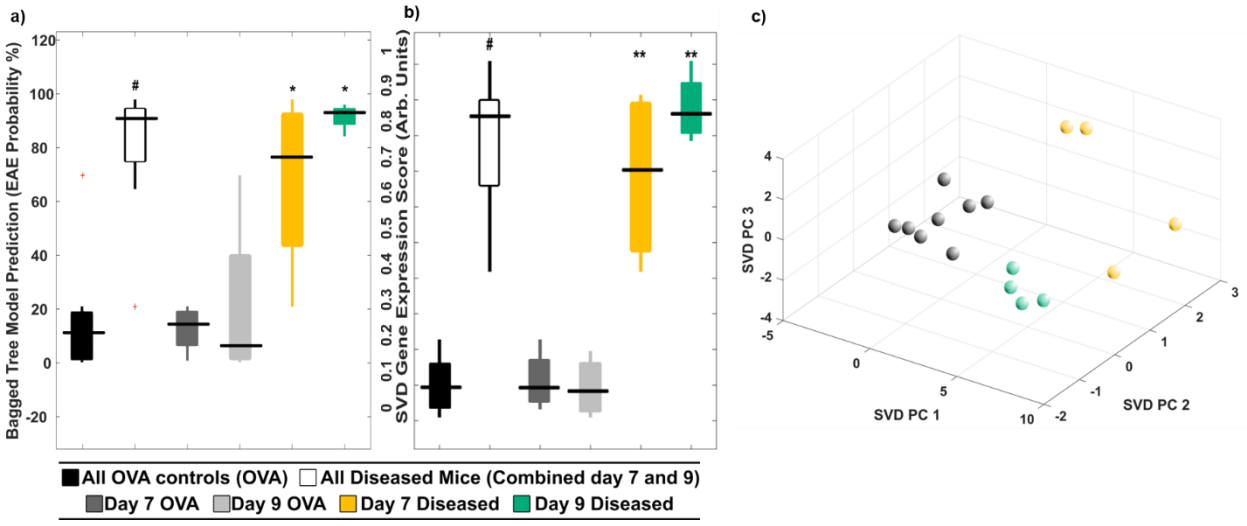


Figure 8.6 Development of SVD and BT model enable classification of mice as healthy or diseased. a) Gene expression data was used to train a bootstrap aggregated (bagged) decision tree ensemble to predict the probability that any given mouse was diseased ($F(1,12) = 26.84$, #p=0.0002) b) An unsupervised dimensionality reduction technique (singular value decomposition – SVD) was used to reduce the gene expression of the 21-gene signature to a score ($F(1,12) = 85.69$, # p = 8.19e-07). Two-way ANOVA was used to compare pooled OVA controls vs diseased mice. A Bonferroni-corrected post-hoc multiple comparisons test was used to compare diseased to time matched controls (*p<0.05, **p<0.0005). c) Three principle components of SVD plotted in a 3D scatter plot. The single SVD scores were computed by calculating the Euclidean distance from the OVA control centroid to any given point (each point represents an independent mouse).

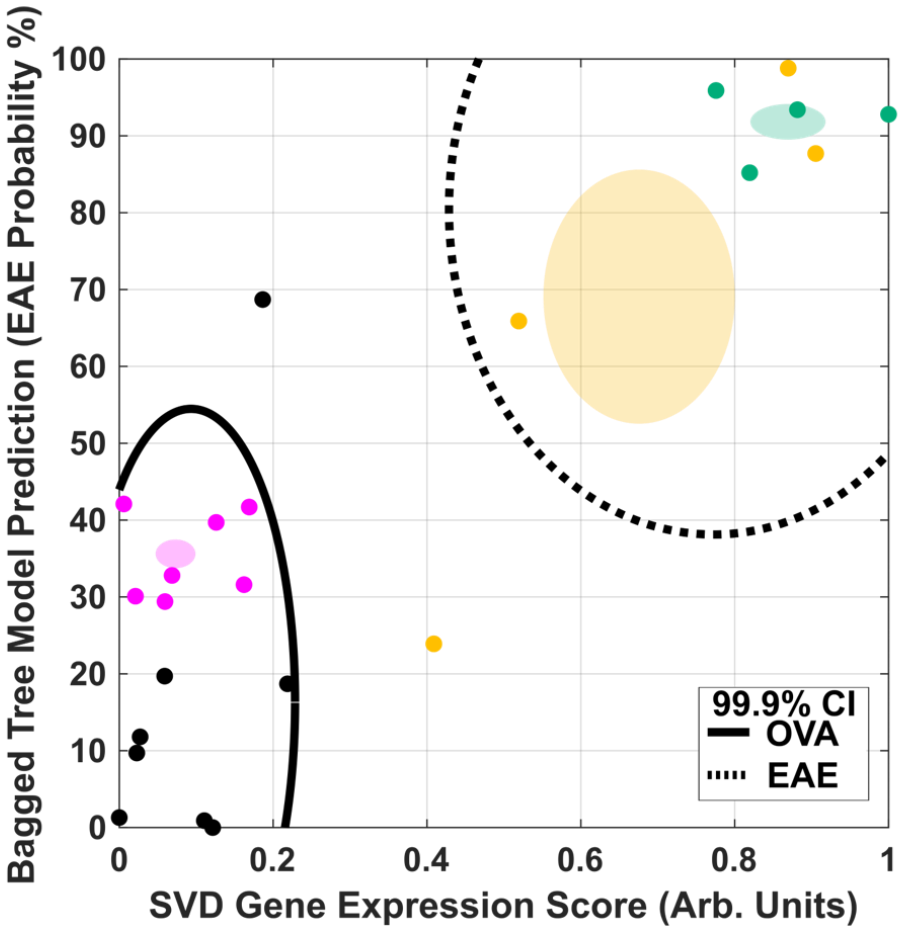


Figure 8.7 INs isolated from healthy mice have similar scores to OVA controls. Plot of the bagged tree (BT) prediction score versus SVD in which pink points represent INs isolated from healthy mice (no adoptively transferred cells), black represent mice that received OVA adoptive transfers and yellow and green PLP adoptive transfers. Black lines indicate 99.9% confidence intervals for pooled diseased or control mice. Filled ovals indicate mean (centroid) and standard error of the mean for each indicated group. Clearly, the signature scores for healthy mice and OVA controls are similar.

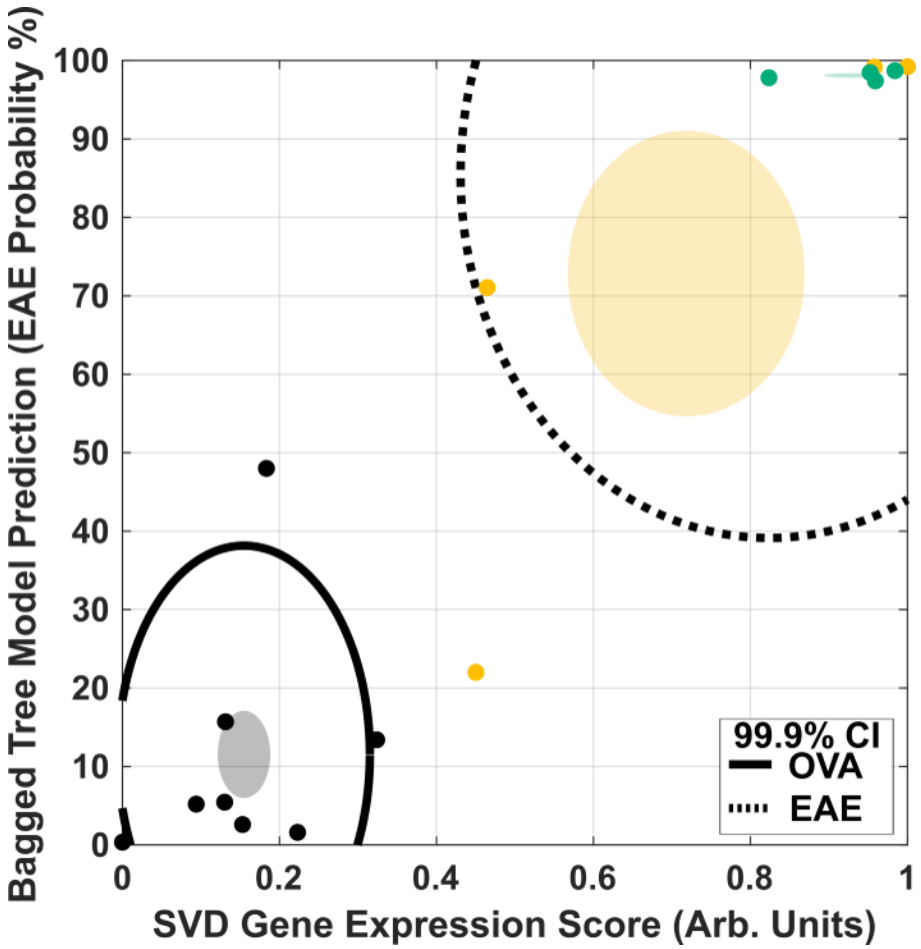


Figure 8.8 Gene expression analysis by qPCR confirms OpenArray findings. The same samples examined via OpenArray were analyzed in-house by qPCR in 384 well plates and signature scores plotted as bagged tree (BT) versus SVD. Black lines indicate 99.9% confidence intervals for pooled diseased or control mice. Filled ovals indicate mean (centroid) and standard error of the mean for each indicated group. Clearly, the results via qPCR indicate similar findings to OpenArray.

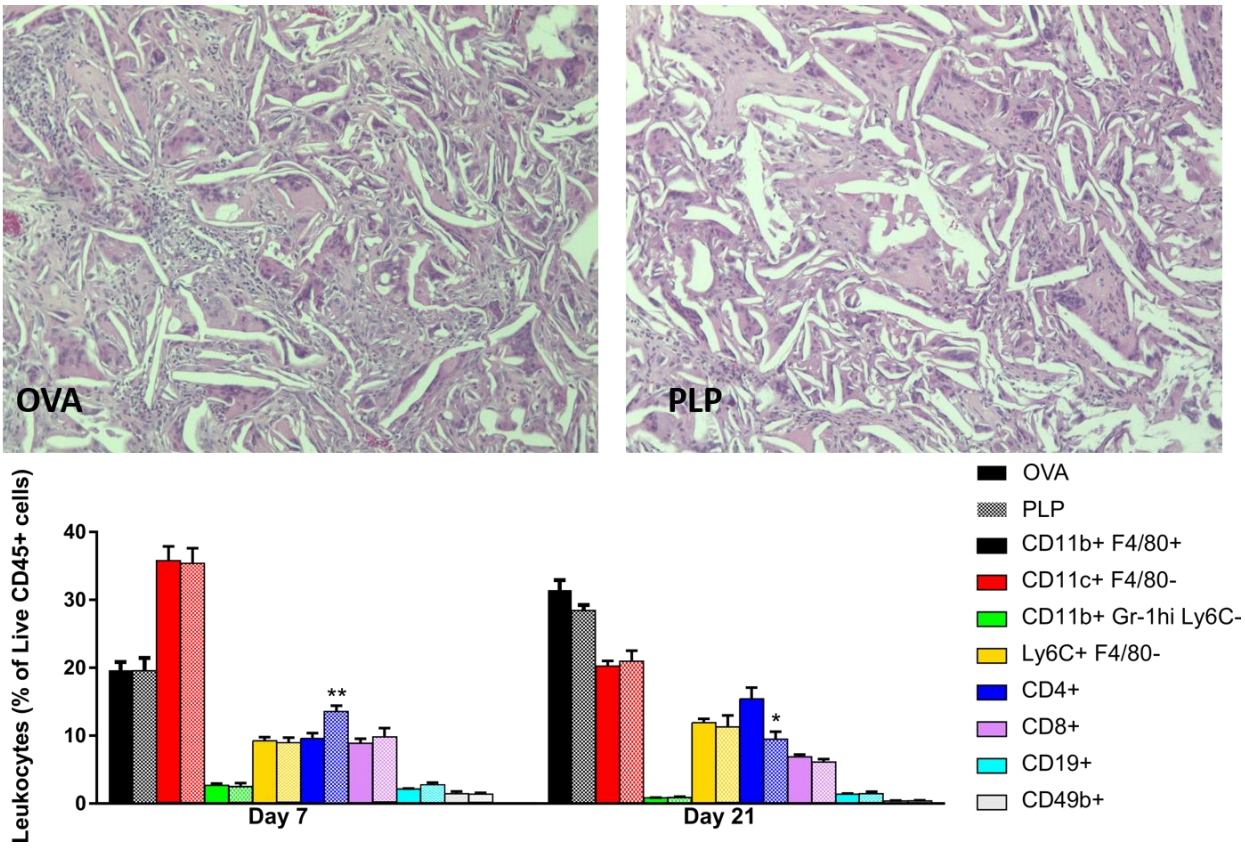


Figure 8.9 Evaluation of immune cells within INs. a) H&E stains indicate a normal FBR for a porous material in both OVA and PLP conditions demonstrating immune infiltrate, foreign body giant cell (FBGC) formation, and tissue ingrowth. b) Flow cytometry for immune cell surface markers demonstrates minor differences between OVA and PLP, but little change in the cell populations within the INs over time. Data are presented as mean + SEM. Statistical analysis performed by student's t-test at individual time points, asterisks indicate change from control (*$p<0.05$, **$p<0.01$). n=7-8 mice per time point.

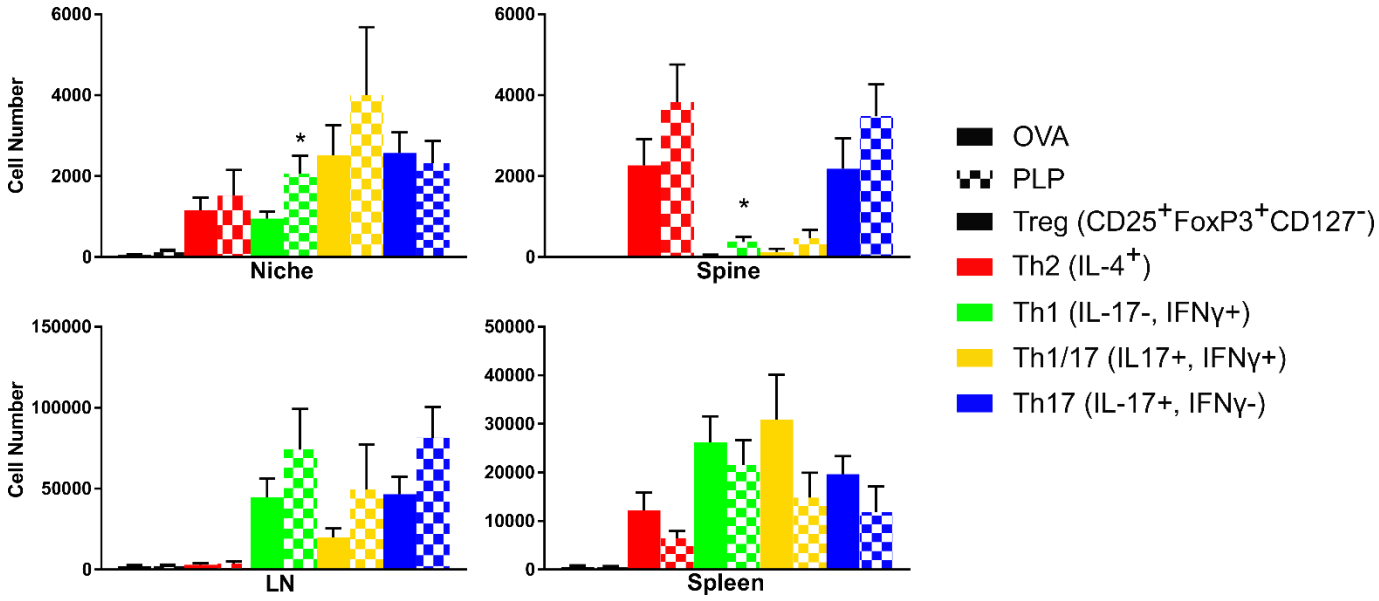


Figure 8.10 Evaluation of T-cell subsets in adoptive transfer model of EAE. Flow cytometry at day 9 post-adoptive transfer demonstrates T-cell subsets present in IN, spinal cord, lymph nodes, and spleens. Data are presented as mean + SEM. Only Th1 (Il-17^{-}, IFN^{+}) cells in scaffolds and spinal cords were significantly increased at this time point. Statistical analysis performed by student's t-test, asterisks indicate change from control for that organ (*$p<0.05$), (n=8).

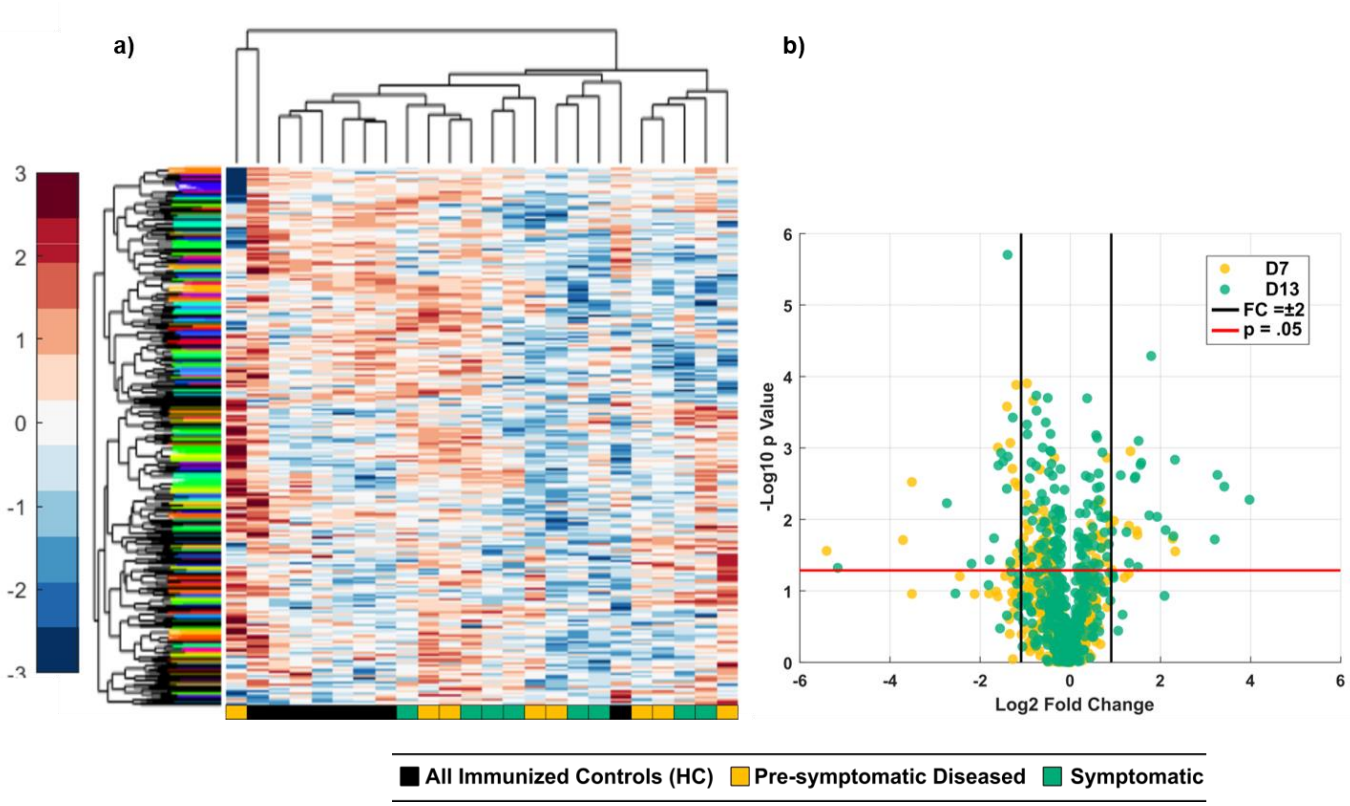


Figure 8.11 Gene expression from entire OpenArray Panel for immunized mice. a) Heatmap and hierarchical clustering of gene expression from entire OpenArray panel (n=8 immunized control [4 at day 7, 4 at day 13] and n= 8 diseased [at each time point]). b) Volcano plot of OpenArray data. Black lines indicate a fold change of ±2 and red line indicates p = 0.05. In total, 222 genes are significantly differentially expressed at the INs between healthy and diseased mice.

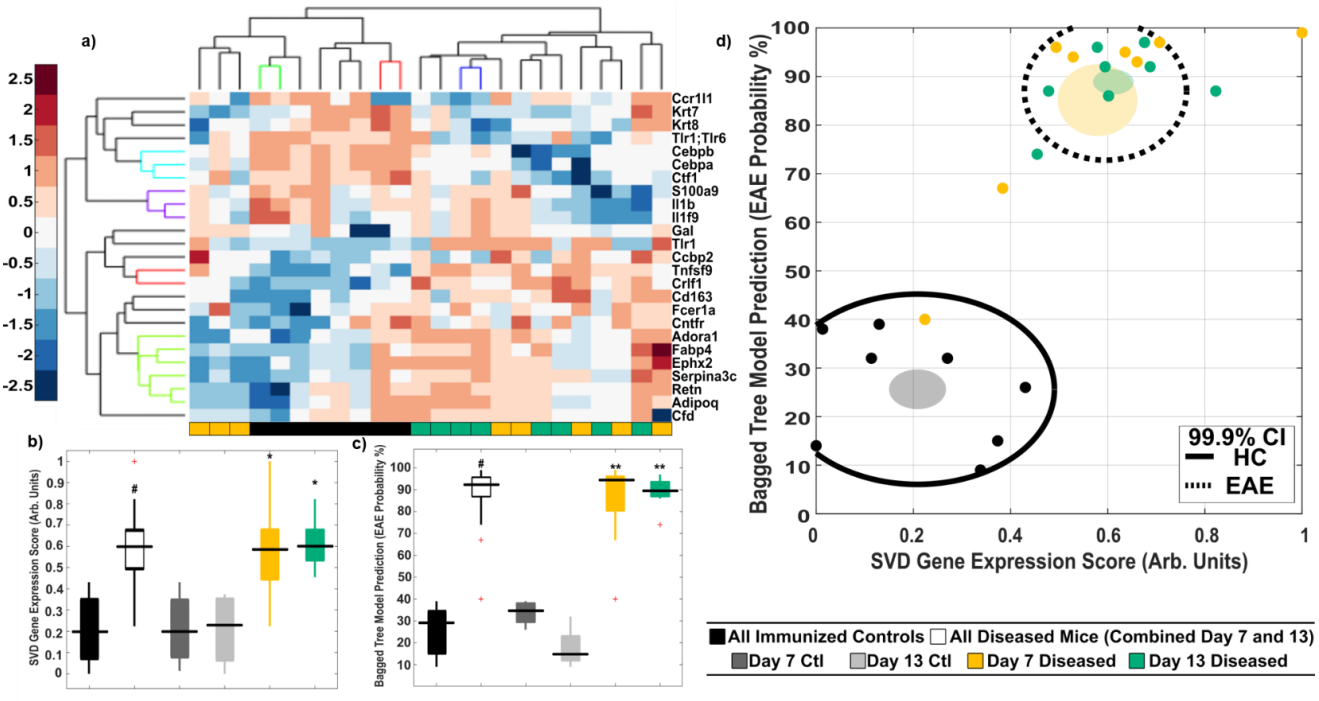


Figure 8.12 IN gene expression changes enables scoring and segmenting of diseased and healthy in an immunization model of EAE. a) Heatmap and hierarchical clustering of 25 identified genes of interest, expression levels standardized by gene (n=8 immunized control [4 at day 7, 4 at day 13] and n= 8 diseased [at each time point]). b) An unsupervised dimensionality reduction technique (singular value decomposition – SVD) was used to reduce the gene expression of the 25-gene signature to a score ($F(1,20) = 23.84$, # $p = 0.000090$). c) Gene expression data was used to train a bootstrap aggregated (bagged) decision tree ensemble to predict the probability that any given mouse was diseased ($F(1,20) = 104.70$, #p=2.1e-9). Two-way ANOVA was used to compare pooled OVA controls vs diseased mice. A Bonferroni-corrected post-hoc multiple comparisons test was used to compare diseased to time matched controls (*p<0.05, **p<0.00005). d) Plot of the bagged tree (BT) prediction score versus SVD indicates separation between groups. Black lines indicate 99.9% confidence intervals for pooled diseased or control mice. Filled ovals indicate mean (centroid) and standard error of the mean for each indicated group.

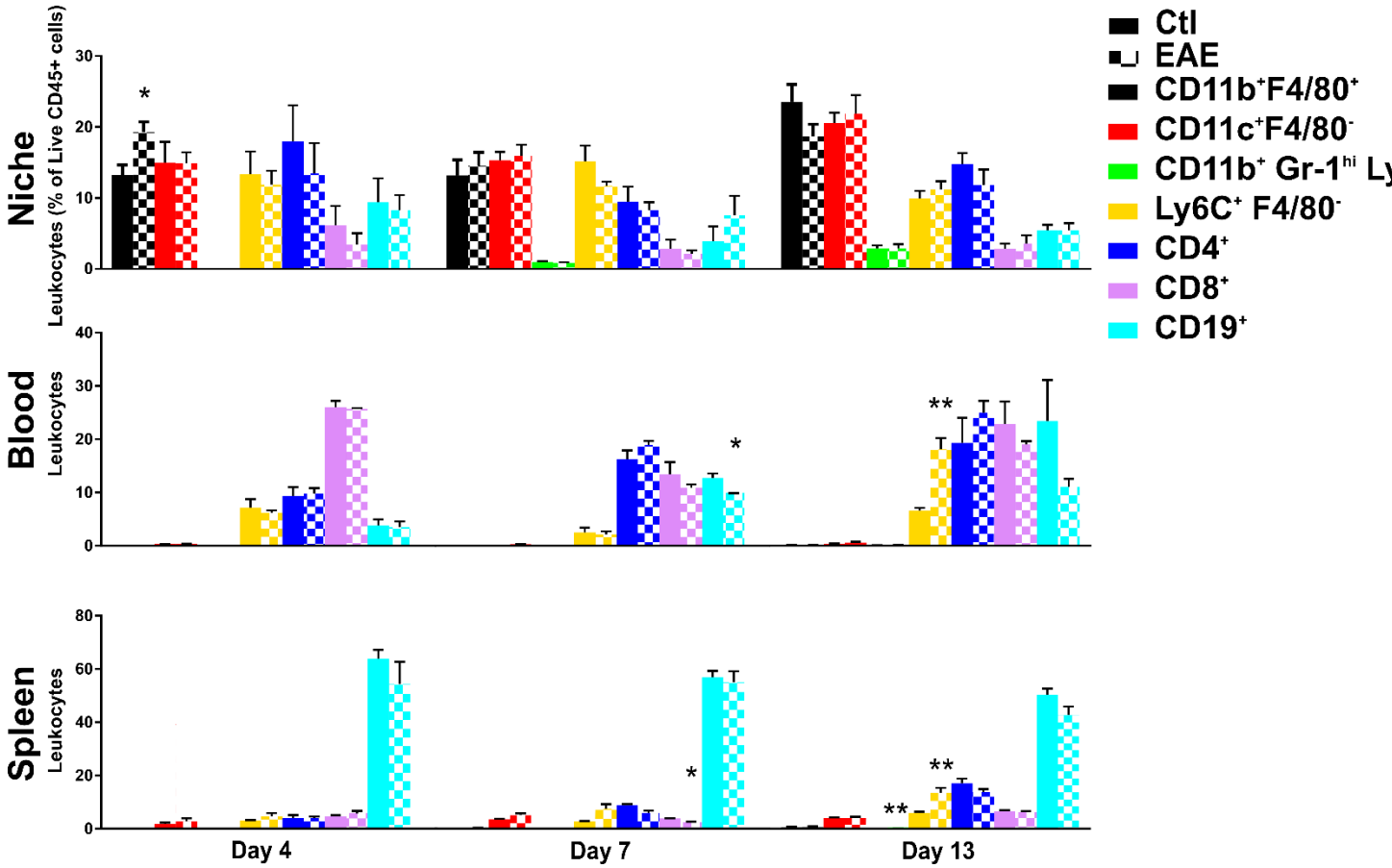


Figure 8.13 Evaluation of immune cell populations during an immunization model of EAE. Flow cytometry for immune cell surface markers demonstrates cell populations through time in IN, blood, and spleens. Data are presented as mean + SEM. Statistical analysis performed by student's t-test at individual time points, asterisks indicate change from control (*$p<0.05$, **$p<0.005$). INs at day 4 and 7: n=4 (Ctl), n=6 (EAE); at day 13: n=14 (Ctl), n=16 (EAE). Blood and spleens at day 4 and 7: n=2 (Ctl), n=3 (EAE); at day 13: n=7 (Ctl), n=8 (EAE).

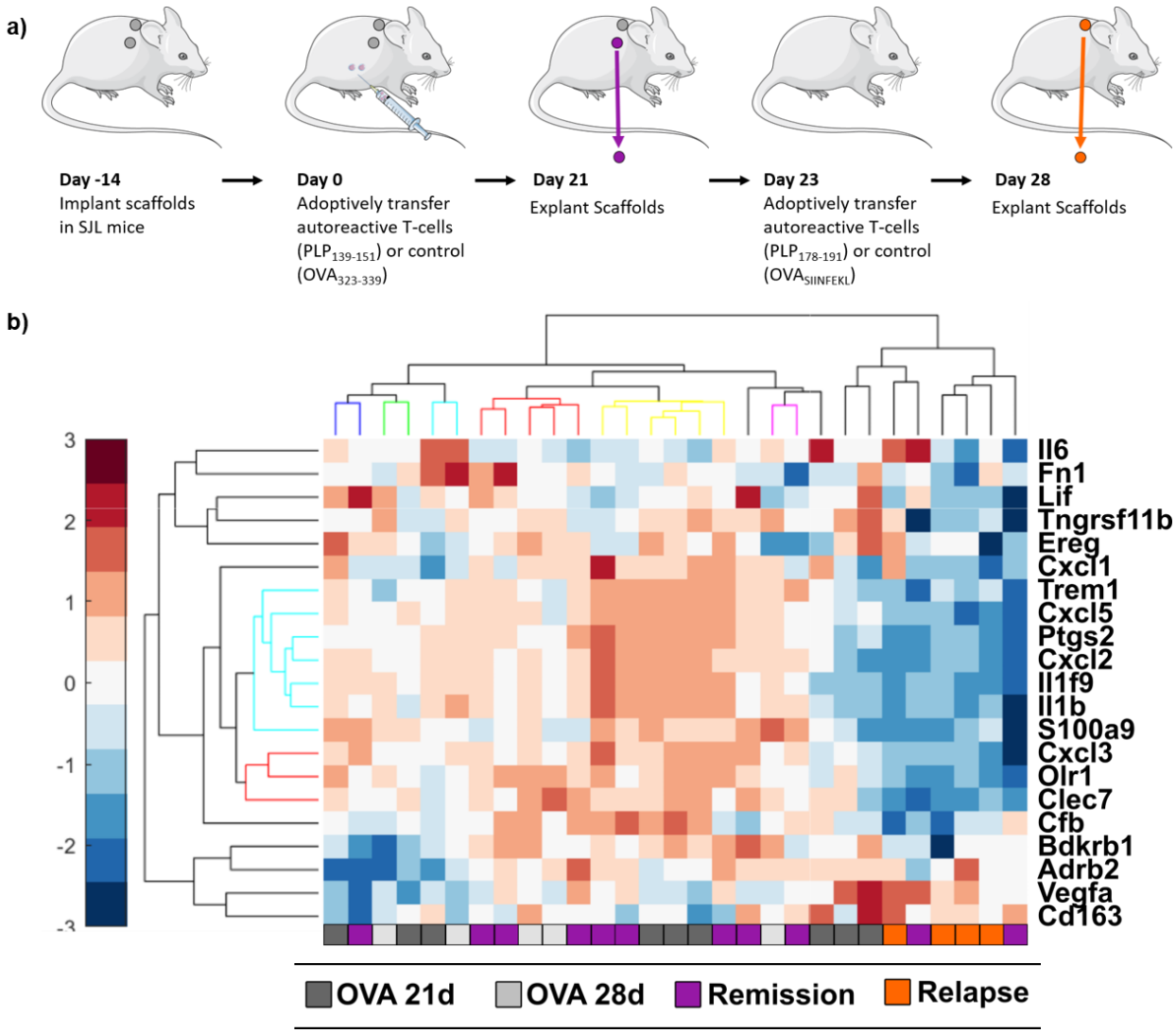


Figure 8.14 Dynamics of EAE disease state are detectable in IN. a) SJL mice were implanted with PCL INs 14 days prior to adoptive transfer of T cells reactive to either $PLP_{139-151}$ (EAE) or $OVA_{323-339}$ (control). INs were subsequently removed at a remission (21 day - purple) or relapse (28 day - orange) time point for analysis via qPCR. A second adoptive transfer of cells reactive against another immunodominant epitope (to mimic epitope spreading in relapse) was performed on day 23 to induce relapse. b) Heatmap and hierarchical clustering of 21 identified genes of interest, expression levels standardized by gene.

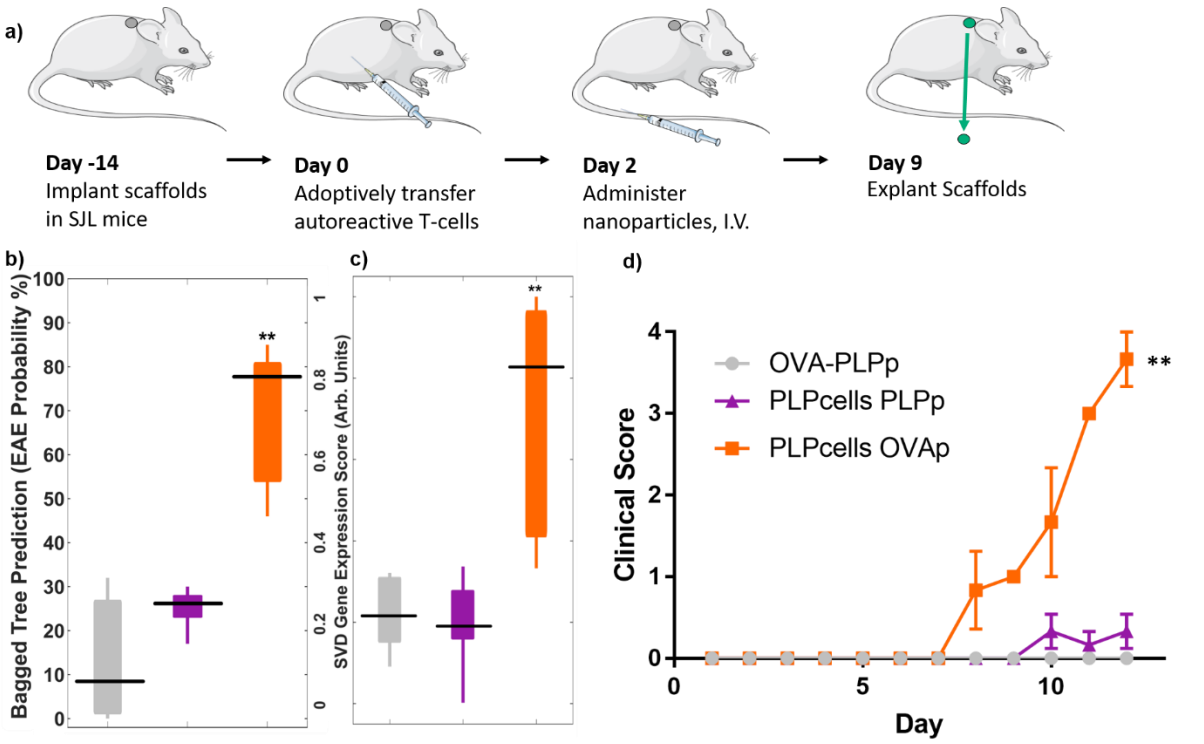


Figure 8.15 IN enables treatment monitoring for nanoparticle induced tolerance. a) SJL mice were implanted with PCL INs 14 days prior to adoptive transfer of T cells reactive to either $PLP_{139-151}$ (EAE) or $OVA_{323-339}$ (control). Nanoparticle treatments were injected intravenously on day 2 and INs subsequently removed on day 9 for analysis via qPCR. Analysis of gene expression by the trained bagged tree ($F(2,15) = 34.2$, $p = 2.6e-06$) (b) and SVD ($F(2,15) = 15.96$, $p = 0.0002$) (c) demonstrated significantly higher scores for mice that received ineffective treatments (and developed symptoms of EAE). One-way ANOVA and a Bonferroni-corrected post-hoc multiple comparisons test was used to compare each group (**$p<0.0005$, different from both control and PLPp treated). d) Mean clinical scores of the mice at each time point demonstrate only the OVA loaded particle treatment demonstrating significantly increased scores from control. A Kruskal-Wallis test (Kruskal-Wallis statistic = 11.69, $p=0.0002$) was used to compare scores for EAE mice and a Dunn's multiple comparisons test was used to compare each group to the OVA control (**$p = 0.0016$).

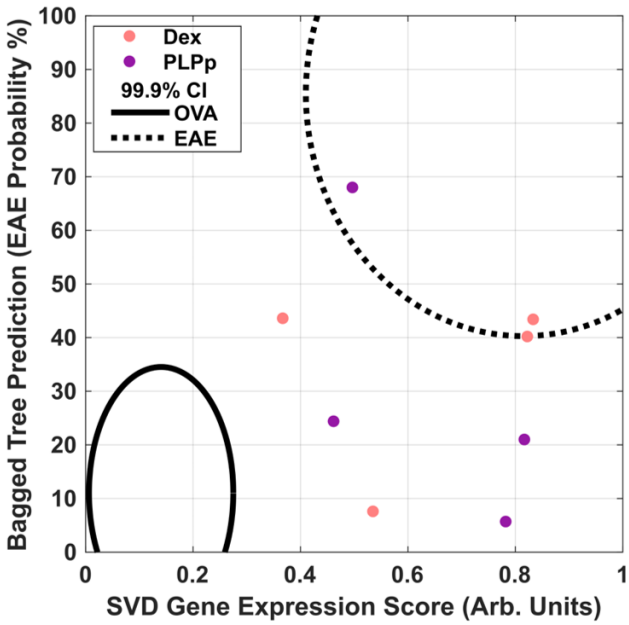


Figure 8.16 INs indicate disease onset and enable pre-emptive treatment. INs were implanted subcutaneously two weeks before adoptive transfer to induce disease. Seven days post-transfer INs were explanted and gene expression analyzed to plot BT score versus SVD which indicated that mice were developing disease. This information was used to enable pre-emptive treatment with either an I.V. injection of 2.5 mg PLGA nanoparticles encapsulating $PLP_{139-151}$ or daily I.P. injections of 5 mg/kg dexamethasone.

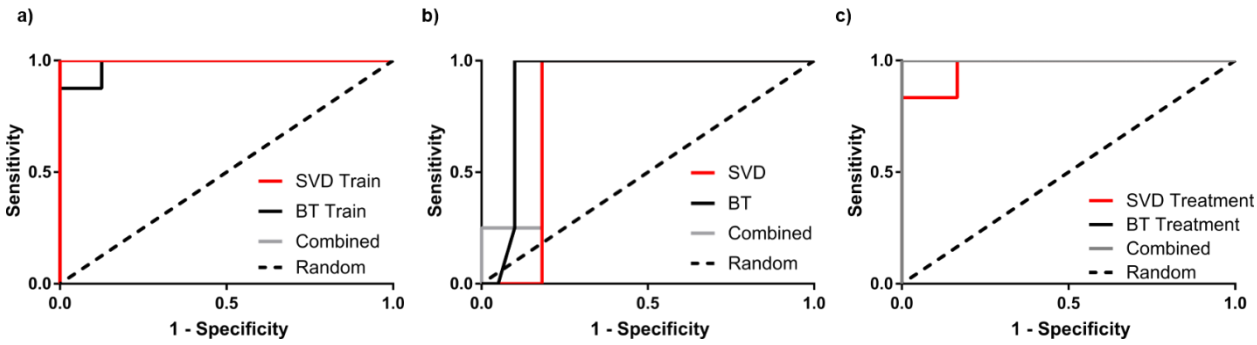


Figure 8.17 ROC curves validate the signature scores from the IN as an effective diagnostic, prognostic, and treatment monitor. ROC curves were plotted for the disease onset data used to train the signature classification model (a), relapse and remission data (b), and particle treatments (c). In each case the area under each curve is > 0.8 indicating successful diagnostic efficacy.

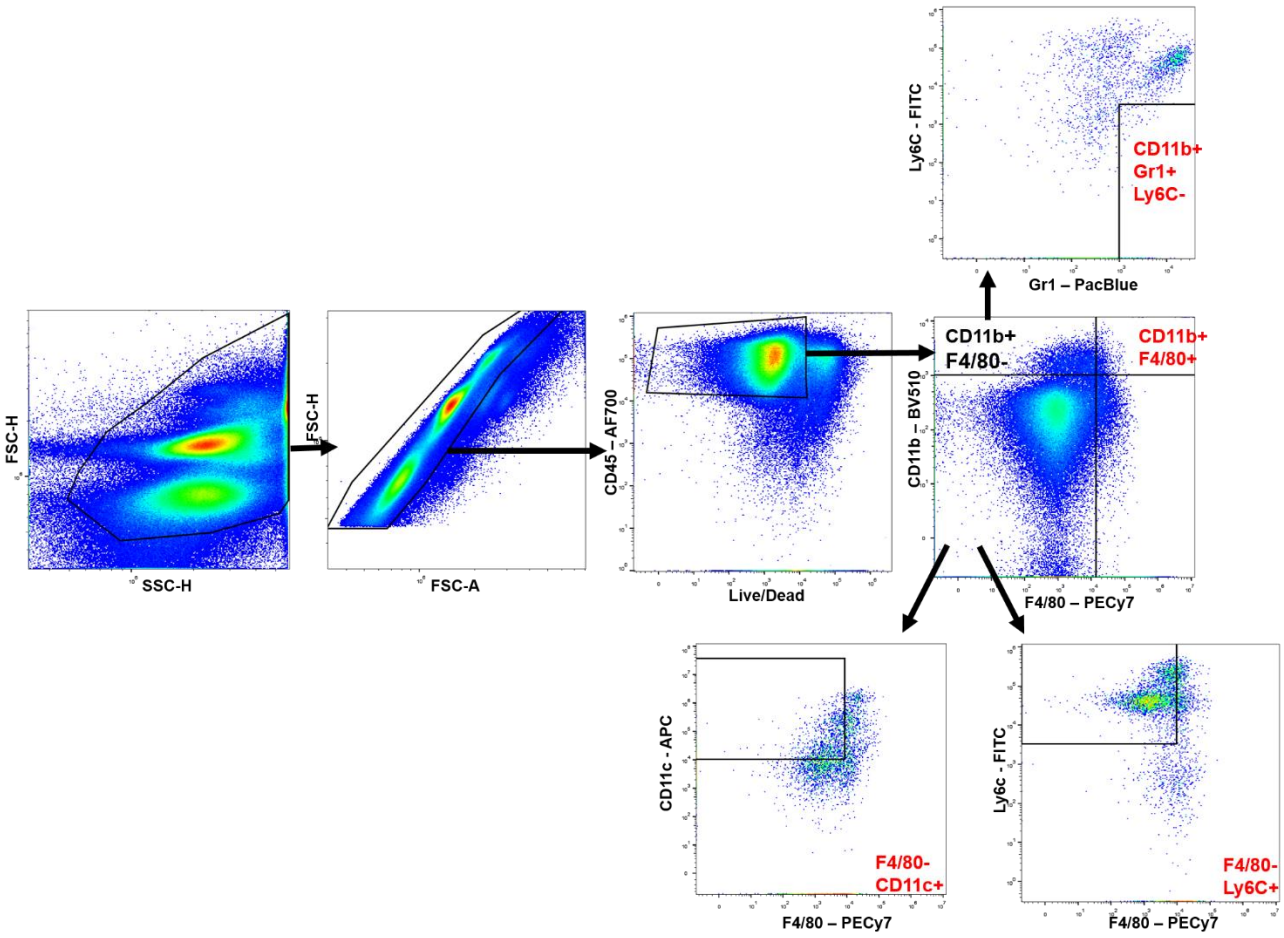


Figure 8.18 Gating Scheme for innate immune panel. All samples were divided in half and half allocated to innate immune panel staining and half to adaptive. Cells were gated using forward scatter area and side scatter height before singlets were gated with forward scatter height and area. Within the singlet population CD45+, live cells (dead cell negative) stains were gated. At this point, CD11b and F480 were plotted to enable selection of CD11b+ F4/80+ cells and subsequent analysis. The CD11b+ gate was used to select Ly6C and Gr-1 to enable the selection of CD11b+ Gr-1+ Ly6C- cells. Then the F4/80 was plotted against Ly6C to enable selection of F4/80- Ly6C+ cells. Finally F4/80 was plotted with CD11c to enable selection of F4/80- CD11c+ cells. Arrows indicate flow of gating and red texts indicates final cell populations used for analysis.

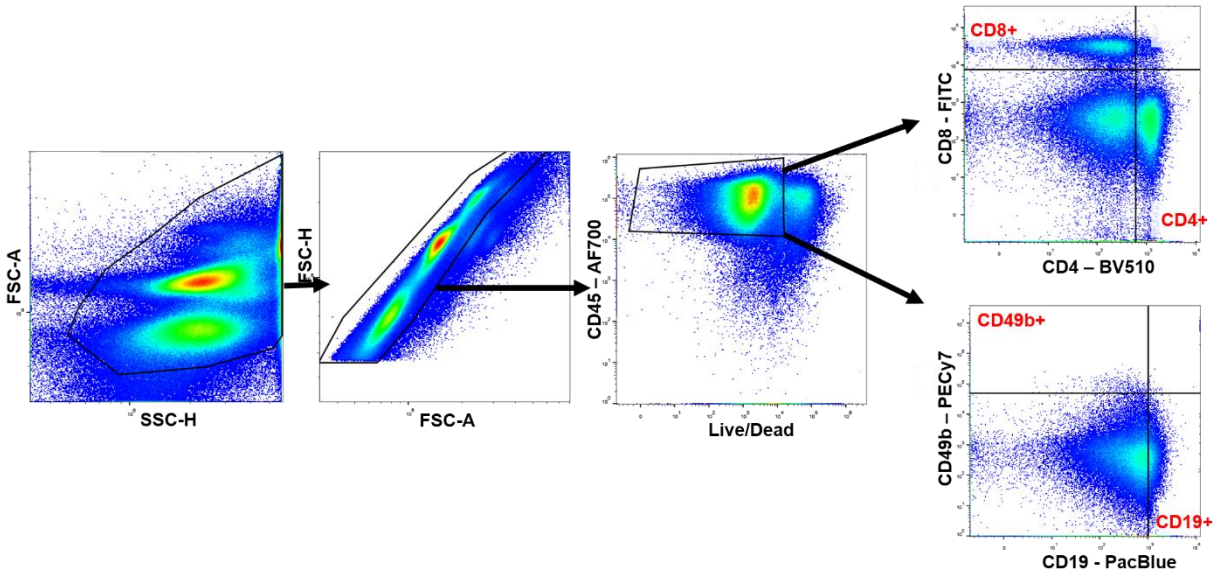


Figure 8.19 Gating Scheme for adaptive immune panel. All samples were divided in half and half allocated to innate immune panel staining and half to adaptive. Cells were gated using forward scatter area and side scatter height before singlets were gated with forward scatter height and area. Within the singlet population CD45+, live cells (dead cell negative) stains were gated. At this point, CD4 and CD8 were plotted to enable selection of CD4+ or CD8+ cells. Next CD19 and CD49B were plotted to select the CD19+ and CD49b+ populations. Arrows indicate flow of gating and red texts indicates final cell populations used for analysis.

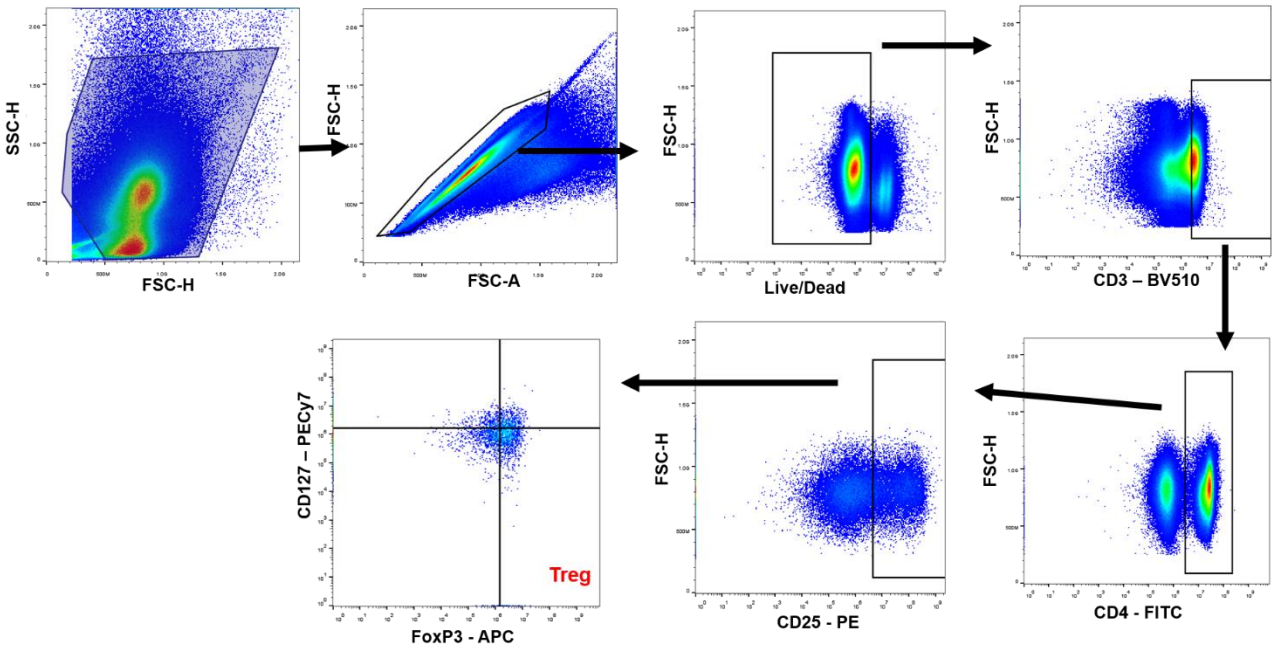


Figure 8.20 Gating scheme for Treg panel. All samples were divided in half and half allocated to Treg panel staining and half to Th panel. Cells were gated using forward scatter and side scatter height before singlets were gated with forward scatter height and area. Within the singlet population live cells (dead cell negative) stains were gated. At this point, CD3 positive cells were selected of which the CD4 positive subset were selected for further analysis. CD25+ T-cells were

selected. Finally, CD127 and FoxP3 were plotted to select the CD127- and FoxP3+ population as regulatory T-cells. Arrows indicate flow of gating and red texts indicates final cell populations used for analysis.

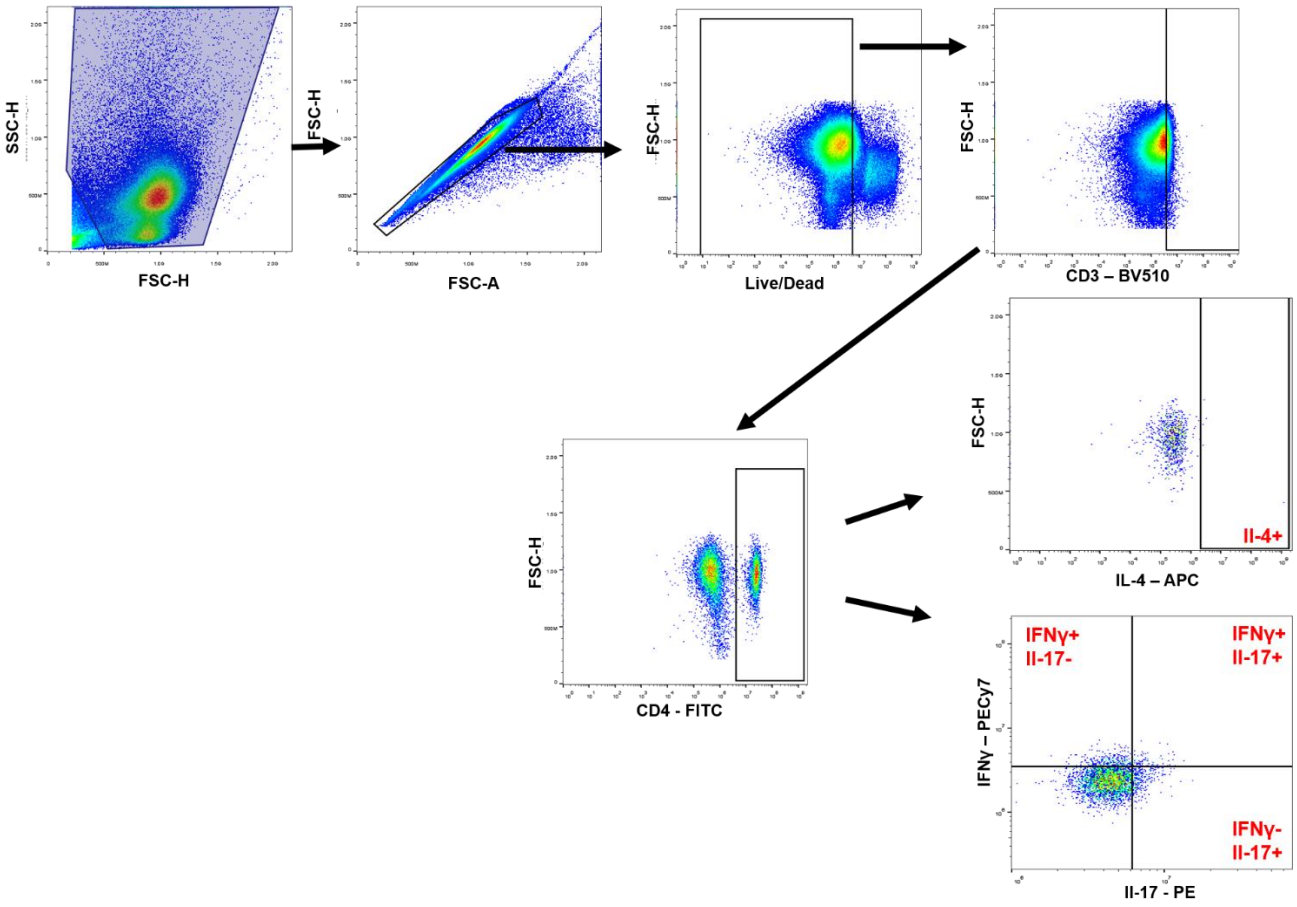


Figure 8.21 Gating scheme for Th panel. All samples were divided in half and half allocated to Treg panel staining and half to Th panel. Cells were gated using forward scatter and side scatter height before singlets were gated with forward scatter height and area. Within the singlet population live cells (dead cell negative) stains were gated. At this point, CD3 positive cells were selected of which the CD4 positive subset were selected for further analysis. The CD4+ gate was used to select Il-4+ to enable the identification of Th2 cells. Finally, the CD4+ population was analyzed by plotting IFNγ stain against IL-17 to enable identification of other Th1/Th17 cell subsets. Arrows indicate flow of gating and red texts indicates final cell populations used for analysis.

Acknowledgements:

This work has been accepted for publication with manuscript information: Morris AM, Hughes KR, Oakes RS, Cai MM, Miller SD, Irani DN, Shea LD. Engineered immunological niches to monitor disease activity and treatment efficacy in relapsing multiple sclerosis, Nature Communications, (2020). We would like to thank the UM Precision Health Scholars grant for funding this work. This work was supported in part by NIH grant R01AI148076. A.H.M. is supported by a Michigan Life Science Fellows award and a NIH T32 grant DE007057-43 and would like to thank both of these funders for their support. Other applicable funding sources include NIH grant R01EB013198, NIH grant R01DK121462, and NIH grant R21AI147677. We would like to thank Christopher Krebs, PhD and the University of Michigan DNA Sequencing Core for assistance in OpenArray processing and analysis. We would also like to thank the University of Michigan Flow Cytometry Core and In Vivo Animal Core for flow cytometry and histology resources, respectively. Finally, we would like to thank Dr. Bethany Moore for helpful conversations and insights.

Conflict of Interest Statement:

This manuscript uses nanoparticles for which L.D.S. and S.D.M. have an interest in Cour Pharmaceutical, who have licensed the technology. L.D.S., A.H.M., R.S.O., and K.R.H. are co-inventors on pending patent applications related to engineered immunological niches. The authors have no other conflicts to declare.

Chapter 9 Conclusion and Future Directions

Summary of Findings

This thesis and the work herein provide several advancements related to biomaterial interventions in instances of aberrant immune function. Utilization of NP to deliver antigen to relevant immune cells is a promising strategy for a variety of immunological disorders. Efforts to deliver multiple antigens with a single NP platform by encapsulation or surface-conjugation are challenging out of necessity to empirically determine synthesis methods to achieve desirable antigen loading, size, and other parameters. Additionally, these methods often result in undesirable burst release or significant alteration of physicochemical properties. Chapter 3 develops a method to achieve targeted loading while avoiding burst release or alteration of physicochemical properties via conjugation of antigen to a PLG backbone prior to nanoparticle synthesis. This strategy was a major advancement in the utility of this and similar platforms and was used routinely throughout this thesis in applications of autoimmunity and transplantation. Chapter 4 develops the technology further by demonstrating the ability to modulate NP efficacy by addition of the bioactive molecule TGF-B. Importantly, this innovation allowed for efficacy with reduced dosages of NP or via subcutaneous injection, which would represent a preferred route of administration for many clinical scenarios.

While the NP platform has shown extensive efficacy in models of Th1/Th17 response and a model of airway inflammation, they had not been investigated in a Th2-mediated model of food allergy prior to this work. These studies are complicated by the fact that intravenous delivery of allergen in pre-sensitized mice may result in anaphylaxis if the amount of surface-expressed

antigen or antigen released from NP upon administration reach a sufficient threshold to induce mast cell degranulation and anaphylactic response. Chapter 5 investigates the quantity of allergen that is tolerated in alum sensitized mice either on the surface or released *in vivo* and demonstrates that a formulation designed following these parameters is well-tolerated and reduces disease symptoms in two separate models of peanut allergy. These are preliminary efforts that are necessary for translation of this therapy to be possible for food allergy, which is a significant clinical need given the shortcomings of the limited options that are available to patients with food allergy. Specifically, current immunotherapies are not effective for all patients, require months to years of treatment for efficacy, have uncertain duration of efficacy, and still possess significant risk for anaphylaxis. Technologies like the NP platform introduced in Chapter 5 are attractive for their potential to provide an off-the-shelf therapy that may reduce risk of anaphylaxis, eliminate the need for time-intensive dose escalation protocols, and have the potential to provide increased duration of efficacy.

Chapter 6 investigates several NP design parameters in an attempt to improve their ability to prevent skin graft rejection. The antigen-polymer conjugation technique developed in Chapter 3 was used extensively to test hypothesized methods to impact NP efficacy, including method of conjugation, location of antigen (i.e. surface-conjugated vs encapsulated antigen), and length of delivered peptide. Interestingly, peptide length played the most significant role in NP efficacy, although it is unclear whether this is a trend that is generalizable to other NP-mediated delivery modalities or whether the observation was the result of altered MHC loading efficacy. Additionally, no NP modification approached the efficacy of apoptotic donor splenocytes, which were used throughout as an effective therapy control. Administration of apoptotic *recipient* splenocytes augmented with peptide containing the amino acid mutations responsible for

allorecognition and rejection was not capable of replicating the efficacy of donor apoptotic splenocytes. The model utilized (BM12 to C57bl/6) features only 3 single amino acid mutations in the hypervariable region of MHC II, which may suggest that intact MHC II is critical for the efficacy of donor apoptotic splenocytes. These studies have motivated additional work from our lab centered on delivery of intact donor membrane components to augment NP efficacy.

While peripheral interventions for allotransplantation may be promising to address underlying causes of allorecognition, considerable research is being conducted related to the development of immunoprivileged sites. This is particularly relevant for models of T1D to enable delivery of allogeneic islets to treat disease while remaining protected from host rejection. Chapter 7 introduces a method to decorate PLG scaffolds with FasL using the bioconjugation technique developed in Chapters 3 and 4. Delivery of allogeneic islets on FasL-decorated scaffolds provided a significant improvement in blood sugar levels relative to non-FasL-decorated scaffolds in diabetic mice. This strategy is unique in that it enables a localized approach to protecting islets that may avoid the off-target effects of systemic therapies like broad immunosuppressives.

There is a significant need for methods to detect disease and response to therapy more rapidly. Chapter 8 introduces a method to interrogate the foreign body response to PCL scaffolds to determine the underlying immune function in mice. This manuscript develops a signature of gene expression within a subcutaneous implant in RR EAE, a murine model of MS. Importantly, we demonstrate that a scaffold "disease score" is highly correlative with the relapsing remitting clinical symptoms in this murine model. Finally, we show that the implant is effective as a complementary diagnostic and is able to detect changes in immune function associated with application of dexamethasone (a control for standard of care) or myelin oligodendrocyte protein

delivery by PLG NP (our novel therapy). These findings are very promising as they may provide a path toward development of a clinical method to improve the timing and selection of therapies for MS patients. Additionally, the biological insights gathered from probing the foreign body response during disease may identify novel pathways involved in disease onset and progression. Together, these findings provide several key improvements and insights related to NP-based therapies and their application. First, there is considerable evidence that conjugation of antigen to polymer backbones is an effective method to enable their delivery to relevant immune cells on NPs or macroscopic implants. Efficacy was observed using peptides of various length and hydrophobicity. Efficacy was also observed within multiple conjugation techniques, including the formation of amide bonds, disulfide bonds, and even relatively stable thioether bonds. Desirable physicochemical properties (antigen loading, polydispersity, size, and Zeta potential) were achievable with this technology and were amenable to augmentation with surface-conjugated TGF-B. These findings will be of particular interest to the field in the selection of strategies for biomaterial intervention. Second, investigation of parameters required for safe and effective delivery of antigen in models of transplant rejection and food allergy were investigated in multiple models. Strategies to incorporate pure peptides and complex, heterogenous protein exracts were developed and demonstrated ability to treat disease. Third, this thesis provides insights related to modification of subcutaneous biomaterial implants to modulate and monitor the immune response to polymeric foreign bodies. Invasion of cytotoxic cells can be limited by decoration with bioactive FasL and the gene expression of invasive cells can be probed to determine underlying immune function. Each of these represent a critical advancement in the field's understanding of biomaterial interventions in immune dysfunction.

Significance and Impact

Development of new strategies to improve control of antigen delivery are highly desirable. Burst release of the contents of NP platforms is a common limitation to their efficacy and methods to conjugate antigen to these platforms often results in unacceptable alterations of physicochemical properties. The work presented in Chapters 3 and 4 and applied in Chapters 6 and 7 provide a method to incorporate multiple antigens in targeted quantities while avoiding burst release of antigen and alteration of surface properties. The finding that method of conjugation of peptide antigen has a relatively small effect on the ability of a NP to effectively deliver the antigen to relevant immune cells and delay skin transplant rejection is a novel finding. Studies presented in Chapter 6 have resulted in the development of membrane coated PLG NPs to enable direct interactions of the platform with T cells and other non-phagocytosing cells that are often challenging to target with NP therapies. For patients with food allergy, therapeutic options are limited to investigational clinical trials and, more recently, a standardized peanut flour for oral immunotherapy. These therapies have multiple shortcomings that have been emphasized several times throughout this thesis, and there is a considerable need for strategies that provide protection with fewer doses more rapidly with reduced risk of anaphylaxis. Chapter 5 investigates critical safety parameters related to the development of intravenously delivered therapies for food allergy by determining tolerable quantities of intravenously administered allergen. Importantly, we demonstrate in two murine models of peanut allergy that there exists a window of therapeutic efficacy for a NP therapy that does not induce adverse anaphylactic events.

Future Directions

The studies presented in this thesis have resulted in the development of several novel avenues of research within our lab. Several of these were discussed in Chapter 1 for the field more broadly and will be revisited here for our technologies more specifically.

Development of strategies to conjugate proteins, lysates, and extracts to polymer backbones of NP formulations

This thesis made routine use of a technological improvement related to conjugation of peptide to PLG polymer for improved control over antigen delivery. This strategy is particularly effective in models where the precise peptide responsible for aberrant immune function is well-characterized and relatively short. However, multiple diseases are the result of inappropriate recognition of large proteins, intact tertiary structures, or an unidentified portion of a lysate or extract. For these models, surface-conjugation or encapsulation of the antigen(s) is commonly utilized, but suffer from many of the shortcomings previously mentioned with these techniques, including altered physicochemical properties, low control over antigen quantities, and high burst release of antigen. Unfortunately, the conjugation techniques presented are not particularly effective due to complications related to protein solubility, conjugation efficiency, inability to efficiently quantify specific sequences or proteins captured, and loss of bioactivity, to name a few. Future studies should investigate strategies that are able to efficiently conjugate a representative population of antigens from proteins, lysates, and extracts. This may involve the development of strategies to separate membrane and cytosolic proteins, controllably degrade larger proteins into more manageable peptide fractions, and considerable troubleshooting of solvent and co-solvents to enable the retention of bioactivity. Translation of the technology will be complicated by the fact that the FDA is likely to perceive each NP formulation (i.e. each antigen or combination of antigens) as a unique drug that will require approval prior to

application clinically. In autoimmune disease, the epitopes involved in initiation and progression of disease are often, but not always, well-characterized. For these, incorporation of the relevant antigen is conceivable. Unfortuatenly, with progression of disease, additional tissue damage is associated with epitope spreading which would require incorporation of multiple antigens. This is less of a concern in allergy, where epitopes involved have been studied extensively and are an attractive application for these technologies. As discussed in Chapter 5, it remains to be seen whether allergen can be delivered by NP safely in human disease and will likely be a major hurdle to translation. In transplant rejection settings, epitope identification will be significantly more challenging. While major antigens are routinely screened to enable HLA-matching, there is a growing appreciation for the involvement of minor antigens during chronic rejection. It is not apparent how the minor antigens responsible for transplant rejection could be identified early enough to enable NP treatment. Given the relative success of apoptotic splenocytes in pre-clinical studies (including in non-human primates), it is possible that NP-mediated delivery of cell lysates would be sufficient to provide protection to minor antigens; however, our efforts to match the efficacy of cell-based therapies (Chapter 6) have demonstrated that improvements (e.g. incorporation of intact MHC) to the platform are necessary. As the complexity of the proteins delivered increases, solvent incompatibility will likely become an issue. Specifically, the formulation strategies typically used for these particles involve dissolving polymer within dichloromethane, acetonitrile, ethyl acetate, or similar solvents. Efforts to develop methods to conjugate peptides to these polymers required the exploration of addition of small amounts DMSO or DMF to enable solubilization of biopolymers; however, for larger peptides and general proteins it is likely that it will be difficult to make the standard emulsion particles while also dissolving such large amino acid sequences. An attractive alternative might invole the use of

larger polymers which may be sufficient to "pull" proteins into the same phase, but care will need to be taken to ensure that the amphiphilic nature of the biopolymers do not spontaneously form micelles or otherwise negatively influence aspects of the synthesis which have been found to be desirable (e.g. size, polydispersity, zeta potential, relative quantities of surface protein…). Additionally, as the percent of the total biopolymer mass that is not protein increases, the total antigen loading of the formulations will decreases at a corresponding amount. Work in the RR-EAE model of multiple sclerosis demonstrated that a total antigen loading of 8μg/mg was sufficient to induce the maximum level of protection that we observed which will hopefully be true in other models and would eliminate concerns over reduced theoretical maxima of loadings. Once these strategies have been developed, a panacea of interesting biological and mechanistic studies will be possible. For example, delivery of one or more NPs containing one or more allergenic regions would provide insights related to the relative contributions of various epitopes in disease models. Alternatively, robust strategies to incorporate intact MHC from donor sources would enable production of platforms capable of directly interacting with recipient T cells, providing a method to impact direct and semi-direct pathways of allorecognition.

Improvement of NP safety and efficacy in murine models of food allergy.

As demonstrated in Chapter 5, there exists a window in which therapeutic efficacy can be achieved by NP delivery of allergen without adverse reactions. As demonstrated in multiple of our disease models, delivery of large quantities of antigen is typically associated with improved therapeutic efficacy. This is possibly related to high zone tolerance mechanisms that the platform is likely to be utilizing in some capacity. In order to improve NP efficacy and to further reduce the risks associated with unacceptably large quantities of surface-exposed or prematurely released allergen, additional strategies to mask allergen from immune recognition are desirable.

PEGylation is a commonly utilized strategy that significantly limits binding, but is likely to also result in alterations to particle biodistribution or physicochemical properties that we believe to be critical to the efficacy of the platform. A variety of techniques exist which could be modified to hide allergens, including layer-by-layer deposition of materials. Due to the variety of chemical and physical properties of the polymeric materials used, there is considerable opportunity to investigate methods to create PLG NPs containing surface-conjugated allergen prior to coating them or encapsulating them in additional layers of PLG with innumerable molecular weights or lactide:glycolide ratios. This would provide a mechanism to deliver allergen to relevant immune cells without eliminating the effects of the base polymer, all while limiting immune recognition of allergen. The field of drug delivery has provided a number of methods to control delivery of protein, but complete masking of antigen has been elusive. Further, we expect that the levels of surface-associated allergen or burst released allergen that are tolerated will vary depending on the murine model used and will almost certainly be different from person-to-person. As such, reliable methods to quantify these amounts are likely to be a prerequisite to clinical translation.

Understanding the mechanism of action of NP therapies

To date, several observations of the mechanism of the NP technology have been made. Reduction in costimulatory molecules on antigen-presenting cells is expected to contribute to the induction/promotion of Tregs, anergy, and reduction of cytokine production in response to NP-delivered antigen. We often consider these biological outcomes to be indicative of tolerance, but several additional manuscripts should explore this to better define what the technology is achieving. Currently, the length of efficacy of the platform are not well-understood in various models. Therapeutic application of NPs in murine models of autoimmunity, allergy, and transplant rejection demonstrate efficacy. If the particles are inducing long-lived tolerance,

attempts to induce the disease weeks or months later would be expected to fail. Further, the majority of our studies involve application of NPs prophylactically within approximately 7 days of disease induction or therapeutically within 3 weeks of disease induction. Investigation of the most-effective timing of administration will be informative for ongoing clinical trials and will also enable a better understanding of the biology involved in their efficacy (e.g. by determining whether application involves transient deletion of antigen-specific T cell repertoirs or by long-lived promotion of Tregs). Many of our studies often involve NP-mediated delivery of irrelevant antigen as a negative control. As expected for an antigen-specific therapy, this has not been associated with reduction in symptoms or recall responses relative to untreated control groups. This is a very promising outcome which should be validated with additional studies. Following treatment of model of disease specific to a particular antigen, ability to fully induce a similar model of disease to a different antigen would provide additional support of antigen-specificity. For example, treatment of RR-EAE specific to $PLP_{139-151}$ should not impact induction of disease specific to $PLP_{178-191}$ and treatment of a model of food allergy to peanut extract should not impact induction of sensitivity to ovalbumin. Alternatively, demonstration of a robust immune response to infection (e.g. influenza or parasite) would be a clinically-relevant strategy to demonstrate that the NPs are not broadly immunosuppressive. With these studies, it will be important to demonstrate that antigen-specific abrogation of aberrant immunity is matched to desired immune response—demonstrating that NPs can treat Th2-mediated allergy without impacting ability to generate a Th1 immune response is important, but may be less-relevant than demonstrating that abrogating Th2-mediated disease does not inhibit induction of desirable Th2 immunity to parasitic infection. While these studies are complicated by the number of possible

combinations of disease kinetics, timing of therapy, and antigen selection, they will be important for safe clinical translation.

Further investigation of implantable complementary diagnostics

Thus far, we have demonstrated that subcutaneously implanted PCL scaffolds can be analyzed to evaluate disease onset, progression, and response to therapy. While these findings are incredibly exciting and have applications in a variety of diseases, considerable efforts are and should continue to be put into development of non-invasive methods to monitor the implants. Currently, the analyses being used would involve biopsy or explantation of subcutaneous implant which will significantly hinder their translational potential. Advancements in non-invasive imaging modalities have enabled the use of ISOCT or ultrasound to monitor these scaffolds in models of cancer and should be investigated in other disease models, including EAE. Technologies like the EverSense glucose monitor currently exist which enable imaging of fluorescence through the skin. The Shea Lab is currently developing strategies to achieve similar results through the use of FRET based-signalling. These are highly promising studies, but may be complicated by unavoidable fluctuations in immune state (e.g. due to onset of irrelevant illness or exposure to adjuvants like pollution) or reduction in signal-to-noise ratio associated with the foreign body response and gradual encapsulation of the implant. Strategies to incorporate stronger signals (e.g. BRET) or to refine the specificity of the platform (e.g. by development of systoms capable of resolving small changes in multiple metabolites) may be critical in enabling their translation. Application of the technology has progressed the furthest as a method to detect metastasis at early timepoints, which was beyond the scope of this thesis but has provided valuable lessons to the Shea lab. Of particular importance to clinicians interested in applying the technology for detection of metastasis is receiving actionable information. For metastatic disease, in which few

therapeutic options exist, it remains to be seen whether early detection will necessarily result in improved outcomes. For wide-spread application in autoimmune diseases like multiple sclerosis, as discussed in this thesis, similar requirements will need to be met. Given the current ability to address symptoms through short-term application of immunosuppressive regimens or corticosteroids, our complementary diagnostic may enable early identification of patients who would benefit from intervention that is otherwise associated with significant risk when applied systemically over long periods of time.

Appendices

Development of immunological niche in murine model of primary progressive multiple sclerosis

Introduction

Currently, 15% of MS patients are diagnosed with Primary Progressive MS (PPMS), a disease characterized by accumulated central nervous system (CNS) damage over time[478]. 50% of PPMS patients are unable to walk without assistance (e.g. a walking stick) within 10 years of diagnosis. Diagnosis of PPMS requires 1 years of disease progression and presence of multiple other indicators of CNS damage[479]. Unfortunately, the inability to diagnose PPMS at early timepoints prevents appropriate pharmacological intervention. Strategies to improve early diagnosis of PPMS and monitor response to therapy is expected to improve patient outcomes. Previously, we have utilized a PLG NP platform for treatment of murine models of relapsing remitting multiple sclerosis (RRMS), but their efficacy in progressive models of disease are unknown. Here, we investigate their application in primary progressive experimental autoimmune encephalomyelitis (PP EAE), a murine model of disease. To enable early detection of disease onset and monitoring of treatment efficacy, we interrogate the foreign body response to a subcutaneously implantable PCL scaffold to extend previous findings in relapsing remitting experimental autoimmune encephalomyelitis (RR EAE).

Methods

Scaffold Fabrication and Subcutaneous implantation

Microporous scaffolds were prepared in the same manner as previously described[458, 474]. All procedures were performed in accordance with the regulations approved by the Animal Care and Use Committee of the University of Michigan. Female C57BL/6 mice were purchased from Jackson Labs at an age of six weeks. Mice were anesthetized with isofluorane, before subcutaneous implantation as previous described[475, 476]. Mice received subcutaneous injections of carprofen (5 mg/kg) immediately before surgery and 24 hours after surgery.

Disease Induction

Mice were immunized as described previously[474, 477]. Briefly, an emulsion was prepared containing 1:1 complete Freund's adjuvant (incomplete Freund's adjuvant [Fisher] with 4 mg/mL heat killed M. tuberculosis H37 Ra [Fisher]) : PBS with 2 mg/mL peptide (MOG_{35-55} or $OVA_{323-339}$ [Genscript]). A total volume of 100 µL CFA with peptide was injected subcutaneously at three sites within each mouse. For studies using active induction of EAE the day of immunization was considered as day 0 and mice were monitored for disease symptoms after this point.

For passive, adoptive transfer disease induction, donor mice were immunized and 10 days later, donor mice were euthanized and spleens and lymph nodes (inguinal, axiallary, and brachial) were harvested before processing into a single cell suspension. Cells were cultured in RPMI with 10% FBS, 2 mM L-glutamine, 100 IU/mL penicillin, 0.1 mg/mL streptomycin, 1x non-essential amino acids solution, 1 mM sodium pyruvate, 10 mM HEPES, and 20 µg/mL peptide antigen. After three days of culture non-adherent cells were harvested, counted, and injected i.p. into recipient mice. After induction of disease, severity was monitored on a 0-5 scale as previously described[330]: 0

= no disease, 1 = hindlimb weakness or limp tail, 2 = hindlimb weakness and limp tail, 3 = partial hindlimb paralysis, 4 = total hindlimb paralysis, 5 = moribund.

Tissue isolation

To harvest biopsies of PCL implants for analysis, mice were anesthetized with isoflurane before an incision was made over the surface of the implant. The implant and any adherent encapsulating tissue were pulled through the incision and excised and the incision was closed with sutures. Tissues for RNA were flash frozen in isopentane on dry ice and stored at -80 °C until analysis. Tissues for flow cytometry were placed into PBS and stored on ice, and tissues for histology were immediately placed in 4% paraformaldehyde. For blood isolation, mice were anesthetized before intracardiac blood draw with EDTA. RBCs were lysed in an ACK solution (Gibco) before washing in PBS. Pellets were resuspended in Trizol and stored at -80 °C until analysis.

RNA isolation and cDNA synthesis

RNA was isolated with the Directzol RNA Miniprep kit (Zymo Research) following manufacturer's instructions. Samples to be used for OpenArray analysis were also assessed for RNA integrity (RIN) with an RNA fragment analysis with an RNA 6000 Nano Kit (Agilent Technologies), and all samples had a RIN>8.

cDNA synthesis was performed with the SuperScript™ VILO™ cDNA Synthesis Kit (ThermoFisher Scientific) according to manufacturers instructions. RT was performed with RNA concentrations of 200 ng/µL. Because RNA isolates from blood typically did not achieve this concentration, an RNA clean-up kit was used to increase concentration and purity according to manufacturer instructions (RNA Clean & Concentrator-5, Zymo Research).

OpenArray High-Throughput RT-qPCR

For high-throughput gene expression analysis, OpenArray panels focused on mouse inflammatory pathways were used. Panels and accompanying reagents were purchased from ThermoFisher (Applied Biosystems™ TaqMan™ OA Mouse Inflammation Panel, Cat. No. 4475393). The panels contained 632 validated genes that have known roles in inflammation as well as 16 endogenous controls (housekeeping genes). cDNA was prepared as described above and OA analysis and quality control was performed on a fee-for-service basis by the UM DNA Sequencing core. The core uses a robotic OA AccuFill system and the QuantStudio 12k Flex RT-PCR system (ThermoFisher Scientific). Analysis was performed as previously described using this system.[26] For OpenArray of adoptive transfer samples a total of n=8 samples per condition (diseased or healthy) were analyzed with 4 from each time point (day 7 or 9). Each sample was from an independent mouse and samples alternated between healthy and diseased in their placement on the chip to minimize spatial bias. For immunization studies, two time points were used for OpenArray, day 7 or 13.

Selection of Genes of Interest

Samples were analyzed first to remove genes that did not have readable data in more than one of the four mice in each condition. Next, any samples that were missing data were filled with the median for the overall dataset. This was required because downstream analysis requires complete matrices. Ultimately, 500 genes of the 648 were used for this study. Each of the 16 reference genes were analyzed via the NormFinder algorithm to select the three most stable reference genes: Hmbs, Polr2a, and Ubc. ΔC_q values were calculated for each gene from the average of the reference genes for that sample. Next, fold change (FC), p-values, and prediction scores derived from elastic net regularization (MATLAB's lasso function, $\alpha = 0.01$, leave one out cross-validation) were

calculated for each gene using time-matched controls.[33] Box-plots show log_2FC, centered on the median of the time matched healthy controls. All identified 21 genes of interest were identified as predictors (elastic net scores>0), had FC>1.5, and $p<0.05$. Additionally, we attempted to include genes that increased and decreased during disease to make the model more robust and ease the eventual construction of a sensor.

Once these genes of interest were identified, all other studies were conducted via RT-qPCR analysis in 384 well plates. The same TaqMan probes used in the OpenArray chips were ordered from ThermoFisher Scientific and samples were alternated between healthy and diseased in their placement on the plate. TaqMan Gene Expression Mastermix was used and a final volume of 9 µL was used for each well of the 384 well plate. RT-qPCR was performed on the QuantStudio ViiA 7 system and C_q values determined by the accompanying software. Non-detects were left blank for any statistical analyses, but were filled with the median of all samples for SVD (because it requires complete matrices). Samples from the original OpenArray data were run on every 384 well plate to allow for a correction factor to be applied to account for variability.

Gene Signature Scores and analysis

Firstly, unsupervised hierarchical clustering analysis was performed using MATLAB's clustergram tool which plots dendrograms to indicate samples and genes that cluster together. Ultimately, genes of interest were identified, and computational approaches were used to create two metrics for evaluating whether mice were sick or healthy. Singular value decomposition (SVD) using MATLAB's svds function was applied to create a gene signature score using an unsupervised technique. Next, a supervised machine learning approach bootstrap aggregated decision tree ensemble (Bagged Tree) was trained to classify samples as healthy or diseased. We employed MATLAB's fitcensemble function with the Bag method.

Nanoparticle Fabrication and Administration

Peptide encapsulating nanoparticles were fabricated with the double emulsion method as previously described.[167]. Briefly, 150 µL of antigen dissolved in PBS (50 mg/mL $PLP_{139-151}$ or $OVA_{323-339}$ [Genscript]) was added to 2 mL of 20% w/v poly(lactide-co-glycolide) (inherent viscosity: 0.17dL/g, Lactel). This solution was sonicated for 30 seconds before the addition of 10 mL of 1% w/v poly(ethylene-alt-maleic anhydride) in water. This was again sonicated to form the double emulsion which was poured into 200 mL of 0.5% w/v poly(ethylene-alt-maleic anhydride) and stirred overnight. Particles were washed extensively before lyophilization in cryoprotectant. The size and zeta potential of the acNPs were determined by dynamic light scattering (DLS) by mixing 10 mL of a 25 mg/mL particle solution into 990 mL of MilliQ water using a Malvern Zetasizer ZSP.

Statistics

All statistics were calculated with MATLAB or GraphPad Prism software. When comparing pooled control vs diseased mice, two-way ANOVA was used to determine significance. A post-hoc multiple comparisons with a Bonferroni correction was then used to compare each time point to its time-matched control. When comparing the scores of EAE mice over time a one-way ANOVA with a Bonferroni corrected post-hoc multiple comparisons test was used. Additionally, the same method was used to compare the three particle treated groups at a single time point. ROC curves were plotted and analyzed in GraphPad. Box plots show the median, 25th-75th percentiles and most extreme data points not considered outliers (outliers are indicated by red +).

Characterization of PLG nanoparticle efficacy in murine model of primary progressive MS

PLG NPs were synthesized as previously described. Briefly, antigen (MOG_{35-55} or $OVA_{323-339}$) were encapsulated using double-emulsion solvent evaporation. Unloaded, “blank” NPs were

synthesized similarly using a single-emulsion method in absence of antigen. NPs were characterized (Fig 1A) and applied after disease induction in a PP EAE (Fig 1B). Mice were evaluated daily for onset and progression of clinical symptoms following an established scoring method[477]. Importantly, PLG(MOG_{35-55}) (but not Blank or PLG($OVA_{323-339}$)) resulted in significant and almost complete abrogation of clinical disease over the course of the study.

	Size (nm)	Zeta (mV)	PDI	Antigen Loading (μg/mg)
Blank	625.8±6.4	-47.5±8.1	0.33	-
PLG(MOG_{35-55})	647.5	-59.4	0.20	13.6
PLG($OVA_{323-339}$)	610.7±6.7	-42.3±1.0	0.388	2.0

Figure A.1 Properties and efficacy of PLG(MOG_{35-55}) treatment of PP EAE. Characterization of nanoparticle properties (A).

To investigate the ability to monitor induction of disease and response to therapy, mice received subcutaneous implantation of PCL scaffolds to enable collection of inflammatory cells recruited through the foreign body response. PP EAE was induced via adoptive transfer of MOG_{35-55}-reactive cells. Scaffolds were removed at Day 9 or 14 for analysis as previously described. An inflammatory OpenArray panel identified genes that significantly changed with disease onset. Singular value decomposition and bagged tree analysis enabled the development of a signature associated with gene expression of recruited cells during disease onset and progression.

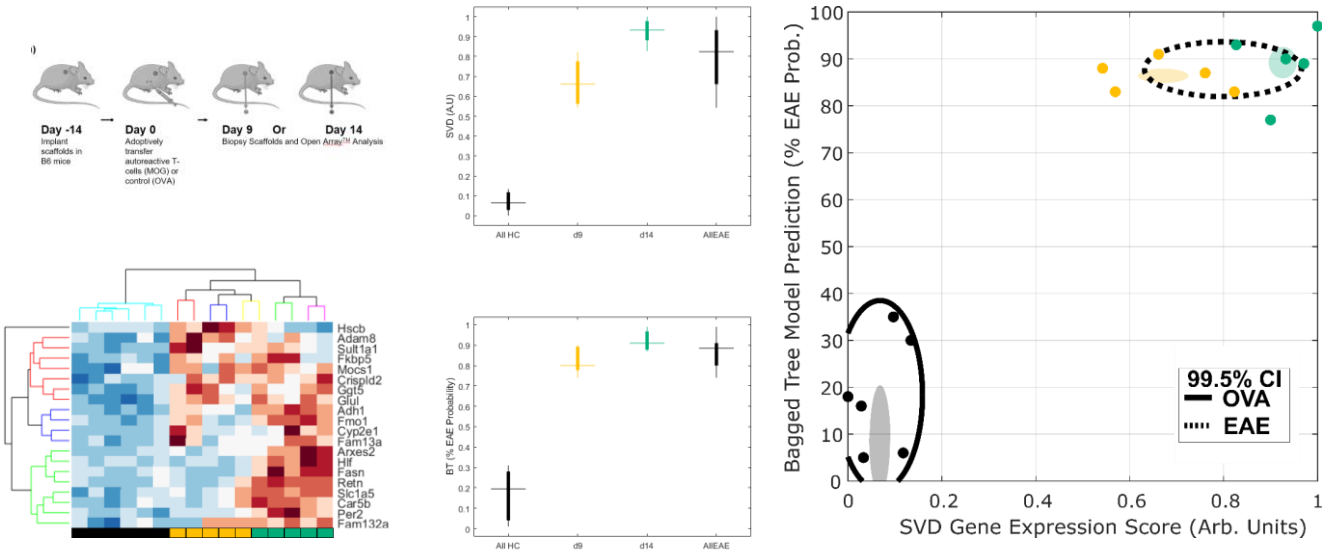


Figure A.2 Implantable scaffold gene expression changes enables scoring and segmenting of diseased and healthy during EAE onset. a) C57BL/6 mice were implanted with PCL scaffolds 14 days prior to adoptive transfer of T cells reactive to either $MOG_{(35-55)}$ (EAE) or $OVA_{323-339}$ (control). INs were subsequently removed at early disease (7 day - yellow) or late (9 day - green) time point for analysis via high-throughput qPCR (OpenArray). b) Heatmap and hierarchical clustering of 20 identified genes of interest, expression levels standardized by gene. e) Plot of the bagged tree (BT) prediction score versus SVD indicates separation between groups. Black lines indicate 99.9% confidence intervals for pooled diseased or control mice. Filled ovals indicate mean (centroid) and standard error of the mean for each indicated group. Each point is from an individual mouse and increasing point size indicates sicker mice (as an average of the day of explant and day after). Mouse cartoon from Servier image bank, https://servier.com/Powerpoint-image-bank.

After demonstrating that disease progression can be monitored by subcutaneous implantation, we next investigated whether response to therapy can be similarly evaluated. Mice received subcutaneous PCL implants and PLG(MOG_{35-55}) therapy on Days 2, 7, or 9 after disease induction. As expected, early delivery of therapy resulted in improved clinical outcomes.

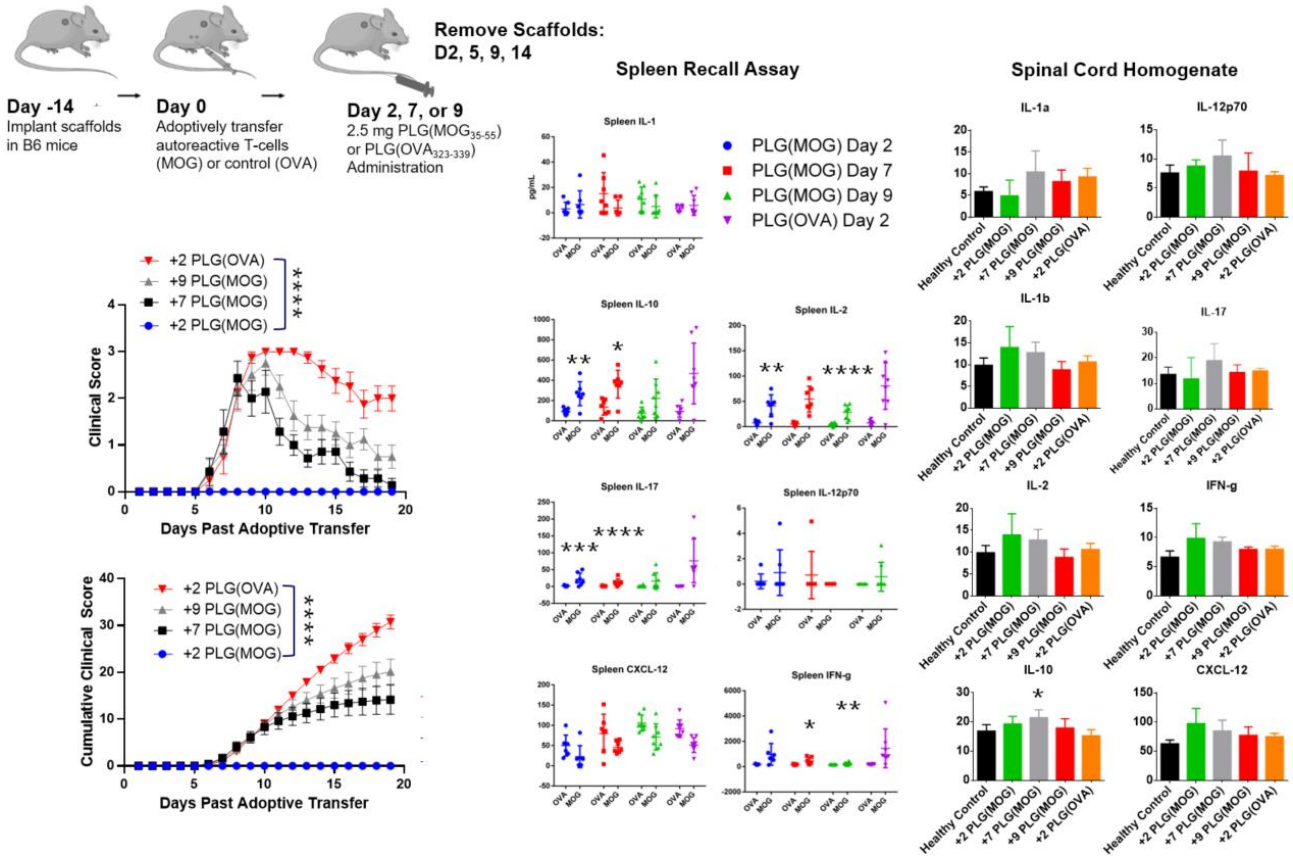


Figure A.3 Treatment of PP EAE with PLG(MOG_{35-55}) provides clinical protection with disease associated with reduced cytokine secretion from plate splenic cells. a) C57BL/6 mice were implanted with PCL scaffolds 14 days prior to adoptive transfer of T cells reactive to either $MOG_{(35-55)}$ (EAE) or $OVA_{323-339}$ (control). INs were subsequently removed at various time points for analysis via Taqman PCR probes. b) Early administration of PLG(MOG_{35-55}) results in improved clinical outcomes. c) Spleens were harvested and plated in 96 well format for stimulation by exposure to $OVA_{323-339}$ or MOG_{35-55} prior to ELISA-based measurement of cytokine production. d) Spinal cords from mice were collected at the conclusion of the study, homogenized, and analyzed by ELISA for cytokine expression within tissue. Mouse cartoon from Servier image bank, https://servier.com/Powerpoint-image-bank.

Evaluation of cytokine secretion of spleen cells was conducted to identify possible mechanisms of PLG(MOG_{35-55}) efficacy and provide insights related to the use of an immunological niche in this setting. Interestingly, ELISA-based cytokine analysis of spinal cord homogenates demonstrated few changes in cytokine expression at the experiment conclusion.

Investigation of PLG NP efficacy in murine model of egg allergy

Previously, we have demonstrated the ability to prevent and treat multiple murine models of peanut allergy. Models of peanut allergy are particularly relevant given the widespread incidence of the allergy and its relatively high risk of lethal anphylaxis; however, they are limited by the variable anaphylactic response in the model and the lack of transgenic models available to study the disease. Here, we investigate therapeutic delivery of ovalbumin (OVA) by PLG NPs (PLG(OVA)) to enable more nuanced studies of mechanistic efficacy.

Materials and Methods:

Ovalbumin (Sigma, Grade V) was used for all intraperitoneal immunizations. For intragastric challenge, ovalbumin was solubilized in PBS and concentrated using a 40,000 MWCO centricon filter unit. Aluminum hydroxide (alum; alhydrogel) was purchased from InvivoGen (San Diego, Calif). PLG (50:50) with a single carboxylic acid end group and an inherent viscosity of 0.17 dL/g in hexafluoro-2-propanol was purchased from Lactel Absorbable Polymers. Poly(ethylene-alt-maleic anhydride) (PEMA) was purchased from Polyscience. Chromogenic LAL endotoxin quantitation kit was purchased from Thermofisher Scientific**.** All other reagents were purchased from Sigma Aldrich unless noted otherwise.

Synthesis of PLG(Greer) nanoparticles:

Greer extract was encapsulated with 50:50 PLG polymer following protocols previously described [299]. Briefly, 150µL of 50mg/mL of protein (ovalbumin or Greer Peanut Extract) was encapsulated in 20% w/v PLG in dichloromethane with PEMA surfactant and allowed to evaporate. Particles were washed three times by centrifugation (5,000xg, 5 minutes, 4°C) prior to freezing and lyophilization with 4% w/v sucrose and 3% w/v mannitol. Carbodiimide chemistry was utilized for conjugation of peanut extract as previously described for other protein [321].

Briefly, solvent evaporation particles were synthesized without incorporation of antigen as described above and were similarly washed and lyophilized. Particles were washed three times with MilliQ water prior to incubation of particles and EDC at 50mg/mL and 20mg/mL, respectively. To achieve varied loadings of surface-exposed antigen, peanut extract was incubated after activation of PLG with EDC at concentrations of 1mg/mL, 2 mg/mL, or 4mg/mL in PBS.

Nanoparticle Characterization

The size, polydispersity, and zeta potential of the NPs were determined by dynamic light scattering (DLS) by mixing 10 mL of a 25 mg/mL particle solution into 990 mL of MilliQ water using a Malvern Zetasizer ZSP. The release of encapsulated antigen from particles was measured over 72 hr as previously descrbed[299]. Briefly, 8 mg of particle was dispersed in PBS and incubated at 37°C. At various timepoints particles were centrifuged at 7000g and 4°C for 5 min and supernatant was collected and stored at 20°C for measurement using the Micro BCA assay (Pierce). Lyophilized particles were washed with MilliQ water to remove the cryoprotectant.

Mice and immunizations

Schedules of immunizations are shown in the figures. Allergic sensitization was induced with intraperitoneal immunization of 20 mg of ovalbumin adsorbed on 2 mg alum Mice were challenged intragastrically with 20 mg of ovalbumin on 7 alternating days during the final 2 weeks of the studies. All animal procedures were performed according to the University of Michigan Institutional Animal Care and Use Committee and the National Institutes of Health ‘‘Guide for the care and use of laboratory animals.’’

Assessment of hypersensitivity reactions.

Reactions were evaluated for at least 1 hour after challenge by using the following scoring system (modified from Li et al[323] and Rodriguez et al[324]): 0, no symptoms; 0.5, transient rubbing and

scratching; 1, prolonged rubbing and scratching around the nose, eyes, or head; 2, puffiness around the eyes or mouth, diarrhea, piloerection, and/or decreased activity with increased respiratory rate; 3, labored respiration, wheezing, stridor, and/or cyanosis around the mouth and tail; 4, tremor, convulsion, no activity after prodding, and/or moribund; and 5, death. Rectal temperature was monitored for at least 60 minutes after challenge. Mice were bled 30 to 90 minutes after challenge, and serum mouse mast cell protease 1 (MCPT-1) levels were determined by using an ELISA (eBioscience).

Statistics

Statistical comparisons were assessed by using the Mann-Whitney test with GraphPad Prism software (version 6; GraphPad Software, La Jolla, Calif). A P value of less than .05 was considered significant.

Timing of therapeutic application of PLG(OVA) impacts efficacy.

It is expected that the timing of PLG NP delivery in murine models of food allergy are important in their efficacy. Mice were sensitized as previously described by i.p. injection of ovalbumin and alum on Days 0 and 14. Mice received either early treatment with PLG(OVA) or PBS or late treatment with PLG(OVA) as shown (Fig 1A). Mice were challenged oral beginning on Days 42 and received 7 total challenges. Interestingly, earlier administration of PLG(OVA) provided reduced incidence of diarrhea, an important anaphylactic outcome that is reflective of human disease.

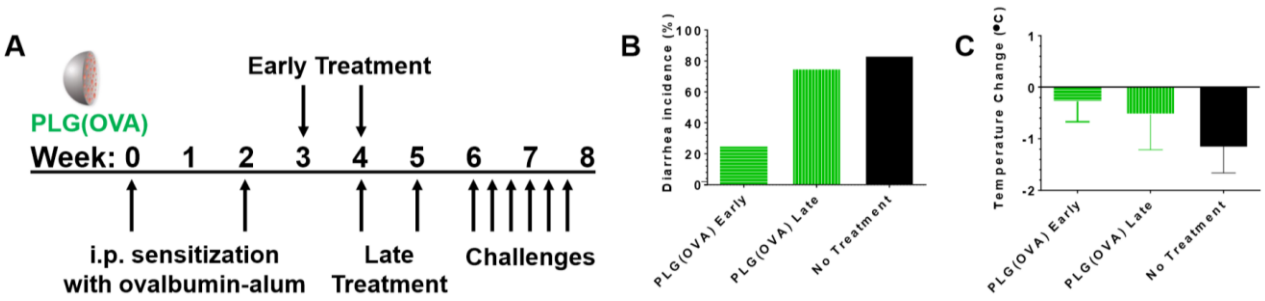


Figure A.4 Mice were sensitized by i.p. administration of alum-adsorbed ovalbumin protein on days 0 and 14. Mice received early (Day 21 and 28) or late (Day 28 and 35) treatment with PLG(OVA) (A). Mice were challenged by 6 oral administrations of ovalbumin on days 42, 44, 46, 49, 51, and 53 and assessed for anaphylactic response. Diarrhea incidence (B) and protection from anaphylactic temperature drop (C) suggest a trend towards protection with early administration of PLG(OVA).

Bibliography

[1] S. Bedoui, T. Gebhardt, G. Gasteiger, W. Kastenmüller, Parallels and differences between innate and adaptive lymphocytes, Nature immunology, 17 (2016) 490-494.
[2] L.L. Lanier, Shades of grey--the blurring view of innate and adaptive immunity.
[3] K.L. Hess, E. Oh, L.H. Tostanoski, J.I. Andorko, K. Susumu, J.R. Deschamps, I.L. Medintz, C.M. Jewell, Engineering Immunological Tolerance Using Quantum Dots to Tune the Density of Self-Antigen Display, Adv Funct Mater, 27 (2017).
[4] R.M. Pearson, J.R. Podojil, L.D. Shea, N.J.C. King, S.D. Miller, D.R. Getts, Overcoming challenges in treating autoimmuntity: Development of tolerogenic immune-modifying nanoparticles, Nanomedicine, 18 (2019) 282-291.
[5] O.S. Fenton, K.N. Olafson, P.S. Pillai, M.J. Mitchell, R. Langer, Advances in Biomaterials for Drug Delivery, Adv Mater, (2018) e1705328.
[6] J.C. Kaczmarek, K.J. Kauffman, O.S. Fenton, K. Sadtler, A.K. Patel, M.W. Heartlein, F. DeRosa, D.G. Anderson, Optimization of a Degradable Polymer-Lipid Nanoparticle for Potent Systemic Delivery of mRNA to the Lung Endothelium and Immune Cells, Nano Lett, 18 (2018) 6449-6454.
[7] X. Clemente-Casares, J. Blanco, P. Ambalavanan, J. Yamanouchi, S. Singha, C. Fandos, S. Tsai, J. Wang, N. Garabatos, C. Izquierdo, S. Agrawal, M.B. Keough, V.W. Yong, E. James, A. Moore, Y. Yang, T. Stratmann, P. Serra, P. Santamaria, Expanding antigen-specific regulatory networks to treat autoimmunity, Nature, 530 (2016) 434-440.
[8] P. Serra, P. Santamaria, Nanoparticle-based approaches to immune tolerance for the treatment of autoimmune diseases, Eur J Immunol, (2018).
[9] R.M. Pearson, L.M. Casey, K.R. Hughes, S.D. Miller, L.D. Shea, In vivo reprogramming of immune cells: technologies for induction of antigen-specific tolerance, Adv Drug Deliv Rev, (2017).
[10] Janeway's Immunobiology. Ninth Edition by Kenneth Murphy, Casey Weaver, Allan Mowat, Leslie Berg, David Chaplin, Charles A. Janeway, Paul Travers, and Mark Walport, The Quarterly Review of Biology, 93 (2018) 59-59.
[11] S.M. Hayter, M.C. Cook, Updated assessment of the prevalence, spectrum and case definition of autoimmune disease, Autoimmun Rev, 11 (2012) 754-765.
[12] S. Chandrashekara, The treatment strategies of autoimmune disease may need a different approach from conventional protocol: a review, Indian J Pharmacol, 44 (2012) 665-671.
[13] D.R. Chen, P.L. Cohen, Living life without B cells: is repeated B-cell depletion a safe and effective long-term treatment plan for rheumatoid arthritis?
[14] A.B. Memon, A. Javed, C. Caon, S. Srivastawa, F. Bao, E. Bernitsas, J. Chorostecki, A. Tselis, N. Seraji-Bozorgzad, O. Khan, Long-term safety of rituximab induced peripheral B-cell depletion in autoimmune neurological diseases, PLoS One, 13 (2018) e0190425.
[15] E.C. Lallana, C.E. Fadul, Toxicities of immunosuppressive treatment of autoimmune neurologic diseases, Curr Neuropharmacol, 9 (2011) 468-477.

[16] E. Saito, R. Kuo, K.R. Kramer, N. Gohel, D.A. Giles, B.B. Moore, S.D. Miller, L.D. Shea, Design of biodegradable nanoparticles to modulate phenotypes of antigen-presenting cells for antigen-specific treatment of autoimmune disease, Biomaterials, 222 (2019) 119432.
[17] F. Heymann, J. Peusquens, I. Ludwig-Portugall, M. Kohlhepp, C. Ergen, P. Niemietz, C. Martin, N. van Rooijen, J.C. Ochando, G.J. Randolph, T. Luedde, F. Ginhoux, C. Kurts, C. Trautwein, F. Tacke, Liver inflammation abrogates immunological tolerance induced by Kupffer cells, Hepatology, 62 (2015) 279-291.
[18] S. Baekkeskov, J.A. Hubbell, E.A. Phelps, Bioengineering strategies for inducing tolerance in autoimmune diabetes, Adv Drug Deliv Rev, 114 (2017) 256-265.
[19] A.J. Grimm, S. Kontos, G. Diaceri, X. Quaglia-Thermes, J.A. Hubbell, Memory of tolerance and induction of regulatory T cells by erythrocyte-targeted antigens, Sci Rep, 5 (2015) 15907.
[20] R.A. LaMothe, P.N. Kolte, T. Vo, J.D. Ferrari, T.C. Gelsinger, J. Wong, V.T. Chan, S. Ahmed, A. Srinivasan, P. Deitemeyer, R.A. Maldonado, T.K. Kishimoto, Tolerogenic Nanoparticles Induce Antigen-Specific Regulatory T Cells and Provide Therapeutic Efficacy and Transferrable Tolerance against Experimental Autoimmune Encephalomyelitis, Front Immunol, 9 (2018) 281.
[21] S. Keshavarz Shahbaz, F. Foroughi, E. Soltaninezhad, T. Jamialahmadi, P.E. Penson, A. Sahebkar, Application of PLGA nano/microparticle delivery systems for immunomodulation and prevention of allotransplant rejection, Expert Opin Drug Deliv, (2020) 1-14.
[22] G.M. Bell, A.E. Anderson, J. Diboll, R. Reece, O. Eltherington, R.A. Harry, T. Fouweather, C. MacDonald, T. Chadwick, E. McColl, J. Dunn, A.M. Dickinson, C.M. Hilkens, J.D. Isaacs, Autologous tolerogenic dendritic cells for rheumatoid and inflammatory arthritis, Ann Rheum Dis, 76 (2017) 227-234.
[23] A. Lutterotti, S. Yousef, A. Sputtek, K.H. Sturner, J.P. Stellmann, P. Breiden, S. Reinhardt, C. Schulze, M. Bester, C. Heesen, S. Schippling, S.D. Miller, M. Sospedra, R. Martin, Antigen-specific tolerance by autologous myelin peptide-coupled cells: a phase 1 trial in multiple sclerosis, Science translational medicine, 5 (2013) 188ra175. PMID: 23740901.
[24] P. Serra, P. Santamaria, Antigen-specific therapeutic approaches for autoimmunity, Nature Biotechnology, 37 (2019) 238-251.
[25] D.M. Richards, B. Kyewski, M. Feuerer, Re-examining the Nature and Function of Self-Reactive T cells, Trends in immunology, 37 (2016) 114-125.
[26] C.A. Akdis, M. Akdis, Mechanisms of immune tolerance to allergens: role of IL-10 and Tregs, The Journal of Clinical Investigation, 124 (2014) 4678-4680.
[27] Y. Gernez, A. Nowak-Węgrzyn, Immunotherapy for Food Allergy: Are We There Yet?, The Journal of Allergy and Clinical Immunology: In Practice, 5 (2017) 250-272.
[28] D.M. Fleischer, M. Greenhawt, G. Sussman, P. Bégin, A. Nowak-Wegrzyn, D. Petroni, K. Beyer, T. Brown-Whitehorn, J. Hebert, J.O.B. Hourihane, D.E. Campbell, S. Leonard, R.S. Chinthrajah, J.A. Pongracic, S.M. Jones, L. Lange, H. Chong, T.D. Green, R. Wood, A. Cheema, S.L. Prescott, P. Smith, W. Yang, E.S. Chan, A. Byrne, A. Assa'ad, J.A. Bird, E.H. Kim, L. Schneider, C.M. Davis, B.J. Lanser, R. Lambert, W. Shreffler, Effect of Epicutaneous Immunotherapy vs Placebo on Reaction to Peanut Protein Ingestion Among Children With Peanut Allergy: The PEPITES Randomized Clinical TrialEffect of Epicutaneous Immunotherapy vs Placebo on Reaction to Peanut Protein in Children With Peanut AllergyEffect of Epicutaneous Immunotherapy vs Placebo on Reaction to Peanut Protein in Children With Peanut Allergy, JAMA, 321 (2019) 946-955.

[29] C.A. Akdis, M. Akdis, Mechanisms of allergen-specific immunotherapy and immune tolerance to allergens, World Allergy Organization Journal, 8 (2015) 17.
[30] G. Cappellano, C. Comi, A. Chiocchetti, U. Dianzani, Exploiting PLGA-Based Biocompatible Nanoparticles for Next-Generation Tolerogenic Vaccines against Autoimmune Disease, Int J Mol Sci, 20 (2019).
[31] C.B. Smarr, W.T. Yap, T.P. Neef, R.M. Pearson, Z.N. Hunter, I. Ifergan, D.R. Getts, P.J. Bryce, L.D. Shea, S.D. Miller, Biodegradable antigen-associated PLG nanoparticles tolerize Th2-mediated allergic airway inflammation pre- and postsensitization, Proceedings of the National Academy of Sciences of the United States of America, 113 (2016) 5059-5064. PMID: 27091976.
[32] Q. Liu, X. Wang, X. Liu, S. Kumar, G. Gochman, Y. Ji, Y.P. Liao, C.H. Chang, W. Situ, J. Lu, J. Jiang, K.C. Mei, H. Meng, T. Xia, A.E. Nel, Use of Polymeric Nanoparticle Platform Targeting the Liver To Induce Treg-Mediated Antigen-Specific Immune Tolerance in a Pulmonary Allergen Sensitization Model, ACS Nano, 13 (2019) 4778-4794.
[33] E. Jensen-Jarolim, A.N. Jensen, G.W. Canonica, Debates in allergy medicine: Molecular allergy diagnosis with ISAC will replace screenings by skin prick test in the future, World Allergy Organization Journal, 10 (2017) 33.
[34] M.F. Bachmann, M.O. Mohsen, M.F. Kramer, M.D. Heath, Vaccination against Allergy: A Paradigm Shift?, Trends Mol Med, 26 (2020) 357-368.
[35] J.H.Y. Siu, V. Surendrakumar, J.A. Richards, G.J. Pettigrew, T cell Allorecognition Pathways in Solid Organ Transplantation, Front Immunol, 9 (2018) 2548.
[36] E.I. Dijke, J.L. Platt, P. Blair, M.R. Clatworthy, J.K. Patel, A.G. Kfoury, M. Cascalho, B cells in transplantation, J Heart Lung Transplant, 35 (2016) 704-710.
[37] M.-L. Alegre, F.G. Lakkis, A.E. Morelli, Antigen Presentation in Transplantation, Trends in immunology, 37 (2016) 831-843.
[38] H. Huang, Y. Lu, T. Zhou, G. Gu, Q. Xia, Innate Immune Cells in Immune Tolerance After Liver Transplantation, Front Immunol, 9 (2018) 2401.
[39] C.M. Lin, R.G. Gill, Direct and indirect allograft recognition: pathways dictating graft rejection mechanisms, Curr Opin Organ Transplant, 21 (2016) 40-44.
[40] K. Patel, C. Atkinson, D. Tran, S.N. Nadig, Nanotechnological Approaches to Immunosuppression and Tolerance Induction, Curr Transplant Rep, 4 (2017) 159-168.
[41] J.D. Fisher, A.P. Acharya, S.R. Little, Micro and nanoparticle drug delivery systems for preventing allotransplant rejection, Clin Immunol, 160 (2015) 24-35.
[42] K.A. Shahzad, M. Naeem, L. Zhang, X. Wan, S. Song, W. Pei, C. Zhao, X. Jin, C. Shen, Design and Optimization of PLGA Particles to Deliver Immunomodulatory Drugs for the Prevention of Skin Allograft Rejection, Immunol Invest, (2019) 1-18.
[43] R.B. Birge, S. Boeltz, S. Kumar, J. Carlson, J. Wanderley, D. Calianese, M. Barcinski, R.A. Brekken, X. Huang, J.T. Hutchins, B. Freimark, C. Empig, J. Mercer, A.J. Schroit, G. Schett, M. Herrmann, Phosphatidylserine is a global immunosuppressive signal in efferocytosis, infectious disease, and cancer, Cell Death Differ, 23 (2016) 962-978.
[44] R.A. Roberts, T.K. Eitas, J.D. Byrne, B.M. Johnson, P.J. Short, K.P. McKinnon, S. Reisdorf, J.C. Luft, J.M. DeSimone, J.P. Ting, Towards programming immune tolerance through geometric manipulation of phosphatidylserine, Biomaterials, 72 (2015) 1-10.
[45] A. Yeste, M.C. Takenaka, I.D. Mascanfroni, M. Nadeau, J.E. Kenison, B. Patel, A.M. Tukpah, J.A. Babon, M. DeNicola, S.C. Kent, D. Pozo, F.J. Quintana, Tolerogenic nanoparticles inhibit T cell-mediated autoimmunity through SOCS2.

[46] J.K. Park, T. Utsumi, Y.E. Seo, Y. Deng, A. Satoh, W.M. Saltzman, Y. Iwakiri, Cellular distribution of injected PLGA-nanoparticles in the liver, Nanomedicine, 12 (2016) 1365-1374.
[47] G. Benichou, B. Gonzalez, J. Marino, K. Ayasoufi, A. Valujskikh, Role of Memory T Cells in Allograft Rejection and Tolerance, Front Immunol, 8 (2017) 170.
[48] Y. Zhang, S. Shen, G. Zhao, C.F. Xu, H.B. Zhang, Y.L. Luo, Z.T. Cao, J. Shi, Z.B. Zhao, Z.X. Lian, J. Wang, In situ repurposing of dendritic cells with CRISPR/Cas9-based nanomedicine to induce transplant tolerance, Biomaterials, 217 (2019) 119302.
[49] X. Luo, S.D. Miller, L.D. Shea, Immune Tolerance for Autoimmune Disease and Cell Transplantation, Annu Rev Biomed Eng, 18 (2016) 181-205.
[50] K. Nazimek, K. Bryniarski, Approaches to inducing antigen-specific immune tolerance in allergy and autoimmunity: Focus on antigen-presenting cells and extracellular vesicles, Scand J Immunol, (2020).
[51] Z. Shen, A. Fisher, W.K. Liu, Y. Li, 1 - PEGylated "stealth" nanoparticles and liposomes, in: A. Parambath (Ed.) Engineering of Biomaterials for Drug Delivery Systems, Woodhead Publishing2018, pp. 1-26.
[52] D. Rosenblum, N. Joshi, W. Tao, J.M. Karp, D. Peer, Progress and challenges towards targeted delivery of cancer therapeutics, Nat Commun, 9 (2018) 1410.
[53] M. Korsgren, M. Andersson, L. Larsson, M. Aldén-Raboisson, L. Greiff, Onset of action of a topical antihistamine as assessed by histamine challenge-induced plasma exudation responses, Annals of Allergy, Asthma & Immunology, 96 (2006) 345-348.
[54] P.J. Gaillard, C.C. Appeldoorn, J. Rip, R. Dorland, S.M. van der Pol, G. Kooij, H.E. de Vries, A. Reijerkerk, Enhanced brain delivery of liposomal methylprednisolone improved therapeutic efficacy in a model of neuroinflammation, J Control Release, 164 (2012) 364-369.
[55] D. Maussang, J. Rip, J. van Kregten, A. van den Heuvel, S. van der Pol, B. van der Boom, A. Reijerkerk, L. Chen, M. de Boer, P. Gaillard, H. de Vries, Glutathione conjugation dose-dependently increases brain-specific liposomal drug delivery in vitro and in vivo, Drug Discov Today Technol, 20 (2016) 59-69.
[56] K.M.S. Kanhai, R. Zuiker, I. Stavrakaki, W. Gladdines, P.J. Gaillard, E.S. Klaassen, G.J. Groeneveld, Glutathione-PEGylated liposomal methylprednisolone in comparison to free methylprednisolone: slow release characteristics and prolonged lymphocyte depression in a first-in-human study, Br J Clin Pharmacol, 84 (2018) 1020-1028.
[57] A. Iacono, M. Wijesinha, K. Rajagopal, N. Murdock, I. Timofte, B. Griffith, M. Terrin, A randomised single-centre trial of inhaled liposomal cyclosporine for bronchiolitis obliterans syndrome post-lung transplantation, ERJ Open Res, 5 (2019).
[58] G.T. Jennings, M.F. Bachmann, The coming of age of virus-like particle vaccines, Biol Chem, 389 (2008) 521-536.
[59] T.M. Kundig, G. Senti, G. Schnetzler, C. Wolf, B.M. Prinz Vavricka, A. Fulurija, F. Hennecke, K. Sladko, G.T. Jennings, M.F. Bachmann, Der p 1 peptide on virus-like particles is safe and highly immunogenic in healthy adults, J Allergy Clin Immunol, 117 (2006) 1470-1476.
[60] G. Senti, P. Johansen, S. Haug, C. Bull, C. Gottschaller, P. Muller, T. Pfister, P. Maurer, M.F. Bachmann, N. Graf, T.M. Kundig, Use of A-type CpG oligodeoxynucleotides as an adjuvant in allergen-specific immunotherapy in humans: a phase I/IIa clinical trial, Clin Exp Allergy, 39 (2009) 562-570.
[61] L. Klimek, J. Willers, A. Hammann-Haenni, O. Pfaar, H. Stocker, P. Mueller, W.A. Renner, M.F. Bachmann, Assessment of clinical efficacy of CYT003-QbG10 in patients with allergic rhinoconjunctivitis: a phase IIb study, Clin Exp Allergy, 41 (2011) 1305-1312.

[62] K.M. Beeh, F. Kanniess, F. Wagner, C. Schilder, I. Naudts, A. Hammann-Haenni, J. Willers, H. Stocker, P. Mueller, M.F. Bachmann, W.A. Renner, The novel TLR-9 agonist QbG10 shows clinical efficacy in persistent allergic asthma, J Allergy Clin Immunol, 131 (2013) 866-874.
[63] S.L. Thrower, L. James, W. Hall, K.M. Green, S. Arif, J.S. Allen, C. Van-Krinks, B. Lozanoska-Ochser, L. Marquesini, S. Brown, F.S. Wong, C.M. Dayan, M. Peakman, Proinsulin peptide immunotherapy in type 1 diabetes: report of a first-in-man Phase I safety study, Clin Exp Immunol, 155 (2009) 156-165.
[64] M. Alhadj Ali, Y.-F. Liu, S. Arif, D. Tatovic, H. Shariff, V.B. Gibson, N. Yusuf, R. Baptista, M. Eichmann, N. Petrov, S. Heck, J.H.M. Yang, T.I.M. Tree, I. Pujol-Autonell, L. Yeo, L.R. Baumard, R. Stenson, A. Howell, A. Clark, Z. Boult, J. Powrie, L. Adams, F.S. Wong, S. Luzio, G. Dunseath, K. Green, A. O'Keefe, G. Bayly, N. Thorogood, R. Andrews, N. Leech, F. Joseph, S. Nair, S. Seal, H. Cheung, C. Beam, R. Hills, M. Peakman, C.M. Dayan, Metabolic and immune effects of immunotherapy with proinsulin peptide in human new-onset type 1 diabetes, Science Translational Medicine, 9 (2017) eaaf7779.
[65] M. Dul, T. Nikolic, M. Stefanidou, M.A. McAteer, P. Williams, J. Mous, B.O. Roep, E. Kochba, Y. Levin, M. Peakman, F.S. Wong, C.M. Dayan, D. Tatovic, S.A. Coulman, J.C. Birchall, E.-A. Consortium, Conjugation of a peptide autoantigen to gold nanoparticles for intradermally administered antigen specific immunotherapy, Int J Pharm, 562 (2019) 303-312.
[66] S.R.J. De, J.M. Irache, A.I. Camacho, G. Gastaminza, M.L. Sanz, M. Ferrer, C. Gamazo, Immunogenicity of peanut proteins containing poly(anhydride) nanoparticles, Clin Vaccine Immunol, 21 (2014) 1106-1112.
[67] A. Brotons-Canto, C. Gamazo, N. Martin-Arbella, M. Abdulkarim, J. Matias, M. Gumbleton, J.M. Irache, Evaluation of nanoparticles as oral vehicles for immunotherapy against experimental peanut allergy, Int J Biol Macromol, 110 (2018) 328-335.
[68] E.R. Gamazon, H.E. Wheeler, K.P. Shah, S.V. Mozaffari, K. Aquino-Michaels, R.J. Carroll, A.E. Eyler, J.C. Denny, G.T. Consortium, D.L. Nicolae, N.J. Cox, H.K. Im, A gene-based association method for mapping traits using reference transcriptome data, Nat Genet, 47 (2015) 1091-1098.
[69] R.A. Maldonado, R.A. LaMothe, J.D. Ferrari, A.H. Zhang, R.J. Rossi, P.N. Kolte, A.P. Griset, C. O'Neil, D.H. Altreuter, E. Browning, L. Johnston, O.C. Farokhzad, R. Langer, D.W. Scott, U.H. von Andrian, T.K. Kishimoto, Polymeric synthetic nanoparticles for the induction of antigen-specific immunological tolerance, Proc Natl Acad Sci U S A, 112 (2015) E156-165.
[70] T.K. Kishimoto, J.D. Ferrari, R.A. LaMothe, P.N. Kolte, A.P. Griset, C. O'Neil, V. Chan, E. Browning, A. Chalishazar, W. Kuhlman, F.-n. Fu, N. Viseux, D.H. Altreuter, L. Johnston, R.A. Maldonado, Improving the efficacy and safety of biologic drugs with tolerogenic nanoparticles, Nature Nanotechnology, 11 (2016) 890-899.
[71] A. Meliani, F. Boisgerault, R. Hardet, S. Marmier, F. Collaud, G. Ronzitti, C. Leborgne, H. Costa Verdera, M. Simon Sola, S. Charles, A. Vignaud, L. van Wittenberghe, G. Manni, O. Christophe, F. Fallarino, C. Roy, A. Michaud, P. Ilyinskii, T.K. Kishimoto, F. Mingozzi, Antigen-selective modulation of AAV immunogenicity with tolerogenic rapamycin nanoparticles enables successful vector re-administration, Nat Commun, 9 (2018) 4098.
[72] J. Bryant, K.A. Hlavaty, X. Zhang, W.T. Yap, L. Zhang, L.D. Shea, X. Luo, Nanoparticle delivery of donor antigens for transplant tolerance in allogeneic islet transplantation, Biomaterials, 35 (2014) 8887-8894.
[73] D.R. Getts, A.J. Martin, D.P. McCarthy, R.L. Terry, Z.N. Hunter, W.T. Yap, M.T. Getts, M. Pleiss, X. Luo, N.J. King, L.D. Shea, S.D. Miller, Microparticles bearing encephalitogenic

peptides induce T-cell tolerance and ameliorate experimental autoimmune encephalomyelitis, Nature Biotechnology, 30 (2012) 1217-1224.
[74] R. Kuo, E. Saito, S.D. Miller, L.D. Shea, Peptide-Conjugated Nanoparticles Reduce Positive Co-stimulatory Expression and T Cell Activity to Induce Tolerance, Mol Ther, 25 (2017) 1676-1685.
[75] R.M. Pearson, L.M. Casey, K.R. Hughes, S.D. Miller, L.D. Shea, In vivo reprogramming of immune cells: Technologies for induction of antigen-specific tolerance, Adv Drug Deliv Rev, 114 (2017) 240-255.
[76] S. Prasad, T. Neef, D. Xu, J.R. Podojil, D.R. Getts, L.D. Shea, S.D. Miller, Tolerogenic Ag-PLG nanoparticles induce tregs to suppress activated diabetogenic CD4 and CD8 T cells, J Autoimmun, 89 (2018) 112-124.
[77] T.L. Freitag, J.R. Podojil, R.M. Pearson, F.J. Fokta, C. Sahl, M. Messing, L.C. Andersson, K. Leskinen, P. Saavalainen, L.I. Hoover, K. Huang, D. Phippard, S. Maleki, N.J.C. King, L.D. Shea, S.D. Miller, S.K. Meri, D.R. Getts, Gliadin Nanoparticles Induce Immune Tolerance to Gliadin in Mouse Models of Celiac Disease, Gastroenterology, 158 (2020) 1667-1681 e1612.
[78] C. Tur, M. Moccia, F. Barkhof, J. Chataway, J. Sastre-Garriga, A.J. Thompson, O. Ciccarelli, Assessing treatment outcomes in multiple sclerosis trials and in the clinical setting, Nat Rev Neurol, 14 (2018) 75-93.
[79] B.O. Roep, Autoreactive T cells in endocrine/organ-specific autoimmunity: why has progress been so slow?, Springer Semin Immunopathol, 24 (2002) 261-271.
[80] T.N. Seyfried, L.C. Huysentruyt, On the origin of cancer metastasis, Critical Reviews in Oncogenesis, 18 (2013) 43-73.
[81] M. Ma, H. Zhu, C. Zhang, X. Sun, X. Gao, G. Chen, "Liquid biopsy"-ctDNA detection with great potential and challenges, Ann Transl Med, 3 (2015) 235-235.
[82] M. Poudineh, E.H. Sargent, K. Pantel, S.O. Kelley, Profiling circulating tumour cells and other biomarkers of invasive cancers, Nat Biomed Eng, 2 (2018) 72-84.
[83] Y.H. Soung, S. Ford, V. Zhang, J. Chung, Exosomes in Cancer Diagnostics, Cancers (Basel), 9 (2017).
[84] A.H. Morris, S.M. Orbach, G.G. Bushnell, R.S. Oakes, J.S. Jeruss, L.D. Shea, Engineered Niches to Analyze Mechanisms of Metastasis and Guide Precision Medicine, Cancer Research, (Accepted 2020).
[85] C. Fiala, E.P. Diamandis, Utility of circulating tumor DNA in cancer diagnostics with emphasis on early detection, BMC Med, 16 (2018) 166.
[86] S.S. Rao, G.G. Bushnell, S.M. Azarin, G. Spicer, B.A. Aguado, J.R. Stoehr, E.J. Jiang, V. Backman, L.D. Shea, J.S. Jeruss, Enhanced Survival with Implantable Scaffolds That Capture Metastatic Breast Cancer Cells In Vivo, Cancer Research, 76 (2016) 5209-5218.
[87] S.M. Azarin, J. Yi, R.M. Gower, B.A. Aguado, M.E. Sullivan, A.G. Goodman, E.J. Jiang, S.S. Rao, Y. Ren, S.L. Tucker, V. Backman, J.S. Jeruss, L.D. Shea, In vivo capture and label-free detection of early metastatic cells, Nat Commun, 6 (2015) 8094.
[88] G.G. Bushnell, X. Hong, R.M. Hartfield, Y. Zhang, R.S. Oakes, S.S. Rao, J.S. Jeruss, J.P. Stegemann, C.X. Deng, L.D. Shea, High Frequency Spectral Ultrasound Imaging to Detect Metastasis in Implanted Biomaterial Scaffolds, Ann Biomed Eng, (2019).
[89] G.L.C. Spicer, S.M. Azarin, J. Yi, L.D. Shea, V. Backman, Detection of extracellular matrix modification in cancer models with inverse spectroscopic optical coherence tomography Detection of extracellular matrix modification in cancer models with inverse spectroscopic optical coherence tomography, Physics in Medicine & Biology, (2019).

[90] R.S. Oakes, G.G. Bushnell, S.M. Orbach, P. Kandagatla, Y. Zhang, A.H. Morris, M.S. Hall, P. LaFaire, J.T. Decker, R.M. Hartfield, M.D. Brooks, M.S. Wicha, J.S. Jeruss, L.D. Shea, Metastatic Conditioning of Myeloid Cells at a Subcutaneous Synthetic Niche Reflects Disease Progression and Predicts Therapeutic Outcomes, Cancer Res, 80 (2020) 602-612.
[91] M.A. Thelin, S. Kissler, F. Vigneault, A.L. Watters, D. White, S.T. Koshy, S.A. Vermillion, D.J. Mooney, T. Serwold, O.A. Ali, In Vivo Enrichment of Diabetogenic T Cells, Diabetes, 66 (2017) 2220-2229.
[92] J.D. Griffin, J.Y. Song, A. Huang, A.R. Sedlacek, K.L. Flannagan, C.J. Berkland, Antigen-specific immune decoys intercept and exhaust autoimmunity to prevent disease, Biomaterials, 222 (2019) 119440.
[93] J.-F. Bach, The Effect of Infections on Susceptibility to Autoimmune and Allergic Diseases, New England Journal of Medicine, 347 (2002) 911-920.
[94] M.K. Jenkins, R.H. Schwartz, Antigen presentation by chemically modified splenocytes induces antigen-specific T cell unresponsiveness in vitro and in vivo, The Journal of experimental medicine, 165 (1987) 302-319.
[95] T. Kheradmand, S. Wang, J. Bryant, J.J. Tasch, N. Lerret, K.L. Pothoven, J.L. Houlihan, S.D. Miller, Z.J. Zhang, X. Luo, Ethylenecarbodiimide-fixed donor splenocyte infusions differentially target direct and indirect pathways of allorecognition for induction of transplant tolerance, J Immunol, 189 (2012) 804-812. PMID: 22696445.
[96] T. Kheradmand, S. Wang, R.F. Gibly, X. Zhang, S. Holland, J. Tasch, J.G. Graham, D.B. Kaufman, S.D. Miller, L.D. Shea, Permanent protection of PLG scaffold transplanted allogeneic islet grafts in diabetic mice treated with ECDI-fixed donor splenocyte infusions, Biomaterials, 32 (2011) 4517-4524.
[97] X.R. Luo, K.L. Pothoven, D. McCarthy, M. DeGutes, A. Martin, D.R. Gettss, G. Xia, J. He, X.M. Zhang, D.B. Kaufman, S.D. Miller, ECDI-fixed allogeneic splenocytes induce donor-specific tolerance for long-term survival of islet transplants via two distinct mechanisms, Proceedings of the National Academy of Sciences of the United States of America, 105 (2008) 14527-14532.
[98] M.F. Bachmann, G.T. Jennings, Vaccine delivery: a matter of size, geometry, kinetics and molecular patterns, Nature Reviews Immunology, 10 (2010) 787-796.
[99] C. Kelly, J. Murray, D. Leffler, A. Bledsoe, G. Smithson, J. Podojil, R. First, A. Morris, M. Boyne, A. Elhofy, and S. Miller, CNP-101 prevents gluten challenge induced immune activation in adults with celiac disease, In United Eur. Gastroenterol. Week Conference, (2019).
[100] I.A. Parish, W.R. Heath, Too dangerous to ignore: self-tolerance and the control of ignorant autoreactive T cells, Immunology and Cell Biology, 86 (2008) 146-152.
[101] D.M. Richards, B. Kyewski, M. Feuerer, Re-examining the Nature and Function of Self-Reactive T cells, Trends in Immunology, 37 (2016) 114-125.
[102] S.D. Miller, D.M. Turley, J.R. Podojil, Antigen-specific tolerance strategies for the prevention and treatment of autoimmune disease, Nature Reviews Immunology, 7 (2007) 665-677.
[103] X. Luo, S.D. Miller, L.D. Shea, Immune Tolerance for Autoimmune Disease and Cell Transplantation, Annual review of biomedical engineering, 18 (2016) 181-205.
[104] A.Y. Peleg, S. Husain, E.J. Kwak, F.P. Silveira, M. Ndirangu, J. Tran, K.A. Shutt, R. Shapiro, N. Thai, K. Abu-Elmagd, Opportunistic infections in 547 organ transplant recipients receiving alemtuzumab, a humanized monoclonal CD-52 antibody, Clinical infectious diseases, 44 (2007) 204-212.

[105] L.H. Calabrese, N. Zein, D. Vassilopoulos, Hepatitis B virus (HBV) reactivation with immunosuppressive therapy in rheumatic diseases: assessment and preventive strategies, Annals of the rheumatic diseases, 65 (2006) 983-989.
[106] J. Adami, H. Gäbel, B. Lindelöf, K. Ekström, B. Rydh, B. Glimelius, A. Ekbom, H.-O. Adami, F. Granath, Cancer risk following organ transplantation: a nationwide cohort study in Sweden, British journal of cancer, 89 (2003) 1221-1227.
[107] A. Lerner, P. Jeremias, T. Matthias, The World Incidence and Prevalence of Autoimmune Diseases is Increasing, International Journal of Celiac Disease, 3 (2016) 151-155.
[108] E. Ingulli, Mechanism of cellular rejection in transplantation, Pediatr Nephrol, 25 (2010) 61-74.
[109] K.D. Stone, C. Prussin, D.D. Metcalfe, IgE, mast cells, basophils, and eosinophils, The Journal of allergy and clinical immunology, 125 (2010) S73-80.
[110] G.E. Kaiko, J.C. Horvat, K.W. Beagley, P.M. Hansbro, Immunological decision-making: how does the immune system decide to mount a helper T-cell response?, Immunology, 123 (2008) 326-338.
[111] M.Z. Atassi, P. Casali, Molecular mechanisms of autoimmunity, Autoimmunity, 41 (2008) 123-132.
[112] S. Sakaguchi, M. Ono, R. Setoguchi, H. Yagi, S. Hori, Z. Fehervari, J. Shimizu, T. Takahashi, T. Nomura, Foxp3(+)CD25(+)CD4(+) natural regulatory T cells in dominant self-tolerance and autoimmune disease, Immunol Rev, 212 (2006) 8-27.
[113] B. Bolon, Cellular and molecular mechanisms of autoimmune disease, Toxicologic pathology, 40 (2012) 216-229.
[114] D.H. Broide, Molecular and cellular mechanisms of allergic disease, Journal of Allergy and Clinical Immunology, 108 (2001) S65-S71.
[115] H.J. Gould, B.J. Sutton, IgE in allergy and asthma today, Nature Reviews Immunology, 8 (2008) 205-217.
[116] B. Priyadharshini, D.L. Greiner, M.A. Brehm, T-cell activation and transplantation tolerance, Transplantation reviews, 26 (2012) 212-222.
[117] J.R. Podojil, S.D. Miller, Molecular mechanisms of T-cell receptor and costimulatory molecule ligation/blockade in autoimmune disease therapy, Immunol Rev, 229 (2009) 337-355.
[118] Y. Xing, K.A. Hogquist, T-cell tolerance: central and peripheral, Cold Spring Harbor perspectives in biology, 4 (2012) a006957.
[119] S.M. Anderton, D.C. Wraith, Selection and fine-tuning of the autoimmune T-cell repertoire, Nature Reviews Immunology, 2 (2002) 487-498.
[120] J.M. Curtsinger, M.F. Mescher, Inflammatory cytokines as a third signal for T cell activation, Curr Opin Immunol, 22 (2010) 333-340.
[121] L. Chen, D.B. Flies, Molecular mechanisms of T cell co-stimulation and co-inhibition, Nature Reviews Immunology, 13 (2013) 227-242.
[122] F.A. Schildberg, S.R. Klein, G.J. Freeman, A.H. Sharpe, Coinhibitory Pathways in the B7-CD28 Ligand-Receptor Family, Immunity, 44 (2016) 955-972.
[123] A.H. Sharpe, Mechanisms of costimulation, Immunol Rev, 229 (2009) 5-11.
[124] S.L. Fink, B.T. Cookson, Apoptosis, pyroptosis, and necrosis: mechanistic description of dead and dying eukaryotic cells, Infect Immun, 73 (2005) 1907-1916.
[125] Y. Lu, S. Xu, H. Chen, M. He, Y. Deng, Z. Cao, H. Pi, C. Chen, M. Li, Q. Ma, P. Gao, Y. Ji, L. Zhang, Z. Yu, Z. Zhou, CdSe/ZnS quantum dots induce hepatocyte pyroptosis and liver inflammation via NLRP3 inflammasome activation, Biomaterials, 90 (2016) 27-39.

[126] A. Hochreiter-Hufford, K.S. Ravichandran, Clearing the dead: apoptotic cell sensing, recognition, engulfment, and digestion, Cold Spring Harbor perspectives in biology, 5 (2013) a008748.
[127] S. Nagata, R. Hanayama, K. Kawane, Autoimmunity and the clearance of dead cells, Cell, 140 (2010) 619-630.
[128] P.A. Leventis, S. Grinstein, The distribution and function of phosphatidylserine in cellular membranes, Annual review of biophysics, 39 (2010) 407-427.
[129] R.B. Birge, S. Boeltz, S. Kumar, J. Carlson, J. Wanderley, D. Calianese, M. Barcinski, R.A. Brekken, X. Huang, J.T. Hutchins, B. Freimark, C. Empig, J. Mercer, A.J. Schroit, G. Schett, M. Herrmann, Phosphatidylserine is a global immunosuppressive signal in efferocytosis, infectious disease, and cancer, Cell death and differentiation, 23 (2016) 962-978.
[130] C.V. Rothlin, S. Ghosh, E.I. Zuniga, M.B. Oldstone, G. Lemke, TAM receptors are pleiotropic inhibitors of the innate immune response, Cell, 131 (2007) 1124-1136.
[131] G. Lemke, T. Burstyn-Cohen, TAM receptors and the clearance of apoptotic cells, Annals of the New York Academy of Sciences, 1209 (2010) 23-29.
[132] L.M. Francisco, P.T. Sage, A.H. Sharpe, The PD-1 pathway in tolerance and autoimmunity, Immunol Rev, 236 (2010) 219-242.
[133] J. He, Y. Hu, M. Hu, B. Li, Development of PD-1/PD-L1 Pathway in Tumor Immune Microenvironment and Treatment for Non-Small Cell Lung Cancer, Scientific Reports, 5 (2015) 13110.
[134] T. Okazaki, S. Chikuma, Y. Iwai, S. Fagarasan, T. Honjo, A rheostat for immune responses: the unique properties of PD-1 and their advantages for clinical application, Nature Immunology, 14 (2013) 1212-1218.
[135] L.T. Nguyen, P.S. Ohashi, Clinical blockade of PD1 and LAG3--potential mechanisms of action, Nature Reviews Immunology, 15 (2015) 45-56.
[136] G. Raposo, W. Stoorvogel, Extracellular vesicles: exosomes, microvesicles, and friends, The Journal of cell biology, 200 (2013) 373-383.
[137] M.F. Ribeiro, H. Zhu, R.W. Millard, G.C. Fan, Exosomes Function in Pro- and Anti-Angiogenesis, Current angiogenesis, 2 (2013) 54-59.
[138] T.A. Chatila, C.B. Williams, Regulatory T cells: exosomes deliver tolerance, Immunity, 41 (2014) 3-5.
[139] I.S. Okoye, S.M. Coomes, V.S. Pelly, S. Czieso, V. Papayannopoulos, T. Tolmachova, M.C. Seabra, M.S. Wilson, MicroRNA-containing T-regulatory-cell-derived exosomes suppress pathogenic T helper 1 cells, Immunity, 41 (2014) 89-103.
[140] A. Agarwal, G. Fanelli, M. Letizia, S.L. Tung, D. Boardman, R. Lechler, G. Lombardi, L.A. Smyth, Regulatory T cell-derived exosomes: possible therapeutic and diagnostic tools in transplantation, Front Immunol, 5 (2014) 555.
[141] R.A. Maldonado, U.H. von Andrian, Chapter 4 - How Tolerogenic Dendritic Cells Induce Regulatory T Cells, in: K.F.A.T.H.F.M.J.W.U. Frederick W. Alt, R.U. Emil (Eds.) Advances in Immunology, Academic Press2010, pp. 111-165.
[142] A. Ten Brinke, C.M.U. Hilkens, N. Cools, E.K. Geissler, J.A. Hutchinson, G. Lombardi, P. Lord, B. Sawitzki, P. Trzonkowski, S.M. Van Ham, E.M. Martinez-Caceres, Clinical Use of Tolerogenic Dendritic Cells-Harmonization Approach in European Collaborative Effort, Mediators of Inflammation, 2015 (2015) 8.
[143] C.M.U. Hilkens, J.D. Isaacs, Tolerogenic dendritic cell therapy for rheumatoid arthritis: where are we now?, Clinical & Experimental Immunology, 172 (2013) 148-157.

[144] T. Kheradmand, S. Wang, J. Bryant, J.J. Tasch, N. Lerret, K.L. Pothoven, J.L. Houlihan, S.D. Miller, Z.J. Zhang, X. Luo, Ethylenecarbodiimide-fixed donor splenocyte infusions differentially target direct and indirect pathways of allorecognition for induction of transplant tolerance, The Journal of Immunology, 189 (2012) 804-812.
[145] X. Luo, K.L. Pothoven, D. McCarthy, M. DeGutes, A. Martin, D.R. Getts, G. Xia, J. He, X. Zhang, D.B. Kaufman, S.D. Miller, ECDI-fixed allogeneic splenocytes induce donor-specific tolerance for long-term survival of islet transplants via two distinct mechanisms, Proceedings of the National Academy of Sciences of the United States of America, 105 (2008) 14527-14532.
[146] S. Kontos, I.C. Kourtis, K.Y. Dane, J.A. Hubbell, Engineering antigens for in situ erythrocyte binding induces T-cell deletion, Proceedings of the National Academy of Sciences, 110 (2013) E60-E68.
[147] K.A. Hlavaty, D.P. McCarthy, E. Saito, W.T. Yap, S.D. Miller, L.D. Shea, Tolerance induction using nanoparticles bearing HY peptides in bone marrow transplantation, Biomaterials, 76 (2016) 1-10. PMID: 26513216.
[148] G.M. Bell, A.E. Anderson, J. Diboll, R. Reece, O. Eltherington, R.A. Harry, T. Fouweather, C. MacDonald, T. Chadwick, E. McColl, J. Dunn, A.M. Dickinson, C.M.U. Hilkens, J.D. Isaacs, Autologous tolerogenic dendritic cells for rheumatoid and inflammatory arthritis, Annals of the Rheumatic Diseases, 76 (2017) 227-234.
[149] A. Lutterotti, S. Yousef, A. Sputtek, K.H. Sturner, J.P. Stellmann, P. Breiden, S. Reinhardt, C. Schulze, M. Bester, C. Heesen, S. Schippling, S.D. Miller, M. Sospedra, R. Martin, Antigen-specific tolerance by autologous myelin peptide-coupled cells: a phase 1 trial in multiple sclerosis, Science translational medicine, 5 (2013) 188ra175.
[150] A.J. Grimm, S. Kontos, G. Diaceri, X. Quaglia-Thermes, J.A. Hubbell, Memory of tolerance and induction of regulatory T cells by erythrocyte-targeted antigens, Scientific Reports, 5 (2015) 15907.
[151] D.R. Getts, L.D. Shea, S.D. Miller, N.J. King, Harnessing nanoparticles for immune modulation, Trends in immunology, 36 (2015) 419-427.
[152] R.M. Pearson, H.-j. Hsu, J. Bugno, S. Hong, Understanding nano-bio interactions to improve nanocarriers for drug delivery, MRS Bulletin, 39 (2014) 227-237.
[153] Q. Jiao, L. Li, Q. Mu, Q. Zhang, Immunomodulation of nanoparticles in nanomedicine applications, BioMed research international, 2014 (2014) 426028.
[154] D.M. Smith, J.K. Simon, J.R. Baker, Jr., Applications of nanotechnology for immunology, Nature Reviews Immunology, 13 (2013) 592-605.
[155] R.M. Pearson, V. Juettner, S. Hong, Biomolecular Corona on Nanoparticles: A Survey of Recent Literature and its Implications in Targeted Drug Delivery, Frontiers in Chemistry, 2 (2014).
[156] F. Leuschner, P. Dutta, R. Gorbatov, T.I. Novobrantseva, J.S. Donahoe, G. Courties, K.M. Lee, J.I. Kim, J.F. Markmann, B. Marinelli, P. Panizzi, W.W. Lee, Y. Iwamoto, S. Milstein, H. Epstein-Barash, W. Cantley, J. Wong, V. Cortez-Retamozo, A. Newton, K. Love, P. Libby, M.J. Pittet, F.K. Swirski, V. Koteliansky, R. Langer, R. Weissleder, D.G. Anderson, M. Nahrendorf, Therapeutic siRNA silencing in inflammatory monocytes in mice, Nature biotechnology, 29 (2011) 1005-1010.
[157] J.D. Fisher, A.P. Acharya, S.R. Little, Micro and nanoparticle drug delivery systems for preventing allotransplant rejection, Clinical immunology, 160 (2015) 24-35.
[158] K.A. Hlavaty, X. Luo, L.D. Shea, S.D. Miller, Cellular and molecular targeting for nanotherapeutics in transplantation tolerance, Clinical immunology, 160 (2015) 14-23.

[159] P. Serra, P. Santamaria, Nanoparticle-based autoimmune disease therapy, Clinical immunology, 160 (2015) 3-13.
[160] D.R. Getts, R.L. Terry, M.T. Getts, C. Deffrasnes, M. Muller, C. van Vreden, T.M. Ashhurst, B. Chami, D. McCarthy, H. Wu, J. Ma, A. Martin, L.D. Shae, P. Witting, G.S. Kansas, J. Kuhn, W. Hafezi, I.L. Campbell, D. Reilly, J. Say, L. Brown, M.Y. White, S.J. Cordwell, S.J. Chadban, E.B. Thorp, S. Bao, S.D. Miller, N.J. King, Therapeutic inflammatory monocyte modulation using immune-modifying microparticles, Science translational medicine, 6 (2014) 219ra217.
[161] D.R. Getts, A.J. Martin, D.P. McCarthy, R.L. Terry, Z.N. Hunter, W.T. Yap, M.T. Getts, M. Pleiss, X. Luo, N.J. King, L.D. Shea, S.D. Miller, Microparticles bearing encephalitogenic peptides induce T-cell tolerance and ameliorate experimental autoimmune encephalomyelitis, Nature biotechnology, 30 (2012) 1217-1224.
[162] R.A. Maldonado, R.A. LaMothe, J.D. Ferrari, A. Zhang, R.J. Rossi, P.N. Kolte, A.P. Griset, C. O'Neil, D.H. Altreuter, E. Browning, L. Johnston, O.C. Farokhzad, R. Langer, D.W. Scott, U.H. von Andrian, T.K. Kishimoto, Polymeric synthetic nanoparticles for the induction of antigen-specific immunological tolerance, Proceedings of the National Academy of Sciences, 112 (2015) E156-165.
[163] A. Yeste, M. Nadeau, E.J. Burns, H.L. Weiner, F.J. Quintana, Nanoparticle-mediated codelivery of myelin antigen and a tolerogenic small molecule suppresses experimental autoimmune encephalomyelitis, Proceedings of the National Academy of Sciences, 109 (2012) 11270-11275.
[164] G. Cappellano, A.D. Woldetsadik, E. Orilieri, Y. Shivakumar, M. Rizzi, F. Carniato, C.L. Gigliotti, E. Boggio, N. Clemente, C. Comi, C. Dianzani, R. Boldorini, A. Chiocchetti, F. Reno, U. Dianzani, Subcutaneous inverse vaccination with PLGA particles loaded with a MOG peptide and IL-10 decreases the severity of experimental autoimmune encephalomyelitis, Vaccine, 32 (2014) 5681-5689.
[165] A. Yeste, M.C. Takenaka, I.D. Mascanfroni, M. Nadeau, J.E. Kenison, B. Patel, A.-M. Tukpah, J.A.B. Babon, M. DeNicola, S.C. Kent, D. Pozo, F.J. Quintana, Tolerogenic nanoparticles inhibit T cell–mediated autoimmunity through SOCS2, Science Signaling, 9 (2016) ra61-ra61.
[166] A. Carambia, B. Freund, D. Schwinge, O.T. Bruns, S.C. Salmen, H. Ittrich, R. Reimer, M. Heine, S. Huber, C. Waurisch, A. Eychmuller, D.C. Wraith, T. Korn, P. Nielsen, H. Weller, C. Schramm, S. Luth, A.W. Lohse, J. Heeren, J. Herkel, Nanoparticle-based autoantigen delivery to Treg-inducing liver sinusoidal endothelial cells enables control of autoimmunity in mice, Journal of hepatology, 6 (2015) 1349-1356.
[167] D.P. McCarthy, J.W. Yap, C.T. Harp, W.K. Song, J. Chen, R.M. Pearson, S.D. Miller, L.D. Shea, An antigen-encapsulating nanoparticle platform for TH1/17 immune tolerance therapy, Nanomedicine : nanotechnology, biology, and medicine, 13 (2017) 191-200. PMID: 27720992.
[168] R. Weissleder, M. Nahrendorf, M.J. Pittet, Imaging macrophages with nanoparticles, Nature materials, 13 (2014) 125-138.
[169] C.B. Smarr, W.T. Yap, T.P. Neef, R.M. Pearson, Z.N. Hunter, I. Ifergan, D.R. Getts, P.J. Bryce, L.D. Shea, S.D. Miller, Biodegradable antigen-associated PLG nanoparticles tolerize Th2-mediated allergic airway inflammation pre-and postsensitization, Proceedings of the National Academy of Sciences, 113 (2016) 5059-5064.
[170] Z. Hunter, D.P. McCarthy, W.T. Yap, C.T. Harp, D.R. Getts, L.D. Shea, S.D. Miller, A Biodegradable Nanoparticle Platform for the Induction of Antigen-Specific Immune Tolerance for Treatment of Autoimmune Disease, ACS Nano, 8 (2014) 2148-2160.

[171] R. Kuo, E. Saito, S.D. Miller, L.D. Shea, Peptide-conjugated nanoparticles reduce positive co-stimulatory expression and T cell activity to induce tolerance, Molecular Therapy, (2017) 10.1016/j.ymthe.2017.1003.1032.
[172] R.M. Pearson, L.M. Casey, K.R. Hughes, L.Z. Wang, M.G. North, D.R. Getts, S.D. Miller, L.D. Shea, Controlled Delivery of Single or Multiple Antigens in Tolerogenic Nanoparticles using Peptide-polymer Bioconjugates, Molecular Therapy, (2017).
[173] S. Tsai, A. Shameli, J. Yamanouchi, X. Clemente-Casares, J. Wang, P. Serra, Y. Yang, Z. Medarova, A. Moore, P. Santamaria, Reversal of autoimmunity by boosting memory-like autoregulatory T cells, Immunity, 32 (2010) 568-580.
[174] W.U. Kim, W.K. Lee, J.W. Ryoo, S.H. Kim, J. Kim, J. Youn, S.Y. Min, E.Y. Bae, S.Y. Hwang, S.H. Park, C.S. Cho, J.S. Park, H.Y. Kim, Suppression of collagen-induced arthritis by single administration of poly(lactic-co-glycolic acid) nanoparticles entrapping type II collagen: a novel treatment strategy for induction of oral tolerance, Arthritis and rheumatism, 46 (2002) 1109-1120.
[175] M.B. Fessler, C. Keijzer, B. Slütter, R. van der Zee, W. Jiskoot, W. van Eden, F. Broere, PLGA, PLGA-TMC and TMC-TPP Nanoparticles Differentially Modulate the Outcome of Nasal Vaccination by Inducing Tolerance or Enhancing Humoral Immunity, PLoS ONE, 6 (2011) e26684.
[176] M.S. Macauley, F. Pfrengle, C. Rademacher, C.M. Nycholat, A.J. Gale, A. von Drygalski, J.C. Paulson, Antigenic liposomes displaying CD22 ligands induce antigen-specific B cell apoptosis, The Journal of clinical investigation, 123 (2013) 3074-3083.
[177] T.K. Kishimoto, J.D. Ferrari, R.A. LaMothe, P.N. Kolte, A.P. Griset, C. O'Neil, V. Chan, E. Browning, A. Chalishazar, W. Kuhlman, F.N. Fu, N. Viseux, D.H. Altreuter, L. Johnston, A.M. R, Improving the efficacy and safety of biologic drugs with tolerogenic nanoparticles, Nature nanotechnology, 11 (2016) 890-899.
[178] I. Schöll, A. Weissenböck, E. Förster-Waldl, E. Untersmayr, F. Walter, M. Willheim, G. Boltz-Nitulescu, O. Scheiner, F. Gabor, E. Jensen-Jarolim, Allergen-loaded biodegradable poly(d,l-lactic-co-glycolic) acid nanoparticles down-regulate an ongoing Th2 response in the BALB/c mouse model, Clinical & Experimental Allergy, 34 (2004) 315-321.
[179] E.G. Marazuela, N. Prado, E. Moro, H. Fernandez-Garcia, M. Villalba, R. Rodriguez, E. Batanero, Intranasal vaccination with poly(lactide-co-glycolide) microparticles containing a peptide T of Ole e 1 prevents mice against sensitization, Clinical & Experimental Allergy, 38 (2008) 520-528.
[180] S.M. Hayter, M.C. Cook, Updated assessment of the prevalence, spectrum and case definition of autoimmune disease, Autoimmunity reviews, 11 (2012) 754-765.
[181] J.A. Bluestone, H. Bour-Jordan, Current and future immunomodulation strategies to restore tolerance in autoimmune diseases, Cold Spring Harbor perspectives in biology, 4 (2012) a007542.
[182] S. Miller, R.P. Wetzig, H.N. Claman, The induction of cell-mediated immunity and tolerance with protein antigens coupled to syngeneic lymphoid cells, The Journal of experimental medicine, 149 (1979) 758-773.
[183] D.M. Turley, S.D. Miller, Peripheral Tolerance Induction Using Ethylenecarbodiimide-Fixed APCs Uses both Direct and Indirect Mechanisms of Antigen Presentation for Prevention of Experimental Autoimmune Encephalomyelitis, The Journal of Immunology, 178 (2007) 2212-2220.

[184] S. Prasad, A.P. Kohm, J.S. McMahon, X. Luo, S.D. Miller, Pathogenesis of NOD diabetes is initiated by reactivity to the insulin B chain 9-23 epitope and involves functional epitope spreading, Journal of Autoimmunity, 39 (2012) 347-353.
[185] D.R. Getts, D.M. Turley, C.E. Smith, C.T. Harp, D. McCarthy, E.M. Feeney, M.T. Getts, A.J. Martin, X. Luo, R.L. Terry, N.J. King, S.D. Miller, Tolerance induced by apoptotic antigen-coupled leukocytes is induced by PD-L1+ and IL-10–producing splenic macrophages and maintained by T regulatory cells, Journal of immunology, 187 (2011) 2405-2417.
[186] C.L. Vanderlugt, S.D. Miller, Epitope spreading in immune-mediated diseases: implications for immunotherapy, Nat Rev Immunol, 2 (2002) 85-95.
[187] C.E. Smith, S.D. Miller, Multi-peptide coupled-cell tolerance ameliorates ongoing relapsing EAE associated with multiple pathogenic autoreactivities, Journal of autoimmunity, 27 (2006) 218-231.
[188] C.B. Smarr, C.L. Hsu, A.J. Byrne, S.D. Miller, P.J. Bryce, Antigen-fixed leukocytes tolerize Th2 responses in mouse models of allergy, Journal of immunology, 187 (2011) 5090-5098.
[189] M. Becker-Hapak, S.S. McAllister, S.F. Dowdy, TAT-mediated protein transduction into mammalian cells, Methods, 24 (2001) 247-256.
[190] J.M. Gump, S.F. Dowdy, TAT transduction: the molecular mechanism and therapeutic prospects, Trends in Molecular Medicine, 13 (2007) 443-448.
[191] T.C. Lei, D.W. Scott, Induction of tolerance to factor VIII inhibitors by gene therapy with immunodominant A2 and C2 domains presented by B cells as Ig fusion proteins, Blood, 105 (2005) 4865-4870.
[192] J. Skupsky, A.H. Zhang, Y. Su, D.W. Scott, B-cell-delivered gene therapy induces functional T regulatory cells and leads to a loss of antigen-specific effector cells, Molecular Therapy, 18 (2010) 1527-1535.
[193] M.P. Matheu, Su, Y., Greenberg, M. L., Blanc, C. a., Parker, I., Scott, D. W., & Cahalan, M. D., Toll-like receptor 4-activated B cells out-compete Toll-like receptor 9-activated B cells to establish peripheral immunological tolerance, (2012).
[194] R.K. Agarwal, Y. Kang, E. Zambidis, D.W. Scott, C.C. Chan, R.R. Caspi, Retroviral gene therapy with an immunoglobulin-antigen fusion construct protects from experimental autoimmune uveitis, The Journal of clinical investigation, 106 (2000) 245-252.
[195] M.E.F. Melo, J. Qian, M. El-Amine, R.K. Agarwal, N. Soukhareva, Y. Kang, D.W. Scott, Gene Transfer of Ig-Fusion Proteins Into B Cells Prevents and Treats Autoimmune Diseases, Journal of immunology, 168 (2002) 4788-4795.
[196] B. Xu, D.W. Scott, A novel retroviral gene therapy approach to inhibit specific antibody production and suppress experimental autoimmune encephalomyelitis induced by MOG and MBP, Clinical immunology, 111 (2004) 47-52.
[197] C.N. Jenne, P. Kubes, Immune surveillance by the liver, Nature Immunology, 14 (2013) 996-1006.
[198] J.-K. Park, T. Utsumi, Y.-E. Seo, Y. Deng, A. Satoh, W.M. Saltzman, Y. Iwakiri, Cellular distribution of injected PLGA-nanoparticles in the liver, Nanomedicine: Nanotechnology, Biology and Medicine, 12 (2016) 1365-1374.
[199] A. Haddadi, P. Elamanchili, A. Lavasanifar, S. Das, J. Shapiro, J. Samuel, Delivery of rapamycin by PLGA nanoparticles enhances its suppressive activity on dendritic cells, Journal of biomedical materials research. Part A, 84 (2008) 885-898.

[200] L.H. Tostanoski, Y.C. Chiu, J.I. Andorko, M. Guo, X. Zeng, P. Zhang, W. Royal, 3rd, C.M. Jewell, Design of Polyelectrolyte Multilayers to Promote Immunological Tolerance, ACS Nano, (2016) in press.
[201] A. Sanchez-Fueyo, T.B. Strom, Immunologic basis of graft rejection and tolerance following transplantation of liver or other solid organs, Gastroenterology, 140 (2011) 51-64.
[202] B. Afzali, G. Lombardi, R.I. Lechler, Pathways of major histocompatibility complex allorecognition, Current Opinon in Organ Transplantation, 13 (2008) 438-444.
[203] G. Chen, T. Kheradmand, J. Bryant, S. Wang, J. Tasch, J.-j. Wang, Z. Zhang, X. Luo, Intragraft CD11b+ IDO+ Cells Mediate Cardiac Allograft Tolerance by ECDI-Fixed Donor Splenocyte Infusions, American Journal of Transplantation, 12 (2012) 2920-2929.
[204] S. Wang, J. Tasch, T. Kheradmand, J. Ulaszek, S. Ely, X. Zhang, B.J. Hering, S.D. Miller, X. Luo, Transient B-cell depletion combined with apoptotic donor splenocytes induces xeno-specific T-and B-cell tolerance to islet xenografts, Diabetes, 62 (2013) 3143-3150.
[205] J. Song, J. Huang, X. Chen, X. Teng, Z. Song, Y. Xing, M. Wang, K. Chen, Z. Wang, P. Yang, Donor-derived exosomes induce specific regulatory T cells to suppress immune inflammation in the allograft heart, Scientific reports, 7 (2016).
[206] X. Li, J.-J. Li, J.-Y. Yang, D.-S. Wang, W. Zhao, W.-J. Song, W.-M. Li, J.-F. Wang, W. Han, Z.-C. Zhang, Tolerance induction by exosomes from immature dendritic cells and rapamycin in a mouse cardiac allograft model, PloS one, 7 (2012) e44045.
[207] B. Ma, J.-Y. Yang, W.-j. Song, R. Ding, Z.-c. Zhang, H.-c. Ji, X. Zhang, J.-l. Wang, X.-s. Yang, K.-s. Tao, Combining Exosomes Derived from Immature DCs with Donor Antigen-Specific Treg Cells Induces Tolerance in a Rat Liver Allograft Model, Scientific Reports, 6 (2016).
[208] A.E. Morelli, A.T. Larregina, W.J. Shufesky, M.L. Sullivan, D.B. Stolz, G.D. Papworth, A.F. Zahorchak, A.J. Logar, Z. Wang, S.C. Watkins, Endocytosis, intracellular sorting, and processing of exosomes by dendritic cells, Blood, 104 (2004) 3257-3266.
[209] M. Larche, C.A. Akdis, R. Valenta, Immunological mechanisms of allergen-specific immunotherapy, Nature Reviews Immunology, 6 (2006) 761-771.
[210] L. Cox, H. Nelson, R. Lockey, C. Calabria, T. Chacko, I. Finegold, M. Nelson, R. Weber, D.I. Bernstein, J. Blessing-Moore, D.A. Khan, D.M. Lang, R.A. Nicklas, J. Oppenheimer, J.M. Portnoy, C. Randolph, D.E. Schuller, S.L. Spector, S. Tilles, D. Wallace, Allergen immunotherapy: a practice parameter third update, J Allergy Clin Immunol, 127 (2011) S1-55.
[211] G. Senti, B.M. Prinz Vavricka, I. Erdmann, M.I. Diaz, R. Markus, S.J. McCormack, J.J. Simard, B. Wüthrich, R. Crameri, N. Graf, P. Johansen, T.M. Kündig, Intralymphatic allergen administration renders specific immunotherapy faster and safer: A randomized controlled trial, Proceedings of the National Academy of Sciences, 105 (2008) 17908-17912.
[212] T. Hylander, L. Latif, U. Petersson-Westin, L.O. Cardell, Intralymphatic allergen-specific immunotherapy: an effective and safe alternative treatment route for pollen-induced allergic rhinitis, J Allergy Clin Immunol, 131 (2013) 412-420.
[213] C.B. Smarr, P.J. Bryce, S.D. Miller, Antigen-specific tolerance in immunotherapy of Th2-associated allergic diseases, Critical reviews in immunology, 33 (2013) 389-414.
[214] H. Fujita, M.B. Soyka, M. Akdis, C.A. Akdis, Mechanisms of allergen-specific immunotherapy, Clinical and translational allergy, 2 (2012) 2.
[215] M.S. Macauley, P.R. Crocker, J.C. Paulson, Siglec-mediated regulation of immune cell function in disease, Nature Reviews Immunology, 14 (2014) 653-666.
[216] A.J. Martin, D. McCarthy, C. Waltenbaugh, G. Goings, X. Luo, S.D. Miller, Ethylenecarbodiimide-Treated Splenocytes Carrying Male CD4 Epitopes Confer

Histocompatability Y Chromosome Antigen Transplant Protection by Inhibiting CD154 Upregulation, The Journal of Immunology, 185 (2010) 3326-3336.
[217] K.M. Lorentz, S. Kontos, G. Diaceri, H. Henry, J.A. Hubbell, Engineered binding to erythrocytes induces immunological tolerance to E. coli asparaginase, Science advances, 1 (2015) e1500112.
[218] J.O. Sestak, B.P. Sullivan, S. Thati, L. Northrup, B. Hartwell, L. Antunez, M.L. Forrest, C.M. Vines, T.J. Siahaan, C. Berkland, Codelivery of antigen and an immune cell adhesion inhibitor is necessary for efficacy of soluble antigen arrays in experimental autoimmune encephalomyelitis, Molecular Therapy - Methods & Clinical Development, 1 (2014) 14008.
[219] J. Idoyaga, C. Fiorese, L. Zbytnuik, A. Lubkin, J. Miller, B. Malissen, D. Mucida, M. Merad, R.M. Steinman, Specialized role of migratory dendritic cells in peripheral tolerance induction, The Journal of clinical investigation, 123 (2013) 844-854.
[220] D.C. Roopenian, S. Akilesh, FcRn: the neonatal Fc receptor comes of age, Nature Reviews Immunology, 7 (2007) 715-725.
[221] F. Nimmerjahn, J.V. Ravetch, FcgammaRs in health and disease, Current Topics in Microbiology and Immunology, 350 (2011) 105-125.
[222] S. Krishnamoorthy, T. Liu, D. Drager, S. Patarroyo-White, E.S. Chhabra, R. Peters, N. Josephson, D. Lillicrap, R.S. Blumberg, G.F. Pierce, H. Jiang, Recombinant factor VIII Fc (rFVIIIFc) fusion protein reduces immunogenicity and induces tolerance in hemophilia A mice, Cellular Immunology, 301 (2016) 30-39.
[223] J.N. Stern, D.B. Keskin, Z. Kato, H. Waldner, S. Schallenberg, A. Anderson, H. von Boehmer, K. Kretschmer, J.L. Strominger, Promoting tolerance to proteolipid protein-induced experimental autoimmune encephalomyelitis through targeting dendritic cells, Proceedings of the National Academy of Sciences, 107 (2010) 17280-17285.
[224] A. Mukhopadhaya, T. Hanafusa, I. Jarchum, Y.G. Chen, Y. Iwai, D.V. Serreze, R.M. Steinman, K.V. Tarbell, T.P. DiLorenzo, Selective delivery of beta cell antigen to dendritic cells in vivo leads to deletion and tolerance of autoreactive CD8+ T cells in NOD mice, Proceedings of the National Academy of Sciences, 105 (2008) 6374-6379.
[225] R. Spiering, B. Margry, C. Keijzer, C. Petzold, A. Hoek, J. Wagenaar-Hilbers, R. van der Zee, W. van Eden, K. Kretschmer, F. Broere, DEC205+ Dendritic Cell-Targeted Tolerogenic Vaccination Promotes Immune Tolerance in Experimental Autoimmune Arthritis, The Journal of Immunology, 194 (2015) 4804-4813.
[226] C. Chittasupho, J. Sestak, L. Shannon, T.J. Siahaan, C.M. Vines, C. Berkland, Hyaluronic acid graft polymers displaying peptide antigen modulate dendritic cell response in vitro, Molecular Pharmaceutics, 11 (2014) 367-373.
[227] S. Sakaguchi, T. Yamaguchi, T. Nomura, M. Ono, Regulatory T Cells and Immune Tolerance, Cell, 133 (2008) 775-787.
[228] M.G. Roncarolo, M. Battaglia, Regulatory T-cell immunotherapy for tolerance to self antigens and alloantigens in humans, Nature Reviews Immunology, 7 (2007) 585-598.
[229] C.T. Ellebrecht, V.G. Bhoj, A. Nace, E.J. Choi, X. Mao, M.J. Cho, G. Di Zenzo, A. Lanzavecchia, J.T. Seykora, G. Cotsarelis, Reengineering chimeric antigen receptor T cells for targeted therapy of autoimmune disease, Science, 353 (2016) 179-184.
[230] D. Blat, E. Zigmond, Z. Alteber, T. Waks, Z. Eshhar, Suppression of murine colitis and its associated cancer by carcinoembryonic antigen-specific regulatory T cells, Molecular Therapy, 22 (2014) 1018-1028.

[231] K.G. MacDonald, R.E. Hoeppli, Q. Huang, J. Gillies, D.S. Luciani, P.C. Orban, R. Broady, M.K. Levings, Alloantigen-specific regulatory T cells generated with a chimeric antigen receptor, The Journal of clinical investigation, 126 (2016) 1413-1424.
[232] D.A. Vignali, L.W. Collison, C.J. Workman, How regulatory T cells work, Nature Reviews Immunology, 8 (2008) 523-532.
[233] N. Arpaia, J.A. Green, B. Moltedo, A. Arvey, S. Hemmers, S. Yuan, P.M. Treuting, A.Y. Rudensky, A Distinct Function of Regulatory T Cells in Tissue Protection, Cell, 162 (2015) 1078-1089.
[234] A.K. Abbas, C. Benoist, J.A. Bluestone, D.J. Campbell, S. Ghosh, S. Hori, S. Jiang, V.K. Kuchroo, D. Mathis, M.G. Roncarolo, A. Rudensky, S. Sakaguchi, E.M. Shevach, D.A. Vignali, S.F. Ziegler, Regulatory T cells: recommendations to simplify the nomenclature, Nat Immunol, 14 (2013) 307-308.
[235] E.M. Shevach, A.M. Thornton, tTregs, pTregs, and iTregs: similarities and differences, Immunol Rev, 259 (2014) 88-102.
[236] T.S. Davidson, E.M. Shevach, Polyclonal Treg cells modulate T effector cell trafficking, European Journal of Immunology, 41 (2011) 2862-2870.
[237] B.H. Nelson, IL-2, regulatory T cells, and tolerance, The Journal of Immunology, 172 (2004) 3983-3988.
[238] Y. Zheng, A.Y. Rudensky, Foxp3 in control of the regulatory T cell lineage, Nature Immunology, 8 (2007) 457-462.
[239] M. Yadav, J. Bluestone, S. Stephan, Peripherally Induced Tregs – Role in Immune Homeostasis and Autoimmunity, Frontiers in Immunology, 4 (2013).
[240] S. Kasagi, P. Zhang, L. Che, B. Abbatiello, T. Maruyama, H. Nakatsukasa, P. Zanvit, W. Jin, J.E. Konkel, W. Chen, In vivo-generated antigen-specific regulatory T cells treat autoimmunity without compromising antibacterial immune response, Science translational medicine, 6 (2014) 241ra278.
[241] G. Gross, T. Waks, Z. Eshhar, Expression of immunoglobulin-T-cell receptor chimeric molecules as functional receptors with antibody-type specificity, Proceedings of the National Academy of Sciences, 86 (1989) 10024-10028.
[242] J.N. Kochenderfer, M.E. Dudley, S.A. Feldman, W.H. Wilson, D.E. Spaner, I. Maric, M. Stetler-Stevenson, G.Q. Phan, M.S. Hughes, R.M. Sherry, B-cell depletion and remissions of malignancy along with cytokine-associated toxicity in a clinical trial of anti-CD19 chimeric-antigen-receptor–transduced T cells, Blood, 119 (2012) 2709-2720.
[243] S.A. Grupp, M. Kalos, D. Barrett, R. Aplenc, D.L. Porter, S.R. Rheingold, D.T. Teachey, A. Chew, B. Hauck, J.F. Wright, Chimeric antigen receptor–modified T cells for acute lymphoid leukemia, New England Journal of Medicine, 368 (2013) 1509-1518.
[244] S.L. Maude, N. Frey, P.A. Shaw, R. Aplenc, D.M. Barrett, N.J. Bunin, A. Chew, V.E. Gonzalez, Z. Zheng, S.F. Lacey, Chimeric antigen receptor T cells for sustained remissions in leukemia, New England Journal of Medicine, 371 (2014) 1507-1517.
[245] P. Joly, H. Mouquet, J.-C. Roujeau, M. D'Incan, D. Gilbert, S. Jacquot, M.-L. Gougeon, C. Bedane, R. Muller, B. Dreno, A single cycle of rituximab for the treatment of severe pemphigus, New England Journal of Medicine, 357 (2007) 545-552.
[246] M. Fransson, E. Piras, J. Burman, B. Nilsson, M. Essand, B. Lu, R.A. Harris, P.U. Magnusson, E. Brittebo, A.S. Loskog, CAR/FoxP3-engineered T regulatory cells target the CNS and suppress EAE upon intranasal delivery, Journal of neuroinflammation, 9 (2012) 1.

[247] P.D. Rios, X. Zhang, X. Luo, L.D. Shea, Mold-casted non-degradable, islet macro-encapsulating hydrogel devices for restoration of normoglycemia in diabetic mice, Biotechnology and Bioengineering, 113 (2016) 2485-2495.
[248] J. Stein-Streilein, R.R. Caspi, Immune privilege and the philosophy of immunology, Frontiers in Immunology, 5 (2014) 110.
[249] T. Desai, L.D. Shea, Advances in islet encapsulation technologies, Nature reviews. Drug discovery, (2016) in press.
[250] J.G. Graham, X. Zhang, A. Goodman, K. Pothoven, J. Houlihan, S. Wang, R.M. Gower, X. Luo, L.D. Shea, PLG scaffold delivered antigen-specific regulatory T cells induce systemic tolerance in autoimmune diabetes, Tissue engineering. Part A, 19 (2013) 1465-1475.
[251] C.L. Vanderlugt, K.L. Neville, K.M. Nikcevich, T.N. Eagar, J.A. Bluestone, S.D. Miller, Pathologic role and temporal appearance of newly emerging autoepitopes in relapsing experimental autoimmune encephalomyelitis, Journal of immunology, 164 (2000) 670-678.
[252] C.E. Smith, T.N. Eagar, J.L. Strominger, S.D. Miller, Differential induction of IgE-mediated anaphylaxis after soluble vs. cell-bound tolerogenic peptide therapy of autoimmune encephalomyelitis, Proceedings of the National Academy of Sciences of the United States of America, 102 (2005) 9595-9600.
[253] S. Prasad, D. Xu, S.D. Miller, Tolerance strategies employing antigen-coupled apoptotic cells and carboxylated PLG nanoparticles for the treatment of type 1 diabetes, The review of diabetic studies : RDS, 9 (2012) 319-327.
[254] J. Conde, J.T. Dias, V. Grazú, M. Moros, P.V. Baptista, J.M. De La Fuente, Revisiting 30 years of Biofunctionalization and Surface Chemistry of Inorganic Nanoparticles for Nanomedicine, Frontiers in Chemistry, 2 (2014).
[255] Y. Yeo, K. Park, Control of encapsulation efficiency and initial burst in polymeric microparticle systems, Archives of Pharmaceutical Research, 27 (2004) 1-12.
[256] C.M. Hu, L. Zhang, S. Aryal, C. Cheung, R.H. Fang, L. Zhang, Erythrocyte membrane-camouflaged polymeric nanoparticles as a biomimetic delivery platform, Proceedings of the National Academy of Sciences of the United States of America, 108 (2011) 10980-10985.
[257] M.G. von Herrath, L.C. Harrison, Antigen-induced regulatory T cells in autoimmunity, Nature Reviews Immunology, 3 (2003) 223-232.
[258] A.M. Bilate, J.J. Lafaille, Induced CD4+Foxp3+ regulatory T cells in immune tolerance, Annual review of immunology, 30 (2012) 733-758.
[259] V.K. Tuohy, M. Yu, L. Yin, J.A. Kawczak, J.M. Johnson, P.M. Mathisen, B. Weinstock-Guttnnan, R.P. Kinkel, The epitope spreading cascade during progression of experimental autoimmune encephalomyelitis and multiple sclerosis, Immunol Rev, 164 (1998) 93-100.
[260] M.B. Lutz, N. Kukutsch, A.L. Ogilvie, S. Rößner, F. Koch, N. Romani, G. Schuler, An advanced culture method for generating large quantities of highly pure dendritic cells from mouse bone marrow, Journal of immunological methods, 223 (1999) 77-92.
[261] S.D. Miller, W.J. Karpus, T.S. Davidson, Experimental autoimmune encephalomyelitis in the mouse, Current protocols in immunology / edited by John E. Coligan ... [et al, Chapter 15 (2010) 15.11.11-15.11.20.
[262] R.M. Pearson, L.M. Casey, K.R. Hughes, S.D. Miller, L.D. Shea, In vivo reprogramming of immune cells: technologies for induction of antigen-specific tolerance, Advanced Drug Delivery Reviews, 114 (2017) 240-255.

[263] L.H. Calabrese, E.S. Molloy, Progressive multifocal leucoencephalopathy in the rheumatic diseases: assessing the risks of biological immunosuppressive therapies, Annals of the Rheumatic Diseases, 67 (2008) iii64-iii65.
[264] D.P. McCarthy, J.W.-T. Yap, C.T. Harp, W.K. Song, J. Chen, R.M. Pearson, S.D. Miller, L.D. Shea, An antigen-encapsulating nanoparticle platform for T H 1/17 immune tolerance therapy, Nanomedicine: Nanotechnology, Biology and Medicine, 13 (2017) 191-200.
[265] L.H. Tostanoski, Y.-C. Chiu, J.M. Gammon, T. Simon, J.I. Andorko, J.S. Bromberg, C.M. Jewell, Reprogramming the local lymph node microenvironment promotes tolerance that is systemic and antigen specific, Cell reports, 16 (2016) 2940-2952.
[266] J.-P. Plard, D. Bazile, Comparison of the safety profiles of PLA 50 and Me. PEG-PLA 50 nanoparticles after single dose intravenous administration to rat, Colloids and Surfaces B: Biointerfaces, 16 (1999) 173-183.
[267] K.B. Ferenz, I.N. Waack, J. Laudien, C. Mayer, M. Broecker-Preuss, H.d. Groot, M. Kirsch, Safety of poly (ethylene glycol)-coated perfluorodecalin-filled poly (lactide-co-glycolide) microcapsules following intravenous administration of high amounts in rats, Results in Pharma Sciences, 4 (2014) 8-18.
[268] B. Phillips, K. Nylander, J. Harnaha, J. Machen, R. Lakomy, A. Styche, K. Gillis, L. Brown, D. Lafreniere, M. Gallo, A microsphere-based vaccine prevents and reverses new-onset autoimmune diabetes, Diabetes, 57 (2008) 1544-1555.
[269] M.A. Travis, D. Sheppard, TGF-β activation and function in immunity, Annual review of immunology, 32 (2014) 51-82.
[270] L. Johns, K. Flanders, G. Ranges, S. Sriram, Successful treatment of experimental allergic encephalomyelitis with transforming growth factor-beta 1, The Journal of Immunology, 147 (1991) 1792-1796.
[271] M.K. Racke, S. Dhib-Jalbut, B. Cannella, P.S. Albert, C.S. Raine, D.E. McFarlin, Prevention and treatment of chronic relapsing experimental allergic encephalomyelitis by transforming growth factor-beta 1, The Journal of Immunology, 146 (1991) 3012-3017.
[272] Y. Laouar, T. Town, D. Jeng, E. Tran, Y. Wan, V.K. Kuchroo, R.A. Flavell, TGF-β signaling in dendritic cells is a prerequisite for the control of autoimmune encephalomyelitis, Proceedings of the National Academy of Sciences, 105 (2008) 10865-10870.
[273] M.E. Keegan, J.L. Falcone, T.C. Leung, W.M. Saltzman, Biodegradable microspheres with enhanced capacity for covalently bound surface ligands, Macromolecules, 37 (2004) 9779-9784.
[274] J.S. Lewis, C. Roche, Y. Zhang, T.M. Brusko, C.H. Wasserfall, M. Atkinson, M.J. Clare-Salzler, B.G. Keselowsky, Combinatorial delivery of immunosuppressive factors to dendritic cells using dual-sized microspheres, Journal of Materials Chemistry B, 2 (2014) 2562-2574.
[275] A.S. Farias, G.S. Spagnol, P. Bordeaux-Rego, C.O. Oliveira, A.G.M. Fontana, R.F. Paula, M. Santos, F. Pradella, A.S. Moraes, E.C. Oliveira, Vitamin D3 induces IDO+ tolerogenic DCs and enhances Treg, reducing the severity of EAE, CNS neuroscience & therapeutics, 19 (2013) 269-277.
[276] E. Henry, C.J. Desmet, V. Garzé, L. Fiévez, D. Bedoret, C. Heirman, P. Faisca, F.J. Jaspar, P. Gosset, A.P. Jacquet, Dendritic cells genetically engineered to express IL-10 induce long-lasting antigen-specific tolerance in experimental asthma, The Journal of immunology, 181 (2008) 7230-7242.
[277] A.P. Robinson, C.T. Harp, A. Noronha, S.D. Miller, The experimental autoimmune encephalomyelitis (EAE) model of MS: utility for understanding disease pathophysiology and treatment, Handbook of clinical neurology, 122 (2014) 173.

[278] A. Schneider, S.A. Long, K. Cerosaletti, C.T. Ni, P. Samuels, M. Kita, J.H. Buckner, In Active Relapsing-Remitting Multiple Sclerosis, Effector T Cell Resistance to Adaptive Tregs Involves IL-6-Mediated Signaling, Science translational medicine, 5 (2013) 170ra115-170ra115.
[279] D.M. Bissell, S.S. Wang, W.R. Jarnagin, F.J. Roll, Cell-specific expression of transforming growth factor-beta in rat liver. Evidence for autocrine regulation of hepatocyte proliferation, The Journal of Clinical Investigation, 96 (1995) 447-455.
[280] J.P. Böttcher, P.A. Knolle, D. Stabenow, Mechanisms Balancing Tolerance and Immunity in the Liver, Digestive Diseases, 29 (2011) 384-390.
[281] A.K. Horst, K. Neumann, L. Diehl, G. Tiegs, Modulation of liver tolerance by conventional and nonconventional antigen-presenting cells and regulatory immune cells, Cellular and Molecular Immunology, 13 (2016) 277.
[282] S.T. Reddy, A. Rehor, H.G. Schmoekel, J.A. Hubbell, M.A. Swartz, In vivo targeting of dendritic cells in lymph nodes with poly(propylene sulfide) nanoparticles, Journal of Controlled Release, 112 (2006) 26-34.
[283] G.J. Randolph, K. Inaba, D.F. Robbiani, R.M. Steinman, W.A. Muller, Differentiation of phagocytic monocytes into lymph node dendritic cells in vivo, Immunity, 11 (1999) 753-761.
[284] S.M. Azarin, J. Yi, R.M. Gower, B.A. Aguado, M.E. Sullivan, A.G. Goodman, E.J. Jiang, S.S. Rao, Y. Ren, S.L. Tucker, V. Backman, J.S. Jeruss, L.D. Shea, In vivo capture and label-free detection of early metastatic cells, Nature Communications, 6 (2015) 1-9.
[285] J.M. Liu, J. Zhang, X. Zhang, K.A. Hlavaty, C.F. Ricci, J.N. Leonard, L.D. Shea, R.M. Gower, Transforming growth factor-beta 1 delivery from microporous scaffolds decreases inflammation post-implant and enhances function of transplanted islets, Biomaterials, 80 (2016) 11-19.
[286] K.J. Peine, M. Guerau-de-Arellano, P. Lee, N. Kanthamneni, M. Severin, G.D. Probst, H. Peng, Y. Yang, Z. Vangundy, T.L. Papenfuss, A.E. Lovett-Racke, E.M. Bachelder, K.M. Ainslie, Treatment of Experimental Autoimmune Encephalomyelitis by Codelivery of Disease Associated Peptide and Dexamethasone in Acetalated Dextran Microparticles, Molecular Pharmaceutics, 11 (2014) 828-835.
[287] D.J. Huss, R.C. Winger, G.M. Cox, M. Guerau-de-Arellano, Y. Yang, M.K. Racke, A.E. Lovett-Racke, TGF-β signaling via Smad4 drives IL-10 production in effector Th1 cells and reduces T-cell trafficking in EAE, European journal of immunology, 41 (2011) 2987-2996.
[288] R.S. Gupta, C.M. Warren, B.M. Smith, J.A. Blumenstock, J. Jiang, M.M. Davis, K.C. Nadeau, The Public Health Impact of Parent-Reported Childhood Food Allergies in the United States. LID - e20181235 [pii] LID - 10.1542/peds.2018-1235 [doi].
[289] R.S. Gupta, C.M. Warren, B.M. Smith, J. Jiang, J.A. Blumenstock, M.M. Davis, R.P. Schleimer, K.C. Nadeau, Prevalence and Severity of Food Allergies Among US Adults, JAMA Netw Open, 2 (2019) e185630-e185630.
[290] M. Akdis, S. Burgler, R. Crameri, T. Eiwegger, H. Fujita, E. Gomez, S. Klunker, N. Meyer, L. O'Mahony, O. Palomares, C. Rhyner, N. Ouaked, A. Schaffartzik, W. Van De Veen, S. Zeller, M. Zimmermann, C.A. Akdis, Interleukins, from 1 to 37, and interferon-gamma: receptors, functions, and roles in diseases, J Allergy Clin Immunol, 127 (2011) 701-721 e701-770. PMID: 21377040
[291] M.C. Berin, S. Sicherer, Food allergy: mechanisms and therapeutics, Current opinion in immunology, 23 (2011) 794-800. PMID: 21943957.
[292] J.A. Boyce, A. Assa'ad, A.W. Burks, S.M. Jones, H.A. Sampson, R.A. Wood, M. Plaut, S.F. Cooper, M.J. Fenton, Guidelines for the diagnosis and management of food allergy in the United

States: summary of the NIAID-sponsored expert panel report, Journal of the American Dietetic Association, 111 (2011) 17-27. PMID: 21185960.
[293] C.B. Smarr, P.J. Bryce, S.D. Miller, Antigen-specific tolerance in immunotherapy of Th2-associated allergic diseases, Critical reviews in immunology, 33 (2013) 389-414. PMID: 24099300.
[294] M.V. Kopp, Role of immunmodulators in allergen-specific immunotherapy, Allergy, 66 (2011) 792-797. PMID: 21332502.
[295] S.T. Holgate, R. Djukanovic, T. Casale, J. Bousquet, Anti-immunoglobulin E treatment with omalizumab in allergic diseases: an update on anti-inflammatory activity and clinical efficacy, Clin Exp Allergy, 35 (2005) 408-416. PMID: 15836747.
[296] Guidelines for the Diagnosis and Management of Food Allergy in the United States: Report of the NIAID-Sponsored Expert Panel, Journal of Allergy and Clinical Immunology, 126 (2010) S1-S58.
[297] A.W. Burks, R.A. Jones Sm Fau - Wood, D.M. Wood Ra Fau - Fleischer, S.H. Fleischer Dm Fau - Sicherer, R.W. Sicherer Sh Fau - Lindblad, D. Lindblad Rw Fau - Stablein, A.K. Stablein D Fau - Henning, B.P. Henning Ak Fau - Vickery, A.H. Vickery Bp Fau - Liu, A.M. Liu Ah Fau - Scurlock, W.G. Scurlock Am Fau - Shreffler, M. Shreffler Wg Fau - Plaut, H.A. Plaut M Fau - Sampson, H.A. Sampson, Oral immunotherapy for treatment of egg allergy in children.
[298] D.M. Turley, S.D. Miller, Peripheral tolerance induction using ethylenecarbodiimide-fixed APCs uses both direct and indirect mechanisms of antigen presentation for prevention of experimental autoimmune encephalomyelitis, J Immunol, 178 (2007) 2212-2220. PMID: 17277126.
[299] R.M. Pearson, L.M. Casey, K.R. Hughes, L.Z. Wang, M.G. North, D.R. Getts, S.D. Miller, L.D. Shea, Controlled Delivery of Single or Multiple Antigens in Tolerogenic Nanoparticles using Peptide-polymer Bioconjugates, Mol Ther, (2017) 1655-1664. PMID: 28479234.
[300] J. Park, Y. Zhang, E. Saito, S.J. Gurczynski, B.B. Moore, B.J. Cummings, A.J. Anderson, L.D. Shea, Intravascular innate immune cells reprogrammed via intravenous nanoparticles to promote functional recovery after spinal cord injury, Proceedings of the National Academy of Sciences, 116 (2019) 14947.
[301] D.R. Getts, D.M. Turley, C.E. Smith, C.T. Harp, D. McCarthy, E.M. Feeney, M.T. Getts, A.J. Martin, X. Luo, R.L. Terry, N.J. King, S.D. Miller, Tolerance induced by apoptotic antigen-coupled leukocytes is induced by PD-L1+ and IL-10-producing splenic macrophages and maintained by T regulatory cells, J Immunol, 187 (2011) 2405-2417. PMID: 21821796.
[302] S. Prasad, T. Neef, D. Xu, J.R. Podojil, D.R. Getts, L.D. Shea, S.D. Miller, Tolerogenic Ag-PLG nanoparticles induce tregs to suppress activated diabetogenic CD4 and CD8 T cells, J Autoimmun, (2017) PMID: 29258717.
[303] L.M. Casey, S. Kakade, J.T. Decker, J.A. Rose, K. Deans, L.D. Shea, R.M. Pearson, Cargo-less nanoparticles program innate immune cell responses to toll-like receptor activation, Biomaterials, 218 (2019) 119333.
[304] J. Swinton, R.M. Schweitzer An Fau - Anderson, R.M. Anderson, Two signal activation as an explanation of high zone tolerance: a mathematical exploration of the nature of the second signal.
[305] H. Grindebacke, K. Wing, A.C. Andersson, E. Suri-Payer, S. Rak, A. Rudin, Defective suppression of Th2 cytokines by CD4+CD25+ regulatory T cells in birch allergics during birch pollen season, Clinical & Experimental Allergy, 34 (2004) 1364-1372.

[306] J. De S. Rebouças, J.M. Irache, A.I. Camacho, G. Gastaminza, M.L. Sanz, M. Ferrer, C. Gamazo, Immunogenicity of Peanut Proteins Containing Poly(Anhydride) Nanoparticles, Clinical and Vaccine Immunology, 21 (2014) 1106.
[307] D.R. Getts, A.J. Martin, D.P. McCarthy, R.L. Terry, Z.H. Hunter, W.T. Yap, M.T. Getts, M. Pleiss, X. Luo, N.J.C. King, L.D. Shea, S.D. Miller, Microparticles bearing encephalitogenic peptides induce T-cell tolerance and ameliorate experimental autoimmune encephalomyelitis, Nature Biotechnology, 30 (2012) 1217-1224. PMID: 23159881.
[308] Z. Hunter, D.P. McCarthy, W.T. Yap, C.T. Harp, D.R. Getts, L.D. Shea, S.D. Miller, A biodegradable nanoparticle platform for the induction of antigen-specific immune tolerance for treatment of autoimmune disease, ACS Nano, 25 (2014) 2148-2160. PMID: 24559284.
[309] A. Sherman, M. Biswas, R.W. Herzog, Innovative Approaches for Immune Tolerance to Factor VIII in the Treatment of Hemophilia A, Front Immunol, 8 (2017) 1604-1604.
[310] P. Kubisz, P. Plamenova I Fau - Holly, J. Holly P Fau - Stasko, J. Stasko, Successful immune tolerance induction with high-dose coagulation factor VIII and intravenous immunoglobulins in a patient with congenital hemophilia and high-titer inhibitor of coagulation factor VIII despite unfavorable prognosis for the therapy.
[311] L. Steinman, P.P. Ho, W.H. Robinson, P.J. Utz, P. Villoslada, Antigen-specific tolerance to self-antigens in protein replacement therapy, gene therapy and autoimmunity.
[312] D.C. Fitzgerald, S. Zhang Gx Fau - Yu, M.L. Yu S Fau - Cullimore, Z. Cullimore Ml Fau - Zhao, A. Zhao Z Fau - Rostami, A. Rostami, Intravenous tolerance effectively overcomes enhanced pro-inflammatory responses and experimental autoimmune encephalomyelitis severity in the absence of IL-12 receptor signaling.
[313] I. Zubizarreta, G. Flórez-Grau, G. Vila, R. Cabezón, C. España, M. Andorra, A. Saiz, S. Llufriu, M. Sepulveda, N. Sola-Valls, E.H. Martinez-Lapiscina, I. Pulido-Valdeolivas, B. Casanova, M. Martinez Gines, N. Tellez, C. Oreja-Guevara, M. Español, E. Trias, J. Cid, M. Juan, M. Lozano, Y. Blanco, L. Steinman, D. Benitez-Ribas, P. Villoslada, Immune tolerance in multiple sclerosis and neuromyelitis optica with peptide-loaded tolerogenic dendritic cells in a phase 1b trial, Proceedings of the National Academy of Sciences, 116 (2019) 8463.
[314] J.M. van Noort, M. Bsibsi, P.J. Nacken, R. Verbeek, E.H.G. Venneker, Therapeutic Intervention in Multiple Sclerosis with Alpha B-Crystallin: A Randomized Controlled Phase IIa Trial, PLOS ONE, 10 (2015) e0143366.
[315] Y. Liu, Y. Sun, L.-J. Chang, N. Li, H. Li, Y. Yu, P.J. Bryce, L.C. Grammer, R.P. Schleimer, D. Zhu, Blockade of peanut allergy with a novel Ara h 2–Fcγ fusion protein in mice, Journal of Allergy and Clinical Immunology, 131 (2013) 213-221.e215.
[316] M.C. Berin, Future Therapies for IgE-Mediated Food Allergy, Curr Pediatr Rep, 2 (2014) 119-126.
[317] E.B. Brandt, R.T. Strait, D. Hershko, Q. Wang, E.E. Muntel, T.A. Scribner, N. Zimmermann, F.D. Finkelman, M.E. Rothenberg, Mast cells are required for experimental oral allergen-induced diarrhea, The Journal of clinical investigation, 112 (2003) 1666-1677.
[318] Z. Amoozgar, Y. Yeo, Recent advances in stealth coating of nanoparticle drug delivery systems.
[319] B.S. Zolnik, A.f. González-Fernández, N. Sadrieh, M.A. Dobrovolskaia, Minireview: Nanoparticles and the Immune System, Endocrinology, 151 (2010) 458-465.
[320] D.P. McCarthy, Z.N. Hunter, B. Chackerian, L.D. Shea, S.D. Miller, Targeted immunomodulation using antigen-conjugated nanoparticles, Wiley Interdiscip Rev Nanomed Nanobiotechnol, 6 (2014) 298-315.

[321] W.T. Yap, W.K. Song, N. Chauhan, P.N. Scalise, R. Agarwal, S.D. Miller, L.D. Shea, Quantification of particle-conjugated or particle-encapsulated peptides on interfering reagent backgrounds, BioTechniques, 57 (2014) 39-44.
[322] J.J. O'Konek, J.J. Landers, K.W. Janczak, R.R. Goel, A.M. Mondrusov, P.T. Wong, J.R. Baker, Jr., Nanoemulsion adjuvant–driven redirection of T_H2 immunity inhibits allergic reactions in murine models of peanut allergy, Journal of Allergy and Clinical Immunology, 141 (2018) 2121-2131.
[323] X.-M. Li, D. Serebrisky, S.-Y. Lee, C.-K. Huang, L. Bardina, B.H. Schofield, J.S. Stanley, A.W. Burks, G.A. Bannon, H.A. Sampson, A murine model of peanut anaphylaxis: T- and B-cell responses to a major peanut allergen mimic human responses, Journal of Allergy and Clinical Immunology, 106 (2000) 150-158.
[324] B. Rodriguez, G. Prioult, F. Hacini-Rachinel, D. Moine, A. Bruttin, C. Ngom-Bru, C. Labellie, I. Nicolis, B. Berger, A. Mercenier, M.-J. Butel, A.-J. Waligora-Dupriet, Infant gut microbiota is protective against cow's milk allergy in mice despite immature ileal T-cell response, FEMS Microbiology Ecology, 79 (2012) 192-202.
[325] S. Smulders, J.-P. Kaiser, S. Zuin, K.L. Van Landuyt, L. Golanski, J. Vanoirbeek, P. Wick, P.H.M. Hoet, Contamination of nanoparticles by endotoxin: evaluation of different test methods, Particle and Fibre Toxicology, 9 (2012) 41.
[326] S. Schulke, M. Albrecht, Mouse Models for Food Allergies: Where Do We Stand?, Cells, 8 (2019).
[327] P.H. Green, B. Lebwohl, R. Greywoode, Celiac disease, J Allergy Clin Immunol, 135 (2015) 1099-1106; quiz 1107.
[328] D.R. Getts, D.P. McCarthy, S.D. Miller, Exploiting apoptosis for therapeutic tolerance induction, Journal of immunology (Baltimore, Md. : 1950), 191 (2013) 5341-5346.
[329] M.C. Michallet, F. Saltel, M. Flacher, J.P. Revillard, L. Genestier, Cathepsin-dependent apoptosis triggered by supraoptimal activation of T lymphocytes: a possible mechanism of high dose tolerance, J Immunol, 172 (2004) 5405-5414.
[330] L.M. Casey, R.M. Pearson, K.R. Hughes, J.M.H. Liu, J.A. Rose, M.G. North, L.Z. Wang, M. Lei, S.D. Miller, L.D. Shea, Conjugation of Transforming Growth Factor Beta to Antigen-Loaded Poly(lactide- co-glycolide) Nanoparticles Enhances Efficiency of Antigen-Specific Tolerance, Bioconjug Chem, 29 (2018) 813-823.
[331] G.R. Shellam, G.J. Nossal, Mechanism of induction of immunological tolerance. IV. The effects of ultra-low doses of flagellin, Immunology, 14 (1968) 273-284.
[332] M. Farazuddin, R.R. Goel, N.J. Kline, J.J. Landers, J.J. O'Konek, J.R. Baker, Jr., Nanoemulsion Adjuvant Augments Retinaldehyde Dehydrogenase Activity in Dendritic Cells via MyD88 Pathway, Front Immunol, 10 (2019) 916.
[333] R. Rachid, D.T. Umetsu, Immunological mechanisms for desensitization and tolerance in food allergy, Semin Immunopathol, 34 (2012) 689-702.
[334] M.C. Berin, L. Mayer, Can we produce true tolerance in patients with food allergy?, J Allergy Clin Immunol, 131 (2013) 14-22.
[335] X.M. Li, S.Y. Serebrisky D Fau - Lee, C.K. Lee Sy Fau - Huang, L. Huang Ck Fau - Bardina, B.H. Bardina L Fau - Schofield, J.S. Schofield Bh Fau - Stanley, A.W. Stanley Js Fau - Burks, G.A. Burks Aw Fau - Bannon, H.A. Bannon Ga Fau - Sampson, H.A. Sampson, A murine model of peanut anaphylaxis: T- and B-cell responses to a major peanut allergen mimic human responses.
[336] AR101 Oral Immunotherapy for Peanut Allergy, New England Journal of Medicine, 379 (2018) 1991-2001.

[337] M.C. Berin, H.A. Sampson, Food allergy: an enigmatic epidemic, Trends in immunology, 34 (2013) 390-397. PMID: 23648309.
[338] K.D. Srivastava, A. Siefert, T.M. Fahmy, M.J. Caplan, X.M. Li, H.A. Sampson, Investigation of peanut oral immunotherapy with CpG/peanut nanoparticles in a murine model of peanut allergy.
[339] D.R. Getts, L.D. Shea, S.D. Miller, N.J. King, Harnessing nanoparticles for immune modulation, Trends in immunology, 36 (2015) 419-427.
[340] C.B. Smarr, J.W.T. Yap, P.J. Bryce, L.D. Shea, S.D. Miller, Biodegradable antigen-associated PLG nanoparticles tolerize Th2-mediated allergic airway inflammation pre- and post-sensitization, Proc. Nat. Acad. Sci. USA, (2015) In review.
[341] J.L. Platt, New directions for organ transplantation, Nature, 392 (1998) 11-17.
[342] C. Ricordi, T.B. Strom, Clinical islet transplantation: advances and immunological challenges, Nat Rev Immunol, 4 (2004) 259-268.
[343] M. Abecassis, S.T. Bartlett, A.J. Collins, C.L. Davis, F.L. Delmonico, J.J. Friedewald, R. Hays, A. Howard, E. Jones, A.B. Leichtman, R.M. Merion, R.A. Metzger, F. Pradel, E.J. Schweitzer, R.L. Velez, R.S. Gaston, Kidney transplantation as primary therapy for end-stage renal disease: A National Kidney Foundation/Kidney Disease Outcomes Quality Initiative (NKF/KDOQI (TM)) conference, Clin J Am Soc Nephro, 3 (2008) 471-480.
[344] R. Girlanda, Deceased organ donation for transplantation: Challenges and opportunities, World J Transplant, 6 (2016) 451-459.
[345] M.D. Duncan, D.S. Wilkes, Transplant-related immunosuppression: a review of immunosuppression and pulmonary infections, Proc Am Thorac Soc, 2 (2005) 449-455.
[346] J.A. Fishman, Infection in solid-organ transplant recipients, N Engl J Med, 357 (2007) 2601-2614.
[347] S.Y. Zafar, D.N. Howell, J.P. Gockerman, Malignancy after solid organ transplantation: an overview, Oncologist, 13 (2008) 769-778.
[348] N.Y. Chokshi, S.H. Sicherer, Interpreting IgE sensitization tests in food allergy, Expert Review of Clinical Immunology, 12 (2016) 389-403.
[349] X. Luo, K.L. Pothoven, D. McCarthy, M. DeGutes, A. Martin, D.R. Getts, G. Xia, J. He, X. Zhang, D.B. Kaufman, S.D. Miller, ECDI-fixed allogeneic splenocytes induce donor-specific tolerance for long-term survival of islet transplants via two distinct mechanisms, Proceedings of the National Academy of Sciences of the United States of America, 105 (2008) 14527-14532. PMID: 18796615.
[350] D.P. McCarthy, J. Bryant, J.P. Galvin, S.D. Miller, X. Luo, Tempering Allorecognition to Induce Transplant Tolerance With Chemically Modified Apoptotic Donor Cells, Am J Transplant, 15 (2015) 1475-1483.
[351] S. Wang, X. Zhang, L. Zhang, J. Bryant, T. Kheradmand, B.J. Hering, S.D. Miller, X. Luo, Preemptive Tolerogenic Delivery of Donor Antigens for Permanent Allogeneic Islet Graft Protection, Cell Transplant, 24 (2015) 1155-1165.
[352] N. Dilek, N. van Rompaey, A. Le Moine, B. Vanhove, Myeloid-derived suppressor cells in transplantation, Curr Opin Organ Transplant, 15 (2010) 765-768.
[353] P. Trzonkowski, R. Bacchetta, M. Battaglia, D. Berglund, H.R. Bohnenkamp, A. ten Brinke, A. Bushell, N. Cools, E.K. Geissler, S. Gregori, S. Marieke van Ham, C. Hilkens, J.A. Hutchinson, G. Lombardi, J.A. Madrigal, N. Marek-Trzonkowska, E.M. Martinez-Caceres, M.G. Roncarolo, S. Sanchez-Ramon, A. Saudemont, B. Sawitzki, Hurdles in therapy with regulatory T cells, Science translational medicine, 7 (2015) 304ps318.

[354] J.M. Lu, X.W. Wang, C. Marin-Muller, H. Wang, P.H. Lin, Q.Z. Yao, C.Y. Chen, Current advances in research and clinical applications of PLGA-based nanotechnology, Expert Rev Mol Diagn, 9 (2009) 325-341.
[355] H.K. Makadia, S.J. Siegel, Poly Lactic-co-Glycolic Acid (PLGA) as Biodegradable Controlled Drug Delivery Carrier, Polymers-Basel, 3 (2011) 1377-1397.
[356] D. Bobo, K.J. Robinson, J. Islam, K.J. Thurecht, S.R. Corrie, Nanoparticle-Based Medicines: A Review of FDA-Approved Materials and Clinical Trials to Date, Pharm Res-Dordr, 33 (2016) 2373-2387.
[357] T. Neef, S.D. Miller, Tolerogenic Nanoparticles to Treat Islet Autoimmunity, Curr Diab Rep, 17 (2017) 84.
[358] T.K. Kishimoto, R.A. Maldonado, Nanoparticles for the Induction of Antigen-Specific Immunological Tolerance, Front Immunol, 9 (2018).
[359] S. Prasad, D. Xu, S.D. Miller, Tolerance strategies employing antigen-coupled apoptotic cells and carboxylated PLG nanoparticles for the treatment of type 1 diabetes, Rev Diabet Stud, 9 (2012) 319-327.
[360] K.R. Mcintyre, J.G. Seidman, Nucleotide-Sequence of Mutant I-a-Beta-Bm12 Gene Is Evidence for Genetic Exchange between Mouse Immune-Response Genes, Nature, 308 (1984) 551-553.
[361] M. Schmaler, M.A. Broggi, S.W. Rossi, Transplantation of tail skin to study allogeneic CD4 T cell responses in mice, J Vis Exp, (2014) e51724.
[362] C. Meydan, H.H. Otu, O.U. Sezerman, Prediction of peptides binding to MHC class I and II alleles by temporal motif mining, Bmc Bioinformatics, 14 (2013).
[363] S.T. Chang, D. Ghosh, D.E. Kirschner, J.J. Linderman, Peptide length-based prediction of peptide-MHC class II binding, Bioinformatics, 22 (2006) 2761-2767.
[364] M. Buettner, M. Bornemann, U. Bode, Skin Tolerance is Supported by the Spleen, Scand J Immunol, 77 (2013) 238-245.
[365] H.H. Lin, D.E. Faunce, M. Stacey, A. Terajewicz, T. Nakamura, J. Zhang-Hoover, M. Kerley, M.L. Mucenski, S. Gordon, J. Stein-Streilein, The macrophage F4/80 receptor is required for the induction of antigen-specific efferent regulatory T cells in peripheral tolerance, Journal of Experimental Medicine, 201 (2005) 1615-1625.
[366] N. Gagliani, T. Jofra, A. Valle, A. Stabilini, C. Morsiani, S. Gregori, S. Deng, D.M. Rothstein, M. Atkinson, M. Kamanaka, R.A. Flavell, M.G. Roncarolo, M. Battaglia, Transplant Tolerance to Pancreatic Islets Is Initiated in the Graft and Sustained in the Spleen, Am J Transplant, 13 (2013) 1963-1975.
[367] A. Goubier, B. Dubois, H. Gheit, G. Joubert, F. Villard-Truc, C. Asselin-Paturel, G. Trinchieri, D. Kaiserlian, Plasmacytoid dendritic cells mediate oral tolerance, Immunity, 29 (2008) 464-475.
[368] P. Martin, G.M. del Hoyo, F. Anjuere, C.F. Arias, H.H. Vargas, A. Fernandez-L, V. Parrillas, C. Ardavin, Characterization of a new subpopulation of mouse CD8 alpha(+) B220(+) dendritic cells endowed with type 1 interferon production capacity and tolerogenic potential, Blood, 100 (2002) 383-390.
[369] T. Liu, L. Soong, G. Liu, R. Konig, A.K. Chopra, CD44 expression positively correlates with Foxp3 expression and suppressive function of CD4(+) T-reg cells, Biol Direct, 4 (2009).
[370] P.A. Roche, K. Furuta, The ins and outs of MHC class II-mediated antigen processing and presentation.

[371] M. Wieczorek, E.T. Abualrous, J. Sticht, M. Alvaro-Benito, S. Stolzenberg, F. Noe, C. Freund, Major Histocompatibility Complex (MHC) Class I and MHC Class II Proteins: Conformational Plasticity in Antigen Presentation.
[372] K.L. Rock, E. Reits, J. Neefjes, Present Yourself! By MHC Class I and MHC Class II Molecules.
[373] Q.Y. Hu, F. Berti, R. Adamo, Towards the next generation of biomedicines by site-selective conjugation, Chem Soc Rev, 45 (2016) 1691-1719.
[374] C.D. Spicer, B.G. Davis, Selective chemical protein modification, Nature Communications, 5 (2014).
[375] M. Di Marco, S. Shamsuddin, K.A. Razak, A.A. Aziz, C. Devaux, E. Borghi, L. Levy, C. Sadun, Overview of the main methods used to combine proteins with nanosystems: absorption, bioconjugation, and encapsulation, Int J Nanomedicine, 5 (2010) 37-49.
[376] S. Takemoto, F.K. Port, F.H.J. Claas, R.J. Duquesnoy, HLA matching for kidney transplantation, Hum Immunol, 65 (2004) 1489-1505.
[377] B. Loveland, E. Simpson, The Non-Mhc Transplantation Antigens - Neither Weak nor Minor, Immunol Today, 7 (1986) 223-229.
[378] H. Waldmann, E. Adams, P.J. Fairchild, S. Cobbold, Infectious tolerance and the long-term acceptance of transplanted tissue, Immunol Rev, 212 (2006) 301-313.
[379] S. Cobbold, H. Waldmann, Infectious tolerance, Current opinion in immunology, 10 (1998) 518-524.
[380] X.C. Li, L.A. Turka, An update on regulatory T cells in transplant tolerance and rejection, Nat Rev Nephrol, 6 (2010) 577-583.
[381] H. Mansour, S. Homs, D. Desvaux, C. Badoual, K. Dahan, M. Matignon, V. Audard, P. Lang, P. Grimbert, Intragraft Levels of Foxp3 mRNA Predict Progression in Renal Transplants with Borderline Change, Journal of the American Society of Nephrology, 19 (2008) 2277-2281.
[382] M.P. Fischbein, J. Yun, H. Laks, Y. Irie, M.C. Fishbein, B. Bonavida, A. Ardehali, Role of CD8(+) lymphocytes in chronic rejection of transplanted hearts, J Thorac Cardiov Sur, 123 (2002) 803-809.
[383] P. Bhat, G. Leggatt, N. Waterhouse, I.H. Frazer, Interferon-gamma derived from cytotoxic lymphocytes directly enhances their motility and cytotoxicity, Cell Death Dis, 8 (2017).
[384] R. Nicolete, D.F. dos Santos, L.H. Faccioli, The uptake of PLGA micro or nanoparticles by macrophages provokes distinct in vitro inflammatory response, Int Immunopharmacol, 11 (2011) 1557-1563.
[385] T.T. Ding, J. Sun, P. Zhang, Immune evaluation of biomaterials in TNF-alpha and IL-1 beta at mRNA level, J Mater Sci-Mater M, 18 (2007) 2233-2236.
[386] J.X. Zhao, J.C. Zhao, S. Perlman, Differential Effects of IL-12 on Tregs and Non-Treg T Cells: Roles of IFN-gamma, IL-2 and IL-2R, Plos One, 7 (2012).
[387] Y. Zhai, R.M. Ghobrial, R.W. Busuttil, J.W. Kupiec-Weglinski, Th1 and Th2 cytokines in organ transplantation: Paradigm lost?, Critical reviews in immunology, 19 (1999) 155-172.
[388] P. Schnorrer, G.M.N. Behrens, N.S. Wilson, J.L. Pooley, C.M. Smith, D. EI-Sukkari, G. Davey, F. Kupresanin, M. Li, E. Maraskovsky, G.T. Belz, F.R. Carbone, K. Shortman, W.R. Heath, J.A. Villadangos, The dominant role of CD8(+) dendritic cells in cross-presentation is not dictated by antigen capture, Proceedings of the National Academy of Sciences of the United States of America, 103 (2006) 10729-10734.

[389] G. Lombardi, L. Barber, S. Sidhu, J.R. Batchelor, R.I. Lechler, The Specificity of Alloreactive T-Cells Is Determined by Mhc Polymorphisms Which Contact the T-Cell Receptor and Which Influence Peptide Binding, Int Immunol, 3 (1991) 769-775.
[390] P.A. Smith, A. Brunmark, M.R. Jackson, T.A. Potter, Peptide-independent recognition by alloreactive cytotoxic T lymphocytes (CTL), Journal of Experimental Medicine, 185 (1997) 1023-1033.
[391] J.A. Villadangos, B. Galocha, J.A.L. Decastro, Unusual Topology of an Hla-B27 Allospecific T-Cell Epitope Lacking Peptide Specificity, Journal of Immunology, 152 (1994) 2317-2323.
[392] M.A. Atkinson, G.S. Eisenbarth, A.W. Michels, Type 1 diabetes, Lancet (London, England), 383 (2014) 69-82.
[393] M.D. Bellin, F.B. Barton, A. Heitman, J.V. Harmon, R. Kandaswamy, A.N. Balamurugan, D.E. Sutherland, R. Alejandro, B.J. Hering, Potent induction immunotherapy promotes long-term insulin independence after islet transplantation in type 1 diabetes, Am J Transplant, 12 (2012) 1576-1583.
[394] M.R. Rickels, M.H. Schutta, R. Mueller, S. Kapoor, J.F. Markmann, A. Naji, K.L. Teff, Glycemic thresholds for activation of counterregulatory hormone and symptom responses in islet transplant recipients, J Clin Endocrinol Metab, 92 (2007) 873-879.
[395] D.M. Thompson, M. Meloche, Z. Ao, B. Paty, P. Keown, R.J. Shapiro, S. Ho, D. Worsley, M. Fung, G. Meneilly, I. Begg, M. Al Mehthel, J. Kondi, C. Harris, B. Fensom, S.E. Kozak, S.O. Tong, M. Trinh, G.L. Warnock, Reduced progression of diabetic microvascular complications with islet cell transplantation compared with intensive medical therapy, Transplantation, 91 (2011) 373-378.
[396] A.M. Shapiro, C. Ricordi, B.J. Hering, H. Auchincloss, R. Lindblad, R.P. Robertson, A. Secchi, M.D. Brendel, T. Berney, D.C. Brennan, E. Cagliero, R. Alejandro, E.A. Ryan, B. DiMercurio, P. Morel, K.S. Polonsky, J.A. Reems, R.G. Bretzel, F. Bertuzzi, T. Froud, R. Kandaswamy, D.E. Sutherland, G. Eisenbarth, M. Segal, J. Preiksaitis, G.S. Korbutt, F.B. Barton, L. Viviano, V. Seyfert-Margolis, J. Bluestone, J.R. Lakey, International trial of the Edmonton protocol for islet transplantation, N Engl J Med, 355 (2006) 1318-1330.
[397] B.J. Hering, W.R. Clarke, N.D. Bridges, T.L. Eggerman, R. Alejandro, M.D. Bellin, K. Chaloner, C.W. Czarniecki, J.S. Goldstein, L.G. Hunsicker, D.B. Kaufman, O. Korsgren, C.P. Larsen, X. Luo, J.F. Markmann, A. Naji, J. Oberholzer, A.M. Posselt, M.R. Rickels, C. Ricordi, M.A. Robien, P.A. Senior, A.M. Shapiro, P.G. Stock, N.A. Turgeon, C. Clinical Islet Transplantation, Phase 3 Trial of Transplantation of Human Islets in Type 1 Diabetes Complicated by Severe Hypoglycemia, Diabetes Care, 39 (2016) 1230-1240.
[398] O. Korsgren, B. Nilsson, C. Berne, M. Felldin, A. Foss, R. Kallen, T. Lundgren, K. Salmela, A. Tibell, G. Tufveson, Current Status of Clinical Islet Transplantation, Transplantation, 79 (2005) 1289-1293.
[399] L. Makhlouf, A. Yamada, T. Ito, R. Abdi, M.J. Ansari, C.Q. Khuong, H.J. Winn, H. Auchincloss, Jr., M.H. Sayegh, Allorecognition and effector pathways of islet allograft rejection in normal versus nonobese diabetic mice, J Am Soc. Nephrol, 14 (2003) 2168-2175.
[400] L. Makhlouf, K. Kishimoto, R.N. Smith, R. Abdi, M. Koulmanda, H.J. Winn, H. Auchincloss, Jr., M.H. Sayegh, The role of autoimmunity in islet allograft destruction: major histocompatibility complex class II matching is necessary for autoimmune destruction of allogeneic islet transplants after T-cell costimulatory blockade, Diabetes, 51 (2002) 3202-3210.

[401] M. Sleater, A.S. Diamond, R.G. Gill, Islet Allograft Rejection by Contact-Dependent CD8(+) T cells: Perforin and FasL Play Alternate but Obligatory Roles, Am J Transplant, 7 (2007) 1927-1933.
[402] A.S. Diamond, R.G. Gill, An essential contribution by IFN-gamma to CD8+ T cell-mediated rejection of pancreatic islet allografts, J. Immunol, 165 (2000) 247-255.
[403] R.G. Gill, A.S. Rosenberg, K.J. Lafferty, A. Singer, Characterization of primary T cell subsets mediating rejection of pancreatic islet grafts., J. Immunol, 143 (1989) 2176-2178.
[404] M.R. Alderson, T.W. Tough, T. Davis-Smith, S. Braddy, B. Falk, K.A. Schooley, R.G. Goodwin, C.A. Smith, F. Ramsdell, D.H. Lynch, Fas ligand mediates activation-induced cell death in human T lymphocytes, J Exp Med, 181 (1995) 71-77.
[405] T.S. Griffith, T. Brunner, S.M. Fletcher, D.R. Green, T.A. Ferguson, FasL ligand-induced apoptosis as a mechanism of immune privilege, Science, 270 (1995) 1189-1192.
[406] D. Bellgrau, D. Gold, H. Selawry, J. Moore, A. Franzusoff, R.C. Duke, A role for CD95 ligand in preventing graft rejection, Nature, 377 (1995) 630-632.
[407] J. Wu, T. Zhou, J. Zhang, J. He, W.C. Gause, J.D. Mountz, Correction of accelerated autoimmune disease by early replacement of the mutated lpr gene with the normal Fas apoptosis gene in the T cells of transgenic MRL-lpr/lpr mice, Proc Natl Acad Sci U S A, 91 (1994) 2344-2348.
[408] S.-T. Ju, D.J. Panka, H. Cul, R. Ettinger, M. El-Khatib, D.H. Sherr, B.Z. Stanger, A. Marshak-Rothstein, Fas(CD95)/FasL interactions required for programmed cell death after T-cell activation, Nature, 373 (1996) 444-448.
[409] E.S. Yolcu, N. Askenasy, N.P. Singh, S.L. Cherradi, H. Shirwan, Cell membrane modification for rapid display of proteins as a novel means of immunomodulation: FasL-decorated cells prevent islet graft rejection, Immunity, 17 (2002) 795-808.
[410] R. Torgler, S. Jakob, E. Ontsouka, U. Nachbur, C. Mueller, D.R. Green, T. Brunner, Regulation of activation-induced Fas (CD95/Apo-1) ligand expression in T cells by the cyclin B1/Cdk1 complex, J Biol Chem, 279 (2004) 37334-37342.
[411] K.U. Lundin, V. Screpanti, H. Omholt, P.O. Hofgaard, H. Yagita, A. Grandien, B. Bogen, CD4+ T cells kill Id+ B-lymphoma cells: FasLigand-Fas interaction is dominant in vitro but is redundant in vivo, Cancer Immunology Immunotherapy, 53 (2004) 1135-1145.
[412] M.R. Alderson, R.J. Armitage, E. Maraskovsky, T.W. Tough, E. Roux, K. Schooley, F. Ramsdell, D.H. Lynch, Fas transduces activation signals in normal human T lymphocytes, J Exp Med, 178 (1993) 2231-2235.
[413] I. Suzuki, S. Martin, T.E. Boursalian, C. Beers, P.J. Fink, Fas Ligand Costimulates the In Vivo Proliferation of CD8+ T Cells, The Journal of Immunology, 165 (2000) 5537-5543.
[414] S.E. Weber, J. Harbertson, E. Godebu, G.A. Mros, R.C. Padrick, B.D. Carson, S.F. Ziegler, L.M. Bradley, Adaptive Islet-Specific Regulatory CD4 T Cells Control Autoimmune Diabetes and Mediate the Disappearance of Pathogenic Th1 Cells In Vivo, The Journal of Immunology, 176 (2006) 4730-4739.
[415] A.V. Gorbachev, R.L. Fairchild, CD4+CD25+ regulatory T cells utilize FasL as a mechanism to restrict DC priming functions in cutaneous immune responses, Eur J Immunol, 40 (2010) 2006-2015.
[416] D.D. Franke, E.S. Yolcu, P. Alard, M.M. Kosiewicz, H. Shirwan, A novel multimeric form of FasL modulates the ability of diabetogenic T cells to mediate type 1 diabetes in an adoptive transfer model, Mol Immunol, 44 (2007) 2884-2892.

[417] E.S. Yolcu, H. Zhao, L. Bandura-Morgan, C. Lacelle, K.B. Woodward, N. Askenasy, H. Shirwan, Pancreatic islets engineered with SA-FasL protein establish robust localized tolerance by inducing regulatory T cells in mice, Journal of immunology, 187 (2011) 5901-5909.
[418] W. Bennet, B. Sundberg, T. Lundgren, A. Tibell, C.G. Groth, A. Richards, D.J. White, G. Elgue, R. Larsson, B. Nilsson, O. Korsgren, Damage to porcine islets of Langerhans after exposure to human blood in vitro, or after intraportal transplantation to cynomologus monkeys: protective effects of sCR1 and heparin, Transplantation, 69 (2000) 711-719.
[419] O. Korsgren, Review article: Acute cellular xenograft rejection, Xenotransplantation, 4 (1997) 11-19.
[420] A.M. Shapiro, H.L. Gallant, E.G. Hao, J.R. Lakey, T. McCready, R.V. Rajotte, R.W. Yatscoff, N.M. Kneteman, The portal immunosuppressive storm: relevance to islet transplantation?, Ther Drug Monit, 27 (2005) 35-37.
[421] R.P. D., S. Michael, L. Jeffrey, Y. Richard, K. Ekaterina, G.A. J., S.L. D., Evaluation of encapsulating and microporous nondegradable hydrogel scaffold designs on islet engraftment in rodent models of diabetes, Biotechnology and Bioengineering, 0.
[422] J.M.H. Liu, X. Zhang, S. Joe, X. Luo, L.D. Shea, Evaluation of biomaterial scaffold delivery of IL-33 as a localized immunomodulatory agent to support cell transplantation in adipose tissue, Journal of Immunology and Regenerative Medicine, 1 (2018) 1-12.
[423] J.M.H. Liu, J. Zhang, X. Zhang, K.A. Hlavaty, C.F. Ricci, J.N. Leonard, L.D. Shea, R.M. Gower, Transforming growth factor-beta 1 delivery from microporous scaffolds decreases inflammation post-implant and enhances function of transplanted islets, Biomaterials, 80 (2016) 11-19.
[424] R.F. Gibly, X. Zhang, W.L. Lowe, L.D. Shea, Porous Scaffolds Support Extrahepatic Human Islet Transplantation, Engraftment, and Function in Mice, Cell Transplantation, 22 (2013) 811-819.
[425] R.F. Gibly, X. Zhang, M.L. Graham, B.J. Hering, D.B. Kaufman, W.L. Lowe, L.D. Shea, Extrahepatic islet transplantation with microporous polymer scaffolds in syngeneic mouse and allogeneic porcine models, Biomaterials, 32 (2011) 9677-9684.
[426] D.M. Salvay, C.B. Rives, X. Zhang, F. Chen, D.B. Kaufman, W.L. Lowe, Jr., L.D. Shea, Extracellular matrix protein-coated scaffolds promote the reversal of diabetes after extrahepatic islet transplantation, Transplantation, 85 (2008) 1456-1464.
[427] H. Blomeier, X. Zhang, C. Rives, M. Brissova, E. Hughes, M. Baker, A.C. Powers, D.B. Kaufman, L.D. Shea, W.L. Lowe, Jr., Polymer scaffolds as synthetic microenvironments for extrahepatic islet transplantation, Transplantation, 82 (2006) 452-459.
[428] R.F. Gibly, X. Zhang, W.L. Lowe, Jr., L.D. Shea, Porous scaffolds support extrahepatic human islet transplantation, engraftment, and function in mice, Cell Transplant, 22 (2013) 811-819.
[429] E. Cantarelli, L. Piemonti, Alternative transplantation sites for pancreatic islet grafts, Curr Diab Rep, 11 (2011) 364-374.
[430] D.J. van der Windt, Echeverri G. J, I.J.N. M., C.D.K. C., The choice of anatomical site for islet transplantation, Cell Transplantation, 17 (2008) 1005-1014.
[431] Z.N. Hunter, D.P. McCarthy, W.T. Yap, C.T. Harp, D.R. Getts, L.D. Shea, S.D. Miller, A biodegradable nanoparticle platform for the induction of antigen-specific immune tolerance for treatment of autoimmune disease, ACS Nano, 8 (2014) 2148-2160.

[432] E.S. Yolcu, X. Gu, C. Lacelle, H. Zhao, L. Bandura-Morgan, N. Askenasy, H. Shirwan, Induction of tolerance to cardiac allografts using donor splenocytes engineered to display on their surface an exogenous fas ligand protein, J. Immunol, 181 (2008) 931-939.
[433] J. Bryant, K.A. Hlavaty, X. Zhang, W.-T. Yap, L. Zhang, L.D. Shea, X. Luo, Nanoparticle delivery of donor antigens for transplant tolerance in allogeneic islet transplantation, Biomaterials, 35 (2014) 8887-8894. PMID: 25066477.
[434] S. Zhao, W. Zhu, S. Xue, D. Han, Testicular defense systems: immune privilege and innate immunity, Cell Mol Immunol, 11 (2014) 428-437.
[435] I. Benhar, A. London, M. Schwartz, The privileged immunity of immune privileged organs: the case of the eye, Front Immunol, 3 (2012) 296.
[436] M.J. Carson, J.M. Doose, B. Melchior, C.D. Schmid, C.C. Ploix, CNS immune privilege: hiding in plain sight, Immunol Rev, 213 (2006) 48-65.
[437] X. Chen, X. Zhang, C. Larson, F. Chen, H. Kissler, D.B. Kaufman, The epididymal fat pad as a transplant site for minimal islet mass, Transplantation, 84 (2007) 122-125.
[438] M. Mehdizadeh, H. Rouhani, N. Sepehri, R. Varshochian, M.H. Ghahremani, M. Amini, M. Gharghabi, S.N. Ostad, F. Atyabi, A. Baharian, R. Dinarvand, Biotin decorated PLGA nanoparticles containing SN-38 designed for cancer therapy, Artif Cells Nanomed Biotechnol, 45 (2017) 495-504.
[439] E.S. Yolcu, H. Zhao, H. Shirwan, Immunomodulation with SA-FasL protein as an effective means of preventing islet allograft rejection in chemically diabetic NOD mice, Transplant Proc, 45 (2013) 1889-1891.
[440] O. Donaldson, Z.J. Huang, N. Comolli, An integrated experimental and modeling approach to propose biotinylated PLGA microparticles as versatile targeting vehicles for drug delivery, Biomaterials, 2 (2013) 1-10.
[441] R.M. Pearson, L.M. Casey, K.R. Hughes, L.Z. Wang, M.G. North, D.R. Getts, S.D. Miller, L.D. Shea, Controlled Delivery of Single or Multiple Antigens in Tolerogenic Nanoparticles Using Peptide-Polymer Bioconjugates, Mol Ther, 25 (2017) 1655-1664.
[442] S. Valetti, S. Mura, M. Noiray, S. Arpicco, F. Dosio, J. Vergnaud, D. Desmaele, B. Stella, P. Couvreur, Peptide conjugation: before or after nanoparticle formation?, Bioconjug Chem, 25 (2014) 1971-1983.
[443] D.J. Mooney, D.F. Baldwin, N.P. Suh, J.P. Vacanti, R. Langer, Novel approach to fabricate porous sponges of poly(D,L-lactic-co-glycolic acid) without the use of organic solvents, Biomaterials, 17 (1996) 1417-1422.
[444] L.D. Shea, E. Smiley, J. Bonadio, D.J. Mooney, DNA delivery from polymer matrices for tissue engineering, Nature Biotechnology, 17 (1999) 551-554.
[445] R.F. Gibly, X. Zhang, M.L. Graham, B.J. Hering, D.B. Kaufman, W.L. Lowe, Jr., L.D. Shea, Extrahepatic islet transplantation with microporous polymer scaffolds in syngeneic mouse and allogeneic porcine models, Biomaterials, 32 (2011) 9677-9684.
[446] R.M. Pearson, S. Sen, H.J. Hsu, M. Pasko, M. Gaske, P. Kral, S. Hong, Tuning the Selectivity of Dendron Micelles Through Variations of the Poly(ethylene glycol) Corona, ACS Nano, 10 (2016) 6905-6914.
[447] P.S. Hume, K.S. Anseth, Inducing local T cell apoptosis with anti-Fas-functionalized polymeric coatings fabricated via surface-initiated photopolymerizations, Biomaterials, 31 (2010) 3166-3174.

[448] E.S. Yolcu, N. Askenasy, N.P. Singh, S.E. Cherradi, H. Shirwan, Cell membrane modification for rapid display of proteins as a novel means of immunomodulation: FasL-decorated cells prevent islet graft rejection, Immunity, 17 (2002) 795-808.
[449] D.M. Headen, K.B. Woodward, M.M. Coronel, P. Shrestha, J.D. Weaver, H. Zhao, M. Tan, M.D. Hunckler, W.S. Bowen, C.T. Johnson, L. Shea, E.S. Yolcu, A.J. Garcia, H. Shirwan, Local immunomodulation with Fas ligand-engineered biomaterials achieves allogeneic islet graft acceptance, Nat Mater, 17 (2018) 732-739.
[450] T.S. Griffith, T. Brunner, S.M. Fletcher, D.R. Green, T.A. Ferguson, Fas ligand-induced apoptosis as a mechanism of immune privilege, Science, 270 (1995) 1189-1192.
[451] Autoimmune disease, Nature Biotechnology, 18 (2000) IT7-IT9.
[452] S.L. Hauser, J.R. Oksenberg, The neurobiology of multiple sclerosis: genes, inflammation, and neurodegeneration, Neuron, 52 (2006) 61-76.
[453] I. Metz, S.D. Weigand, B.F. Popescu, J.M. Frischer, J.E. Parisi, Y. Guo, H. Lassmann, W. Bruck, C.F. Lucchinetti, Pathologic heterogeneity persists in early active multiple sclerosis lesions, Annals of neurology, 75 (2014) 728-738.
[454] C. Lucchinetti, W. Bruck, J. Parisi, B. Scheithauer, M. Rodriguez, H. Lassmann, Heterogeneity of multiple sclerosis lesions: implications for the pathogenesis of demyelination, Annals of neurology, 47 (2000) 707-717.
[455] A. Billiau, P. Matthys, Modes of action of Freund's adjuvants in experimental models of autoimmune diseases, Journal of Leukocyte Biology, 70 (2001) 849-860.
[456] O. Alter, P.O. Brown, D. Botstein, Singular value decomposition for genome-wide expression data processing and modeling, Proceedings of the National Academy of Sciences, 97 (2000) 10101.
[457] <randomforest2001.pdf>.
[458] S.S. Rao, G.G. Bushnell, S.M. Azarin, G. Spicer, B.A. Aguado, J.R. Stoehr, E.J. Jiang, V. Backman, L.D. Shea, J.S. Jeruss, Enhanced Survival with Implantable Scaffolds That Capture Metastatic Breast Cancer Cells In Vivo, Cancer research, 76 (2016) 5209-5218.
[459] K.C. Navegantes, R. de Souza Gomes, P.A.T. Pereira, P.G. Czaikoski, C.H.M. Azevedo, M.C. Monteiro, Immune modulation of some autoimmune diseases: the critical role of macrophages and neutrophils in the innate and adaptive immunity, Journal of translational medicine, 15 (2017) 36.
[460] Z. Yan, S.A. Gibson, J.A. Buckley, H. Qin, E.N. Benveniste, Role of the JAK/STAT signaling pathway in regulation of innate immunity in neuroinflammatory diseases, Clin Immunol, 189 (2018) 4-13.
[461] I.L. King, T.L. Dickendesher, B.M. Segal, Circulating Ly-6C+ myeloid precursors migrate to the CNS and play a pathogenic role during autoimmune demyelinating disease, Blood, 113 (2009) 3190-3197.
[462] L. Mayo, F.J. Quintana, H.L. Weiner, The innate immune system in demyelinating disease, Immunol Rev, 248 (2012) 170-187.
[463] D. Nickles, H.P. Chen, M.M. Li, P. Khankhanian, L. Madireddy, S.J. Caillier, A. Santaniello, B.A. Cree, D. Pelletier, S.L. Hauser, J.R. Oksenberg, S.E. Baranzini, Blood RNA profiling in a large cohort of multiple sclerosis patients and healthy controls, Human molecular genetics, 22 (2013) 4194-4205.
[464] M. Comabella, R. Martin, Genomics in multiple sclerosis--current state and future directions, Journal of neuroimmunology, 187 (2007) 1-8.

[465] M. Ramanathan, L.T. Weinstock-Guttman B Fau - Nguyen, D. Nguyen Lt Fau - Badgett, C. Badgett D Fau - Miller, K. Miller C Fau - Patrick, C. Patrick K Fau - Brownscheidle, L. Brownscheidle C Fau - Jacobs, L. Jacobs, In vivo gene expression revealed by cDNA arrays: the pattern in relapsing-remitting multiple sclerosis patients compared with normal subjects.
[466] R. Ratzer, J.R. Sondergaard Hb Fau - Christensen, L. Christensen Jr Fau - Bornsen, R. Bornsen L Fau - Borup, P.S. Borup R Fau - Sorensen, F. Sorensen Ps Fau - Sellebjerg, F. Sellebjerg, Gene expression analysis of relapsing-remitting, primary progressive and secondary progressive multiple sclerosis.
[467] N. Safari-Alighiarloo, M. Rezaei-Tavirani, M. Taghizadeh, S.M. Tabatabaei, S. Namaki, Network-based analysis of differentially expressed genes in cerebrospinal fluid (CSF) and blood reveals new candidate genes for multiple sclerosis, PeerJ, 4 (2016) e2775-e2775.
[468] L.A.A. Orellano, S.A. de Almeida, L.X. Pereira, L.C. Couto, M.G.T. de Lazari, C.T.R. Viana, S.P. Andrade, P.P. Campos, Upregulation of Foreign Body Response in Obese Mice, Obesity (Silver Spring, Md.), 26 (2018) 531-539.
[469] G.S.A. Boersema, L. Utomo, Y. Bayon, N. Kops, E. van der Harst, J.F. Lange, Y.M. Bastiaansen-Jenniskens, Monocyte subsets in blood correlate with obesity related response of macrophages to biomaterials in vitro, Biomaterials, 109 (2016) 32-39.
[470] D. Hachim, N. Wang, S.T. Lopresti, E.C. Stahl, Y.U. Umeda, R.D. Rege, S.T. Carey, D. Mani, B.N. Brown, Effects of aging upon the host response to implants, J Biomed Mater Res A, 105 (2017) 1281-1292.
[471] R.S. Oakes, G.G. Bushnell, S.M. Orbach, P. Kandagatla, Y. Zhang, A.H. Morris, M.S. Hall, P. LaFaire, J.T. Decker, R.M. Hartfield, M.D. Brooks, M.S. Wicha, J.S. Jeruss, L.D. Shea, Metastatic conditioning of myeloid cells at a subcutaneous synthetic niche reflects disease progression and predicts therapeutic outcomes, Cancer research, (2019) canres.1932.2019.
[472] S.L. Bailey, B. Schreiner, E.J. McMahon, S.D. Miller, CNS myeloid DCs presenting endogenous myelin peptides 'preferentially' polarize CD4+ T(H)-17 cells in relapsing EAE, Nature immunology, 8 (2007) 172-180.
[473] T. Derfuss, Personalized medicine in multiple sclerosis: hope or reality?, BMC Medicine, 10 (2012) 116.
[474] B.A. Aguado, R.M. Hartfield, G.G. Bushnell, J.T. Decker, S.M. Azarin, D. Nanavati, M.J. Schipma, S.S. Rao, R.S. Oakes, Y. Zhang, J.S. Jeruss, L.D. Shea, Biomaterial Scaffolds as Pre-metastatic Niche Mimics Systemically Alter the Primary Tumor and Tumor Microenvironment, Advanced healthcare materials, 7 (2018) e1700903.
[475] A.H. Morris, R.S. Mahal, J. Udell, M. Wu, T.R. Kyriakides, Multicompartment Drug Release System for Dynamic Modulation of Tissue Responses, Advanced healthcare materials, 6 (2017).
[476] A.H. Morris, D.K. Stamer, B. Kunkemoeller, J. Chang, H. Xing, T.R. Kyriakides, Decellularized materials derived from TSP2-KO mice promote enhanced neovascularization and integration in diabetic wounds, Biomaterials, 169 (2018) 61-71.
[477] S.D. Miller, W.J. Karpus, Experimental autoimmune encephalomyelitis in the mouse, Current protocols in immunology, Chapter 15 (2007) Unit 15.11.
[478] N.J. Holland, D.M. Schneider, R. Rapp, R.C. Kalb, Meeting the needs of people with primary progressive multiple sclerosis, their families, and the health-care community, Int J MS Care, 13 (2011) 65-74.
[479] Z. Khaleeli, F. Ciccarelli O Fau - Manfredonia, F. Manfredonia F Fau - Barkhof, B. Barkhof F Fau - Brochet, M. Brochet B Fau - Cercignani, V. Cercignani M Fau - Dousset, M. Dousset V

Fau - Filippi, X. Filippi M Fau - Montalban, C. Montalban X Fau - Polman, M. Polman C Fau - Rovaris, A. Rovaris M Fau - Rovira, J. Rovira A Fau - Sastre-Garriga, M. Sastre-Garriga J Fau - Vellinga, D. Vellinga M Fau - Miller, A. Miller D Fau - Thompson, A. Thompson, Predicting progression in primary progressive multiple sclerosis: a 10-year multicenter study.